CHAPTER 5

TRANSIENT SUBCOOLED FLOW BOILING OF FC-72 OVER A SMALL HEATED COPPER PLATE

The experimental data obtained in the second part of this study are presented in this chapter to illustrate how the FC-72 mass flux oscillation affects the transient subcooled flow boiling heat transfer of FC-72 over a small heated circular copper flat plate flush mounted on the bottom of a horizontal rectangular channel. The present experiments are carried out for the mean FC-72 mass flux fixed at 300 and 400 kg/m^2s, inlet liquid cooling of 5^oC and $10\ ^oC$, and imposed heat flux varying from 0.1 W/cm^2 to 10 W/cm^2. Besides, the amplitude of the coolant mass flux oscillation is set at 0%, 5% and 10% of the mean coolant mass flux. At the inlet of the test section the period of the mass flux oscillation is fixed at 10, 20 and 30 seconds. The coolant is at slightly subatmospheric pressure of 99 kPa with T_{sat} = 55^oC for FC-72. In the following, the effects of the experimental parameters, namely, the mean level and the amplitude and period of the coolant mass flux oscillation, inlet coolant subcooling, imposed heat flux, on the transient FC-72 subcooled flow boiling heat transfer performance are examined in detail. Note that for the limiting case of 0% mass flux oscillation we have stable subcooled boiling of FC-72 in the test section. The heat transfer performance is presented in terms of the time variations of the space average surface temperature of the copper plate and boiling heat transfer coefficients. Besides, the photos of the boiling flow and the bubble departure diameter and frequency and active nucleation site density at selected time instants in a typical periodic cycle are presented.

5.1 Stable and Time-average Subcooled Flow Boiling Curves and Heat Transfer Coefficients

Effects of the mean coolant mass flux $\overline{G}$, inlet subcooling ΔT_{sub}, and the amplitude γ and period t_p of the coolant mass flux oscillation on the time-average boiling curves measured in the stable and transient FC-72 subcooled flow boiling are shown in Figures 5.1 - 5.4. Figure 5.1 shows the effects of the coolant mass flux oscillation on the measured time-average boiling curves for the stable and transient subcooled flow boiling for γ= 5% and t_p varied from 10s to 30s for ΔT_{sub} = 5°C. The data for a higher γ of 10% are given in Figure 5.2. In Figures 5.3 and 5.4 the data for a higher inlet liquid subcooling of 10°C are shown. These results indicate that for each boiling curve the space-average temperature of the copper plate increases gradually with the imposed heat flux from the subcooled temperature of the coolant at a low q to a certain value just slightly higher than the saturated temperature and no bubble nucleation is observed. The heat transfer in this region is completely due to the single-phase forced convection. With the continuing increase in the surface heat flux, bubbles begin to appear on the surface and the boiling curve is characterized by a sharp increase in the surface heat flux for a small rise in the temperature of the copper surface. We have onset of nucleate boiling (ONB) in the flow. A significant drop in the copper plate temperature occurs at ONB. The reason causing the sudden drop in the copper surface temperature at ONB is due to a significant increase in the wall heat transfer by the boiling processes. A close inspection of the data for the single-phase region further reveals that at a higher mass flux the temperature of the copper plate is somewhat lower for the same imposed heat flux. This obviously results from the increase in the single-phase convection heat transfer coefficient with the coolant mass flux. Note that except for the imposed heat flux slightly beyond that for ONB the amplitude and period of the coolant mass flux oscillation exhibit little effects on the

time-average boiling curves, suggesting that the dominance of the wall heat transfer by the fully developed nucleate boiling. However at a higher G the wall superheat and heat flux at ONB are substantially higher. This can be attributed to the fact that at a higher G more energy is needed for the vapor to nucleate from the cavities in the wall since the residence time of the coolant on the heated surface is shorter. A scrutiny of these data further suggests that the fully developed nucleate boiling prevails in the flow after ONB. It is worth to note that in the subcooled flow boiling significant temperature undershoot occurs at ONB. Besides, the temperature undershoot is smaller when the coolant mass flux oscillates at 5% and 10%. However, the effects of the period of the mass flux oscillation on the temperature are rather slight. Next, the effects of the inlet liquid subcooling on the time-average subcooled boiling curves are shown in Figures 5.5 – 5.11. The results indicate that during ONB a substantial increase in the temperature undershoot occurs when the inlet liquid subcooling is raised from 5°C to 10 °C. Beyond ONB the effects of the inlet liquid subcooling on the time-average boiling curves are small.

We proceed to examine how the time-average subcooled flow boiling heat transfer coefficients $\overline{h}_{2\phi,sub}$ are affected by the FC-72 coolant mass flux oscillation. The results for the variations of $\overline{h}_{2\phi,sub}$ with the imposed surface heat flux presented in Figures 5.12 - 5.15 reveal that the mean level, amplitude and period of the coolant mass flux oscillation shows negligible influences on the time-average subcooled flow boiling heat transfer coefficients. However, for a given coolant mass flux the boiling heat transfer coefficient increases substantially with the imposed heat flux. For example, at $\triangle T_{sub}$ =5°C and $\overline{G}$ =400 kg/m^{2}s, the subcooled boiling heat transfer coefficient for q =9.7 W/cm^2 is about 53.6% higher than that for q =5.0 W/cm^2 (Figure 5.12(a)). Moreover, the inlet liquid subcooling of the coolant also shows a significant effect on the time-average boiling heat transfer coefficient, as evident from

the data in Figures 5.16 – 5.22. Specifically, $\bar{h}_{2\phi,sub}$ is higher for a lower the inlet liquid subcooling.

5.2 Stable and Transient Subcooled Flow Boiling Heat Transfer Characteristics

The transient subcooled boiling heat transfer characteristics for FC-72 flow over the heated copper plate resulting from the temporal coolant mass flux oscillation are illustrated by presenting the time variations of the space-average heated surface temperature T_w and heat transfer coefficient $h_{2\phi}$ for various imposed heat fluxes and mass fluxes. For comparison purpose the results for T_w for the limiting cases of constant coolant mass fluxes are shown in Figure 5.23. These data for γ= 0% indicate that the fluctuations of the space average heated surface temperature with time for various q and G are relatively small. The subcooled boiling hence can be regarded as at a statistically stable state.

Now when the coolant mass flux oscillates periodically in time in a form of nearly a triangular wave, significant temporal oscillations in the space average heated surface temperature occur for the imposed heat flux slightly higher than that for the time average ONB, as evident from the data shown in Figures 5.24 -5.48 for the oscillation amplitude being 5% and 10% of the mean mass flux. Note that the temporal oscillation of the heated surface temperature is also periodic in time and is at the same frequency as the mass flux. Besides, the T_w oscillation gets slightly stronger for higher imposed heat flux and higher amplitude of the mass flux oscillation. Moreover, a longer period of the mass flux oscillation results in a larger amplitude of the T_w oscillation with $\triangle G$ being 10% of $\bar{G}$. Even in the single-phase forced convection for γ= 10% the space average heated surface temperature also oscillates

noticeably with time at a relatively low imposed heat flux with $q < \bar{q}_{ONB}$ (Figures 5.30 – 5.35). Here $\bar{q}_{ONB}$ is the time-average heat flux for ONB for the cases with the oscillating mass flux. A close inspection of the data given in Figures 5.24 – 5.35 further reveals that the T_w oscillation slightly lags the mass flux oscillation. Moreover for q substantially above $\bar{q}_{ONB}$, in the period of time at which the instantaneous mass flux is higher than the average level, the T_w is higher than the time-average level suggesting that the flow boiling heat transfer over the heated surface is poorer at a higher instantaneous G. But in the single-phase region the opposite is the case (Figures 5.30 – 5.35). The trend for the single-phase flow is apparently due to the better convection heat transfer for a higher mass flux. The somewhat unusual trend for the subcooled boiling flow requires more investigation into the associated bubble characteristics which will be examined later.

The measured temporal variations of the space average heated surface temperature for a higher inlet liquid subcooling of 10 ^{o}C are given in Figures 5.36 – 5.48. These results resemble that presented in Fugures 5.23 – 5.35 for $\triangle T_{sub}$ =5^{o}C except that at the higher inlet liquid subcooling T_w oscillates in a somewhat larger amplitude.

The corresponding time variations of the space-average subcooled flow boiling heat transfer coefficient affected by the coolant mass flux oscillation are shown in Fugures 5.49 – 5.60 for the inlet liquid subcooling of 5 ^{o}C. The results manifest that the flow boiling heat transfer coefficients also oscillate periodically in time and at the same frequency as the G oscillation. At a higher imposed heat flux and for the larger amplitude and longer period in the mass flux oscillation, the subcooled boiling heat transfer coefficients oscillate stronger. Besides in the period of time at which the mass flux is higher than the mean level, the boiling heat transfer coefficient is lower than

the time-average level. Note that at the higher inlet liquid subcoling of 10 ^{o}C the oscillation in the boiling heat transfer coefficient is stronger, as evident from the data shown in Figures 5.61 – 5.72. Moreover, the oscillation in $h_{2\phi}$ also lags slightly behind the mass flux oscillation.

In this transient oscillatory boiling flow the time variation of the coolant pressure at the inlet of the test section is also of interest in thermal-fluid design. These data are shown in Figures 5.73 - 5.96 for various cases. The results indicate that the inlet coolant pressure oscillates nearly in phase with the mass flux oscillation. Note that the inlet coolant pressure oscillation becomes more irregular for the cases with a longer period of the mass flux oscillation and a higher average mass flux. Besides, at the higher inlet liquid subcooling of 10^{o}C the oscillation in the inlet coolant pressure is stronger. Finally, the quantitative data evaluated from the above results are summarized in Tables 5.1 and 5.2 for the relative oscillation amplitudes of the space average heated surface temperature and boiling heat transfer coefficient $A_{T_w}/\Delta\bar{T}_{sat}$ and $A_{h2\varphi}/\bar{h}_{2\varphi}$ at various imposed heat fluxes and the amplitude and period of the coolant mass flux oscillation.

5.3 Transient Bubble Characteristics in Subcooled Flow Boiling

To elucidate the transient FC-72 subcooled flow boiling heat transfer characteristics affected by the mass flux oscillation, the data for the bubble characteristics obtained from the present flow visualization are examined in the following. The top views of the boiling flow in a small region around the geometric center of the heated surface for various coolant mass fluxes and imposed heat fluxes are shown in Figs. 5.97 – 5.146 for the transient subcooled flow boiling. In the flow visualization we note that as the wall superheat exceeds that for the boiling incipience, the vapor bubbles

generated from the heated plate begin to appear. At first, the bubble characteristics for the limiting cases of constant mass fluxes are illustrated by the photos in Figures 5.97 for $\triangle T_{sub}$ =5°C and 5.122 for $\triangle T_{sub}$ =10°C for the stable subcooled flow boiling. In the beginning, tiny bubbles are observed in the active nucleation sites. The tiny bubbles keep growing until their diameters reach to a certain size and they detach from the active nucleation sites immediately. Then they slide along the heating surface for some distance. The processes of bubble growth and departure are nearly regular and the bubbles are nearly spherical at low imposed heat flux. The formation, growth, and detachment processes of the bubbles on the heated copper plate obviously depend on the flow and thermal conditions and on the geometry of the cavities.

Next, the bubble characteristics in the transient flow boiling are illustrated by presenting the photos of the subcooled boiling flow at eight selected time instants in a typical periodic cycle in Figures 5.98 – 5.121 for $\triangle T_{sub}$ =5°C and in Figures 5.123 – 5.146 for $\triangle T_{sub}$ =10°C. In these figures the symbol " $t=t_o$ " signifies the time instant at which the instantaneous mass flux is at the mean level and starts to increase with time. The results indicate that for given imposed heat flux and inlet liquid subcooling and fixed mean level, amplitude and period of the mass flux oscillation the bubbles get smaller and become more dispersed in the period of time in which the instantaneous mass flux increases. The opposite processes take place when the instantaneous mass flux decreases with time. These changes of the bubble characteristics with the instantaneous mass flux become more significant for an increase in the amplitude of the mass flux oscillation (Figures 5.98 and 5.110 and Figures 5.99 and 5.111) and for a higher imposed heat flux. It is of interest to note that the mean level of the mass flux oscillation exhibits larger influences on the bubble characteristics in the transient flow boiling, as evident by comparing Figures 5.99 and 5.100. Besides, the bubble characteristics are only affected slightly by the period of the mass flux oscillation.

Finally, it should be mentioned that in the subcooled flow boiling with $\triangle T_{sub}$ =5°C and 10°C the bubble coalescence is less significant than the saturated flow boiling.

To quantify the bubble characteristics, the measured data for the time variations of the space-average bubble departure diameter and frequency and active nucleation site density in a typical periodic cycle are shown in Figures 5.147 – 5.200 for various experimental parameters. The results in Figures 5.147 and 5.174 indicate that the mean size of the bubbles departing from the heated surface is somewhat smaller for the mass flux raised from 300 to 400 kg/m^{2}s in stable subcooled flow boiling. It reflects the fact that the coolant at a higher mass flux and hence at a higher speed tends to sweep the bubbles more quickly away from the heating surface. Now as the coolant mass flux oscillates, the bubble departure diameter varies significantly with time (Figures 5.147(b) - (c) and 5.174(b) - (c)). More specifically, the size of the departing bubbles decreases in the first and fourth quarters of the periodic cycle in which the instantaneous mass flux increases with time. While in the second and third quarters of the cycle an opposite process is noted since the instantaneous mass flux decreases with time. Besides, at a higher imposed heat flux the departing bubbles are larger. Similar trend is noted in Figures 5.148 – 5.150 and 5.175 – 5.177. Comparing the results in Figure 5.147 with Figure 5.148 and Figure 5.149 with Figure 5.150 indicates that at the larger amplitude of the mass flux oscillation the effects of the imposed heat flux on the bubble departure diameter are slightly smaller. Figures 5.151 – 5.154 and 5.178 – 5.181 indicate that the bubble departure diameters are only affected slightly by the period of the mass flux oscillation. At the small amplitude of the mass flux oscillation of 5% the bubble departure diameters are slightly larger than that at the large amplitude of the mass flux oscillation of 10% (Figures 5.155 and 5.182).

Next, the data for the variations of the space-average bubble departure frequency

with time for various cases are shown in Figures 5.156 – 5.159 for $\triangle T_{sub}$ =5°C and Figures 5.183 – 5.186 for $\triangle T_{sub}$ =10°C. In the stable flow boiling the results in Figures 5.156(a) and 5.183(a) indicate that the increase in the bubble departure frequency with the imposed heat flux and coolant mass flux is clearly seen. The increase of f with G is ascribed again to the higher drag on the bubbles still attaching to the heated surface by the liquid coolant moving at a higher speed for a higher G. This, in turn, causes an earlier departure of the bubbles from the surface, resulting in a higher departure frequency. For an oscillation mass flux the bubbles depart from the heated surface at a slightly faster rate in the first and fourth quarters of the periodic cycle in which the coolant mass flux rises with time. Apparently, in the second and third quarters of the cycle in which G decreases with time the bubble departing rate reduces slightly. It is also observed that the mean bubble departure frequency increases noticeably with the imposed heat flux. It should be pointed out that the time variations of the bubble departure frequency are somewhat weaker than the bubble departure diameter. Figures 5.160 – 5.163 and 5.187 – 5.190 indicate that the bubble departure frequencies are only affected slightly by the period of the mass flux oscillation. At the large amplitude of the mass flux oscillation of 10% the bubble departure frequencies are slightly higher than that at the small amplitude of the mass flux oscillation of 5% (Figures 5.164 and 5.191).

Finally, the space-average active nucleation site density on the heated surface affected by the coolant mass flux oscillation is illustrated in Figures 5.165 – 5.168 for $\triangle T_{sub}$ =5°C and Figures 5.192 – 5.195 for $\triangle T_{sub}$ =10°C. The results Figures 5.165(a) and 5.192(a) indicate that in stable flow boiling the active nucleation site density increases substantially with the imposed heat flux. But the increase is also significant for the mass flux reduced from 400 to 300 kg/m^{2}s. Note that in transient flow boiling the active nucleation site density decreases with time in the first and fourth quarters of

the periodic cycle in which G increases. The reverse process appears in the second and third quarters of the cycle in which the coolant decelerates. At a higher amplitude of the mass flux oscillation the temporal variations of N_{ac} is stronger (Figures 5.166, 5.168, 5.193 and 5.195). The effects of the period of the mass flux oscillation are weaker. Figures 5.169 – 5.172 and 5.196 – 5.199 indicate that the active nucleation site density is only affected slightly by the period of the mass flux oscillation. At the large amplitude of the mass flux oscillation of 10% the active nucleation site densities are less than that at the small amplitude of the mass flux oscillation of 5% (Figures 5.173 and 5.200).

5.4 Correlation Equations

According to the present experimental data, empirical correlations for the space-average bubble departure diameter in FC-72 stable and transient subcooled flow boiling on the heated circular copper flat plate flush mounted on the bottom of the rectangular channel estimated from the present flow visualization are proposed as

$$\frac{d_p}{\sqrt{\sigma/g\cdot\Delta\rho}} = \frac{0.37\cdot(\rho_l/\rho_v)^{1.32}}{\overline{Re_D}^{0.2}\cdot[Ja' + \frac{0.6\cdot(\rho_l/\rho_v)^{0.9}}{\overline{Bo}^{0.3}\overline{Re_D}^{0.1}}]} \quad \text{for stable flow boiling} \tag{5.1}$$

where $\overline{Re_D}$ and $\overline{Bo}$ are the mean Reynolds and Boiling numbers respectively. They are defined as

$$\overline{Re_D} = \frac{\bar{G}\cdot D}{\mu_l} \tag{5.2}$$

$$\overline{Bo} = \frac{q''}{\bar{G}\cdot i_{lv}} \tag{5.3}$$

and

$$\frac{d_p}{\sqrt{\sigma/g\cdot\Delta\rho}} = \frac{0.37\cdot(\rho_l/\rho_v)^{1.29}}{Re_D^{0.2}\cdot[Ja' + \frac{0.6\cdot(\rho_l/\rho_v)^{0.9}}{Bo^{0.3}Re_D^{0.1}}]} \quad \text{for transient flow boiling} \tag{5.4}$$

where Re_D and Bo are respectively the instantaneous Reynolds and Boiling numbers. They are defined as

$$Re_D = \frac{G\cdot D}{\mu_l} \tag{5.5}$$

$$Bo = \frac{q''}{G \cdot i_{lv}} \tag{5.6}$$

Here Ja' is the modified Jacob number based on the coolant inlet subcooled temperature ΔT_{sub} which is defined as

$$Ja' = \frac{\rho_l \cdot c_{pl} \cdot \Delta T_{sub}}{\rho_v \cdot i_{lv}} \tag{5.7}$$

where $G(=\bar{G}+\Delta G)$ is the instantaneous coolant mass flux, $\bar{G}$ is the average coolant mass flux, ΔG is the amplitude of the mass flux oscillation, c_{pl} is the liquid specific heat, ρ_l is the liquid density, and D is the copper diameter. Figures 5.201 and 5.202 show that the present experimental data fall within ± 15 % and ± 20 % of the correlations given in Equations (5.1) and (5.4). In addition, empirical equations are provided to correlate the data for the space-average bubble departure frequency as

$$\frac{f \cdot d_p}{\mu_l/\rho_l \cdot D_h} = 0.65\overline{Re_D}^{1.4} \cdot Ja'^{-0.3} \cdot \overline{Bo}^{0.5} \quad \text{for stable flow boiling} \tag{5.8}$$

and

$$\frac{f \cdot d_p}{\mu_l/\rho_l \cdot D_h} = 0.63Re_D^{1.41} \cdot Ja'^{-0.3} \cdot Bo^{0.54} \quad \text{for transient flow boiling} \tag{5.9}$$

Figures 4.203 and 4.204 reveal that the present experimental data for $f \cdot d_p$ can be correlated with the deviation less than ± 25 % by the above two equations. Moreover, empirical correlations for the space-average active nucleation site density in the FC-72 subcooled flow boiling deduced from the present flow visualization are proposed as

$$N_{ac} \cdot d_p^{\,2} = -0.09+(80 \cdot \overline{Bo}^{0.8} \cdot \overline{Re_D}^{-0.15} \cdot Ja'^{-0.05}) \quad \text{for stable flow boiling} \tag{5.10}$$

and

$$N_{ac} \cdot d_p^{\,2} = -0.09+(68 \cdot Bo^{0.8} \cdot Re_D^{-0.15} \cdot Ja'^{-0.05}) \quad \text{for transient flow boiling} \tag{5.11}$$

The comparisons in Figs. 4.205 and 4.206 show that more than 80 % of the present experimental data fall within ± 30 % and ± 40 % of the correlation given in Equations (5.10) and (5.11). Finally, the total heat flux input to the stable boiling flow q_t is considered to be roughly composed of two parts: one resulting from the bubble

nucleation q_b and another due to the single phase forced convection q_c. Thus

$$q_t = q_b + q_c \tag{5.12}$$

Here q_b and q_c can be individually calculated from the quantitative data for the bubble characteristics examined in section 5.3 and single phase liquid forced convection as

$$q_b = \rho_v \cdot V_v \cdot f \cdot N_{ac} \cdot i_{lv} \tag{5.13}$$

where ρ_v is the vapor density, V_v is the vapor volume of the mean departing bubble defined as $\frac{4\pi}{3}(\frac{d_p}{2})^3$, f is the space-average bubble departure frequency, N_{ac} is the space-average active nucleation site density, i_{lv} is the enthalpy of vaporization, and

$$q_c = E \cdot \bar{h}_{1\phi} \cdot \Delta T_{sat} \tag{5.14}$$

where E is an enhancement factor added to account for the agitating motion of the bubbles which can enhance the single phase liquid convection heat transfer. From the experimental data, E can be empirically correlated as

$$E = 4.5 \cdot N_{conf}{}^{0.5} \cdot \overline{Fr_l}^{0.15} \cdot (1 + 280 \cdot \overline{Bo})^2 \quad \text{for stable flow boiling} \tag{5.15}$$

Here $\overline{Fr_l}$ is the Froude number and N_{conf} is the Confinement number. They are respectively defined as

$$N_{conf} = \frac{(\sigma / g \cdot \Delta\rho)^{0.5}}{D_h} \tag{5.16}$$

and

$$\overline{Fr_l} = \frac{\bar{G}^2}{\rho_l{}^2 \cdot g \cdot D_h} \tag{5.17}$$

where g is the acceleration due to gravity, D_h is the hydraulic diameter of the test section, and ΔT_{sat} (= T_w - T_{sat}) is the wall superheat. The results given in Figure 5.207 indicate that the present data can be correlated with the deviation less than ± 25% by the empirical correlation given in Equations (5.12) - (5.17).

Table 5.1 Relative amplitudes of heated surface temperature and heat transfer coefficient oscillations in transient oscillatory subcooled flow boiling at ΔT_{sub} = 5°C for various imposed heat fluxes and the amplitudes and periods of the coolant mass flux oscillation.

$\Delta G/\bar{G}$	t_p (sec)	$\bar{G}$ =300 kg/m^{2}s			$\bar{G}$ =400 kg/m^{2}s		
		q(W/cm^2)	$A_{T_w}/\Delta\bar{T}_{sat}$	$A_{h_{2\phi}}/\bar{h}_{2\phi}$	q(W/cm^2)	$A_{T_w}/\Delta\bar{T}_{sat}$	$A_{h_{2\phi}}/\bar{h}_{2\phi}$
±5%	10	4.98	0.0147	0.0114	5.55	0.0158	0.0123
		6.16	0.0162	0.0128	6.78	0.0160	0.0126
		8.19	0.0144	0.0116	8.17	0.0183	0.0147
		9.69	0.0145	0.0119	9.67	0.0159	0.0130
	20	4.96	0.0208	0.0160	5.46	0.0291	0.0226
		6.10	0.0188	0.0150	6.72	0.0267	0.0211
		8.17	0.0192	0.0155	8.11	0.0284	0.0229
		9.67	0.0213	0.0173	9.62	0.0286	0.0234
	30	4.95	0.0177	0.0137	5.48	0.0304	0.0235
		6.12	0.0193	0.0151	6.71	0.0306	0.0242
		8.15	0.0206	0.0165	8.10	0.0293	0.0236
		9.65	0.0225	0.0183	9.62	0.0272	0.0222
±10%	10	5.50	0.0280	0.0219	5.50	0.0287	0.0224
		6.78	0.0283	0.0226	6.73	0.0327	0.0260
		8.14	0.0309	0.0250	8.12	0.0360	0.0292
		9.64	0.0289	0.0237	9.63	0.0347	0.0285
	20	5.45	0.0329	0.0256	5.02	0.0297	0.0230
		6.70	0.0351	0.0279	6.78	0.0430	0.0313
		8.10	0.0358	0.0289	8.19	0.0432	0.0352
		9.61	0.0346	0.0284	9.70	0.0443	0.0366
	30	5.48	0.0338	0.0264	4.88	0.0375	0.0292
		6.72	0.0384	0.0305	6.72	0.0459	0.0368
		8.11	0.0378	0.0306	8.12	0.0476	0.0389
		9.62	0.0378	0.0309	9.63	0.0516	0.0426

Table 5.2 Relative amplitudes of heated surface temperature and heat transfer coefficient oscillations in transient oscillatory subcooled flow boiling at $\Delta T_{sub} = 10^{o}C$ for various imposed heat fluxes and the amplitudes and periods of the coolant mass flux oscillation.

$\Delta G/\bar{G}$	t_p (sec)	$\bar{G}$ =300 kg/m^{2}s			$\bar{G}$ =400 kg/m^{2}s		
		q(W/cm^2)	$A_{T_w}/\Delta\bar{T}_{sat}$	$A_{h_{2\varphi}}/\bar{h}_{2\varphi}$	q(W/cm^2)	$A_{T_w}/\Delta\bar{T}_{sat}$	$A_{h_{2\varphi}}/\bar{h}_{2\varphi}$
±5%	10	5.48	0.0221	0.0139	6.13	0.0157	0.0090
		6.72	0.0243	0.0158	7.39	0.0275	0.0151
		8.12	0.0244	0.0165	8.81	0.0252	0.0170
		9.60	0.0250	0.0172	10.36	0.0246	0.0170
	20	5.54	0.0306	0.0193	6.04	0.0230	0.0147
		6.67	0.0280	0.0183	7.35	0.0259	0.0170
		8.05	0.0306	0.0206	8.78	0.0285	0.0194
		9.56	0.0307	0.0211	10.37	0.0277	0.0192
	30	5.98	0.0329	0.0209	5.96	0.0259	0.0167
		7.29	0.0300	0.0197	7.28	0.0284	0.0191
		8.74	0.0297	0.0202	8.73	262	0.0179
		10.32	0.0265	0.0184	10.30	0.0288	0.0200
±10%	10	5.50	0.0389	0.0244	5.58	0.0247	0.0154
		6.69	0.0415	0.0270	6.82	0.0356	0.0231
		8.10	0.0445	0.0299	8.22	0.0397	0.0266
		9.61	0.0470	0.0320	9.75	0.0404	0.0277
	20	5.49	0.0543	0.0339	5.47	0.0220	0.0136
		6.67	0.0613	0.0397	6.70	0.0462	0.0296
		8.06	0.0612	0.0407	8.08	0.0529	0.0353
		9.56	0.0584	0.0400	9.58	0.0584	0.0402
	30	5.47	0.0609	0.0382	5.44	0.0249	0.0154
		6.67	0.0656	0.0426	6.72	0.0551	0.0356
		8.05	0.0676	0.0452	8.07	0.0527	0.0350
		9.55	0.0624	0.0429	9.61	0.0565	0.0387

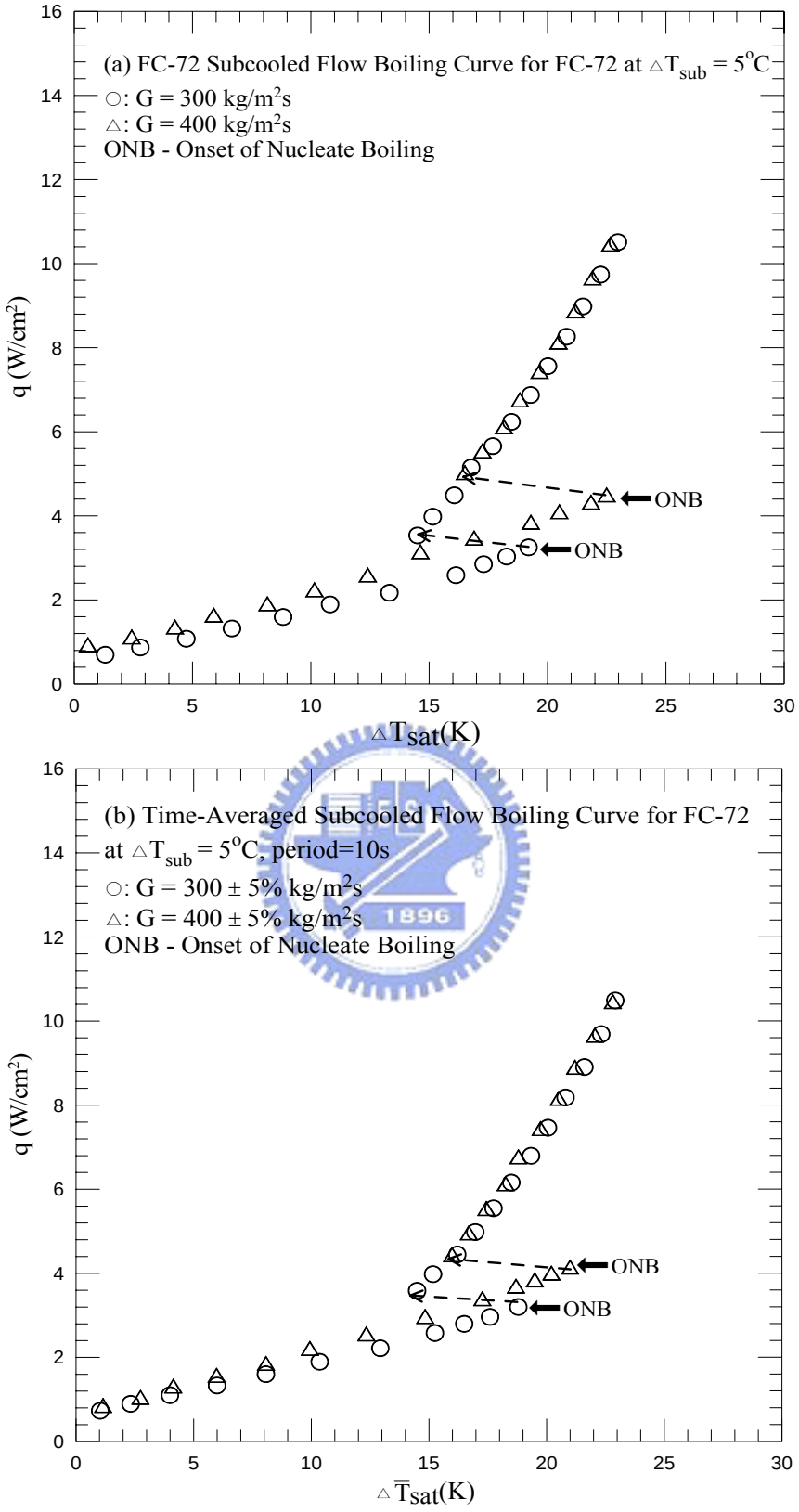

Fig. 5.1 Time-average flow boiling curves for various coolant mass fluxes for stable subcooled flow boiling (a) and transient subcooled flow boiling at $\triangle T_{sub}$ =5°C for t_p=10 sec (b), 20 sec (c) and 30 sec (d).

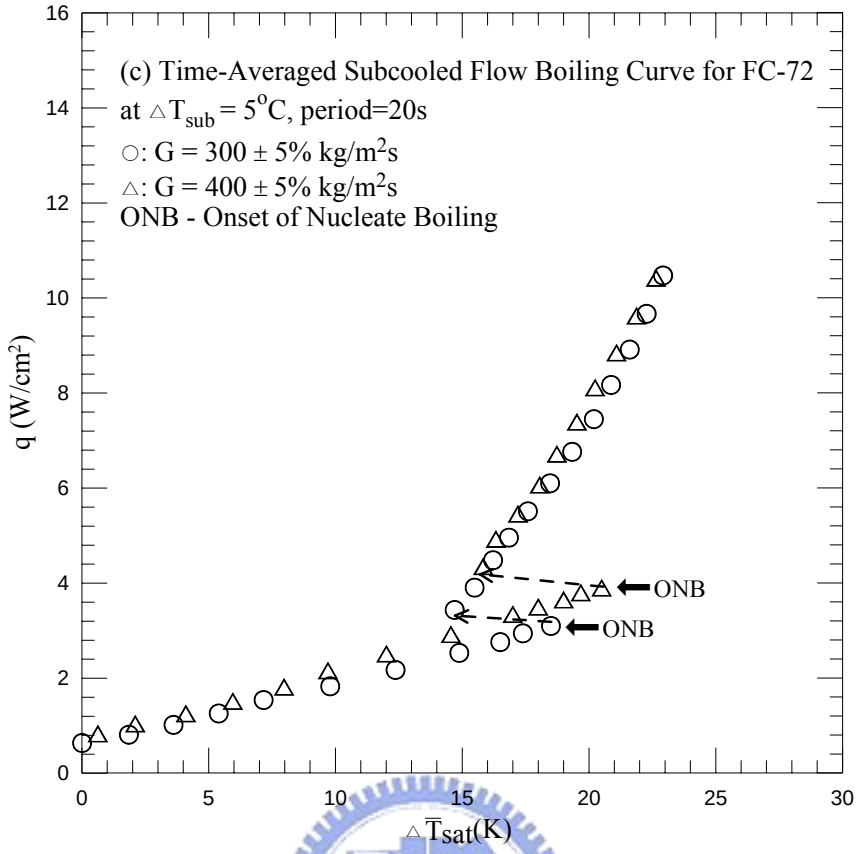

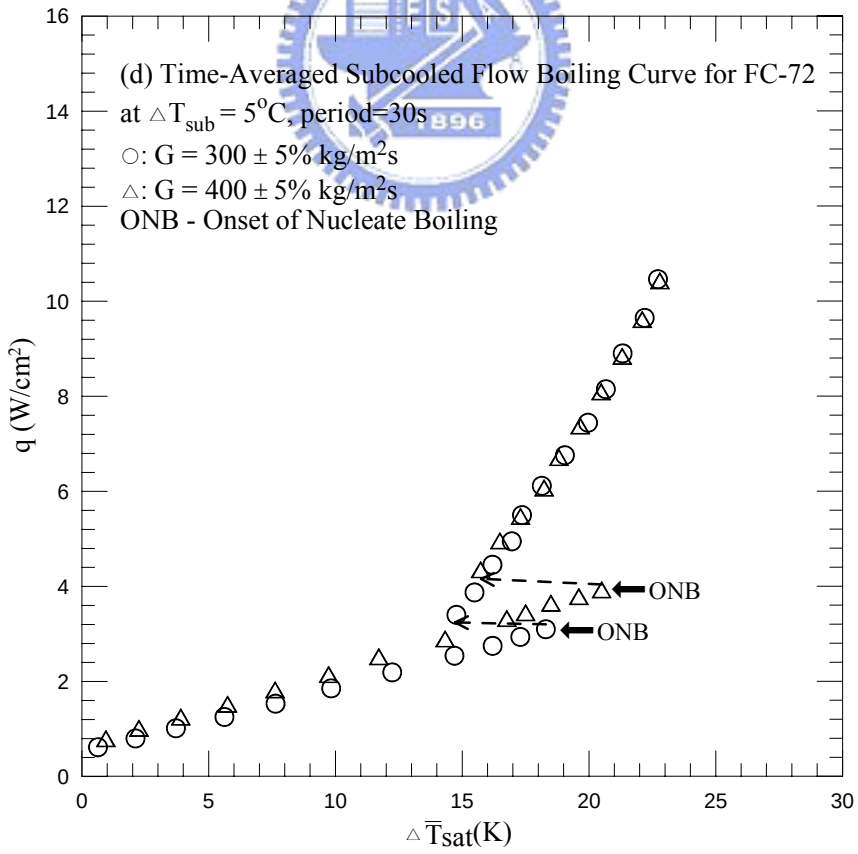

Fig. 5.1 Continued.

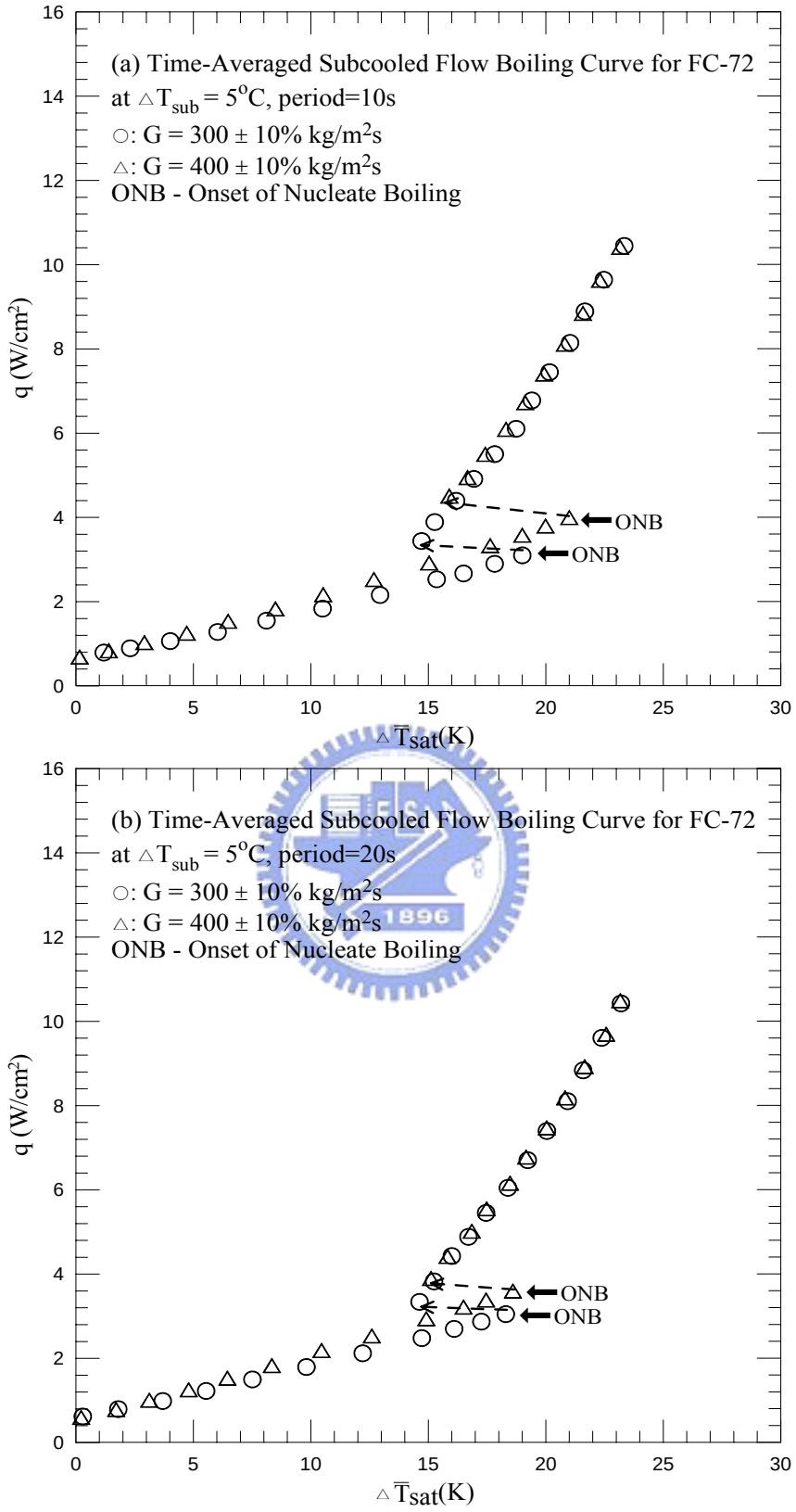

Fig. 5.2 Time-average flow boiling curves for various coolant mass fluxes for transient subcooled flow boiling at $\triangle T_{sub}$ =5°C for t_p=10 sec (a), 20 sec (b) and 30 sec (c).

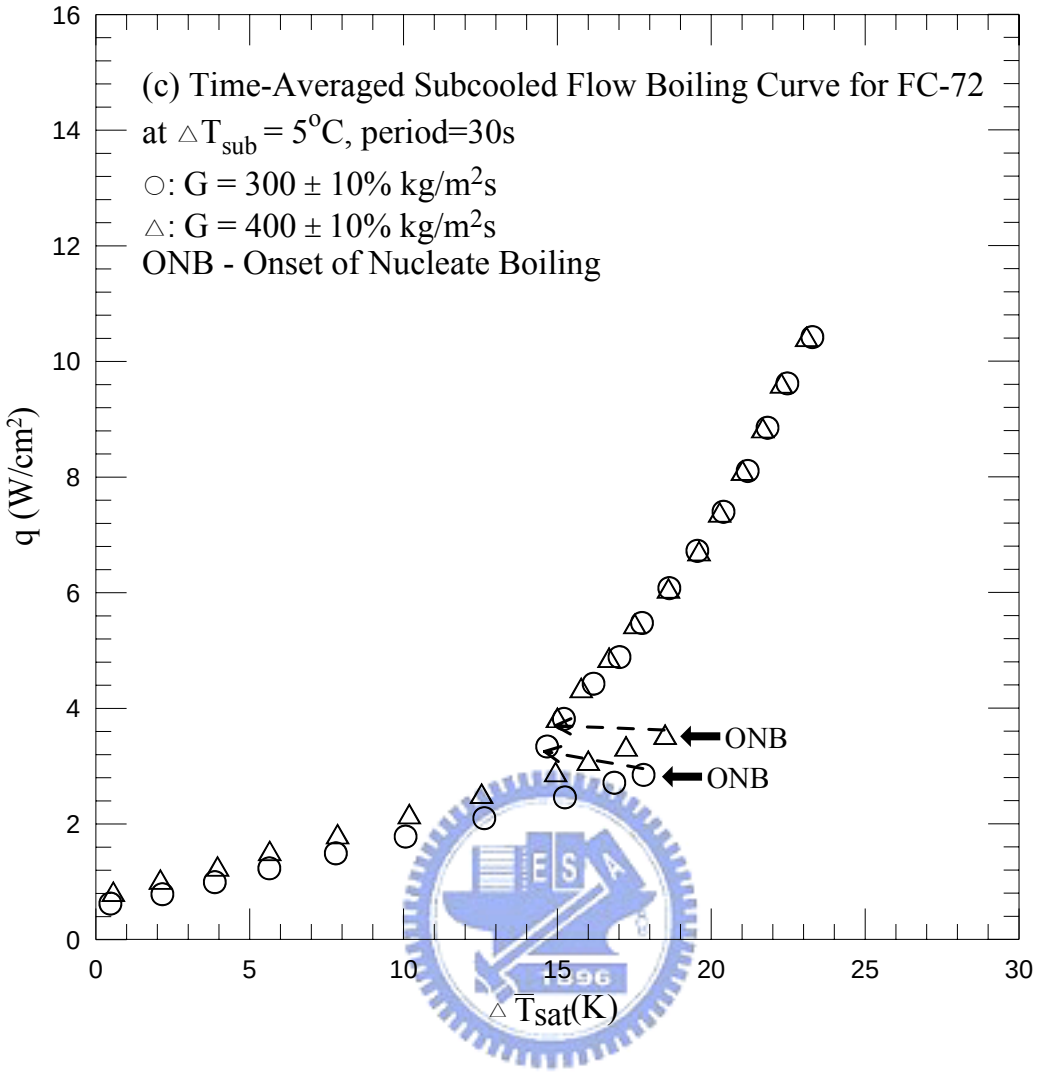

Fig. 5.2 Continued.

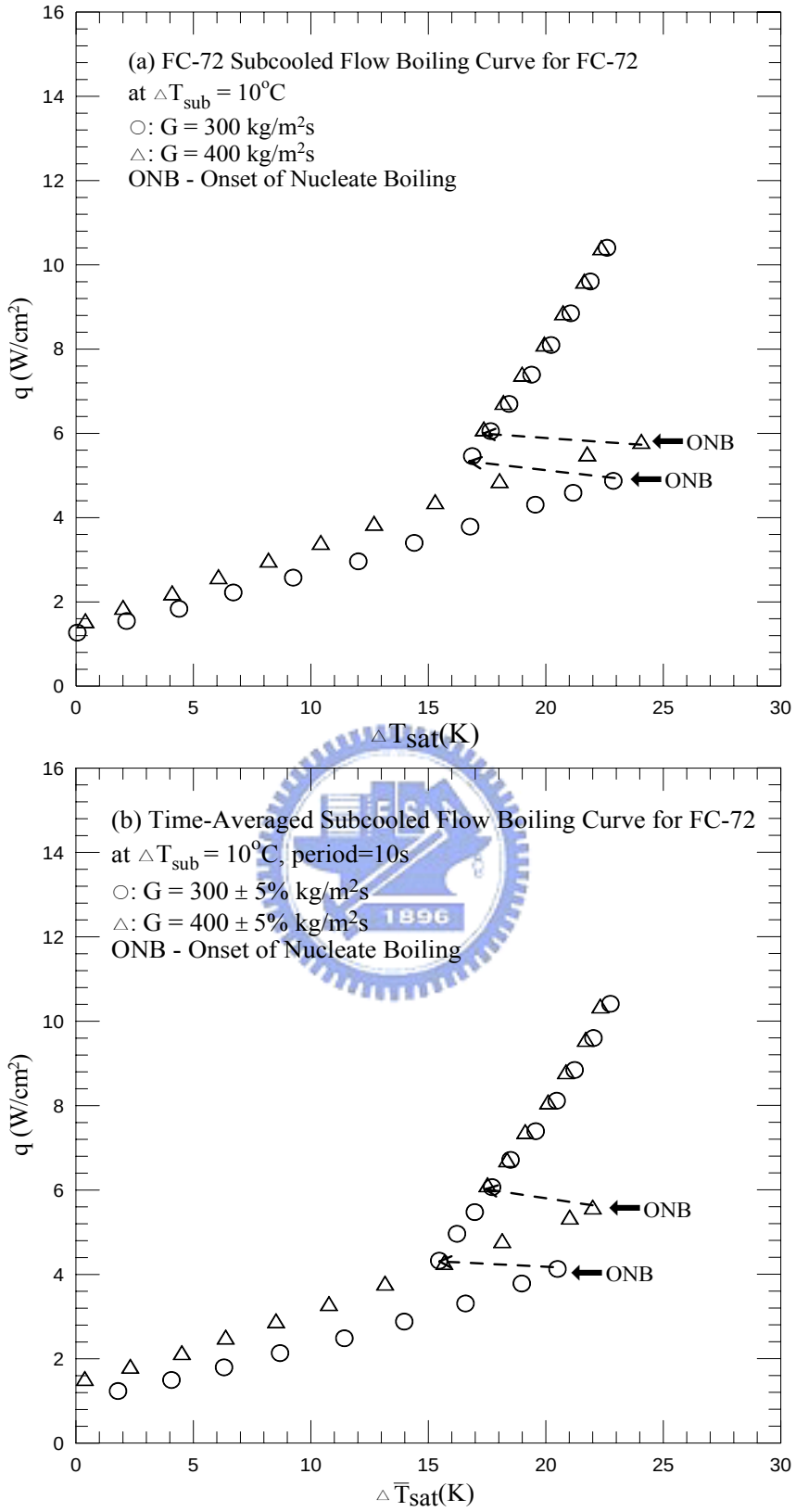

Fig. 5.3 Time-average flow boiling curves for various coolant mass fluxes for stable subcooled flow boiling (a) and transient subcooled flow boiling at $\triangle T_{sub}$ =10°C for t_p=10 sec (b), 20 sec (c) and 30 sec (d).

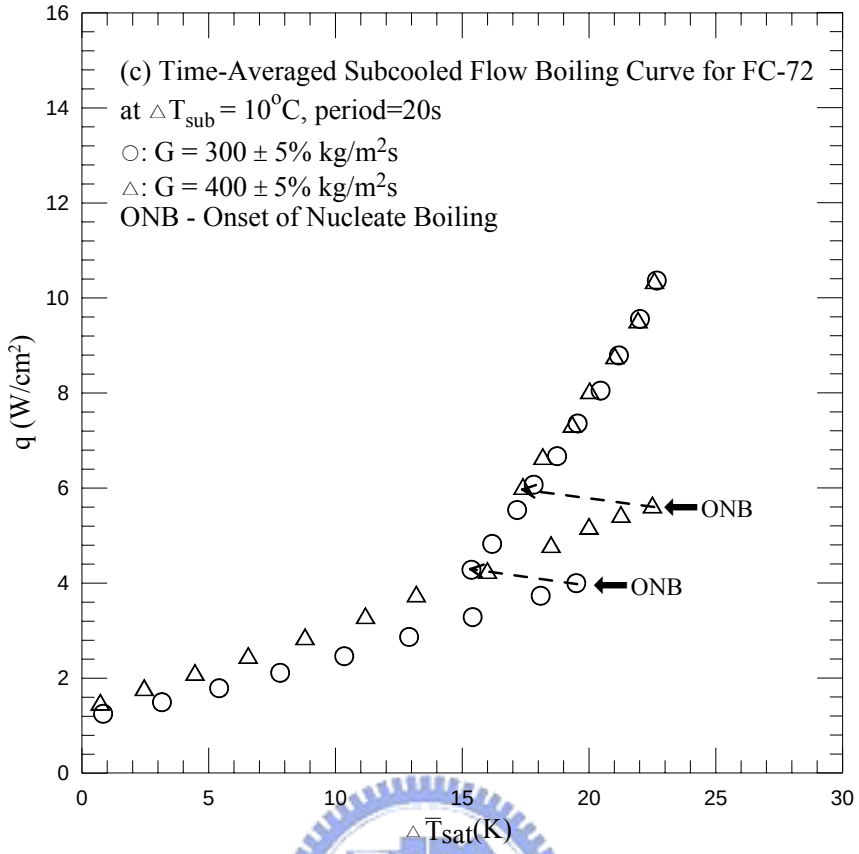

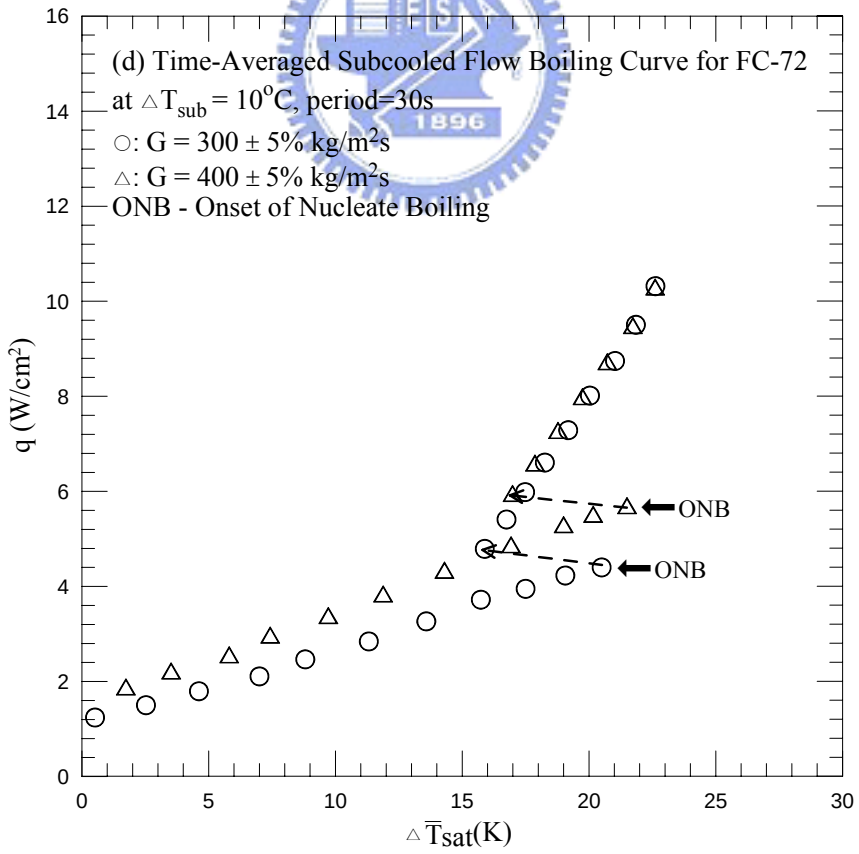

Fig. 5.3 Continued.

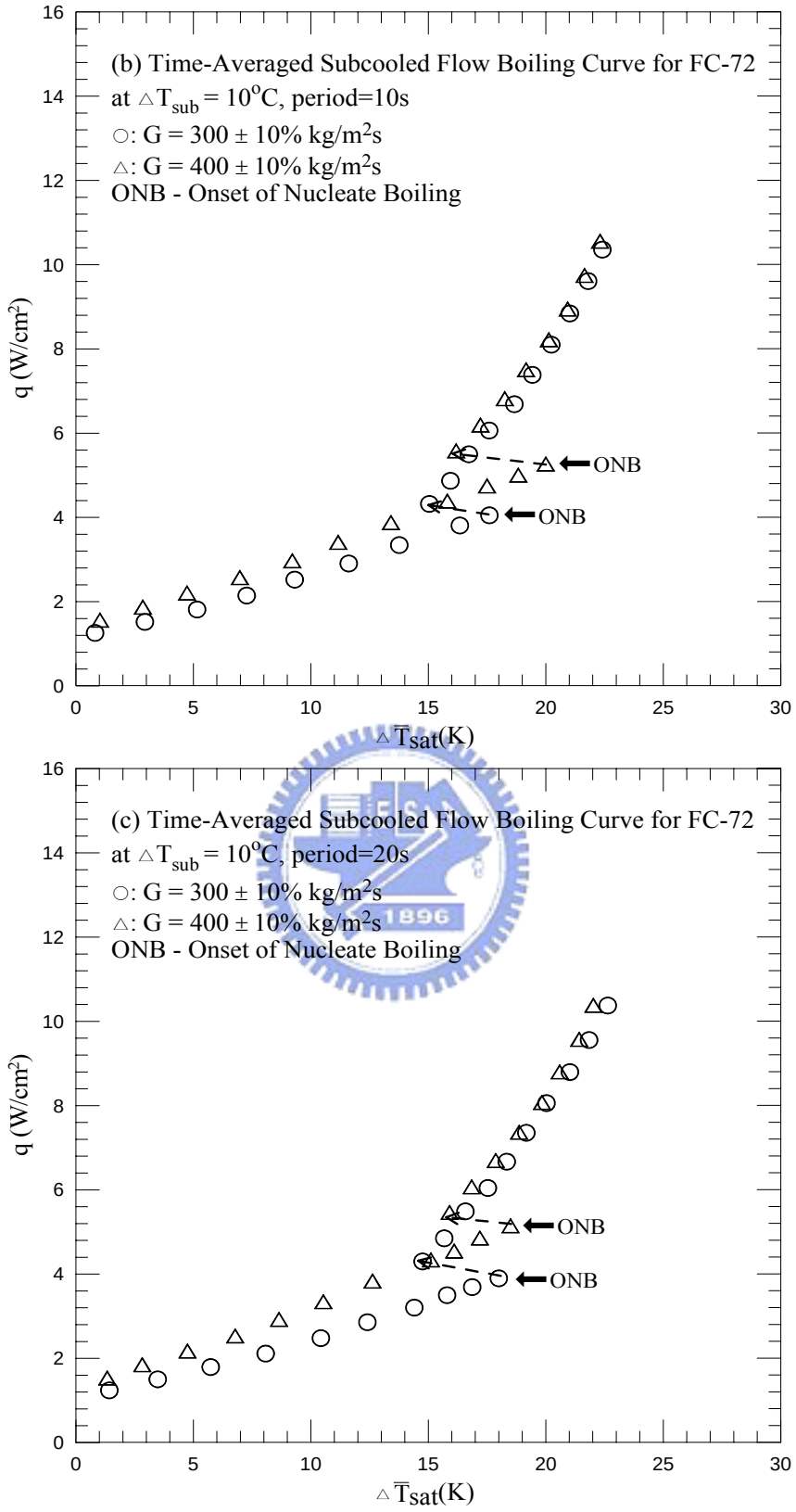

Fig. 5.4 Time-average flow boiling curves for various coolant mass fluxes for transient subcooled flow boiling at $\triangle T_{sub}$ =10°C for t_p=10 sec (a), 20 sec (b) and 30 sec (c).

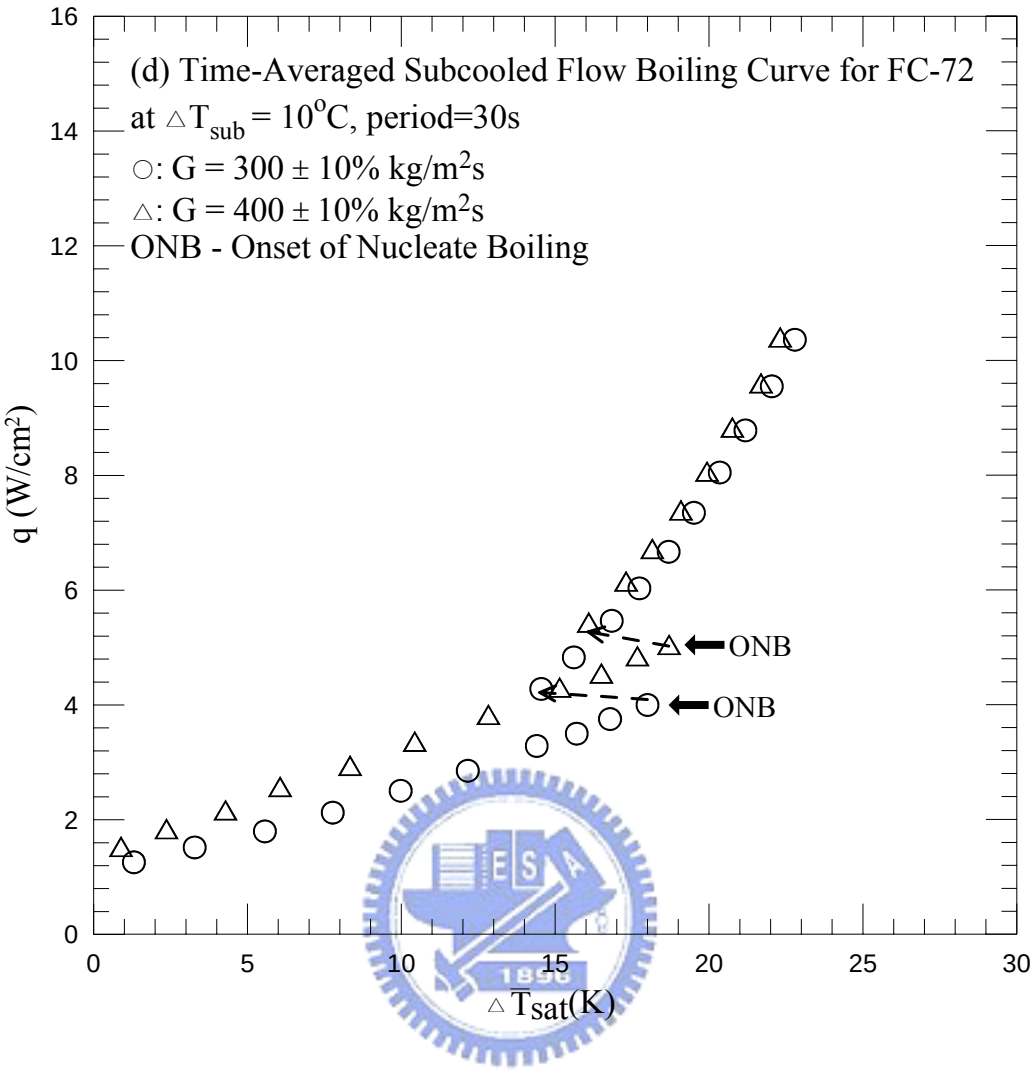

Fig. 5.4 Continued.

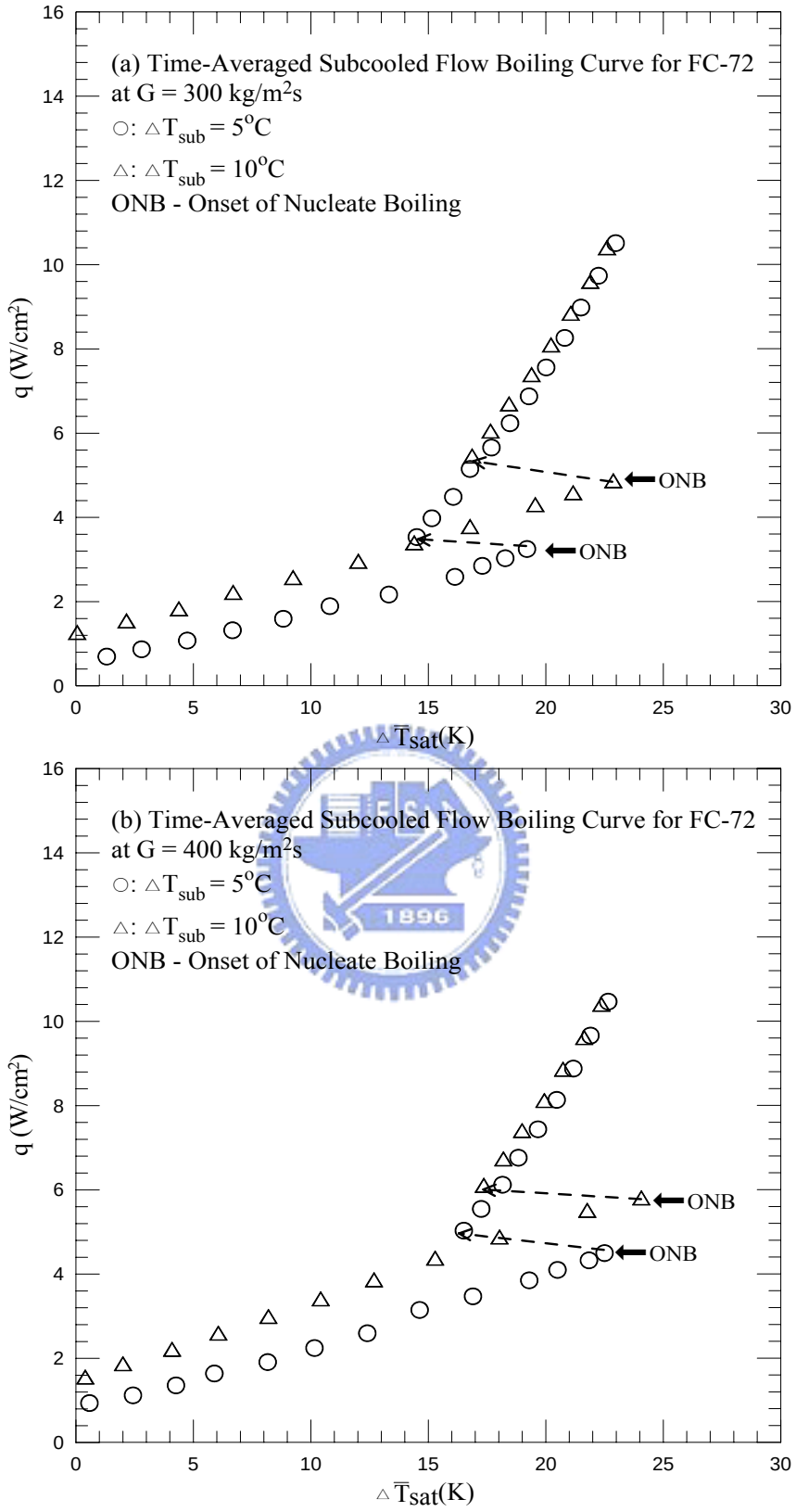

Fig. 5.5 Time-average flow boiling curves for various inlet subcoolings for stable subcooled flow boiling at (a) G=300 kg/m^{2}s and (b) G=400 kg/m^{2}s.

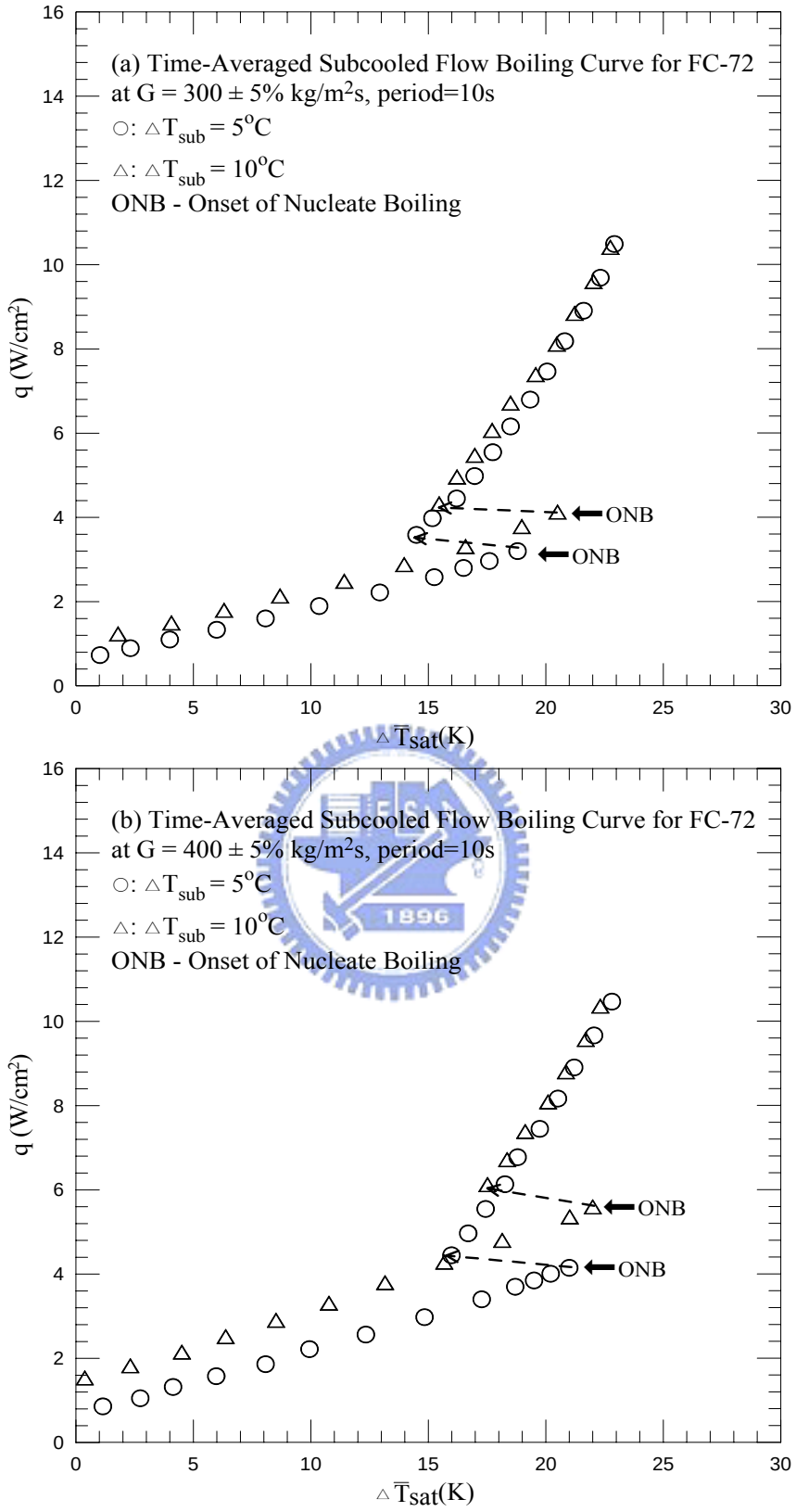

Fig. 5.6 Time-average flow boiling curves for various inlet subcoolings for transient subcooled flow boiling at (a) G=300±5% kg/m^{2}s and (b) G=400±5% kg/m^{2}s at t_p=10 sec.

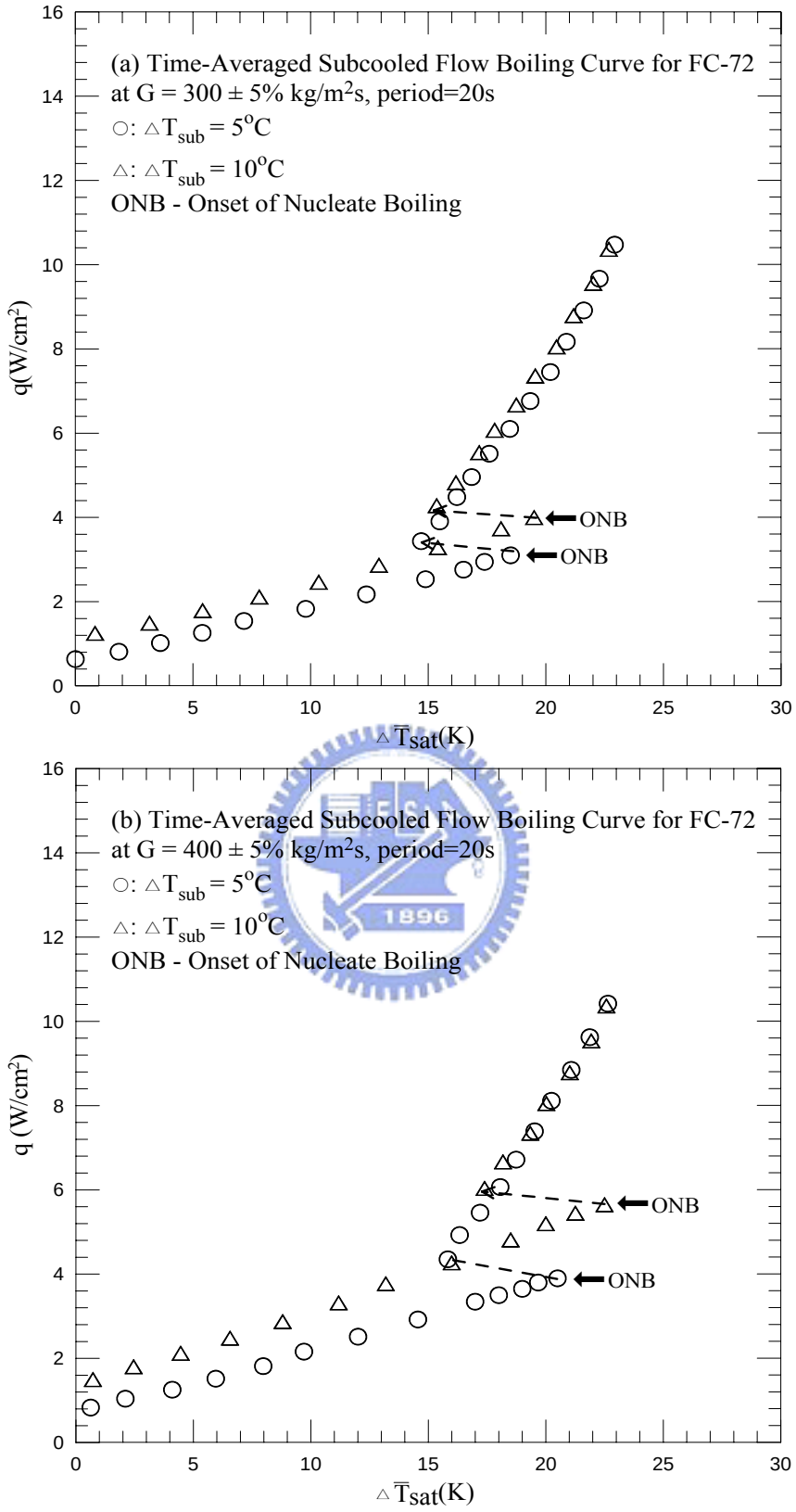

Fig. 5.7 Time-average flow boiling curves for various inlet subcoolings for transient subcooled flow boiling at (a) G=300±5% kg/m^{2}s and (b) G=400±5% kg/m^{2}s at t_p=20 sec.

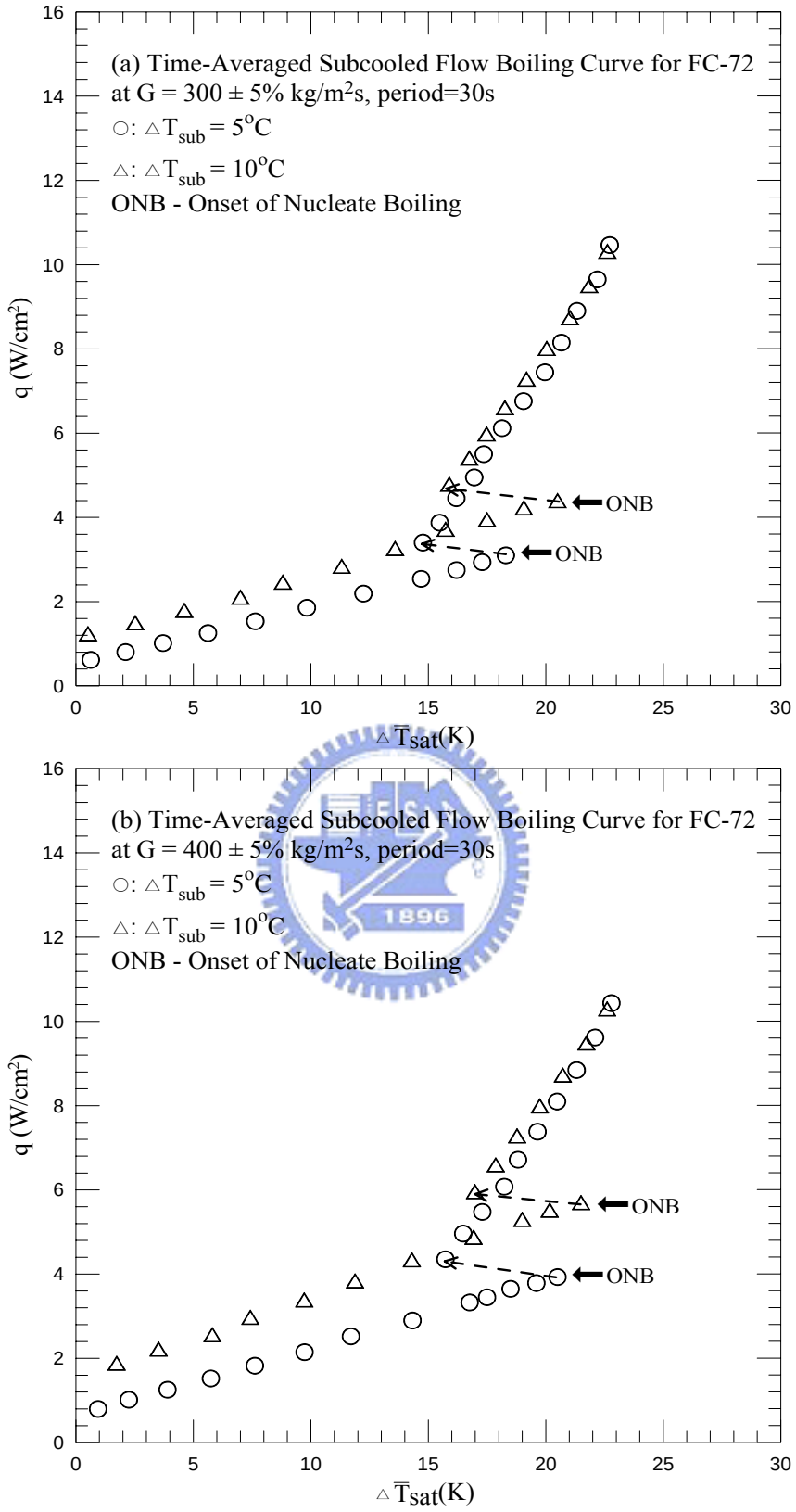

Fig. 5.8 Time-average flow boiling curves for various inlet subcoolings for transient subcooled flow boiling at (a) G=300±5% kg/m^{2}s and (b) G=400±5% kg/m^{2}s at t_p=30 sec.

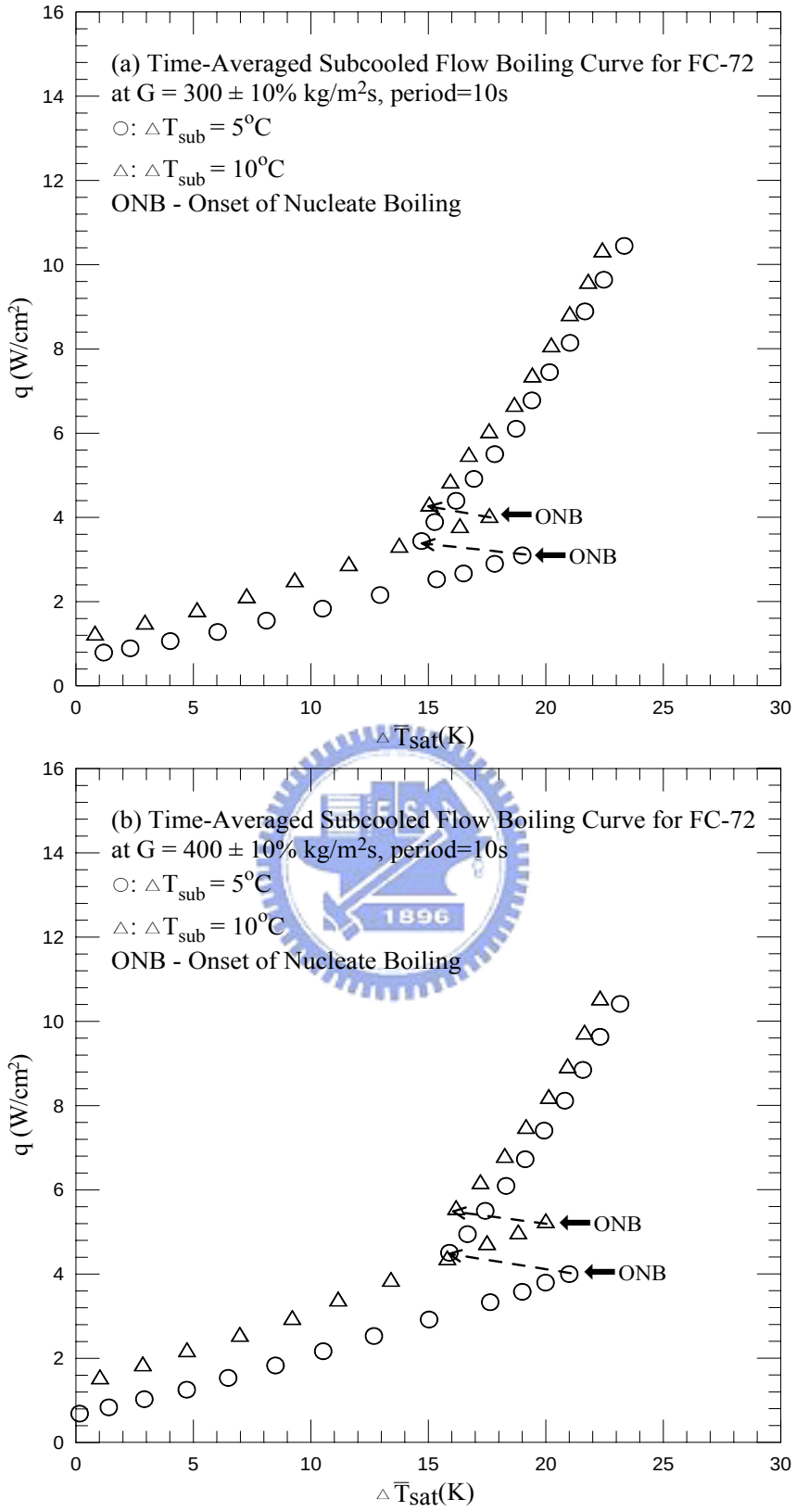

Fig. 5.9 Time-average flow boiling curves for various inlet subcoolings for transient subcooled flow boiling at (a) G=300±10% kg/m^{2}s and (b) G=400±10% kg/m^{2}s at t_p=10 sec.

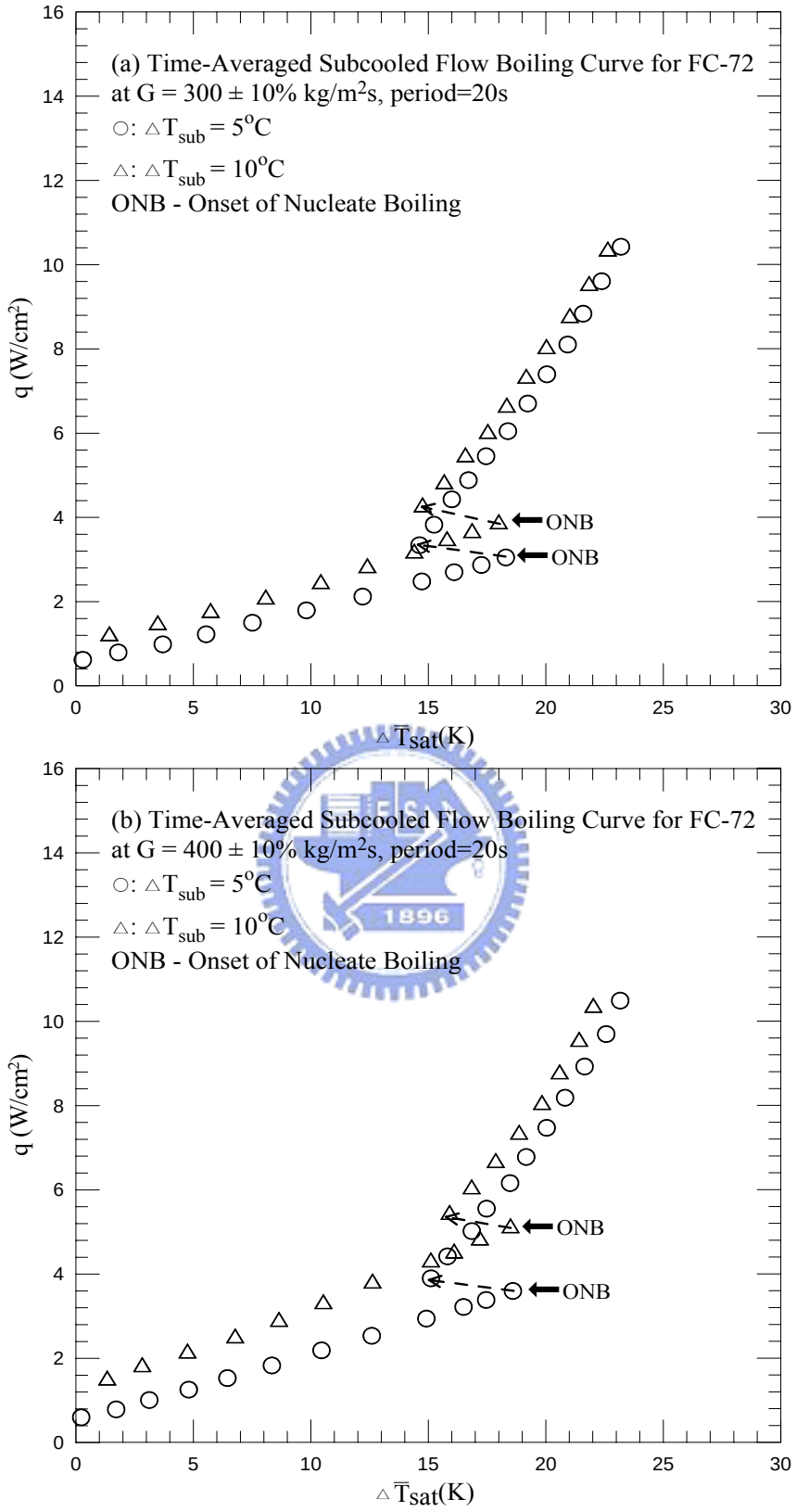

Fig. 5.10 Time-average flow boiling curves for various inlet subcoolings for transient subcooled flow boiling at (a) G=300±10% kg/m^{2}s and (b) G=400±10% kg/m^{2}s at t_p=20 sec.

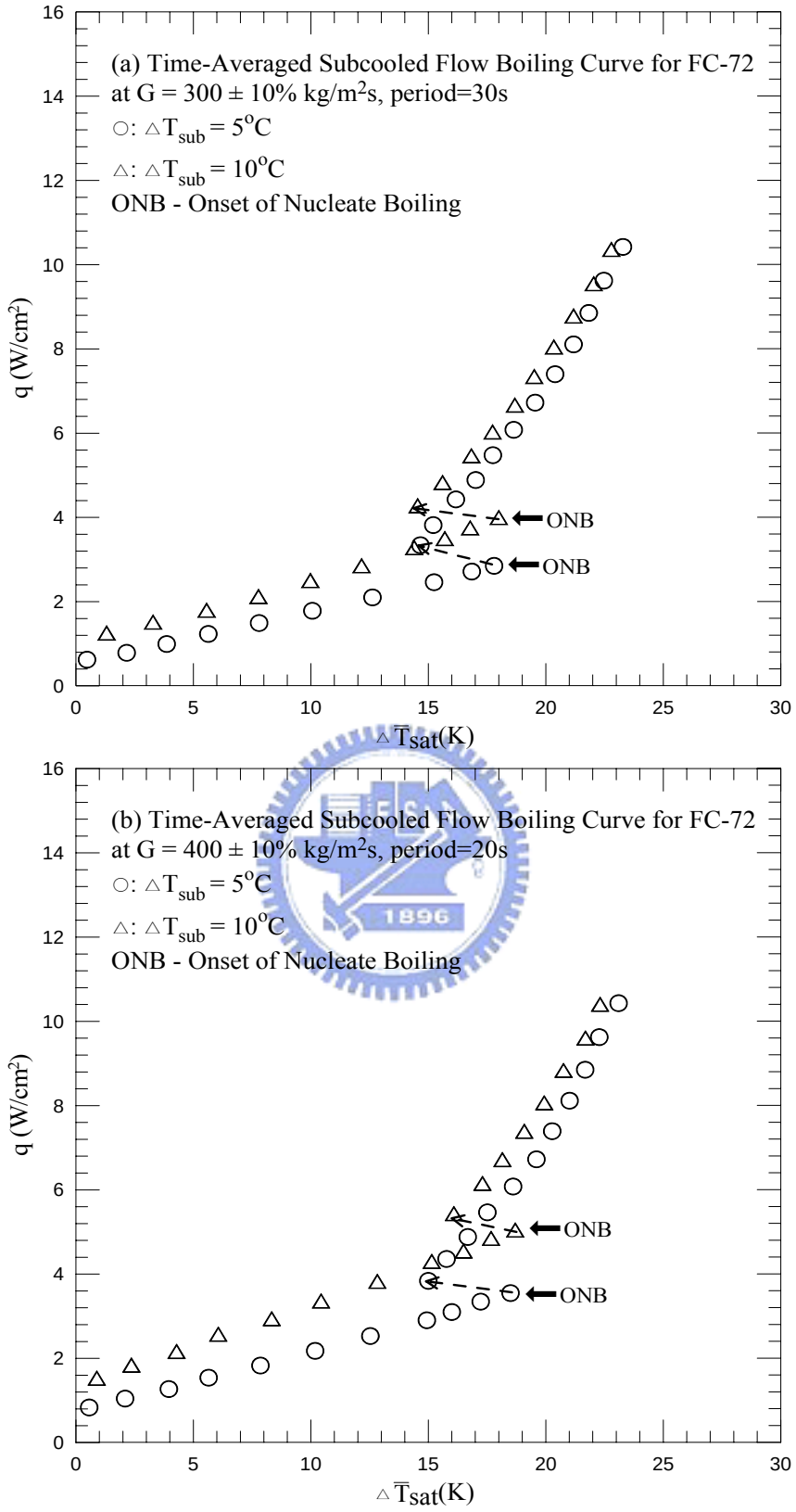

Fig. 5.11 Time-average flow boiling curves for various inlet subcoolings for transient subcooled flow boiling at (a) G=300±10% kg/m^{2}s and (b) G=400±10% kg/m^{2}s at t_p=30 sec.

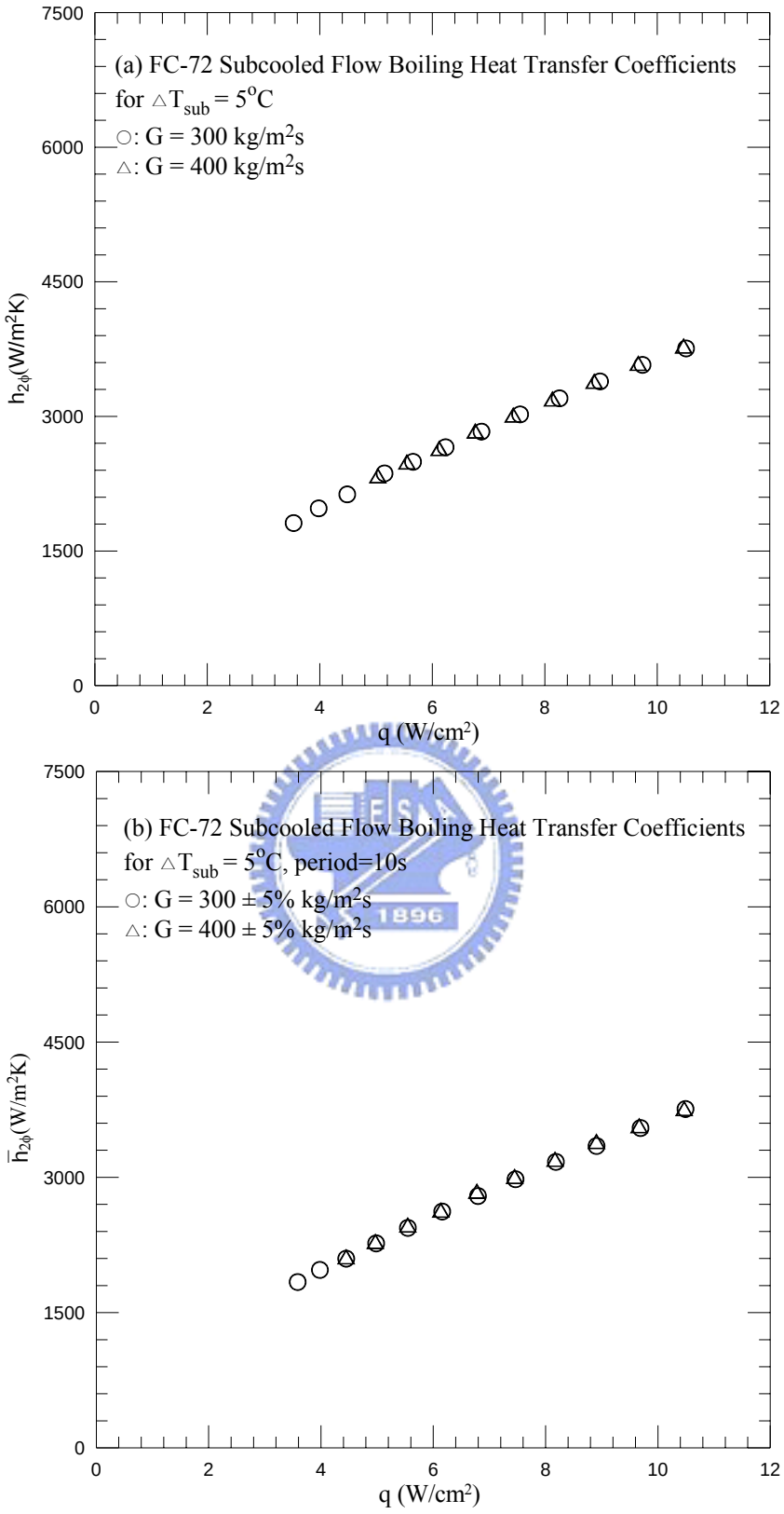

Fig. 5.12 Time-average flow boiling heat transfer coefficients for various coolant mass fluxes for stable subcooled flow boiling (a) and transient subcooled flow boiling at ΔT_{sub} =5°C for t_p=10 sec (b), 20 sec (c) and 30 sec (d).

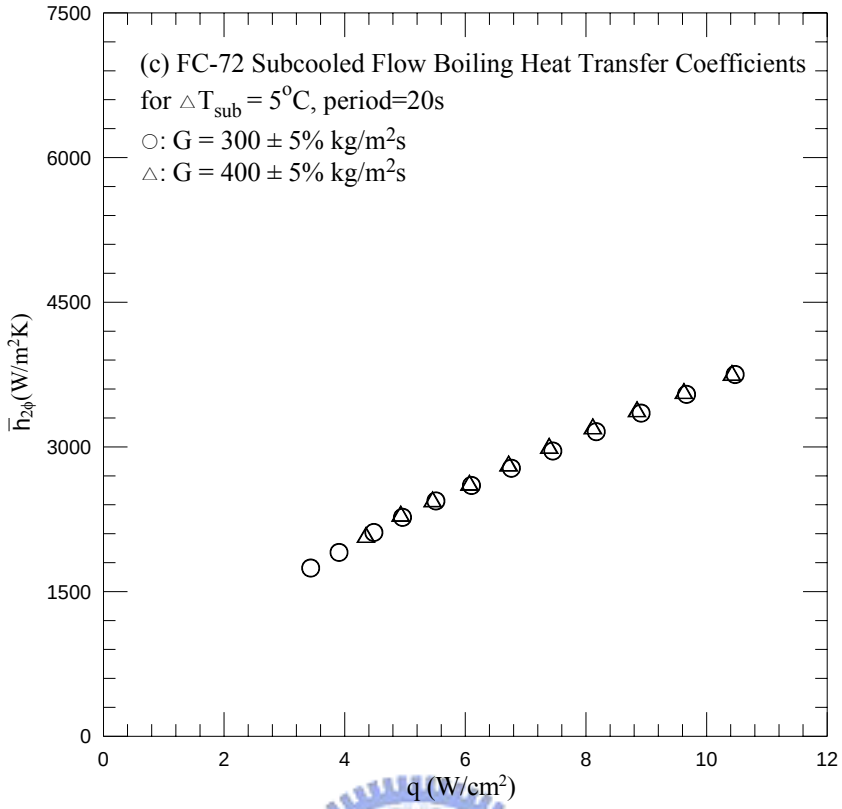

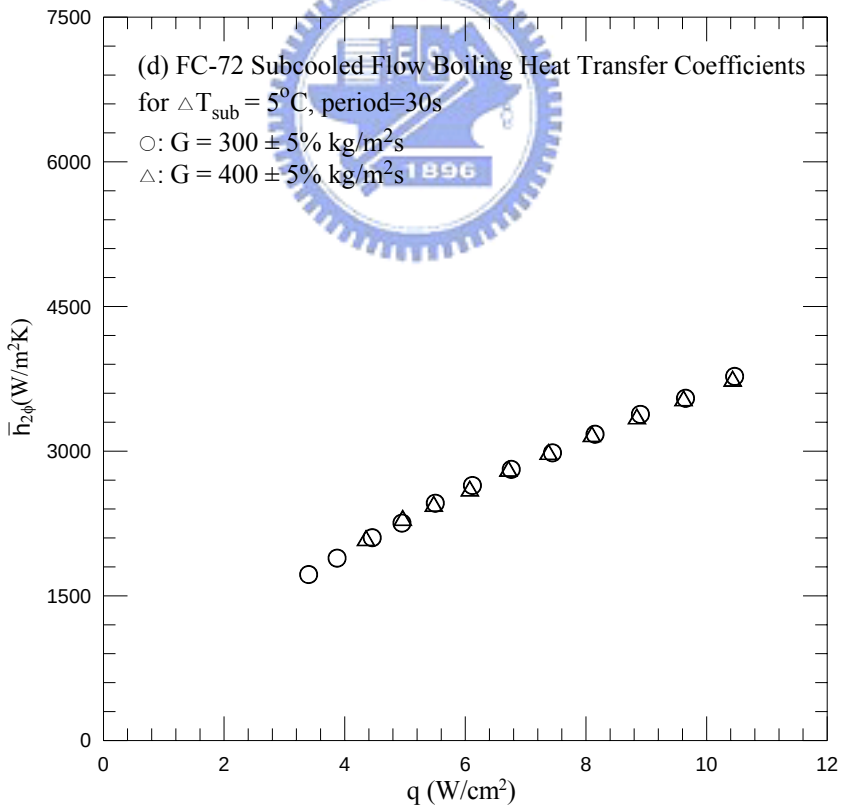

Fig. 5.12 Continued.

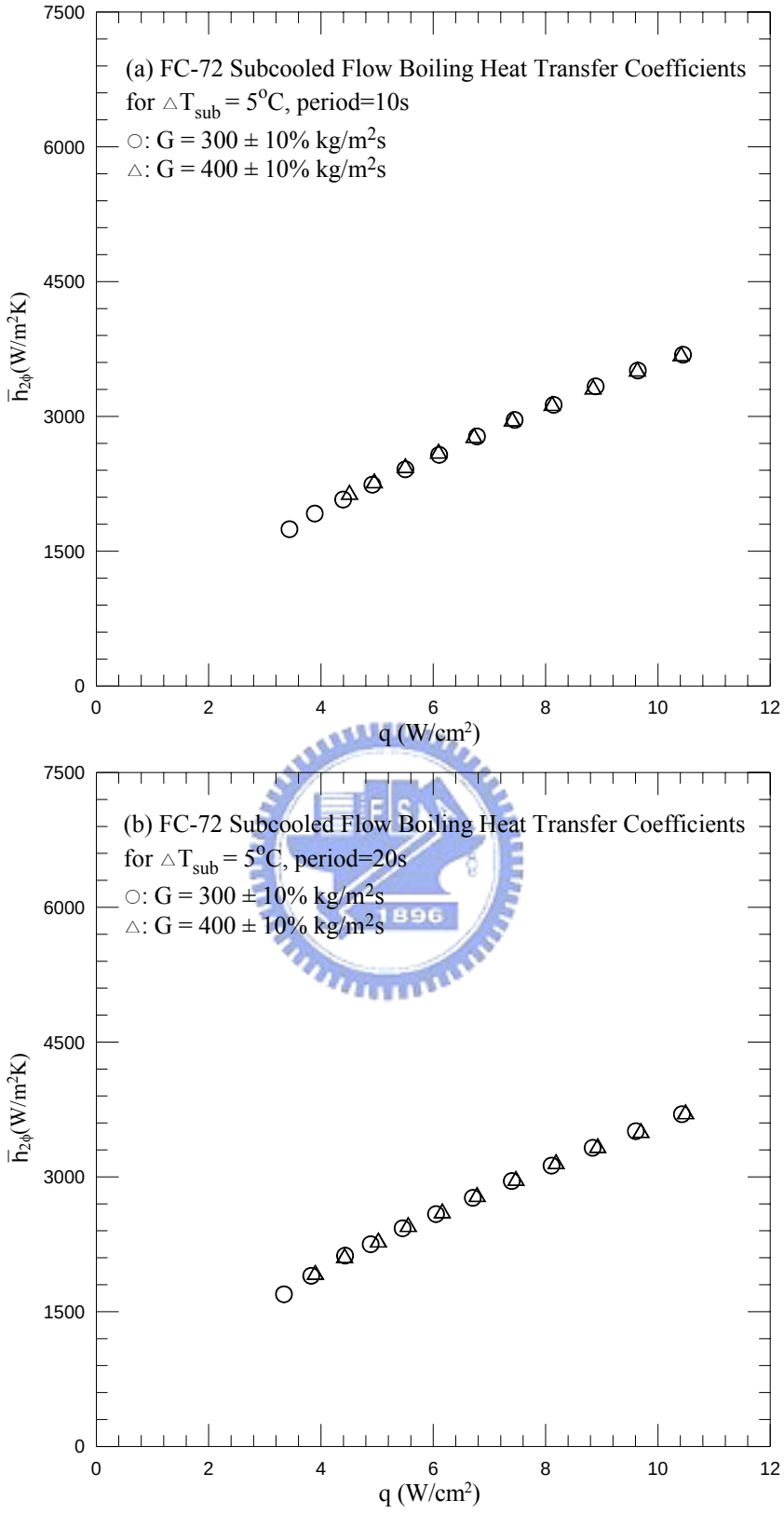

Fig. 5.13 Time-average flow boiling heat transfer coefficients for various coolant mass fluxes for transient subcooled flow boiling at ΔT_{sub} =5°C for t_p=10 sec (a), 20 sec (b) and 30 sec (c).

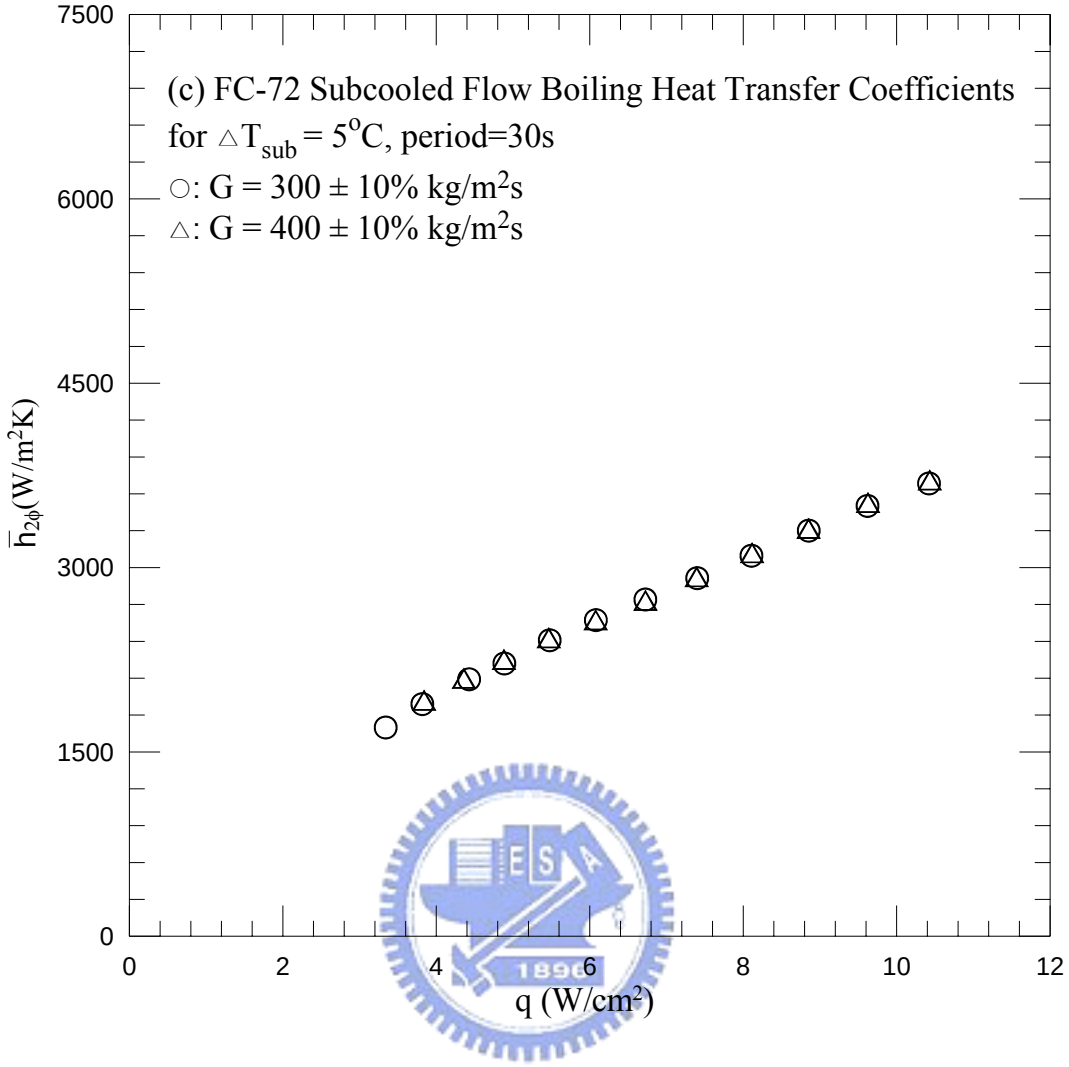

Fig. 5.13 Continued.

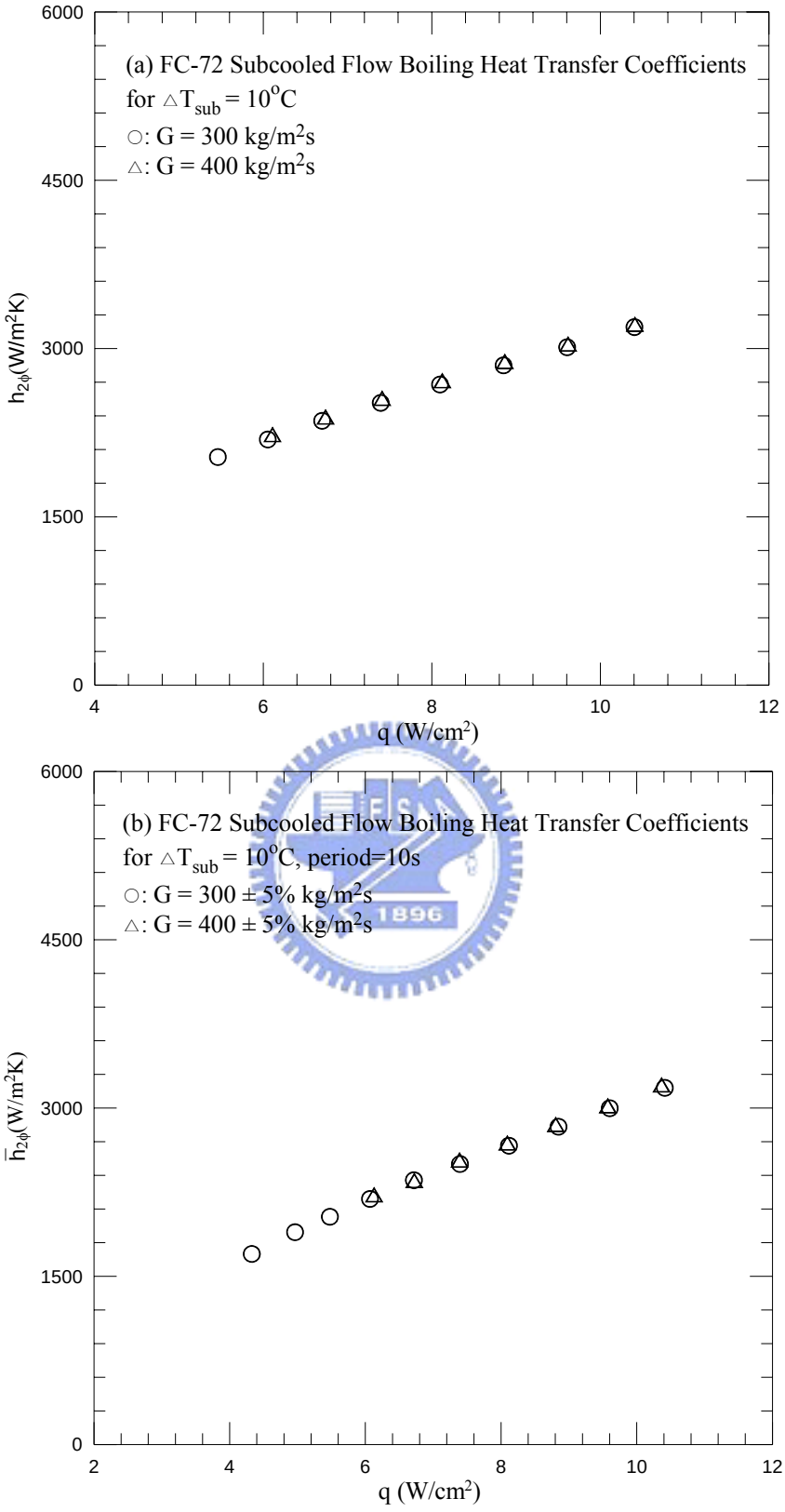

Fig. 5.14 Time-average flow boiling heat transfer coefficients for various coolant mass fluxes for stable subcooled flow boiling (a) and transient subcooled flow boiling at ΔT_{sub} =10°C for t_p=10 sec (b), 20 sec (c) and 30 sec (d).

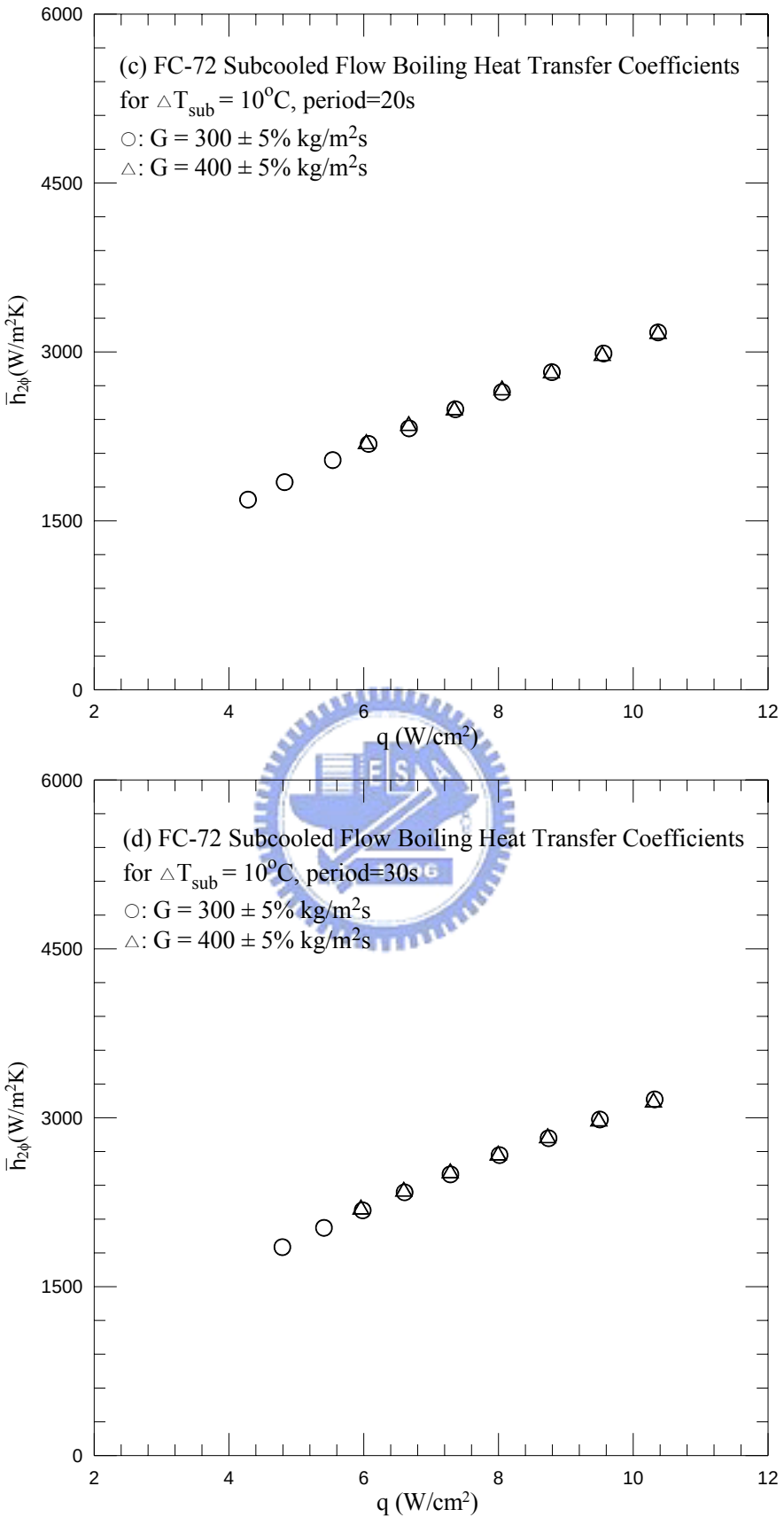

Fig. 5.14 Continued.

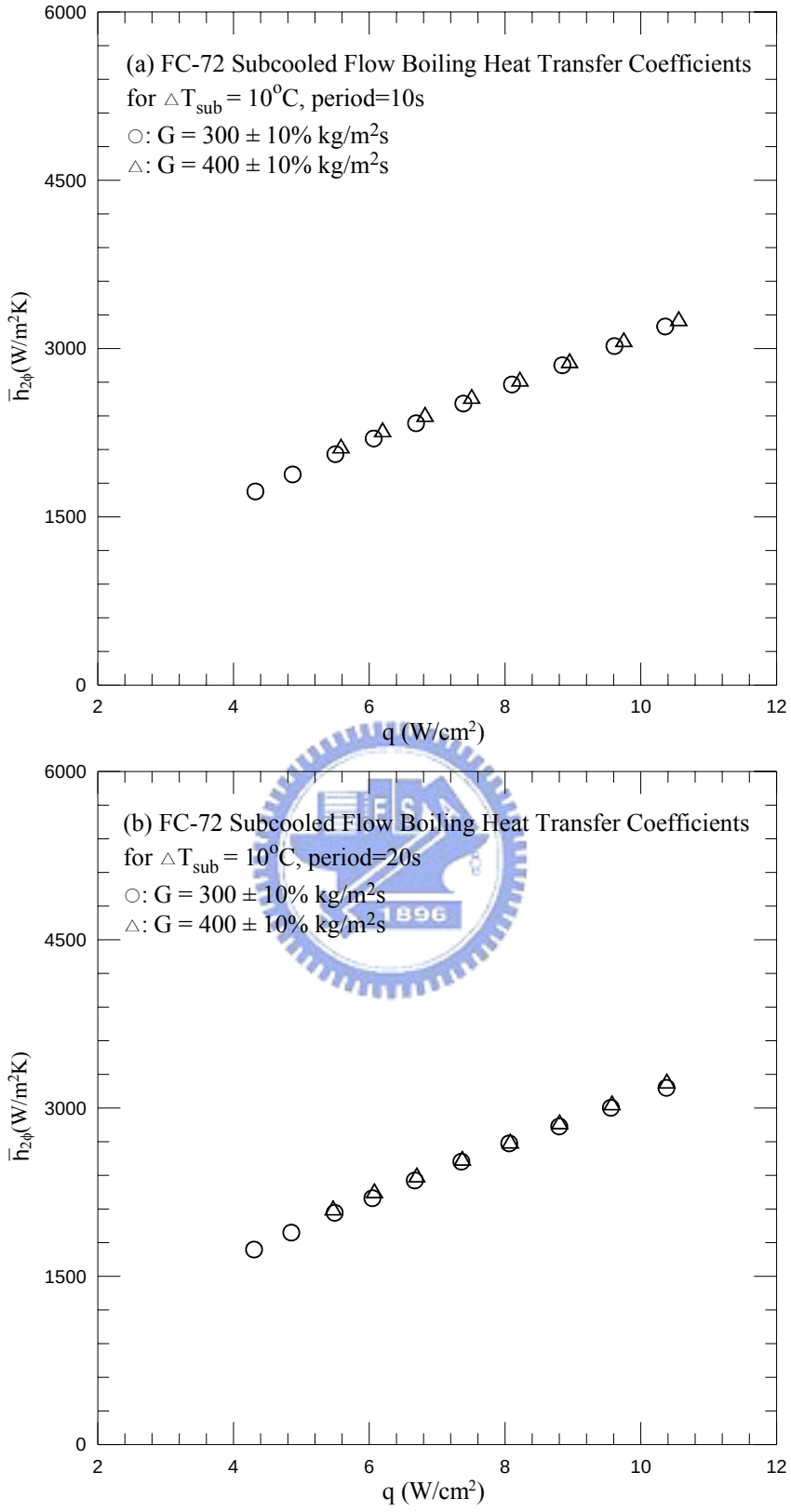

Fig. 5.15 Time-average flow boiling heat transfer coefficients for various coolant mass fluxes for transient subcooled flow boiling at ΔT_{sub} =10°C for t_p=10 sec (a), 20 sec (b) and 30 sec (c).

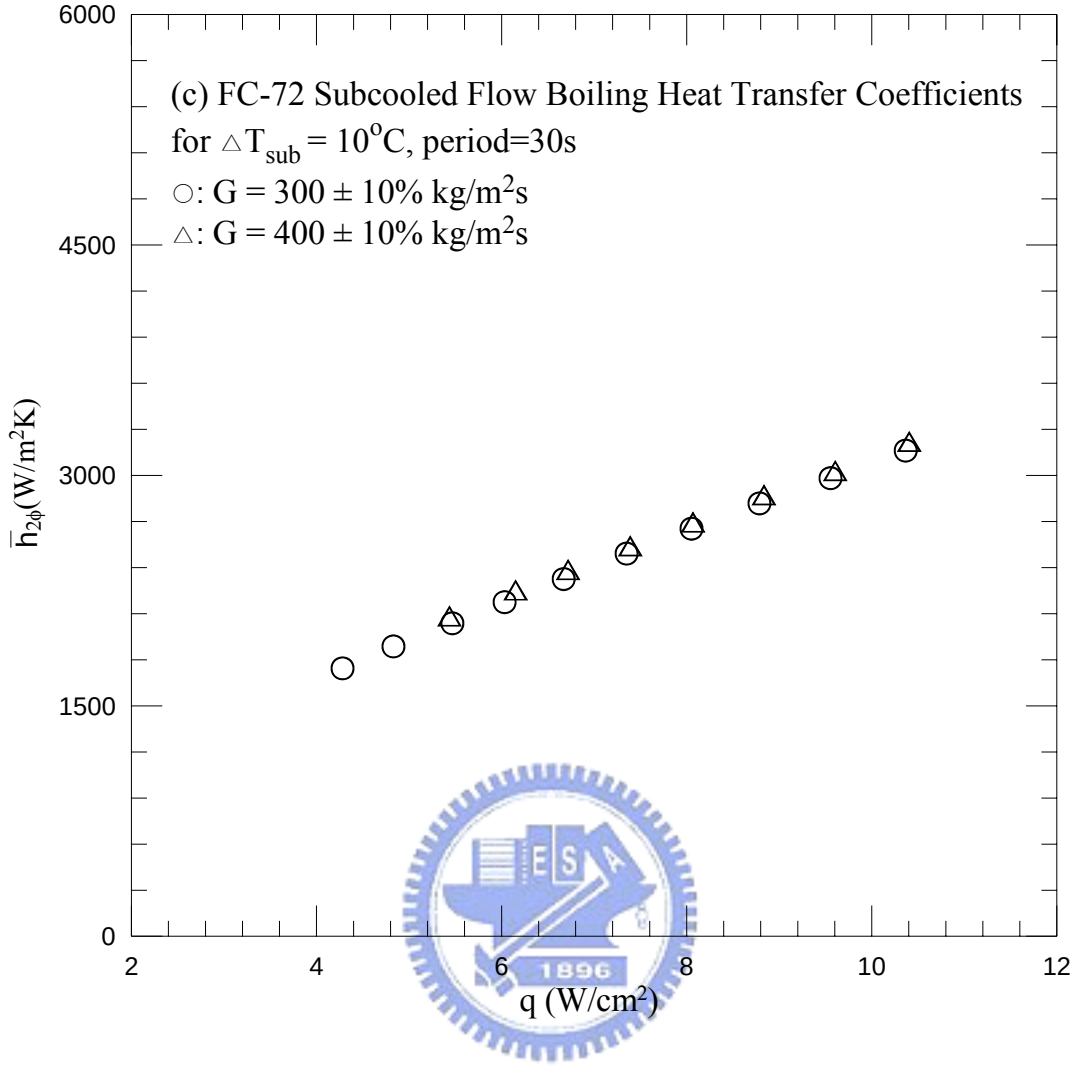

Fig. 5.15 Continued.

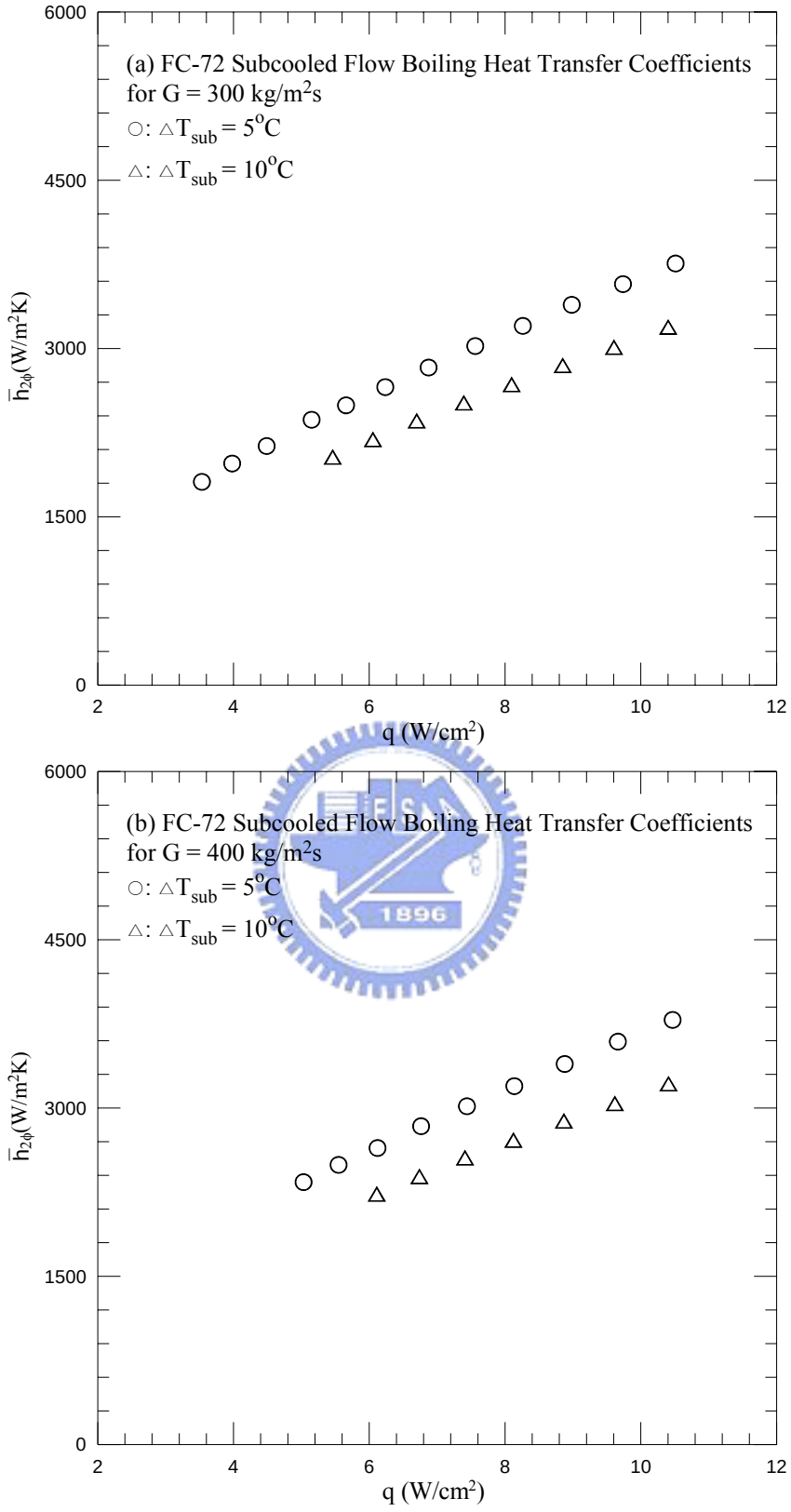

Fig. 5.16 Time-average flow boiling heat transfer coefficients for various inlet subcoolings for stable subcooled flow boiling at (a) G=300 kg/m^{2}s and (b) G=400 kg/m^{2}s.

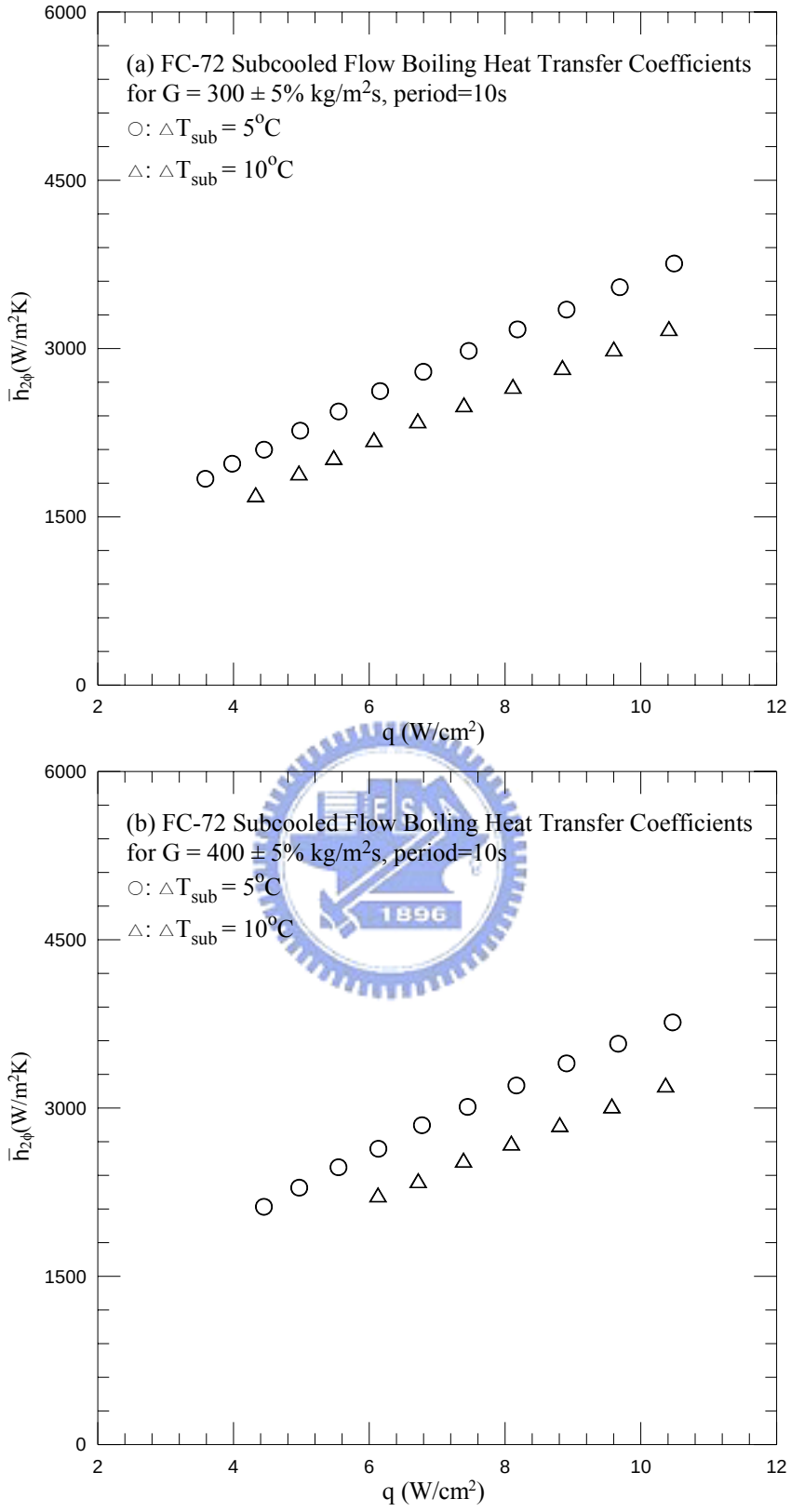

Fig. 5.17 Time-average flow boiling heat transfer coefficients for various inlet subcoolings for stable subcooled flow boiling at (a) G=300±5% kg/m^{2}s and (b) G=400±5% kg/m^{2}s at t_p=10 sec.

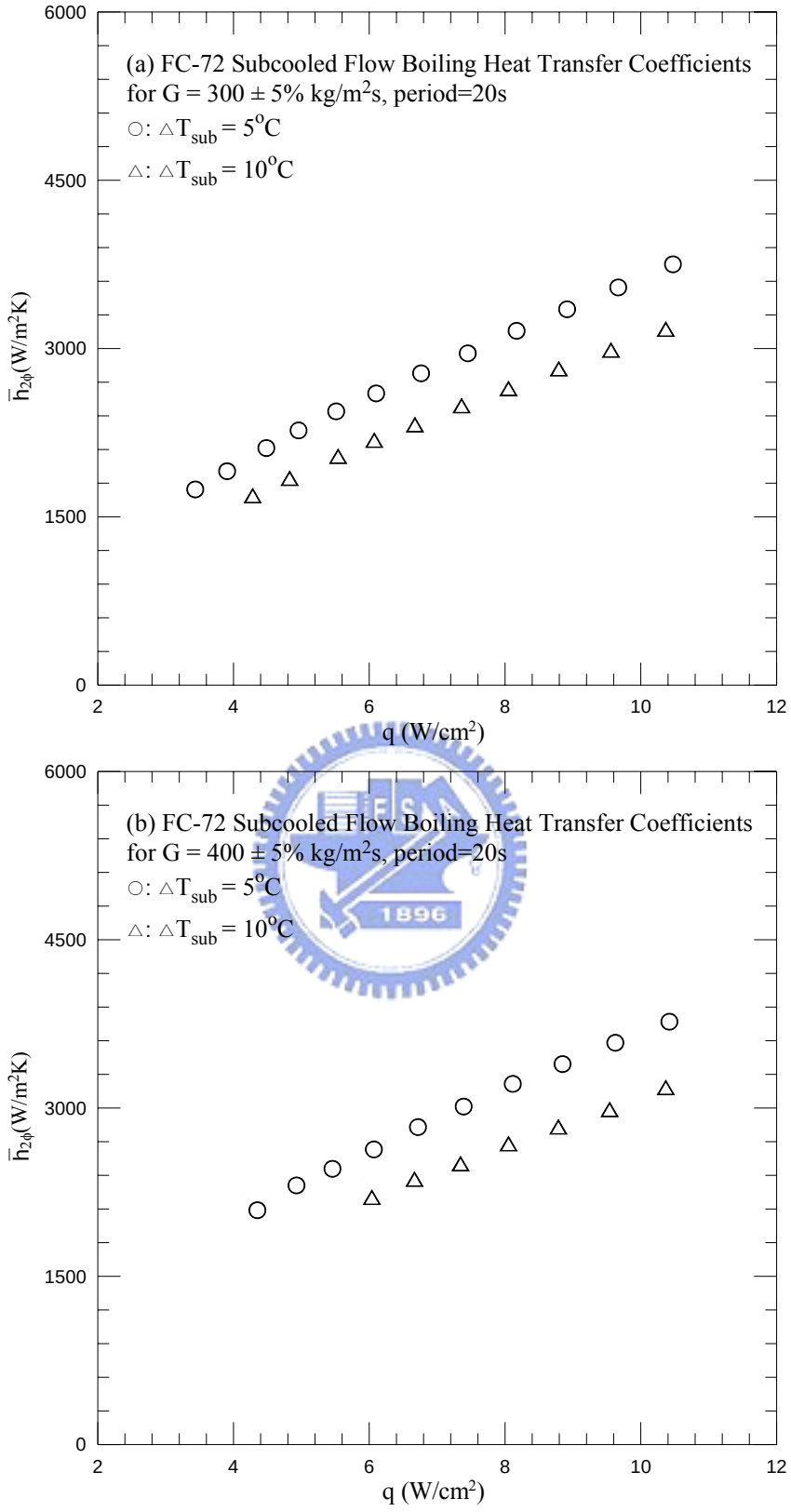

Fig. 5.18 Time-average flow boiling heat transfer coefficients for various inlet subcoolings for stable subcooled flow boiling at (a) G=300±5% kg/m^{2}s and (b) G=400±5% kg/m^{2}s at t_p=20 sec.

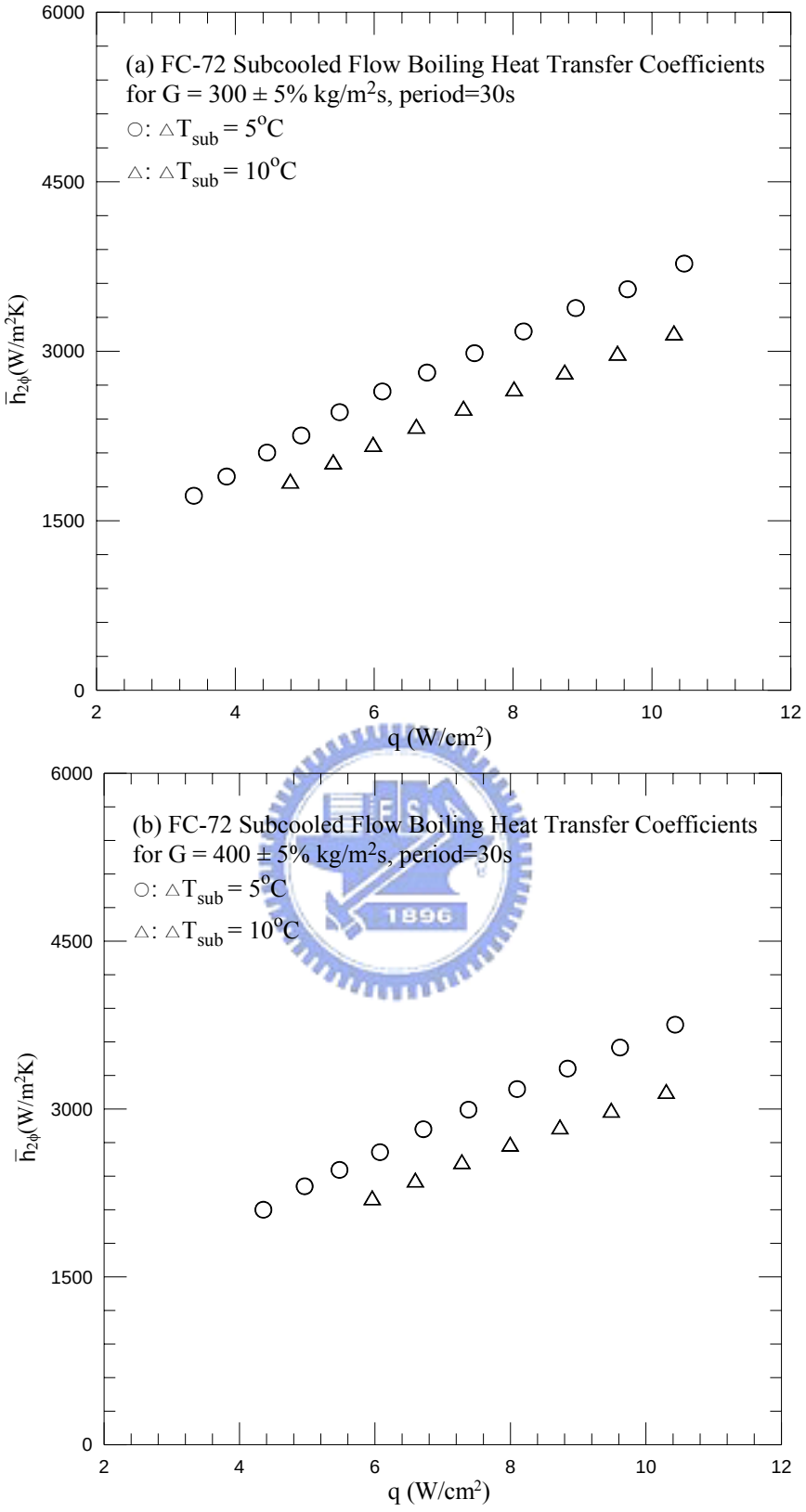

Fig. 5.19 Time-average flow boiling heat transfer coefficients for various inlet subcoolings for stable subcooled flow boiling at (a) G=300±5% kg/m^{2}s and (b) G=400±5% kg/m^{2}s at t_p=30 sec.

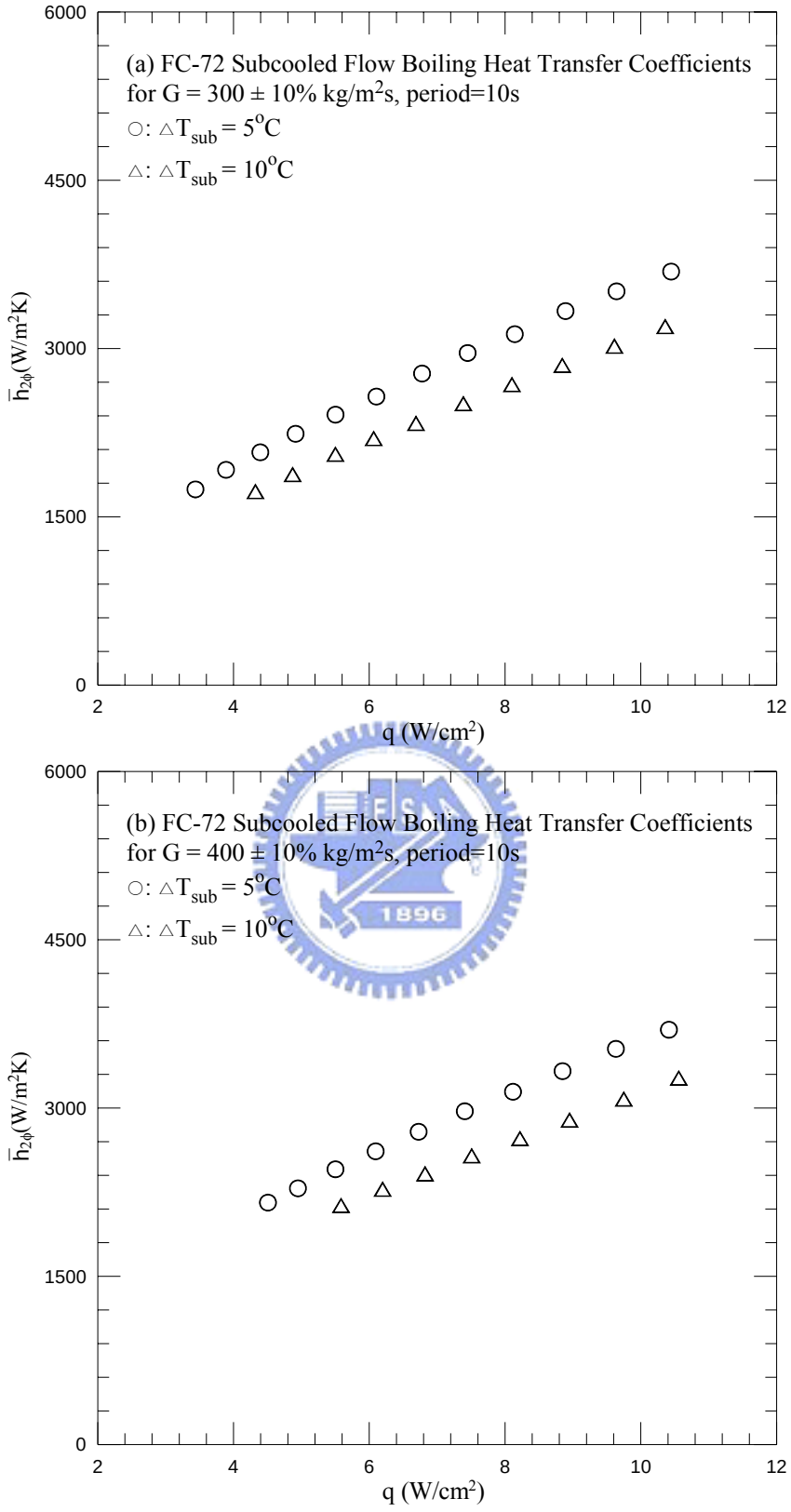

Fig. 5.20 Time-average flow boiling heat transfer coefficients for various inlet subcoolings for stable subcooled flow boiling at (a) G=300±10% kg/m^{2}s and (b) G=400±10% kg/m^{2}s at t_p=10 sec.

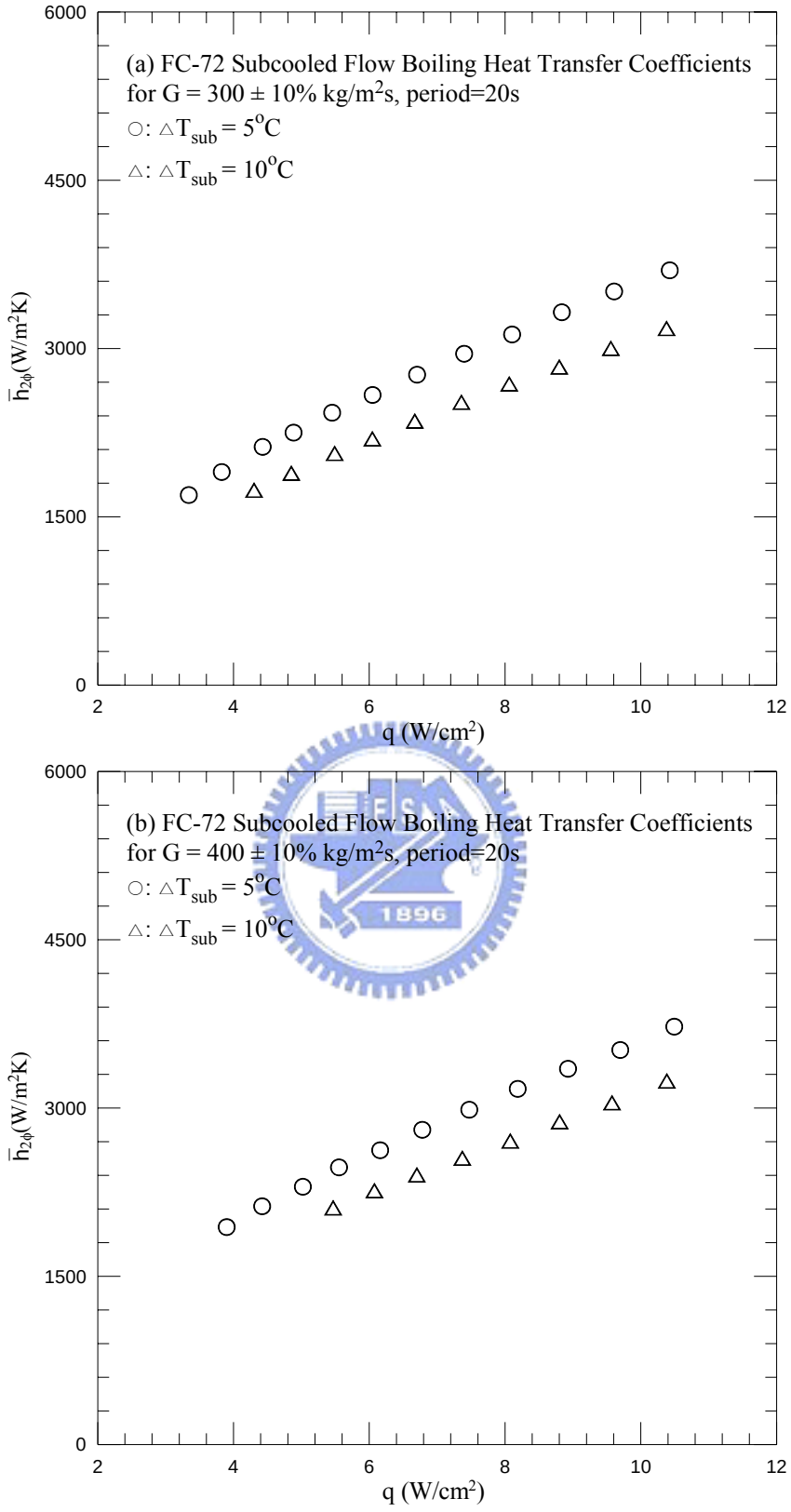

Fig. 5.21 Time-average flow boiling heat transfer coefficients for various inlet subcoolings for stable subcooled flow boiling at (a) G=300±10% kg/m^{2}s and (b) G=400±10% kg/m^{2}s at t_p=20 sec.

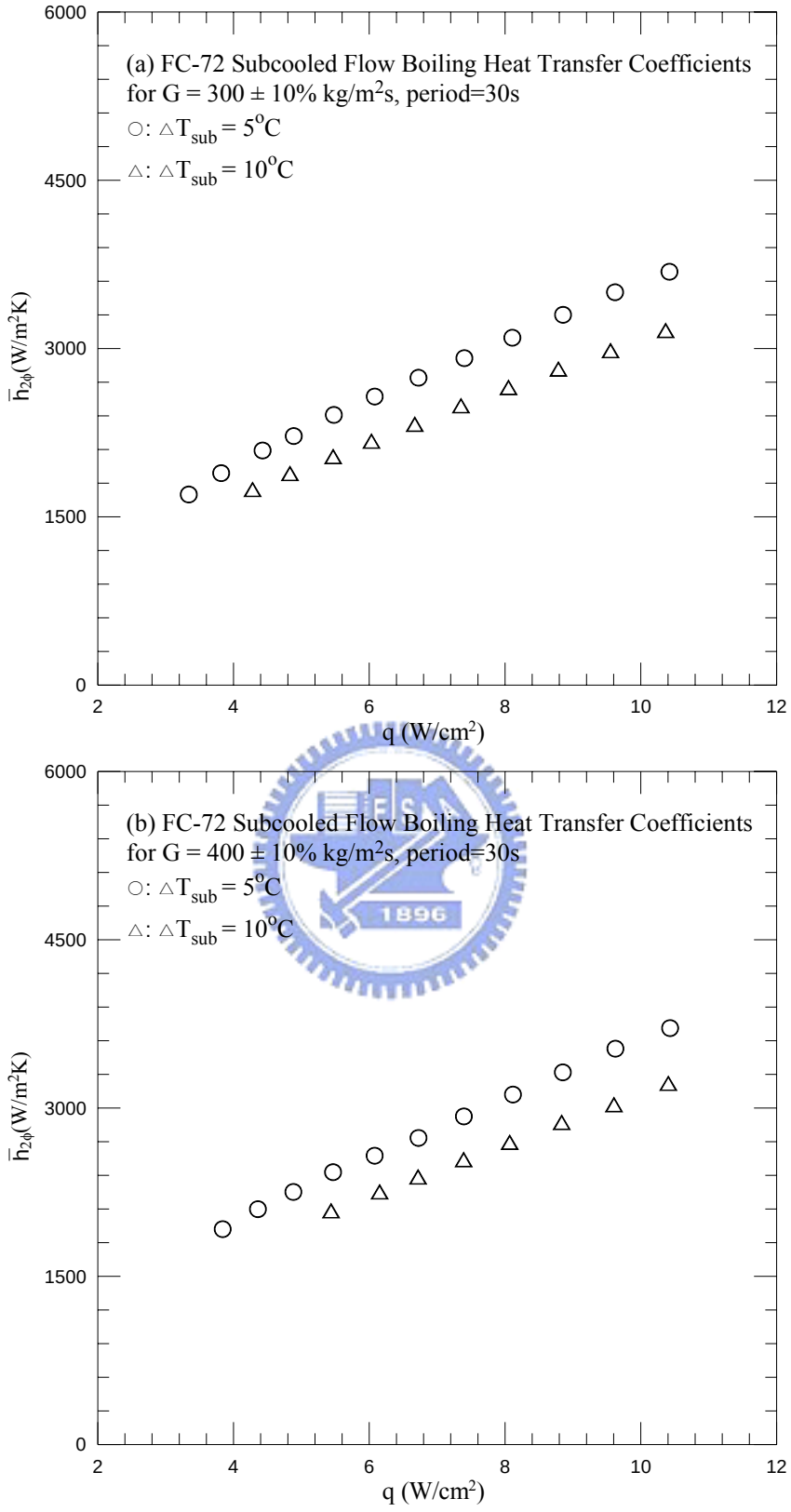

Fig. 5.22 Time-average flow boiling heat transfer coefficients for various inlet subcoolings for stable subcooled flow boiling at (a) G=300±10% kg/m^{2}s and (b) G=400±10% kg/m^{2}s at t_p=30 sec.

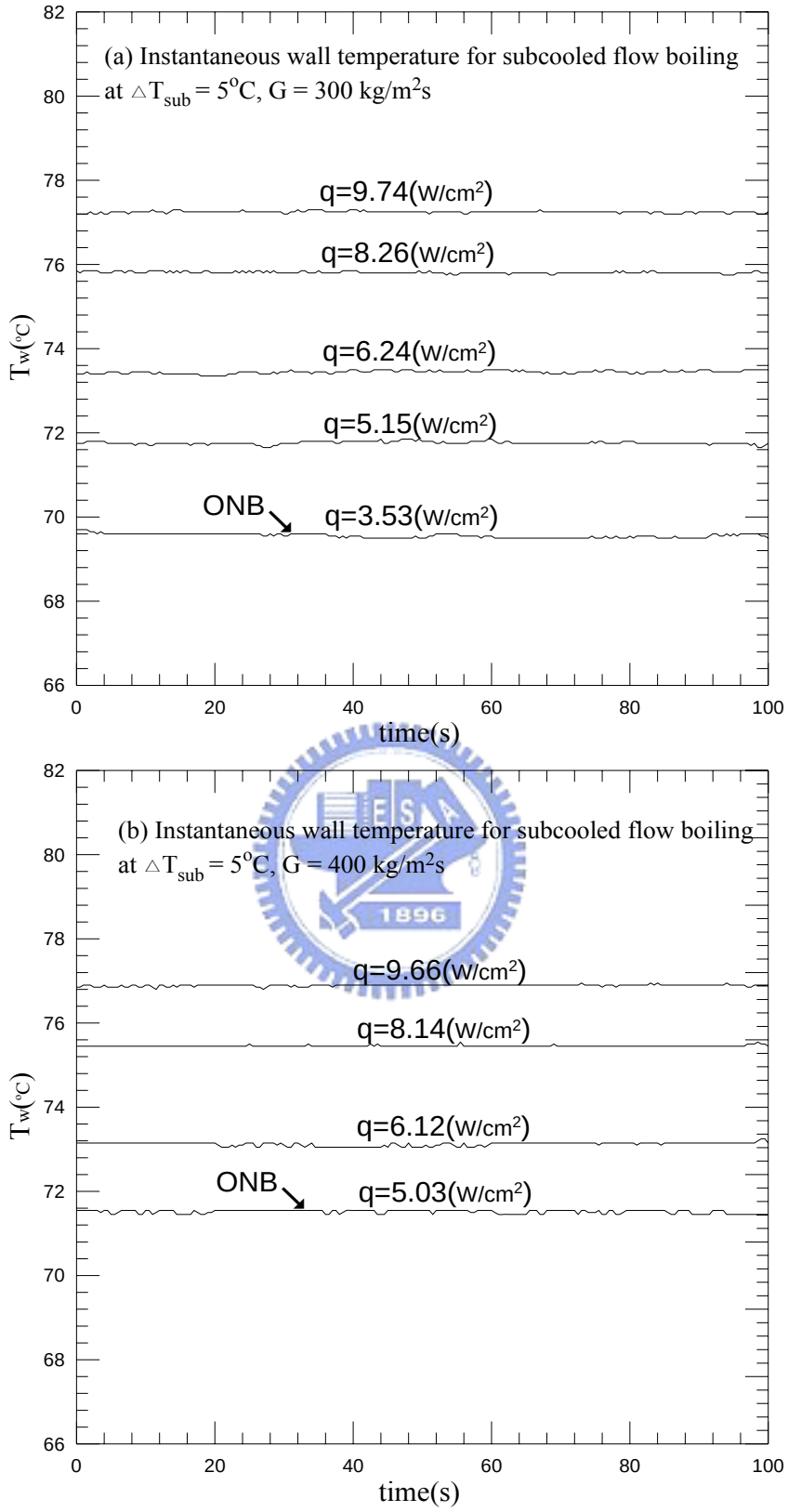

Fig. 5.23 Time variations of the copper plate temperature in stable subcooled flow boiling for various imposed heat fluxes for ΔT_{sub} =5°C at (a) G=300 kg/m^{2}s and (b) G=400 kg/m^{2}s.

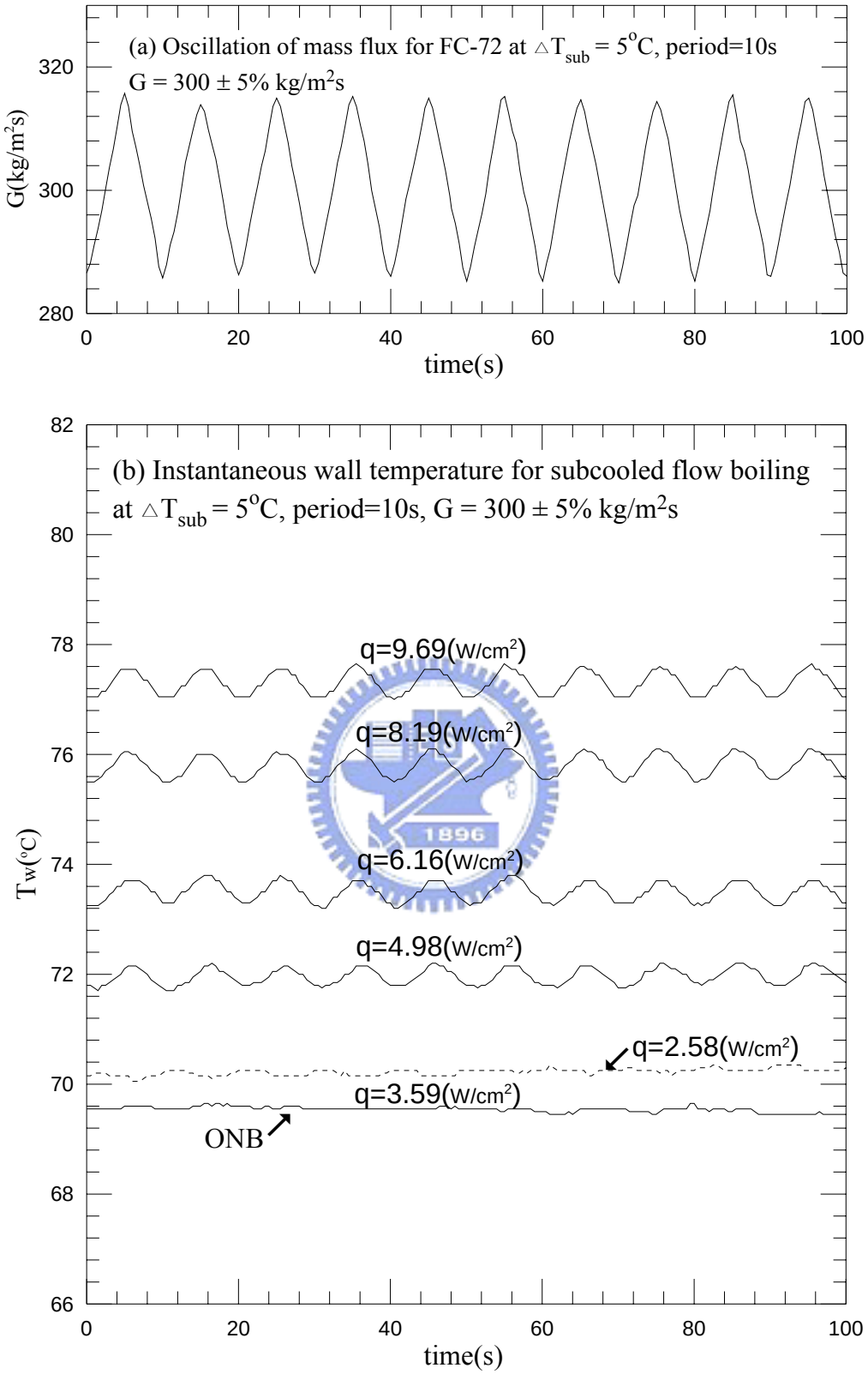

Fig. 5.24 Time variations of (a) imposed coolant mass flux and (b) copper plate temperature in transient oscillatory subcooled flow boiling for various imposed heat fluxes for G=300±5% kg/m^{2}s with t_p=10 sec.($\overline{q}_{ONB}$ =3.59 w/cm^2 at G =300 kg/m^{2}s)

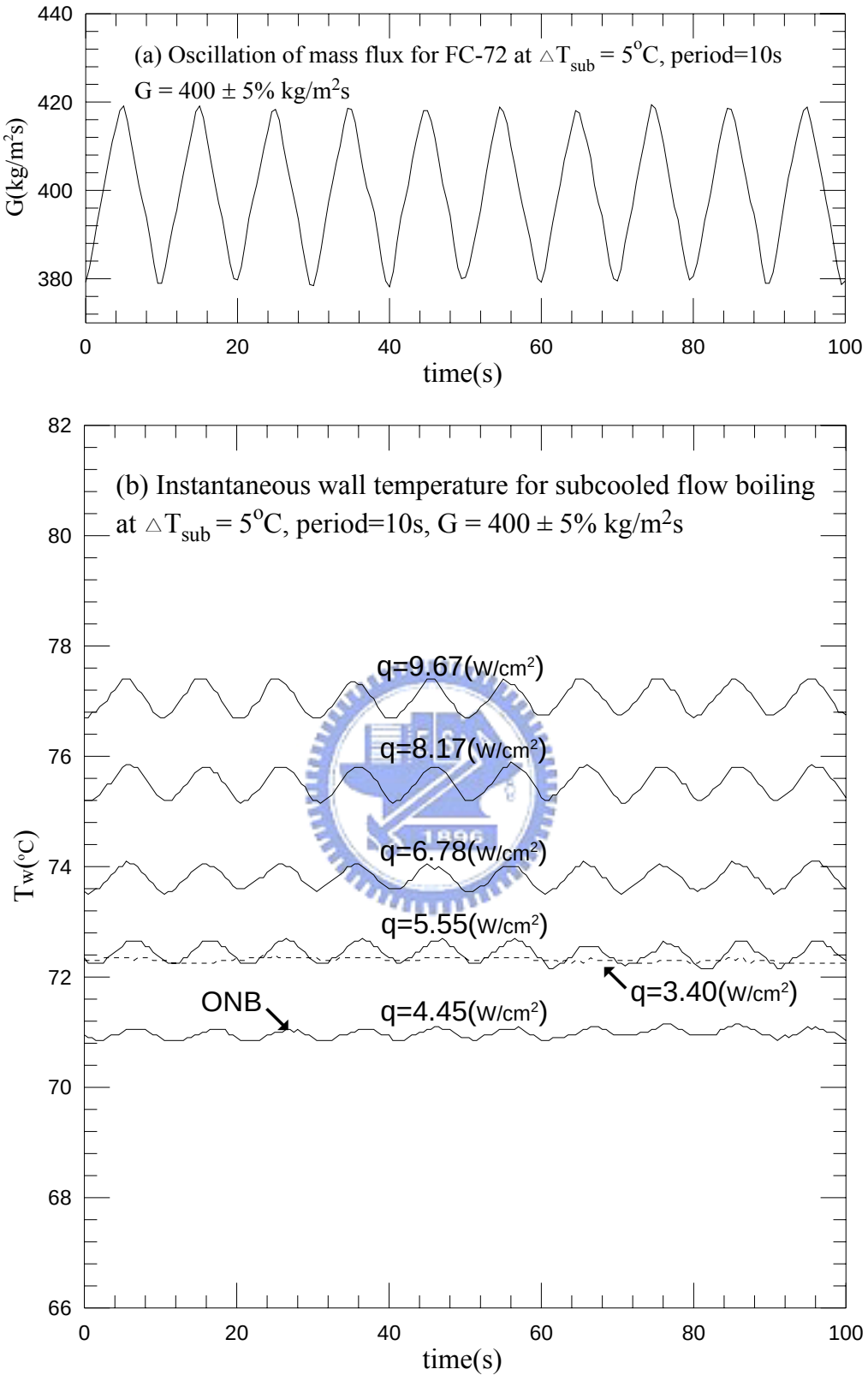

Fig. 5.25 Time variations of (a) imposed coolant mass flux and (b) copper plate temperature in transient oscillatory subcooled flow boiling for various imposed heat fluxes for G=400±5% kg/m^{2}s with t_p=10 sec.($\bar{q}_{ONB}$ =4.45 w/cm^2 at G =400 kg/m^{2}s)

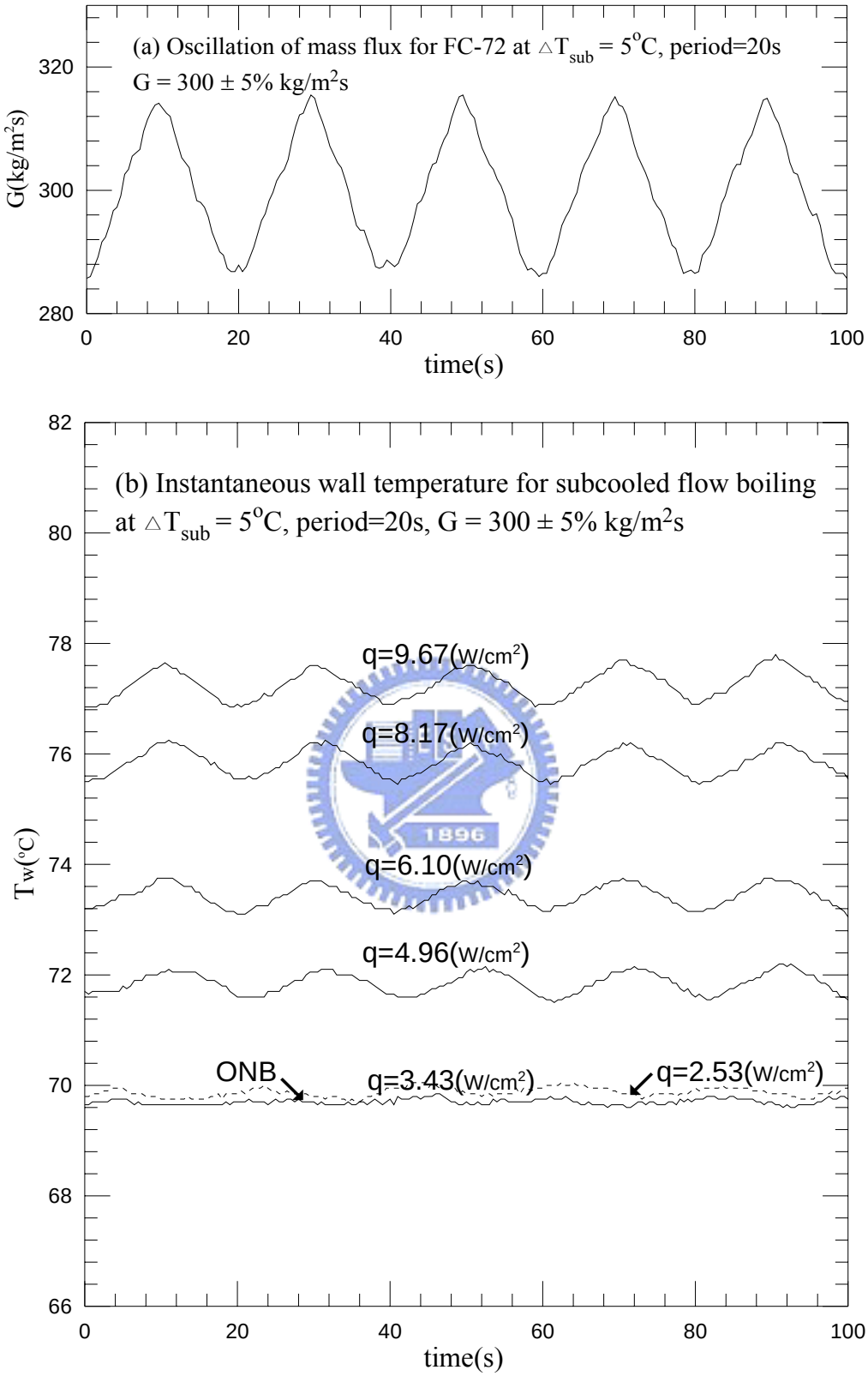

Fig. 5.26 Time variations of (a) imposed coolant mass flux and (b) copper plate temperature in transient oscillatory subcooled flow boiling for various imposed heat fluxes for G=300±5% kg/m^{2}s with t_p =20 sec.($\overline{q}_{ONB}$ =3.43 w/cm^2 at G =300 kg/m^{2}s)

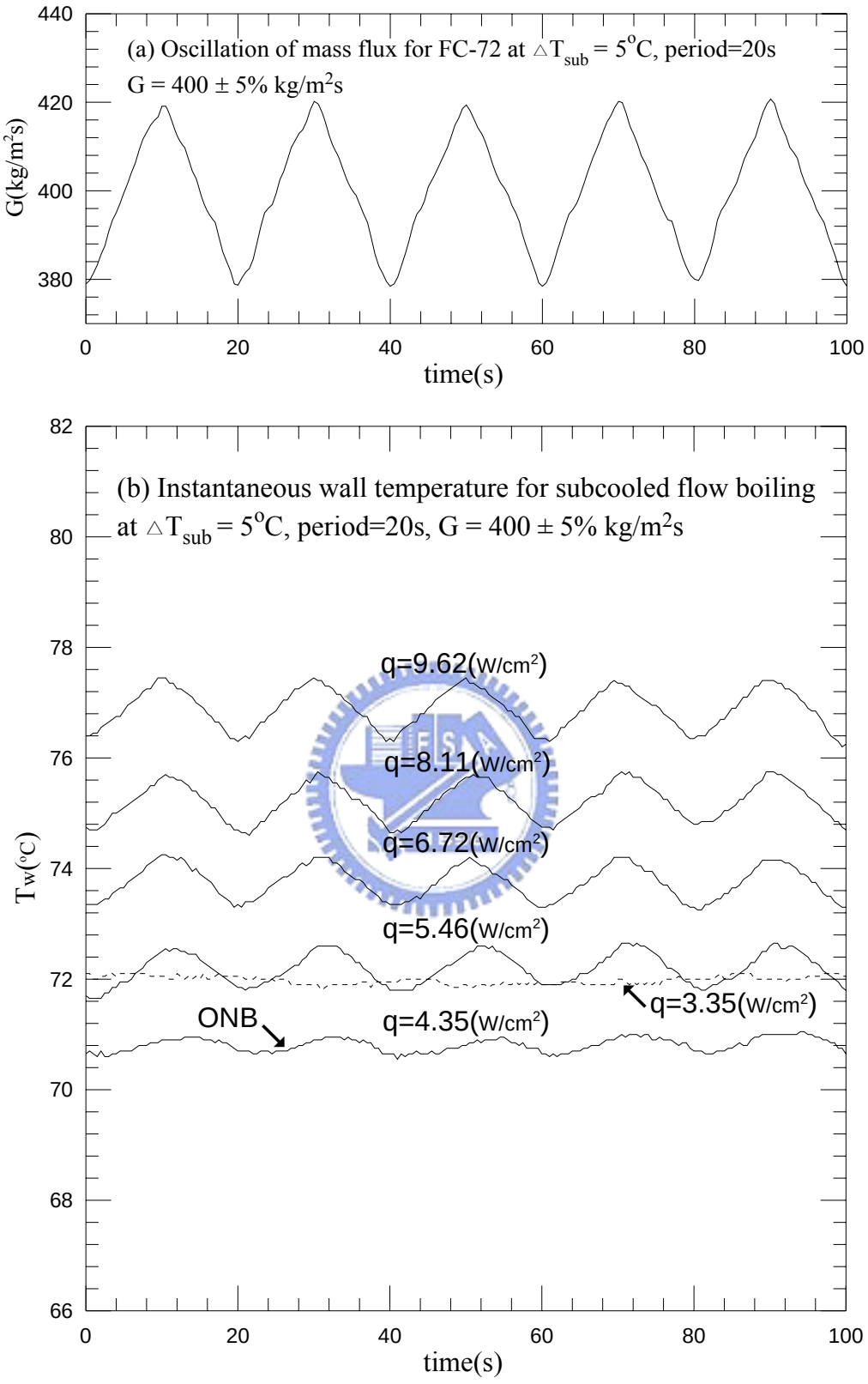

Fig. 5.27 Time variations of (a) imposed coolant mass flux and (b) copper plate temperature in transient oscillatory subcooled flow boiling for various imposed heat fluxes for G=400±5% kg/m^{2}s with t_p =20 sec.($\overline{q}_{ONB}$ =4.35 w/cm^2 at G =400 kg/m^{2}s)

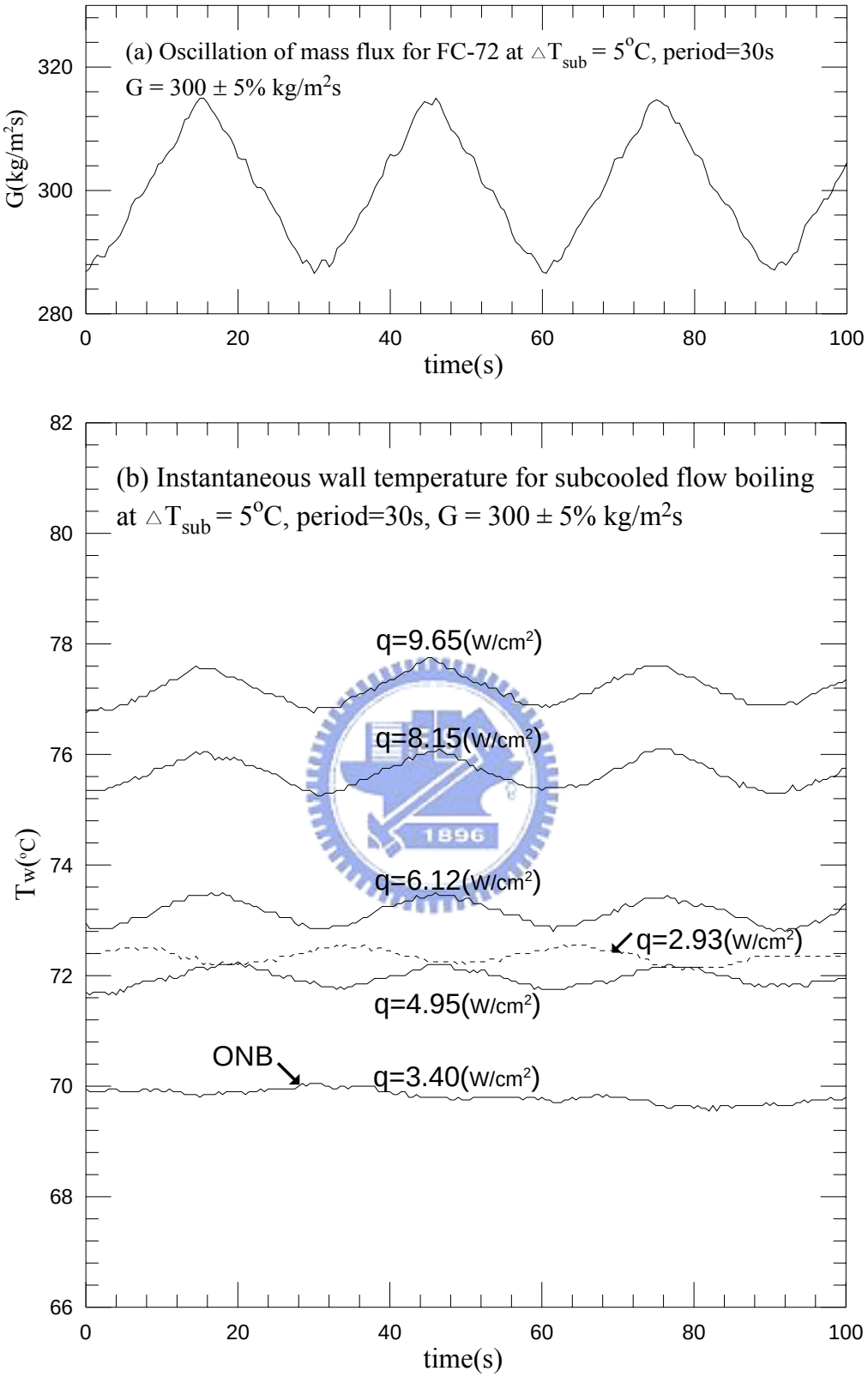

Fig. 5.28 Time variations of (a) imposed coolant mass flux and (b) copper plate temperature in transient oscillatory subcooled flow boiling for various imposed heat fluxes for G=300±5% kg/m^{2}s with t_p =30 sec.($\overline{q}_{ONB}$ =3.40 w/cm^2 at G =300 kg/m^{2}s)

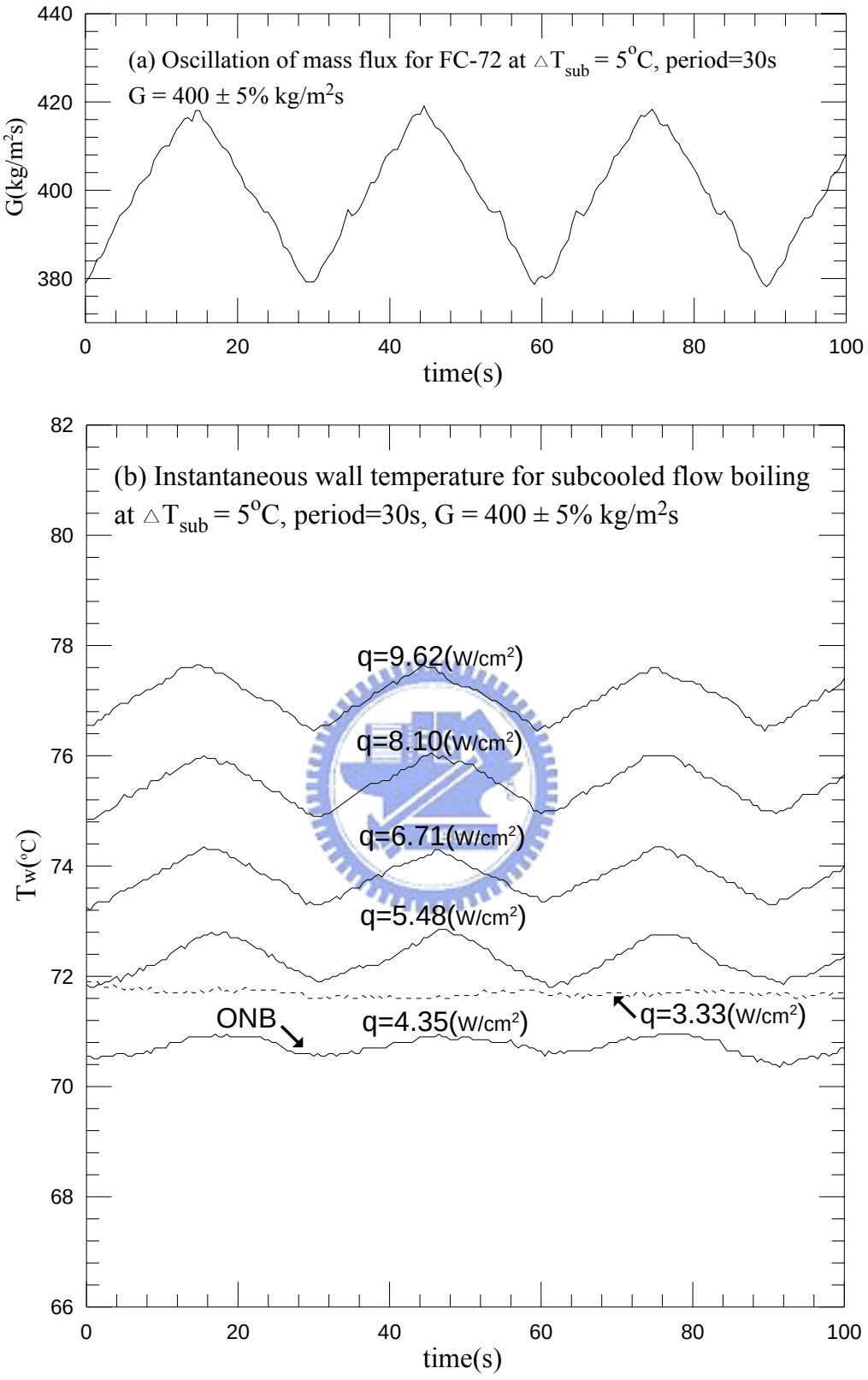

Fig. 5.29 Time variations of (a) imposed coolant mass flux and (b) copper plate temperature in transient oscillatory subcooled flow boiling for various imposed heat fluxes for G=400±5% kg/m^{2}s with t_p =30 sec.($\overline{q}_{ONB}$ =4.35 w/cm^2 at G =400 kg/m^{2}s)

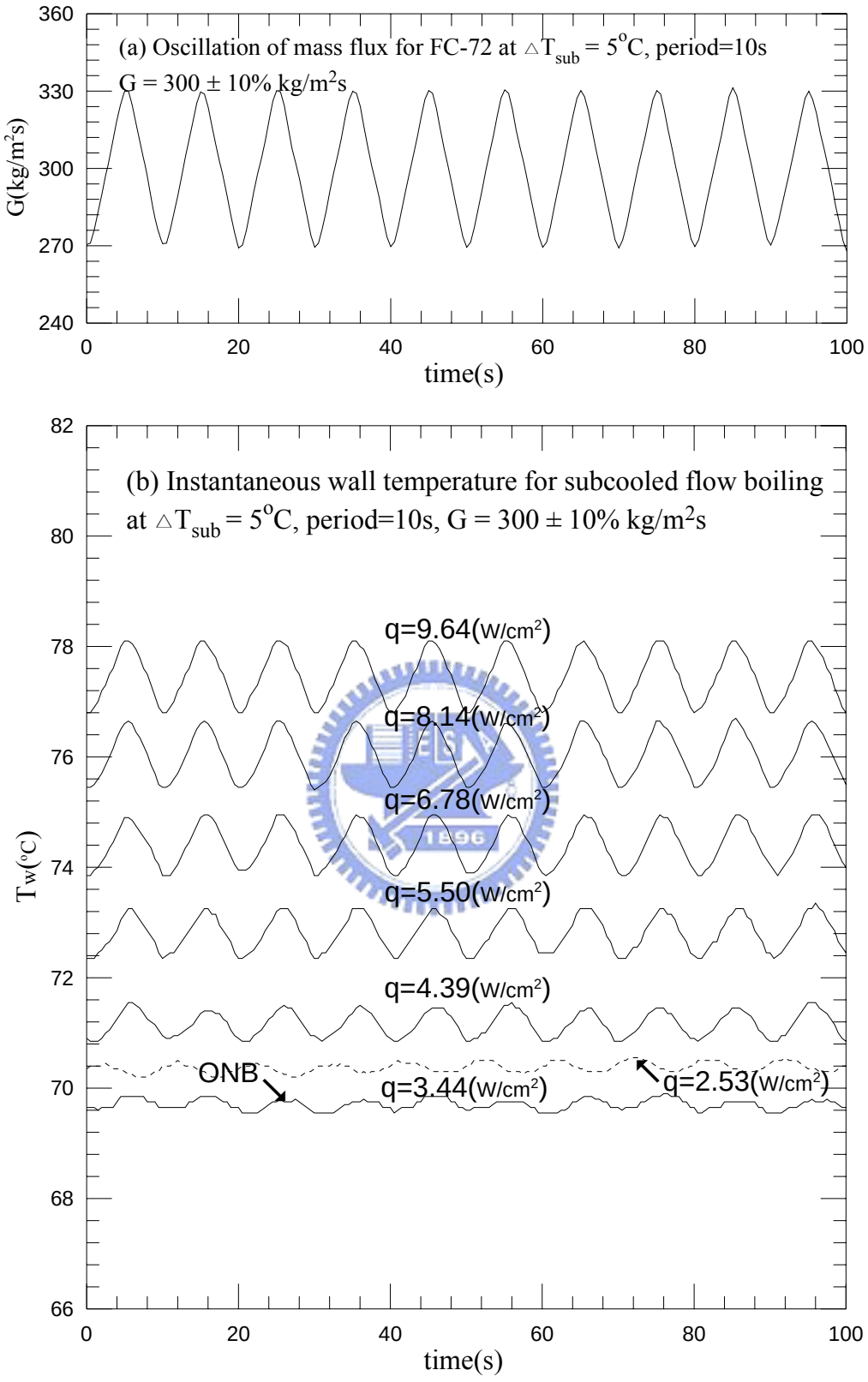

Fig. 5.30 Time variations of (a) imposed coolant mass flux and (b) copper plate temperature in transient oscillatory subcooled flow boiling for various imposed heat fluxes for G=300±10% kg/m^{2}s with t_p=10 sec.($\bar{q}_{ONB}$ =3.44 w/cm^2 at G =300 kg/m^{2}s)

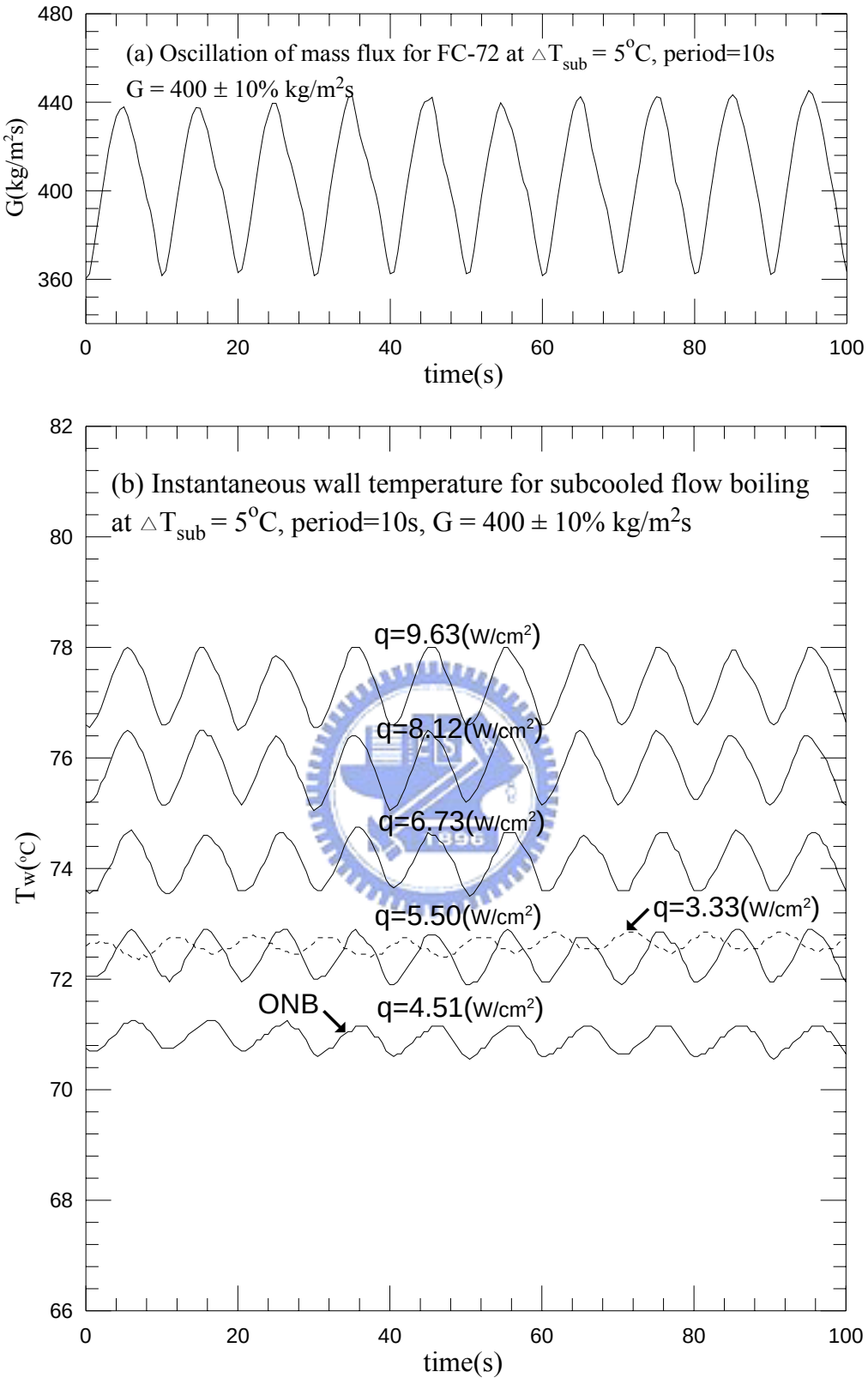

Fig. 5.31 Time variations of (a) imposed coolant mass flux and (b) copper plate temperature in transient oscillatory subcooled flow boiling for various imposed heat fluxes for G=400±10% kg/m^{2}s with t_p=10 sec.($\bar{q}_{ONB}$ =4.51 w/cm^2 at G =400 kg/m^{2}s)

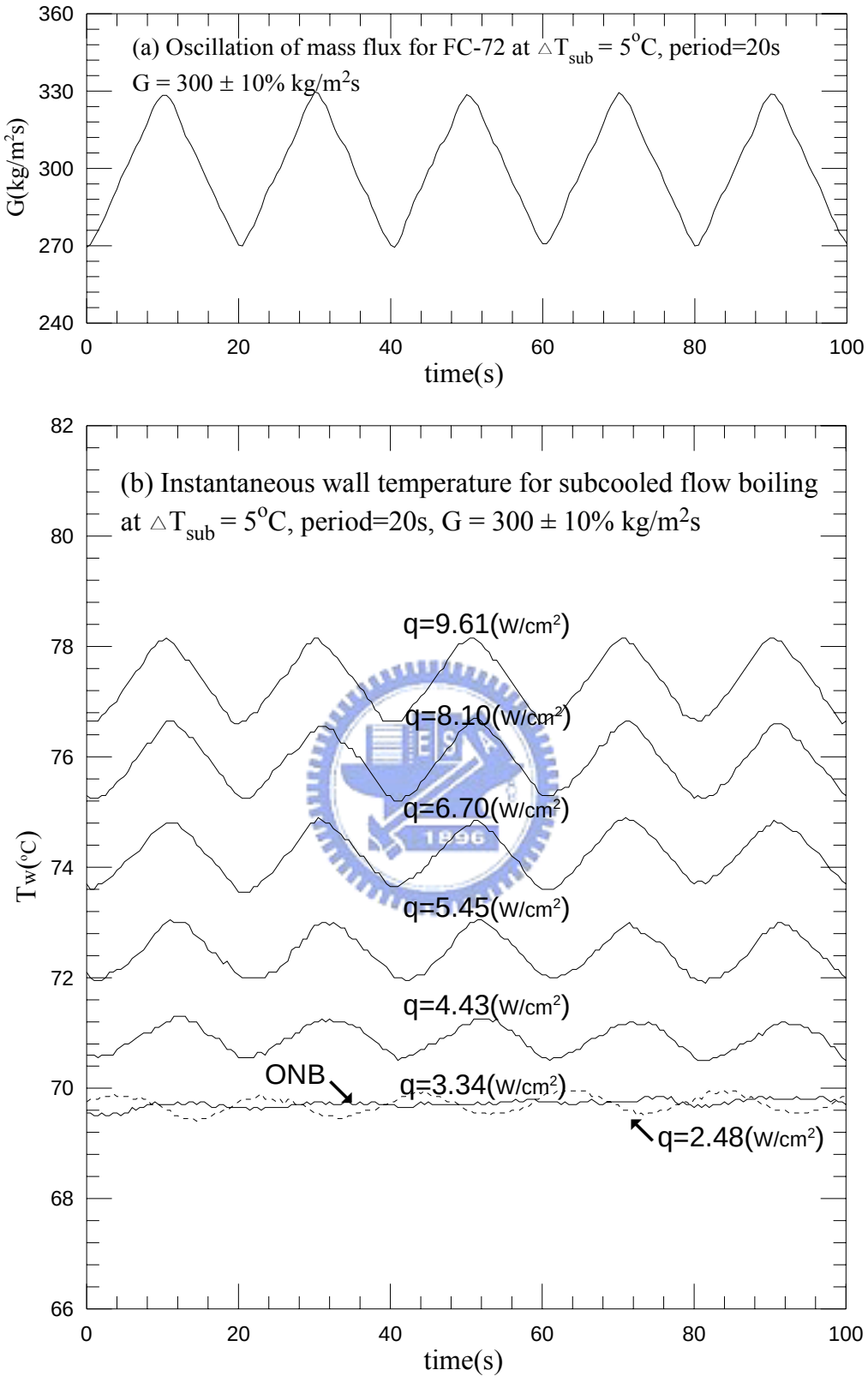

Fig. 5.32 Time variations of (a) imposed coolant mass flux and (b) copper plate temperature in transient oscillatory subcooled flow boiling for various imposed heat fluxes for G=300±10% kg/m^{2}s with t_p =20 sec.($\bar{q}_{ONB}$ =3.34 w/cm^2 at G =300 kg/m^{2}s)

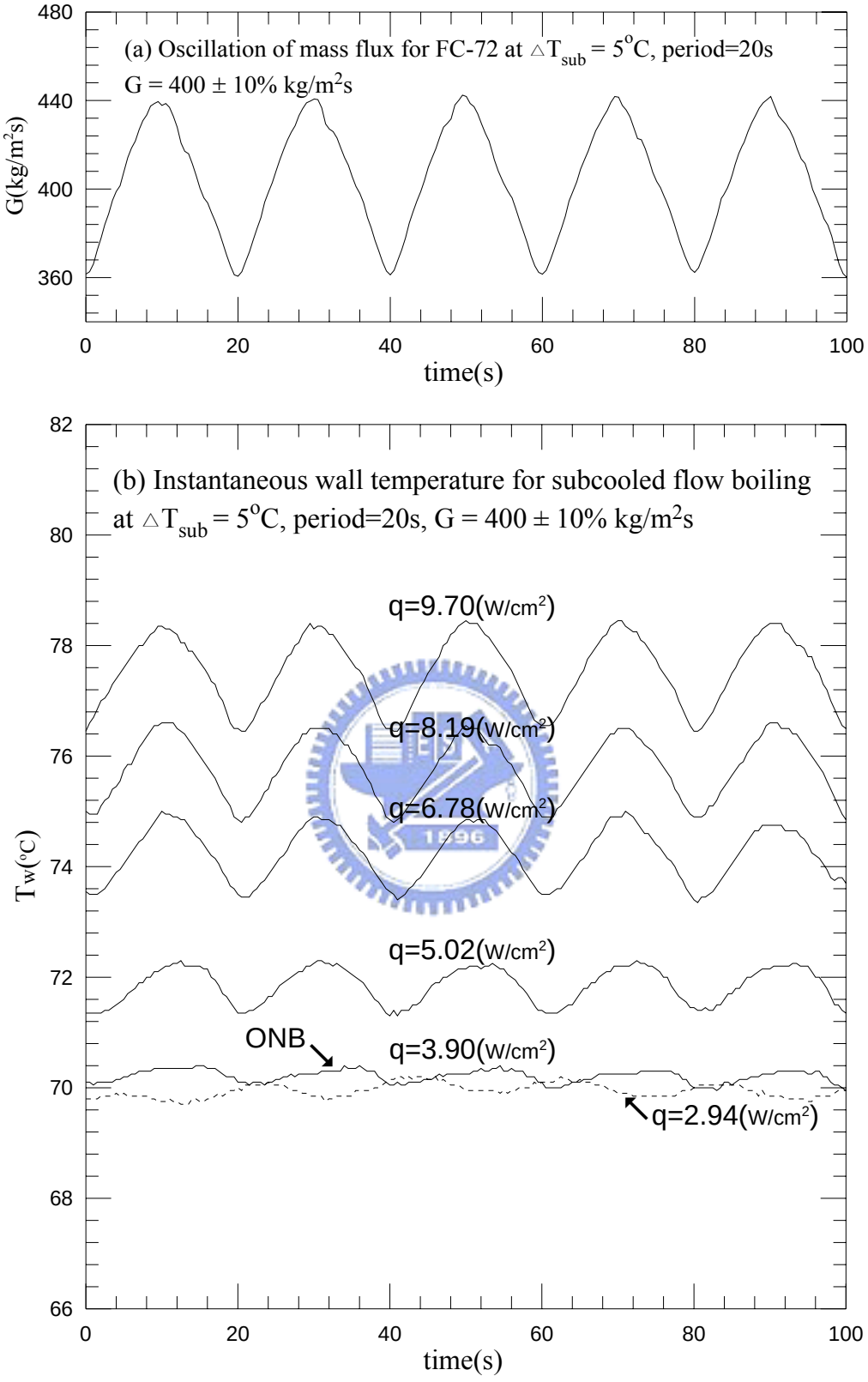

Fig. 5.33 Time variations of (a) imposed coolant mass flux and (b) copper plate temperature in transient oscillatory subcooled flow boiling for various imposed heat fluxes for G=400±10% kg/m^{2}s with t_p =20 sec.($\overline{q}_{ONB}$ =3.90 w/cm^2 at G =400 kg/m^{2}s)

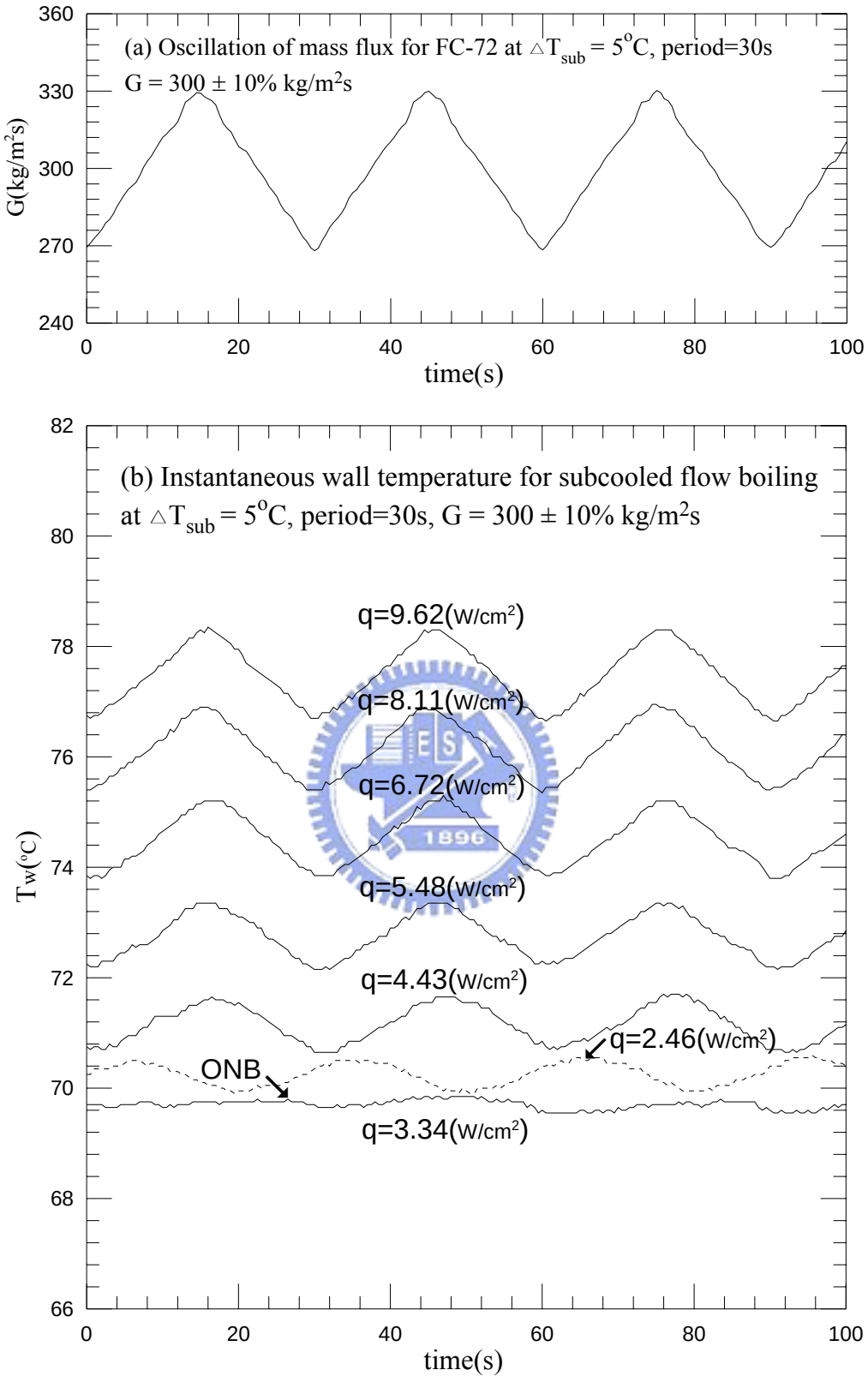

Fig. 5.34 Time variations of (a) imposed coolant mass flux and (b) copper plate temperature in transient oscillatory subcooled flow boiling for various imposed heat fluxes for G=300±10% kg/m^{2}s with t_p =30 sec.($\bar{q}_{ONB}$ =3.34 w/cm^2 at G =300 kg/m^{2}s)

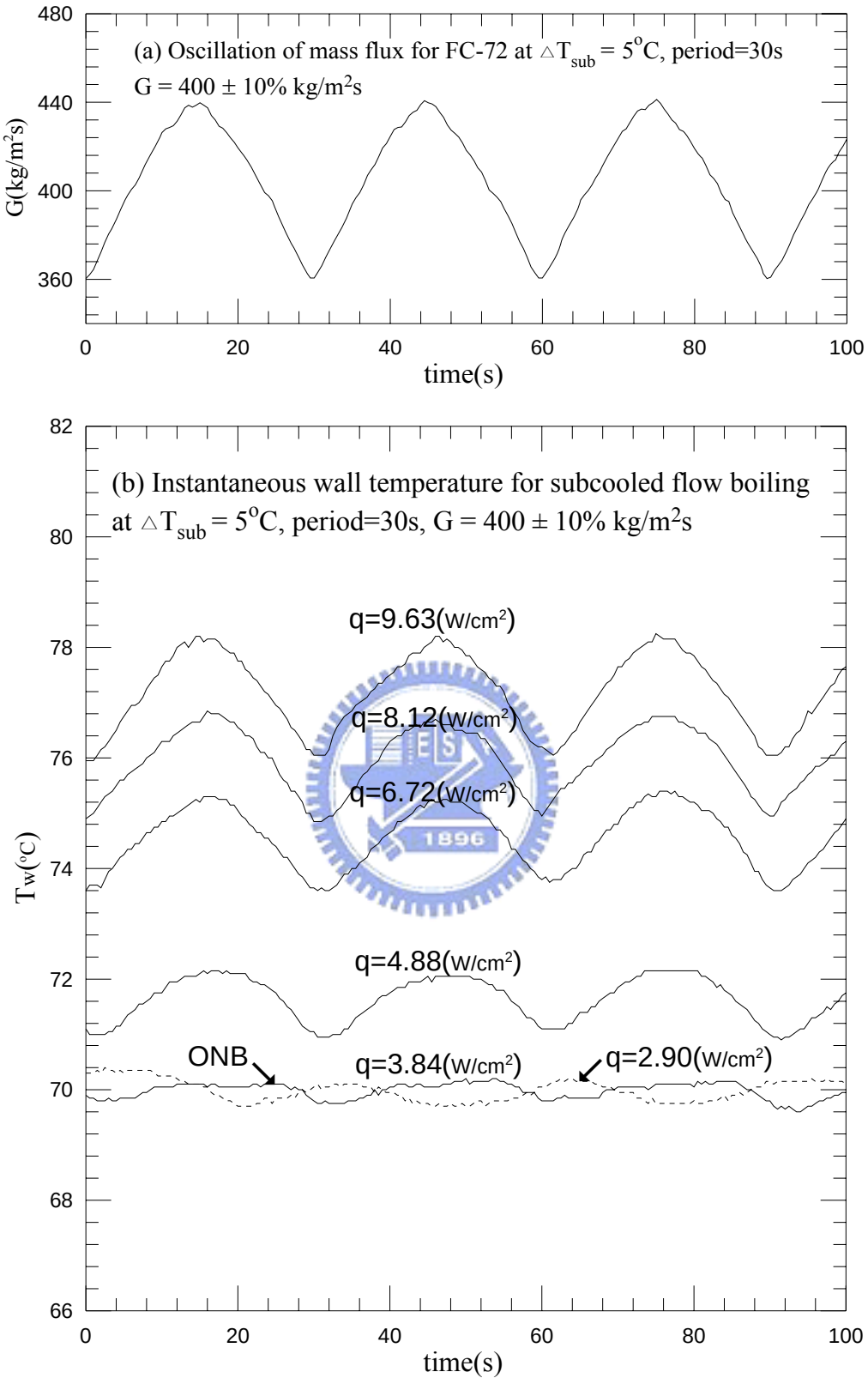

Fig. 5.35 Time variations of (a) imposed coolant mass flux and (b) copper plate temperature in transient oscillatory subcooled flow boiling for various imposed heat fluxes for G=400±10% kg/m^{2}s with t_p =30 sec.($\bar{q}_{ONB}$ =3.84 w/cm^2 at G =400 kg/m^{2}s)

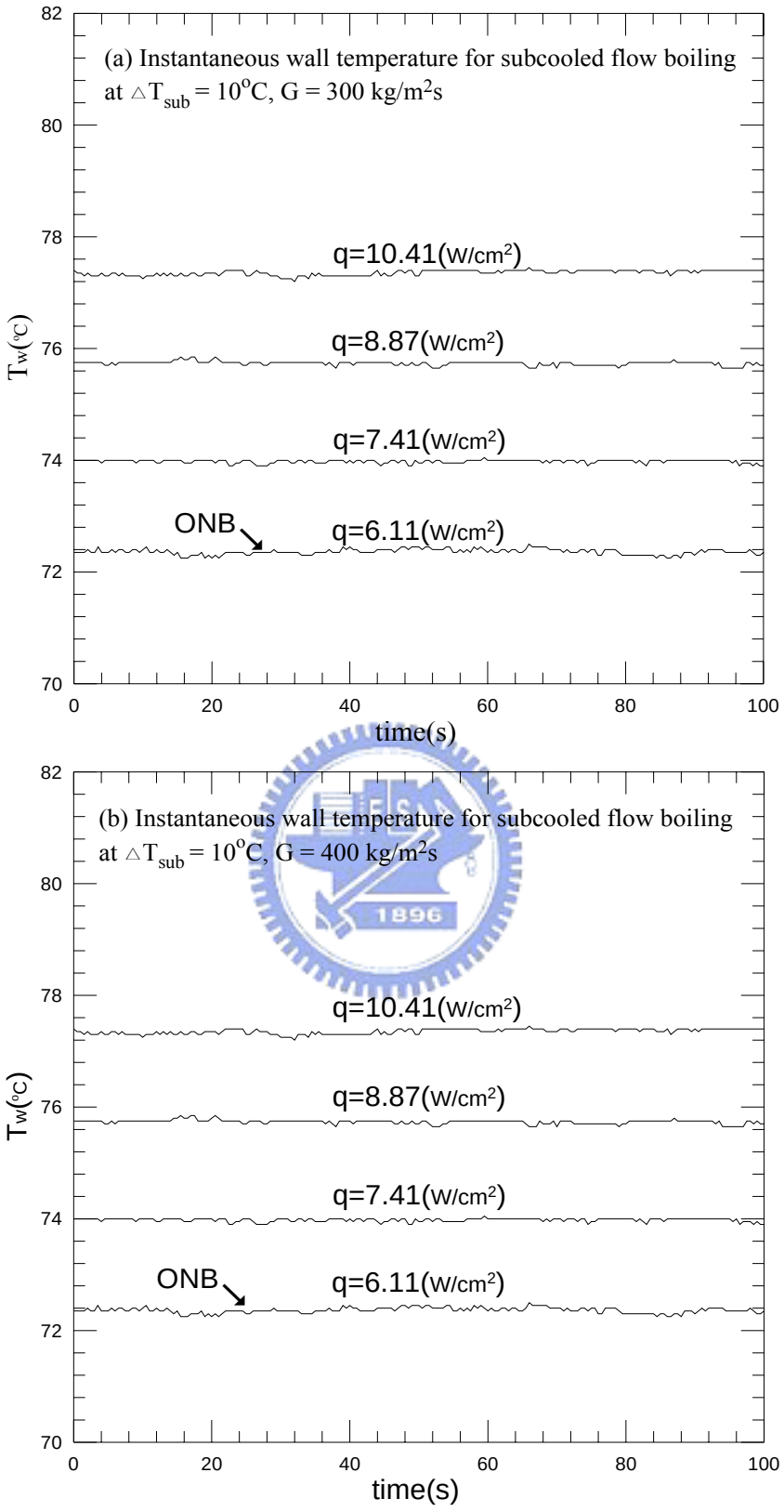

Fig. 5.36 Time variations of the copper plate temperature in stable subcooled flow boiling for various imposed heat fluxes for $\triangle T_{in}$=10°C at (a) G=300 kg/m^{2}s and (b) G=400 kg/m^{2}s.

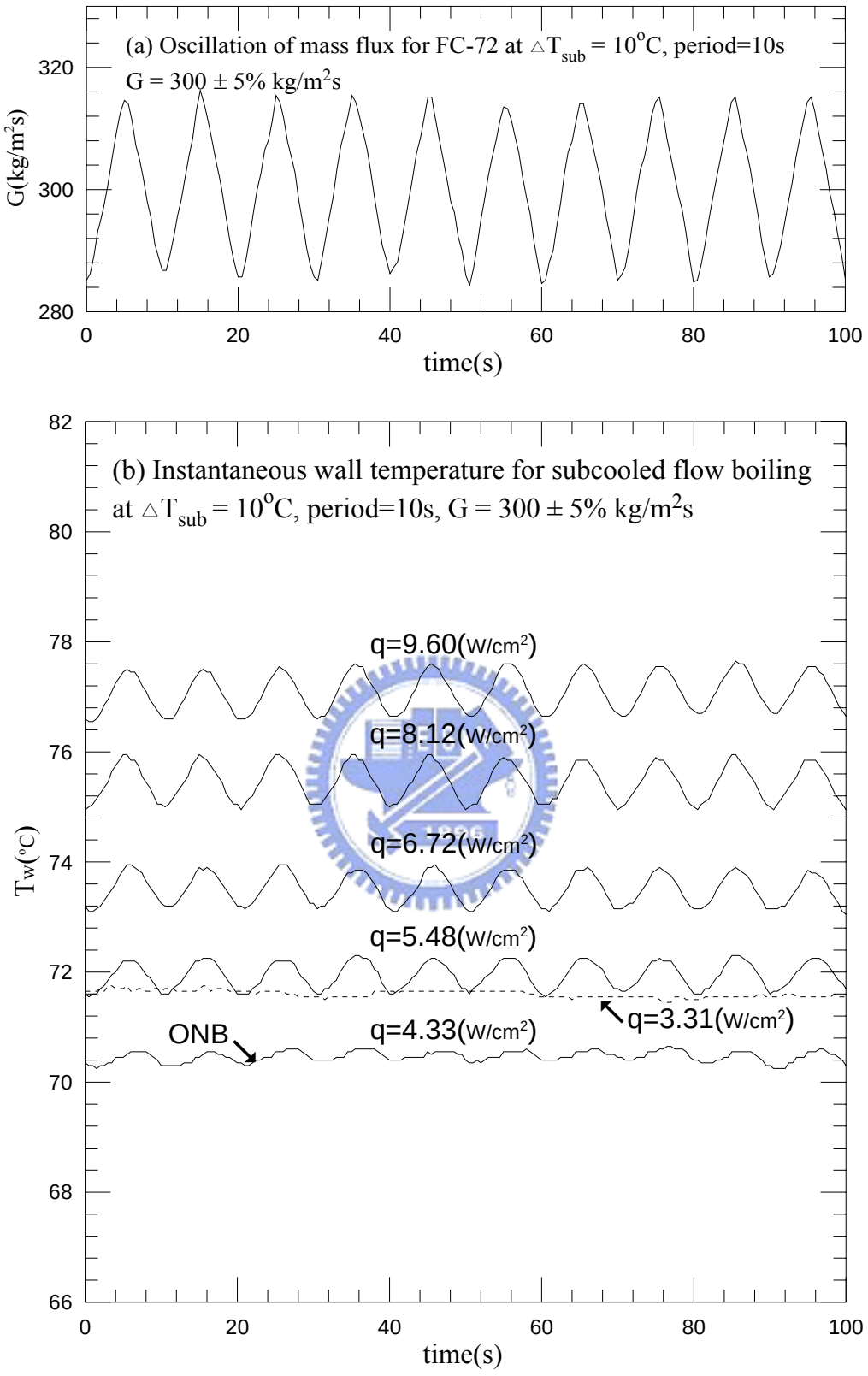

Fig. 5.37 Time variations of (a) imposed coolant mass flux and (b) copper plate temperature in transient oscillatory subcooled flow boiling for various imposed heat fluxes for G=300±5% kg/m^{2}s with t_p=10 sec.($\overline{q}_{ONB}$ =4.33 w/cm^2 at G =300 kg/m^{2}s)

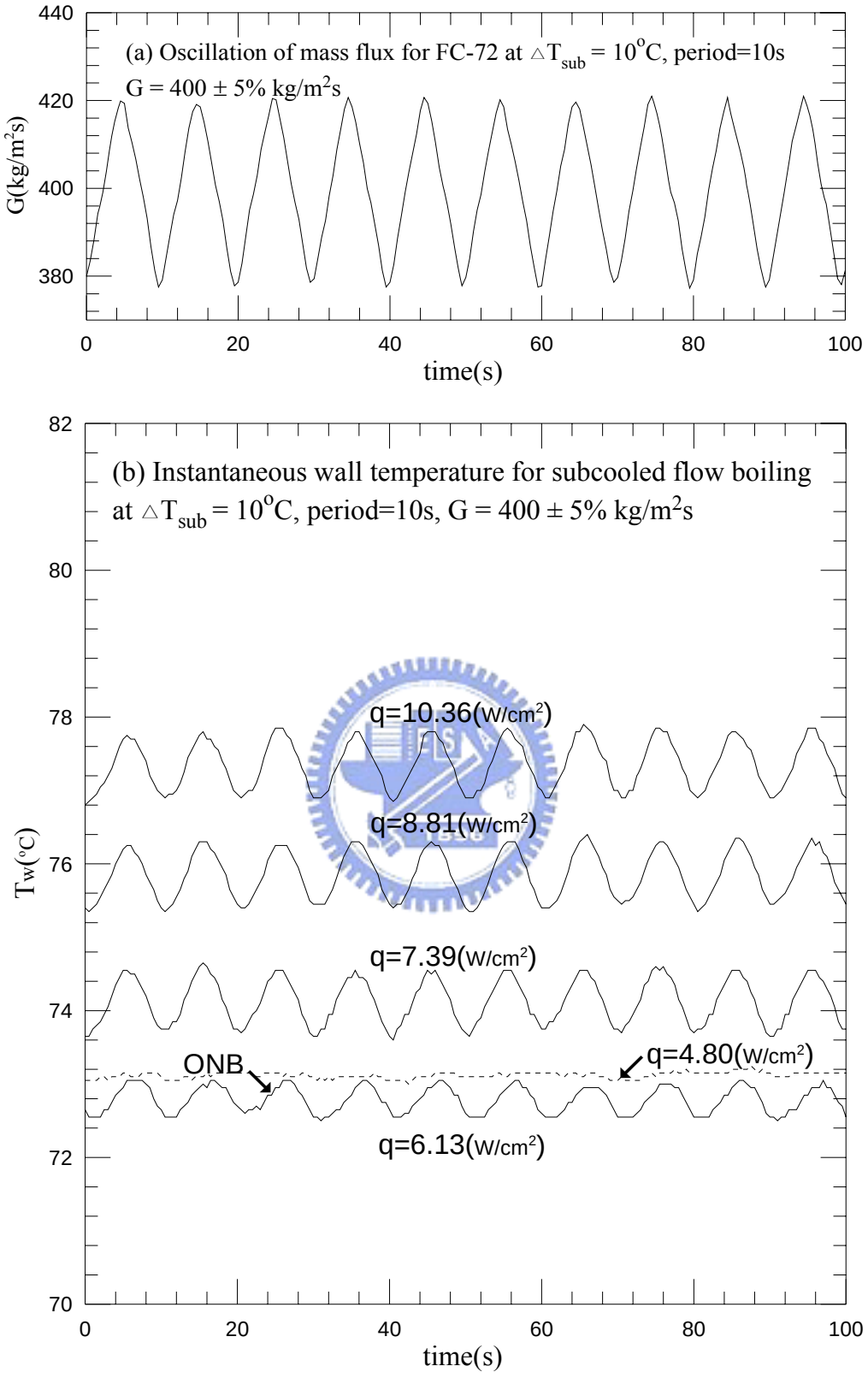

Fig. 5.38 Time variations of (a) imposed coolant mass flux and (b) copper plate temperature in transient oscillatory subcooled flow boiling for various imposed heat fluxes for G=400±5% kg/m^{2}s with t_p=10 sec.($\bar{q}_{ONB}$ =6.13 w/cm^2 at G =400 kg/m^{2}s)

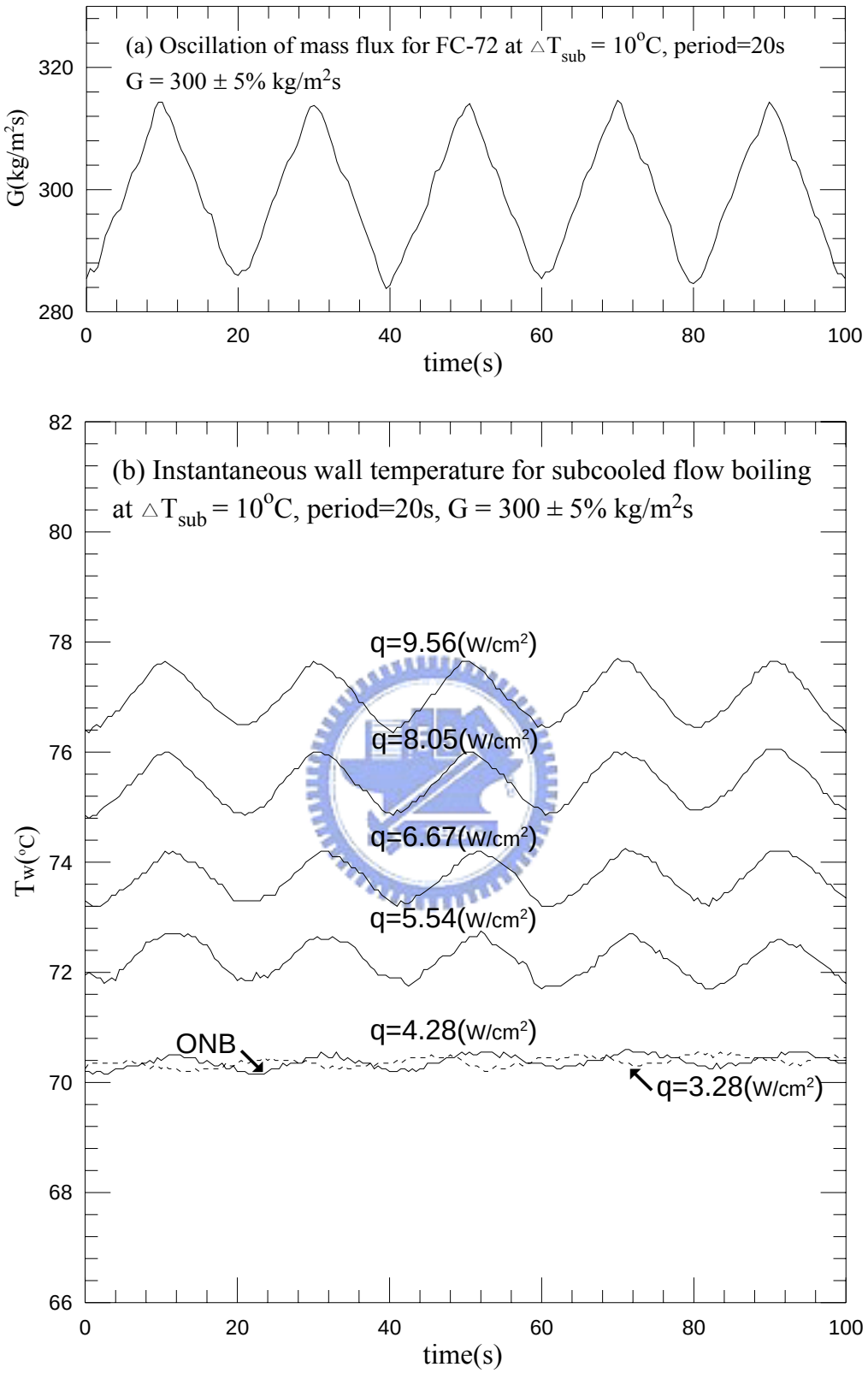

Fig. 5.39 Time variations of (a) imposed coolant mass flux and (b) copper plate temperature in transient oscillatory subcooled flow boiling for various imposed heat fluxes for G=300±5% kg/m^{2}s with t_p =20 sec.($\bar{q}_{ONB}$ =4.28 w/cm^2 at G =300 kg/m^{2}s)

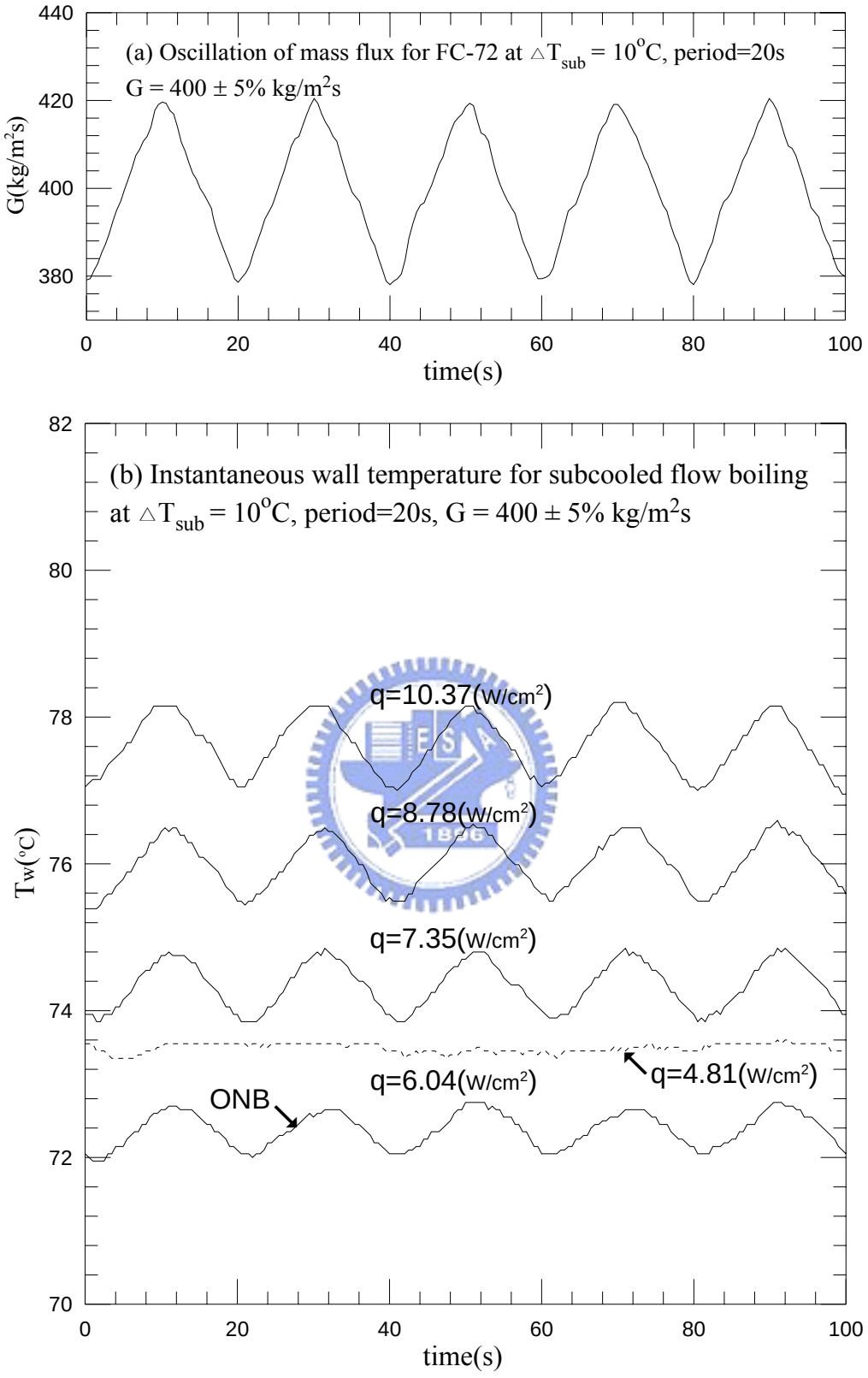

Fig. 5.40 Time variations of (a) imposed coolant mass flux and (b) copper plate temperature in transient oscillatory subcooled flow boiling for various imposed heat fluxes for G=400±5% kg/m^{2}s with t_p =20 sec.($\overline{q}_{ONB}$ =6.04 w/cm^2 at G =400 kg/m^{2}s)

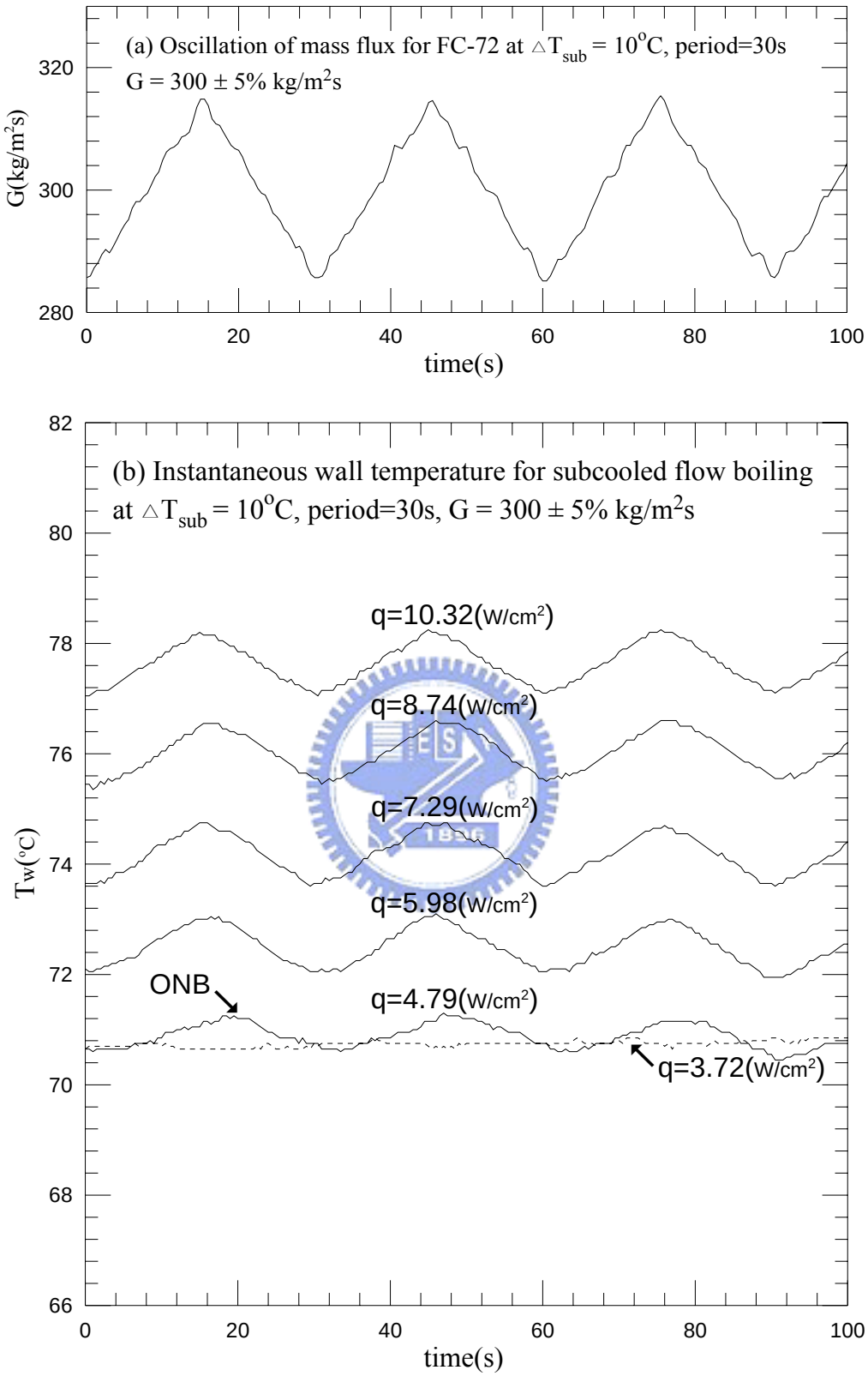

Fig. 5.41 Time variations of (a) imposed coolant mass flux and (b) copper plate temperature in transient oscillatory subcooled flow boiling for various imposed heat fluxes for G=300±5% kg/m^{2}s with t_p =30 sec.($\overline{q}_{ONB}$ =4.79 w/cm^2 at G =300 kg/m^{2}s)

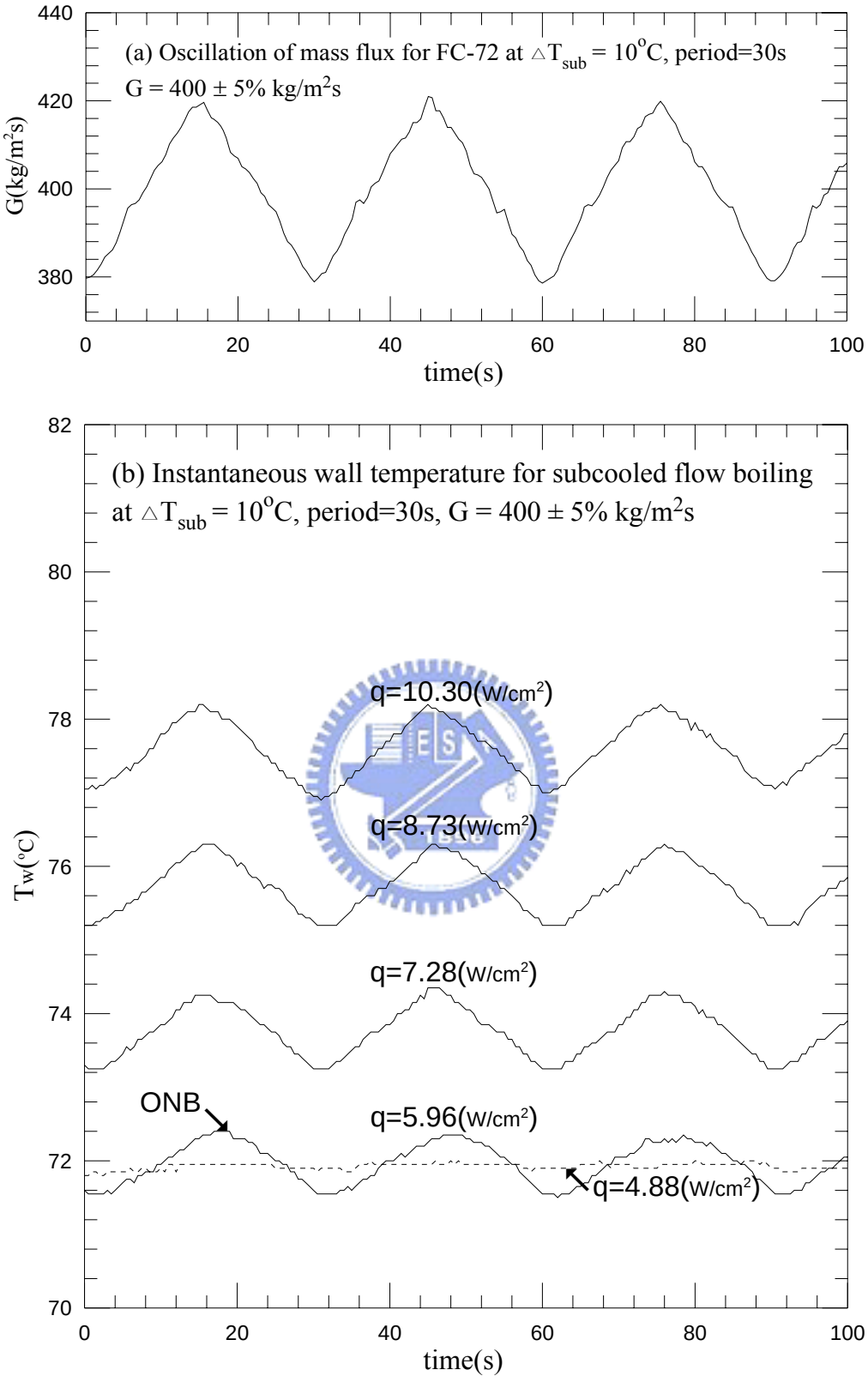

Fig. 5.42 Time variations of (a) imposed coolant mass flux and (b) copper plate temperature in transient oscillatory subcooled flow boiling for various imposed heat fluxes for G=400±5% kg/m^{2}s with t_p =30 sec.($\overline{q}_{ONB}$ =5.96 w/cm^2 at G =400 kg/m^{2}s)

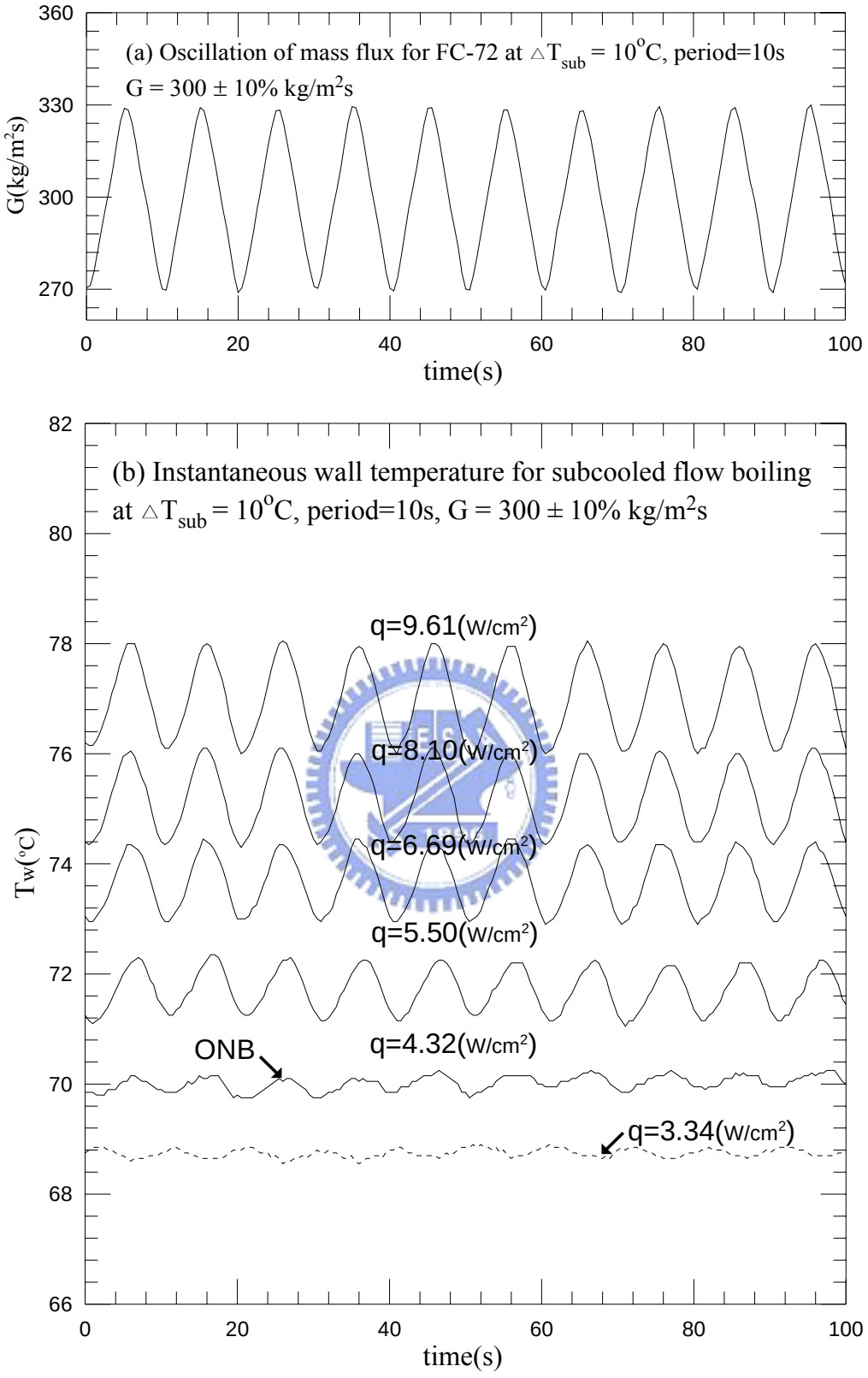

Fig. 5.43 Time variations of (a) imposed coolant mass flux and (b) copper plate temperature in transient oscillatory subcooled flow boiling for various imposed heat fluxes for G=300±10% kg/m^{2}s with t_p=10 sec.($\bar{q}_{ONB}$ =4.32 w/cm^2 at G =300 kg/m^{2}s)

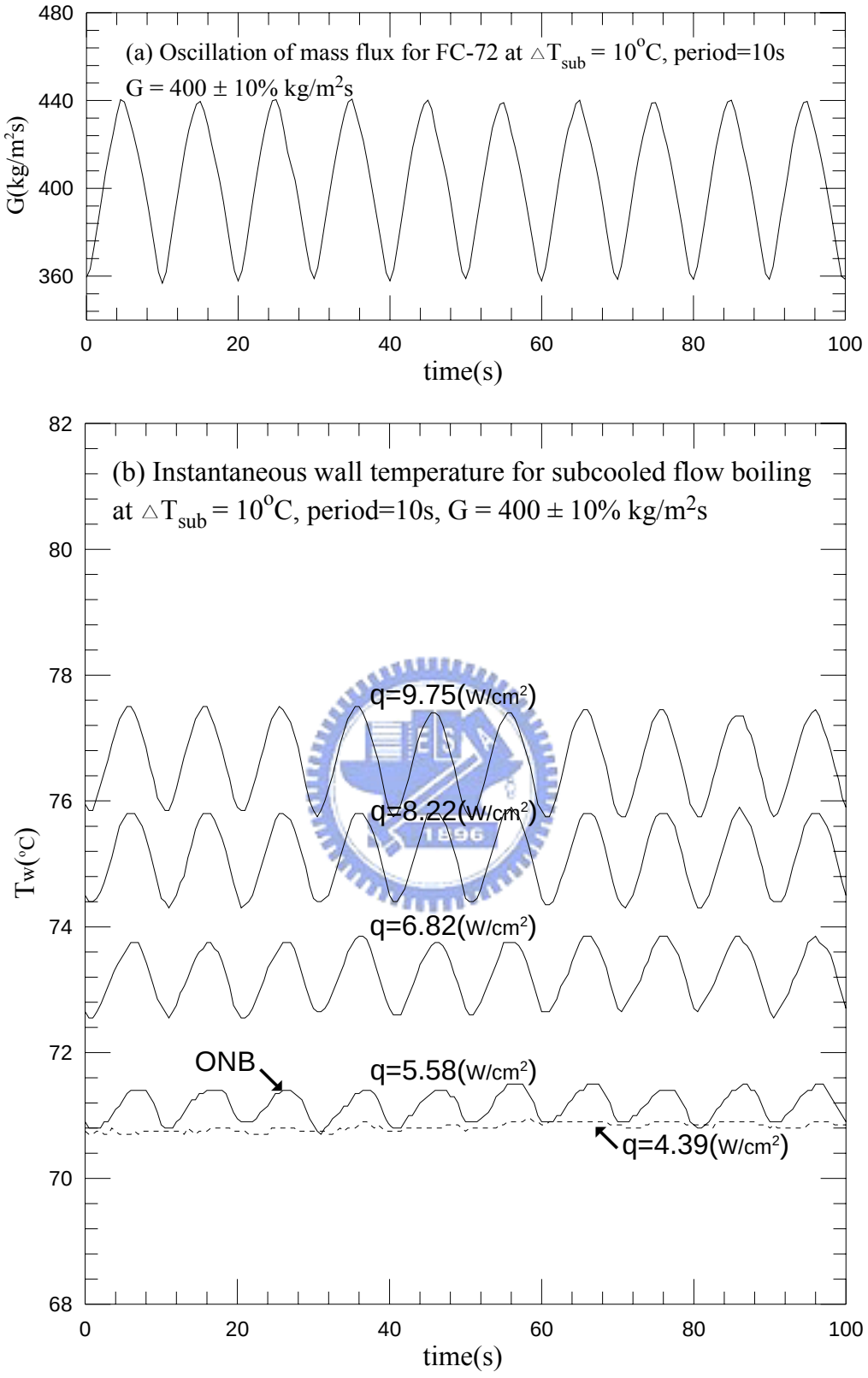

Fig. 5.44 Time variations of (a) imposed coolant mass flux and (b) copper plate temperature in transient oscillatory subcooled flow boiling for various imposed heat fluxes for G=400±10% kg/m^{2}s with t_p=10 sec.($\bar{q}_{ONB}$ =5.58 w/cm^2 at G =400 kg/m^{2}s)

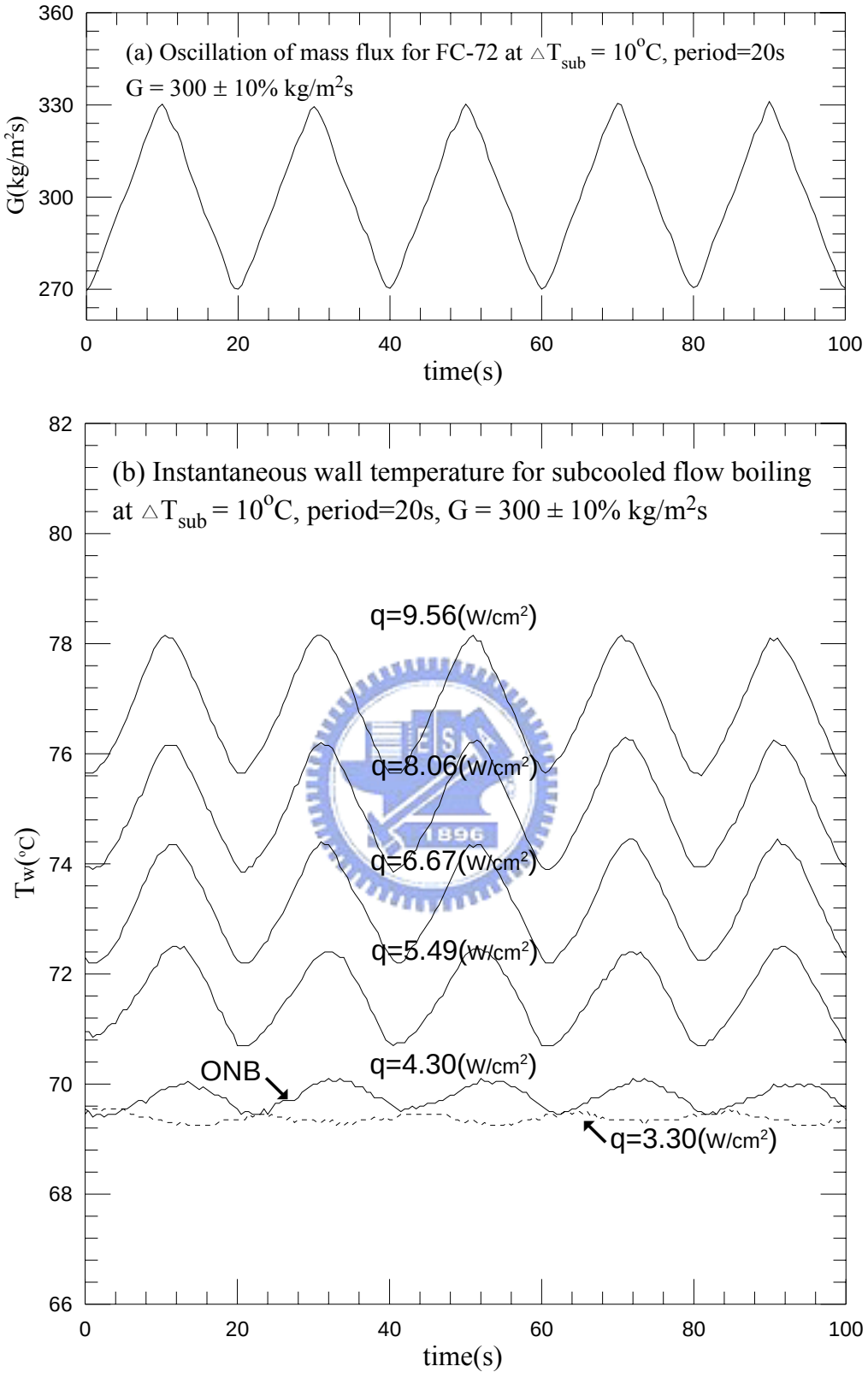

Fig. 5.45 Time variations of (a) imposed coolant mass flux and (b) copper plate temperature in transient oscillatory subcooled flow boiling for various imposed heat fluxes for G=300±10% kg/m^{2}s with t_p =20 sec.($\overline{q}_{ONB}$ =4.30 w/cm^2 at G =300 kg/m^{2}s)

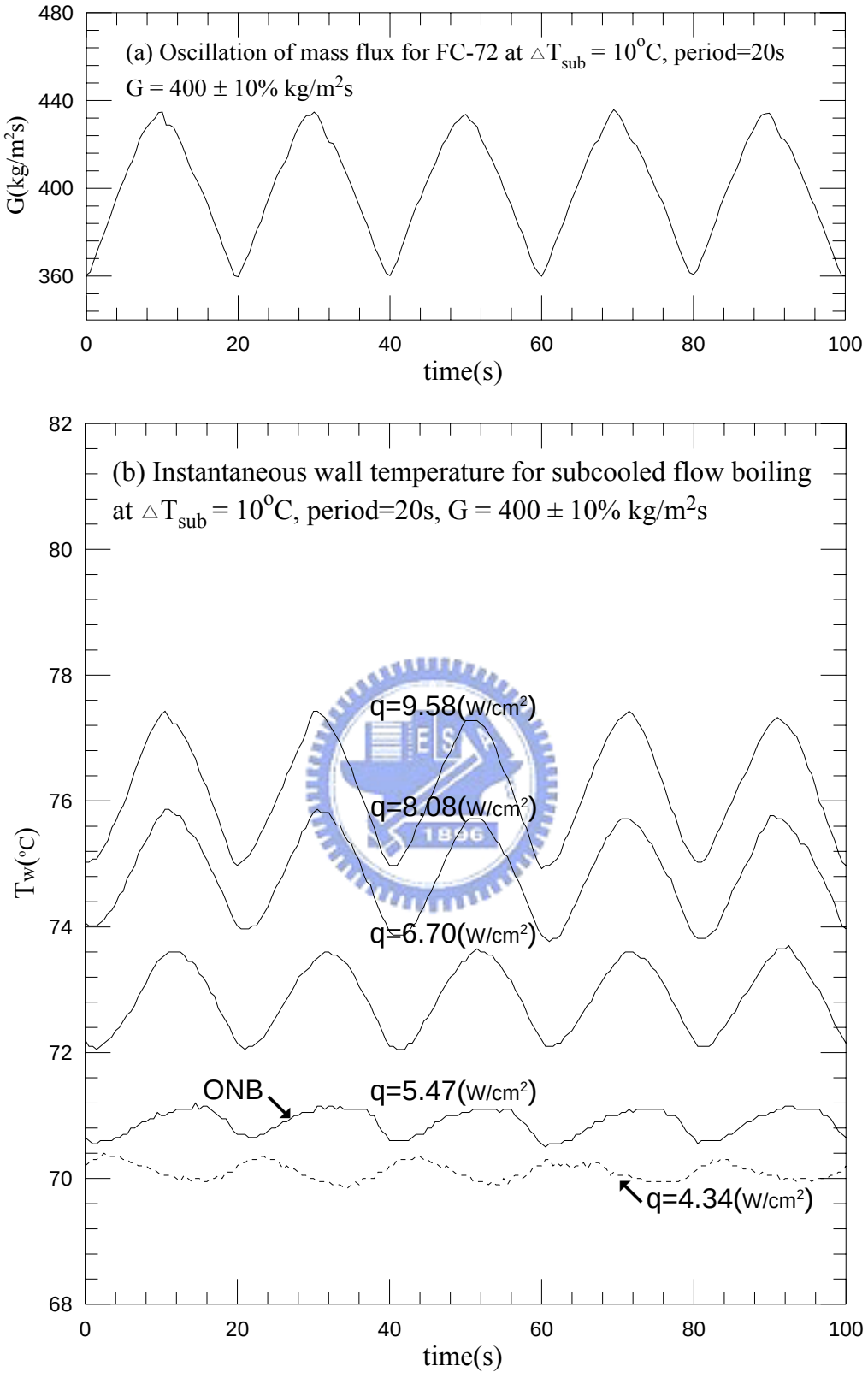

Fig. 5.46 Time variations of (a) imposed coolant mass flux and (b) copper plate temperature in transient oscillatory subcooled flow boiling for various imposed heat fluxes for G=400±10% kg/m^{2}s with t_p =20 sec.($\bar{q}_{ONB}$ =5.47 w/cm^2 at G =400 kg/m^{2}s)

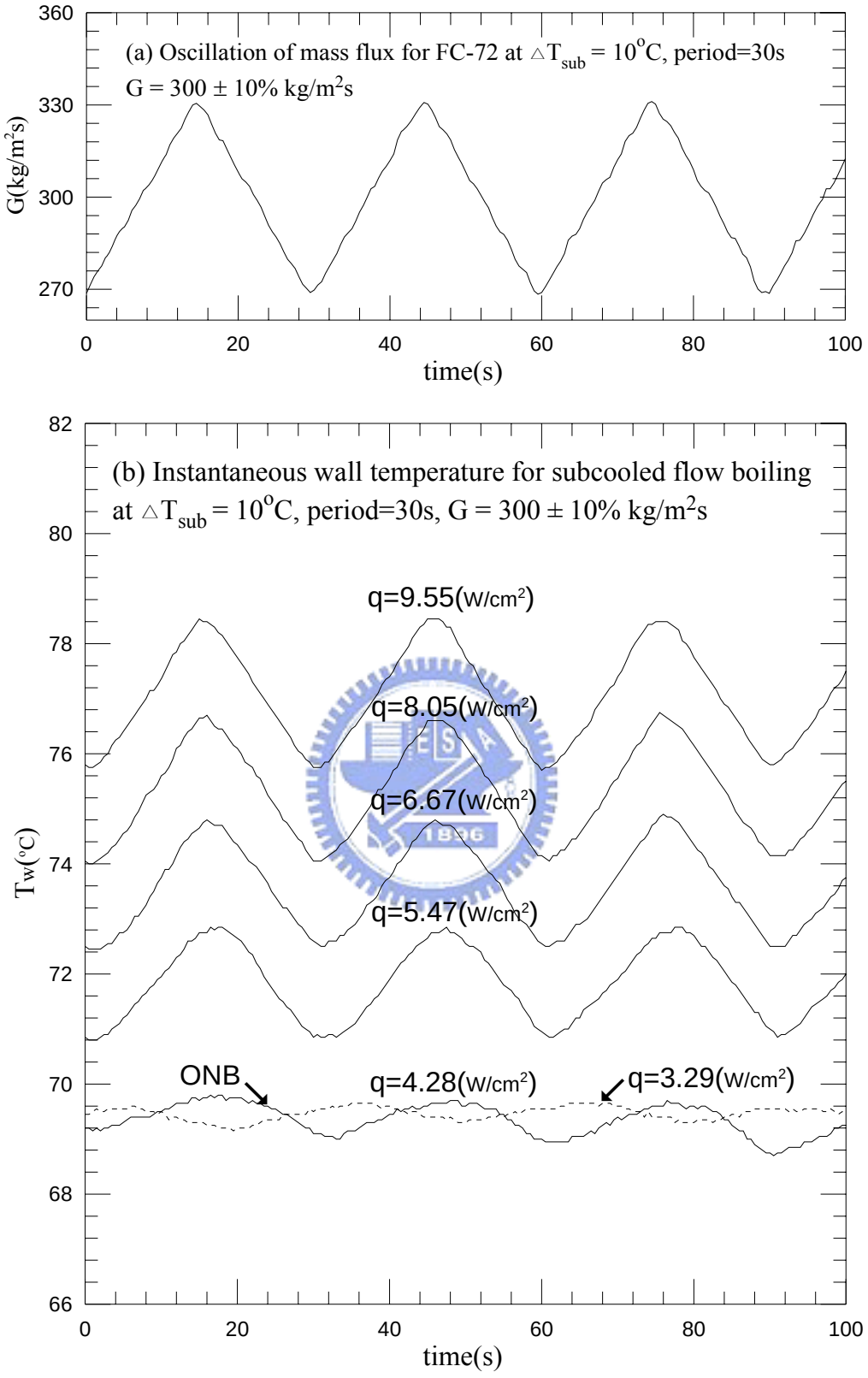

Fig. 5.47 Time variations of (a) imposed coolant mass flux and (b) copper plate temperature in transient oscillatory subcooled flow boiling for various imposed heat fluxes for G=300±10% kg/m^{2}s with t_p =30 sec.($\overline{q}_{ONB}$ =4.28 w/cm^2 at G =300 kg/m^{2}s)

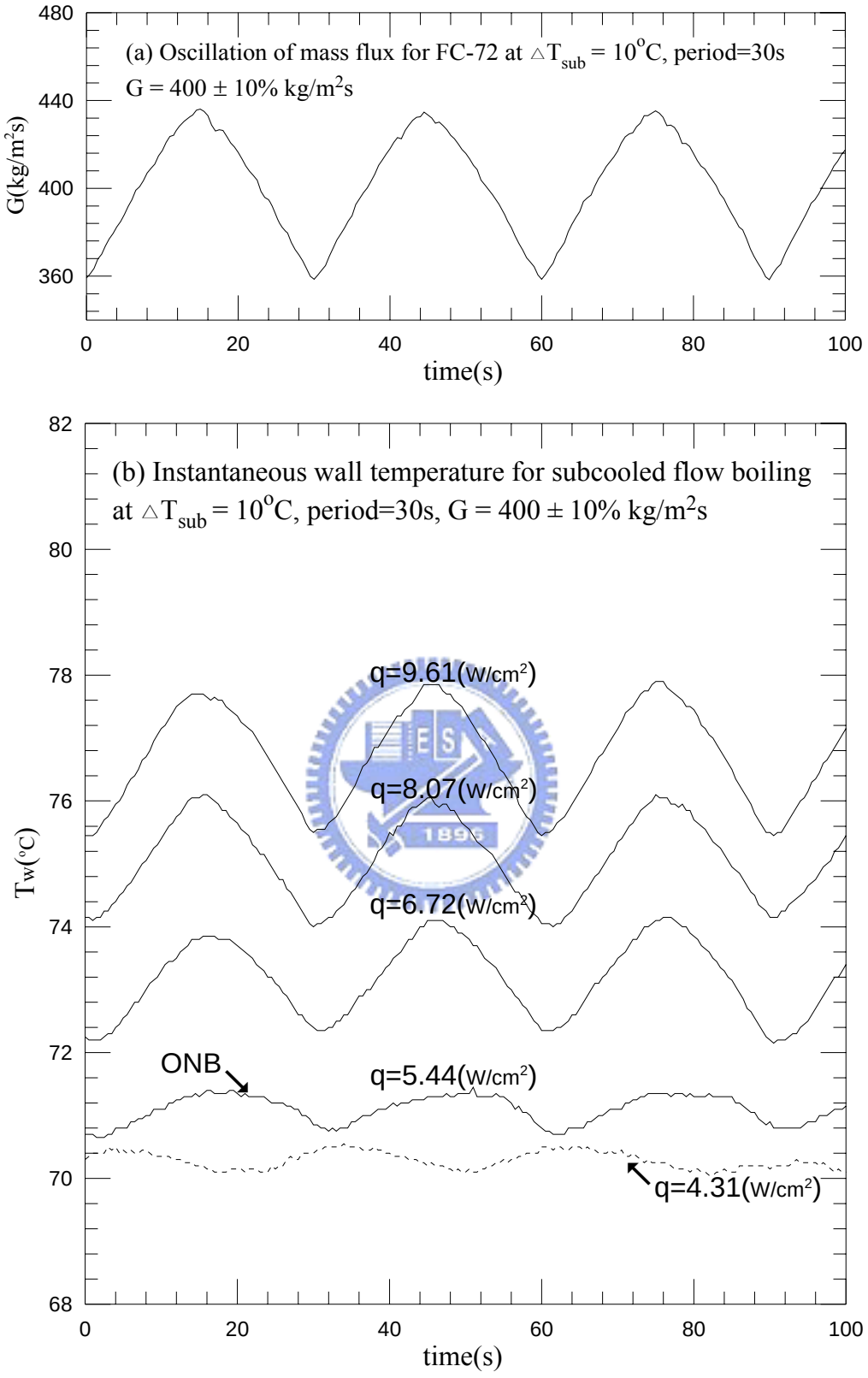

Fig. 5.48 Time variations of (a) imposed coolant mass flux and (b) copper plate temperature in transient oscillatory subcooled flow boiling for various imposed heat fluxes for G=400±10% kg/m^{2}s with t_p =30 sec.($\bar{q}_{ONB}$ =5.44 w/cm^2 at G =400 kg/m^{2}s)

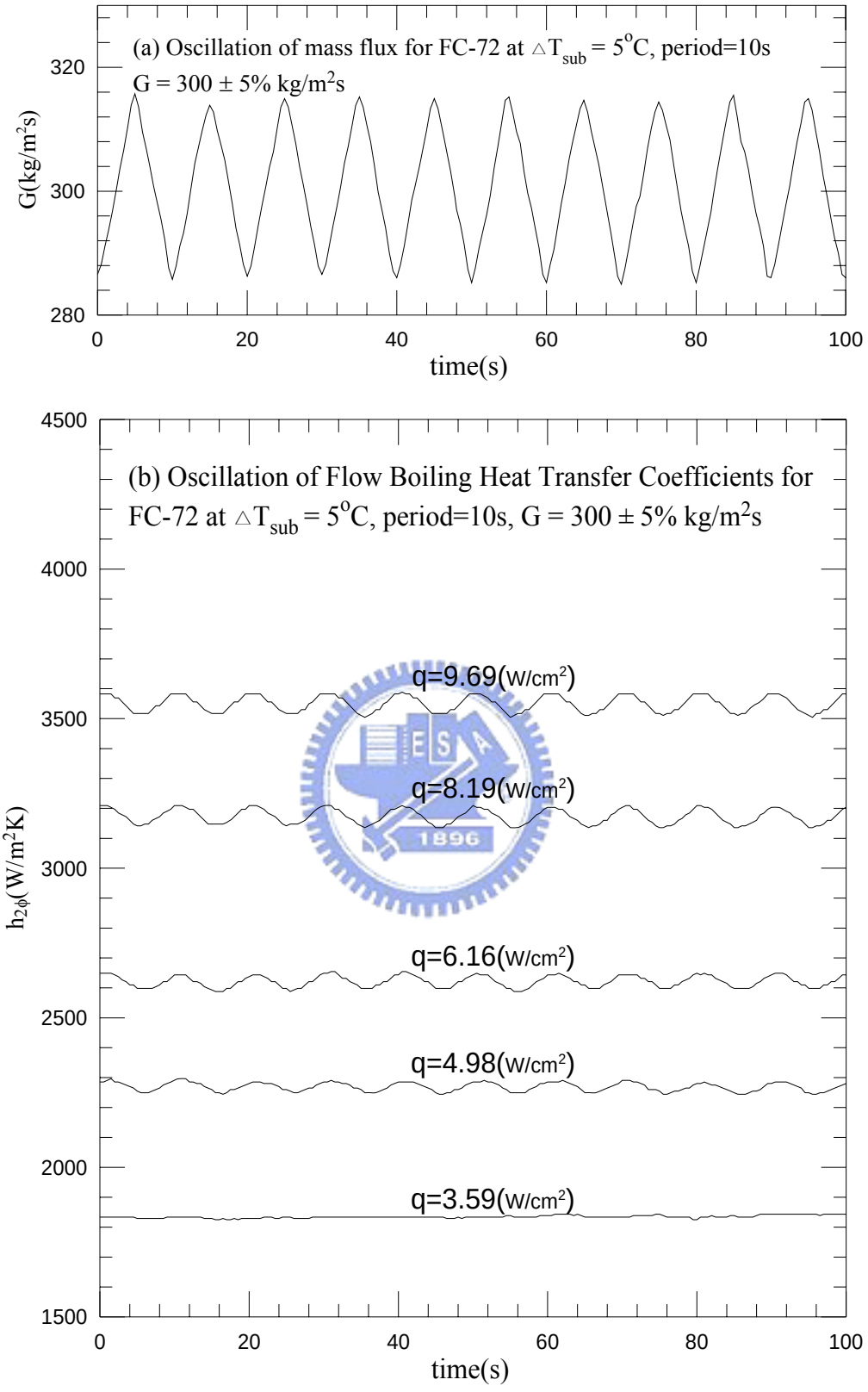

Fig. 5.49 Time variations of (a) imposed coolant mass flux and (b) flow boiling heat transfer coefficients in transient oscillatory subcooled flow boiling for various imposed heat fluxes for G=300±5% kg/m^{2}s with t_p=10 sec.

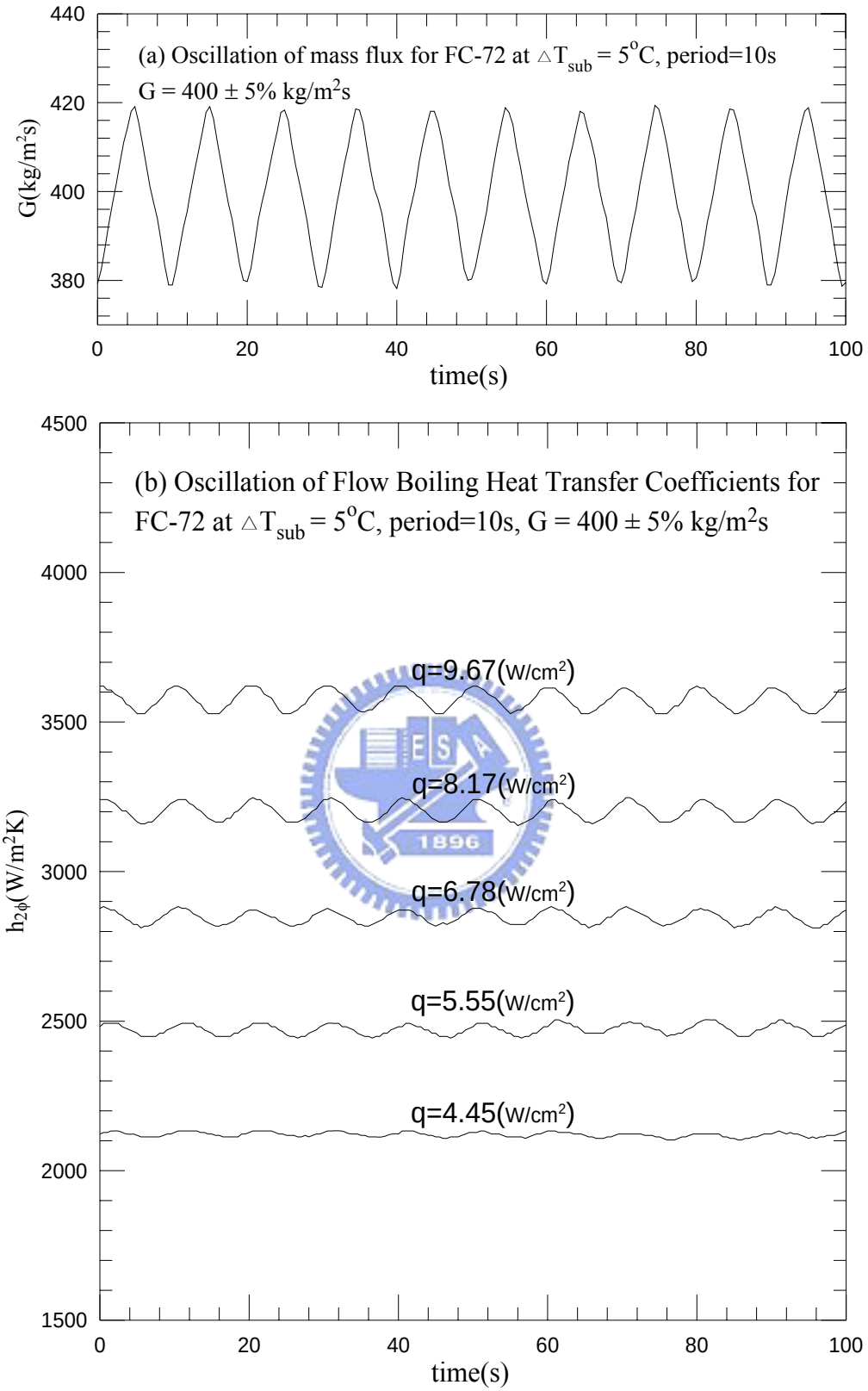

Fig. 5.50 Time variations of (a) imposed coolant mass flux and (b) flow boiling heat transfer coefficients in transient oscillatory subcooled flow boiling for various imposed heat fluxes for G=400±5% kg/m^{2}s with t_p=10 sec.

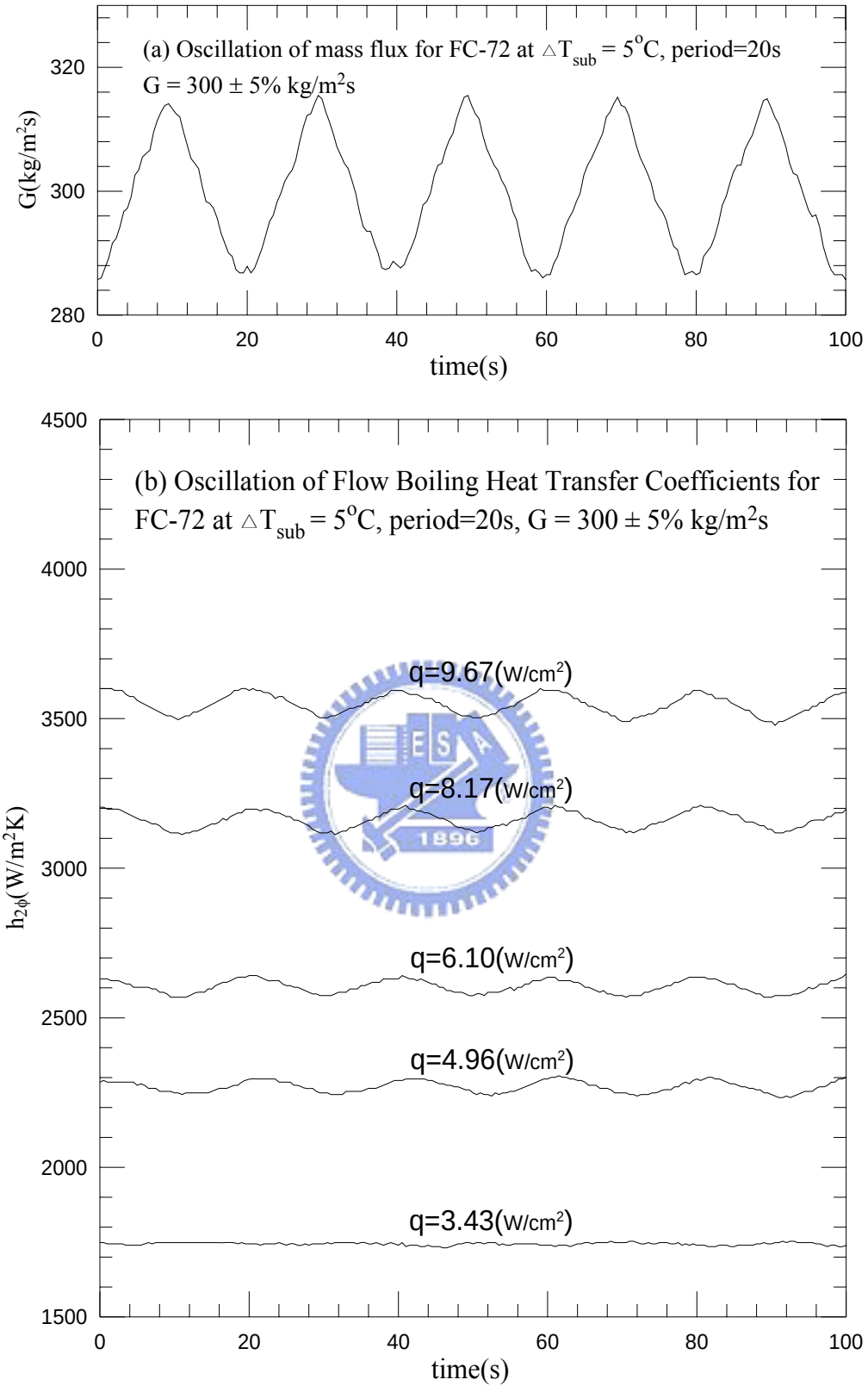

Fig. 5.51 Time variations of (a) imposed coolant mass flux and (b) flow boiling heat transfer coefficients in transient oscillatory subcooled flow boiling for various imposed heat fluxes for G=300±5% kg/m^{2}s with t_p=20 sec.

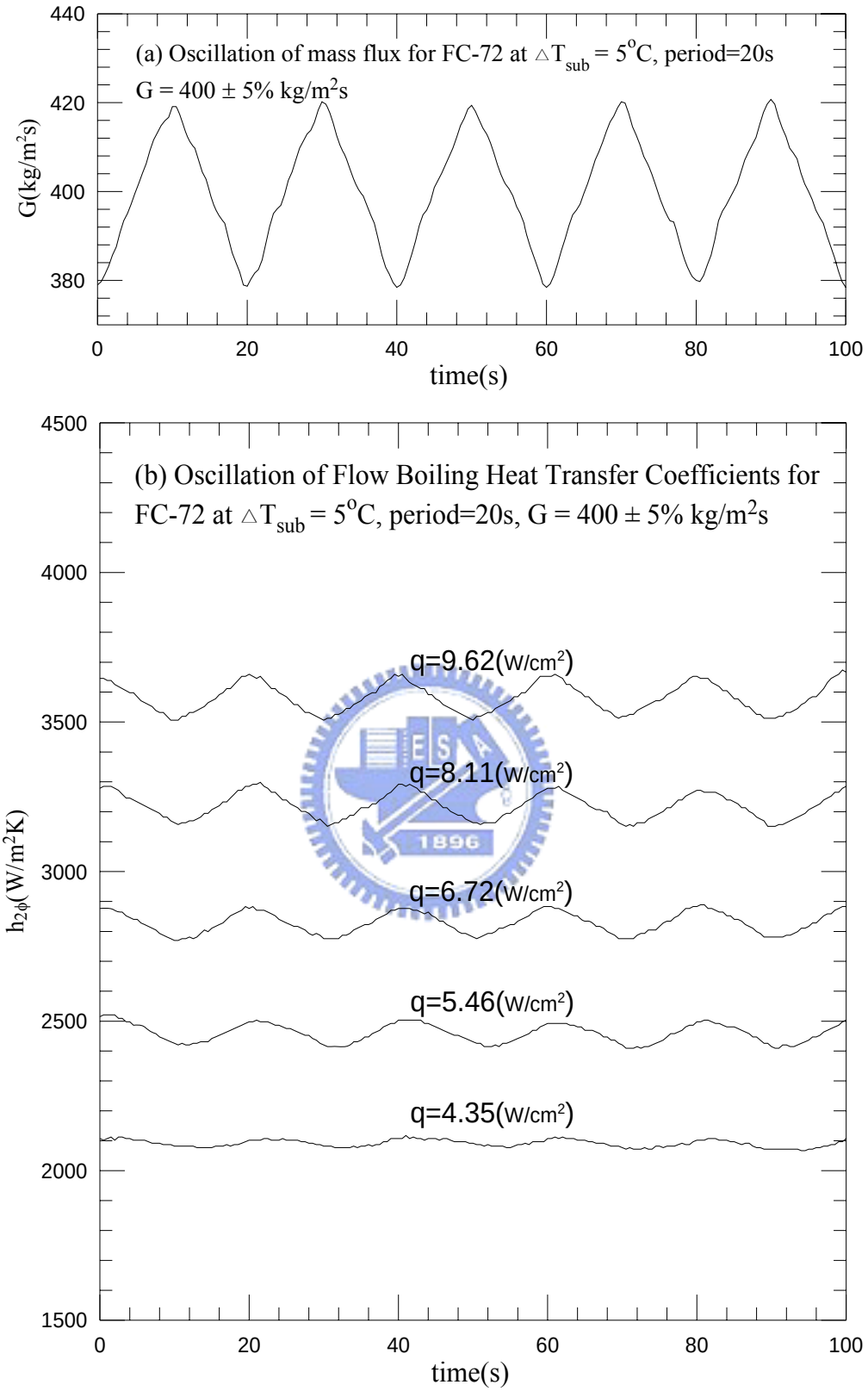

Fig. 5.52 Time variations of (a) imposed coolant mass flux and (b) flow boiling heat transfer coefficients in transient oscillatory subcooled flow boiling for various imposed heat fluxes for G=400±5% kg/m^{2}s with t_p=20 sec.

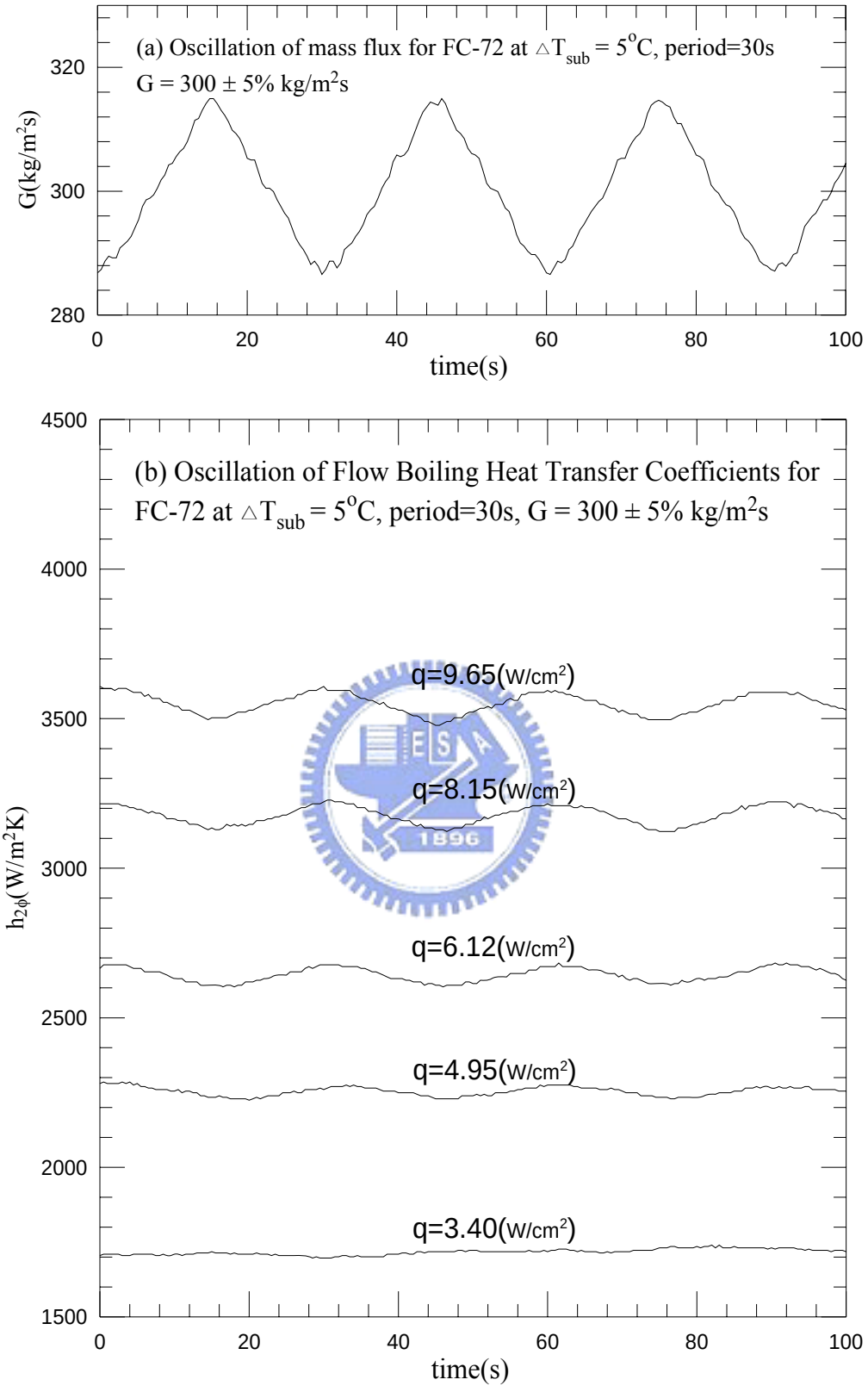

Fig. 5.53 Time variations of (a) imposed coolant mass flux and (b) flow boiling heat transfer coefficients in transient oscillatory subcooled flow boiling for various imposed heat fluxes for G=300±5% kg/m^{2}s with t_p=30 sec.

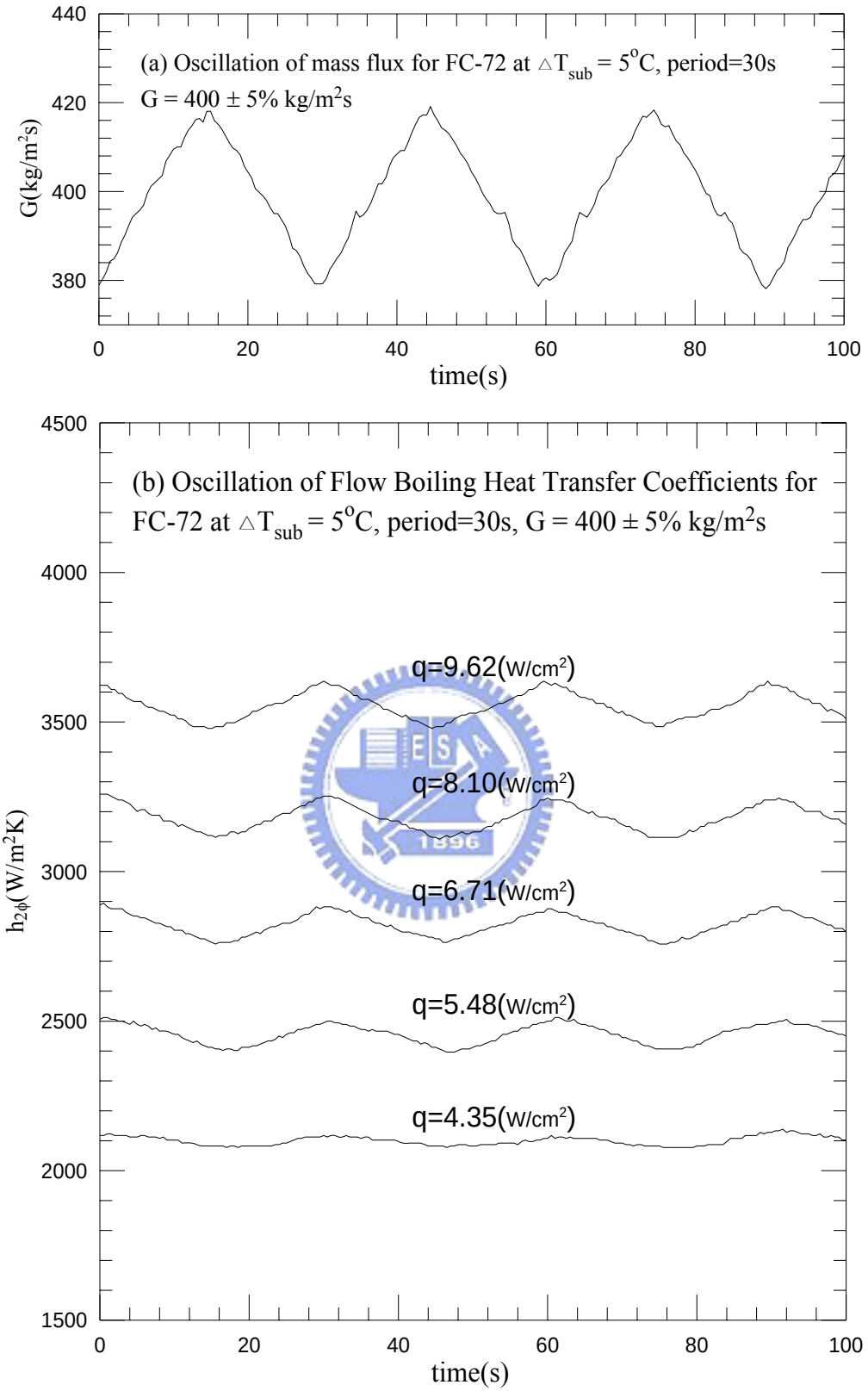

Fig. 5.54 Time variations of (a) imposed coolant mass flux and (b) flow boiling heat transfer coefficients in transient oscillatory subcooled flow boiling for various imposed heat fluxes for G=400±5% kg/m^{2}s with t_p=30 sec.

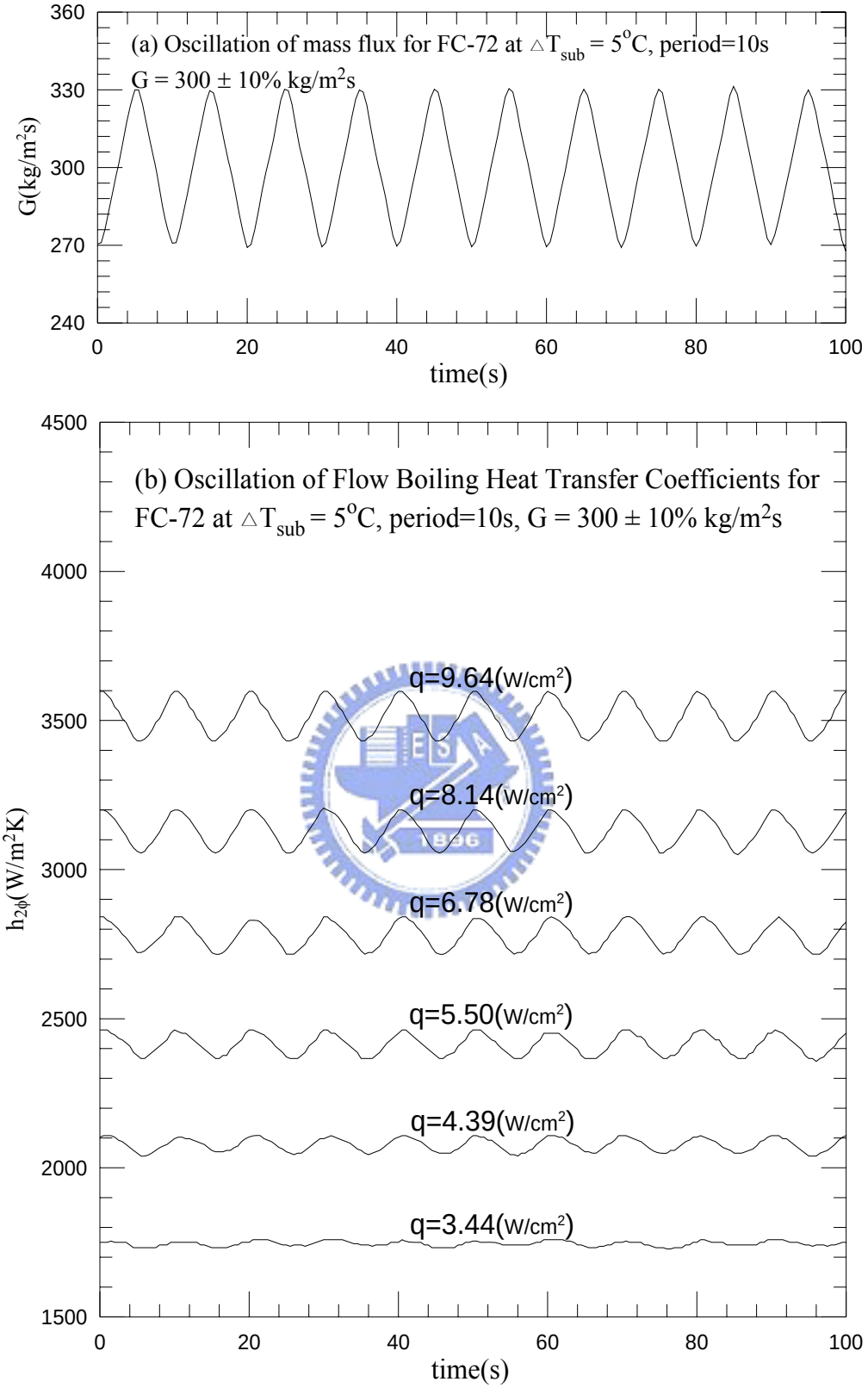

Fig. 5.55 Time variations of (a) imposed coolant mass flux and (b) flow boiling heat transfer coefficients in transient oscillatory subcooled flow boiling for various imposed heat fluxes for G=300±10% kg/m^{2}s with t_p=10 sec.

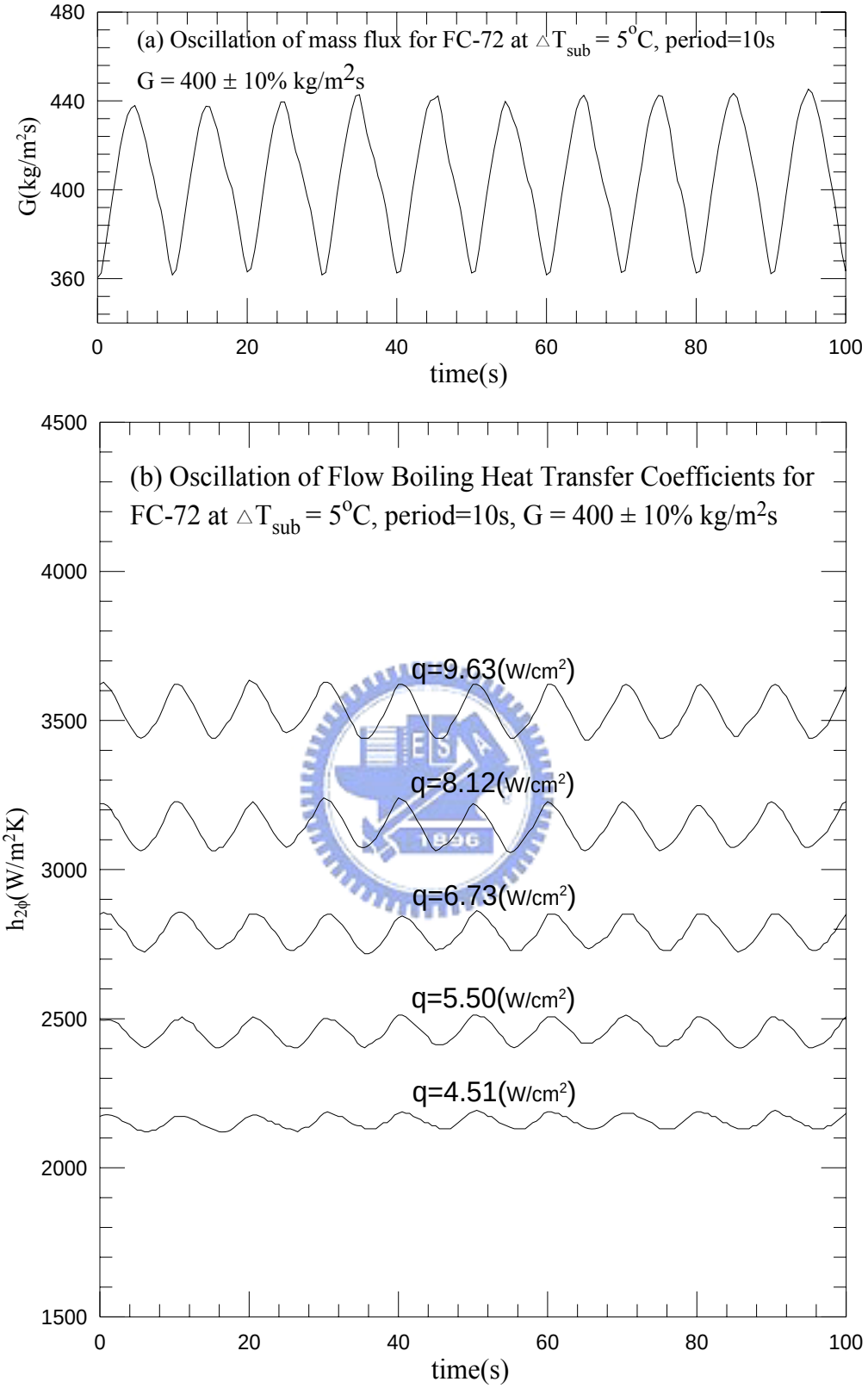

Fig. 5.56 Time variations of (a) imposed coolant mass flux and (b) flow boiling heat transfer coefficients in transient oscillatory subcooled flow boiling for various imposed heat fluxes for G=400±10% kg/m^{2}s with t_p=10 sec.

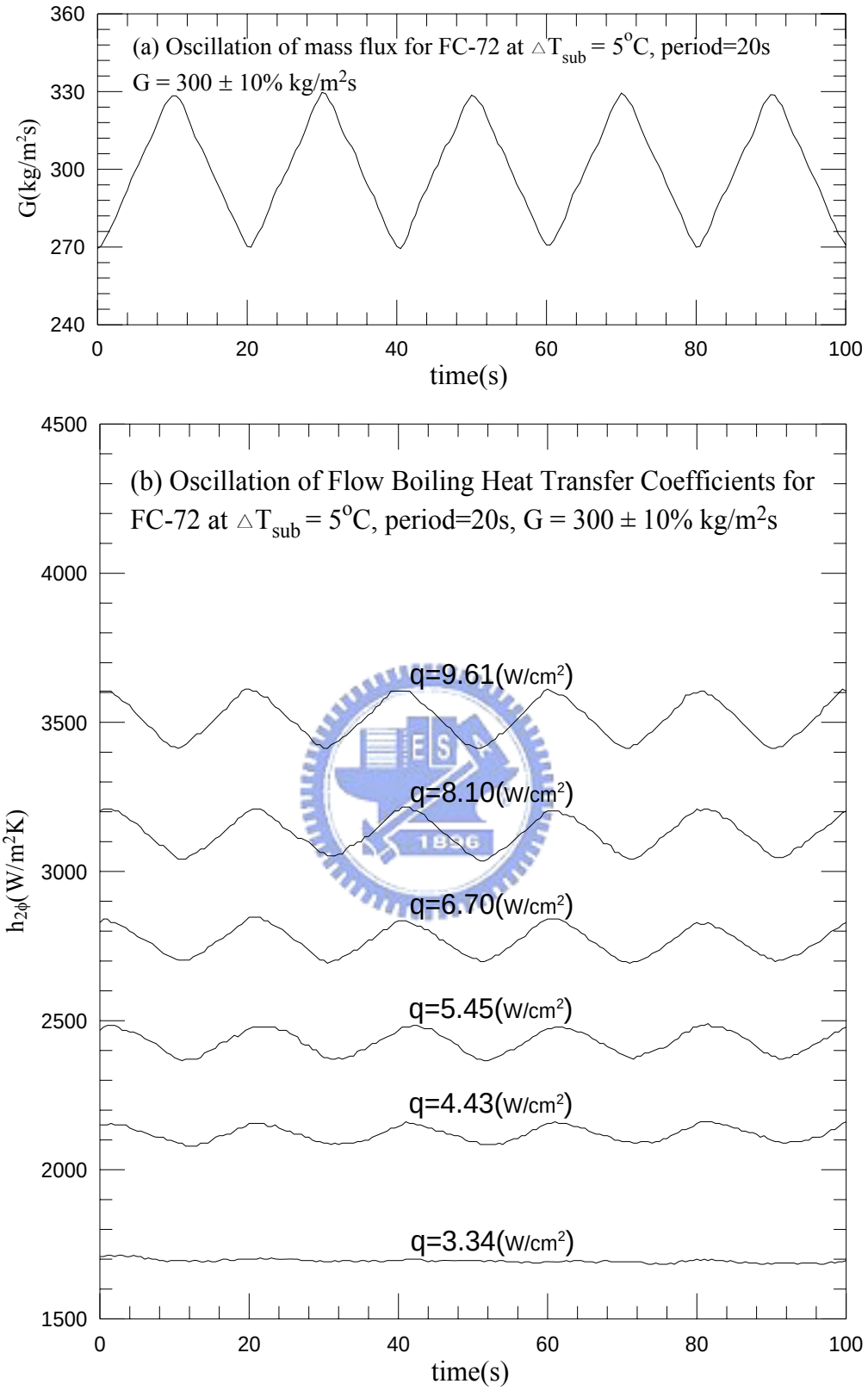

Fig. 5.57 Time variations of (a) imposed coolant mass flux and (b) flow boiling heat transfer coefficients in transient oscillatory subcooled flow boiling for various imposed heat fluxes for G=300±10% kg/m^{2}s with t_p=20 sec.

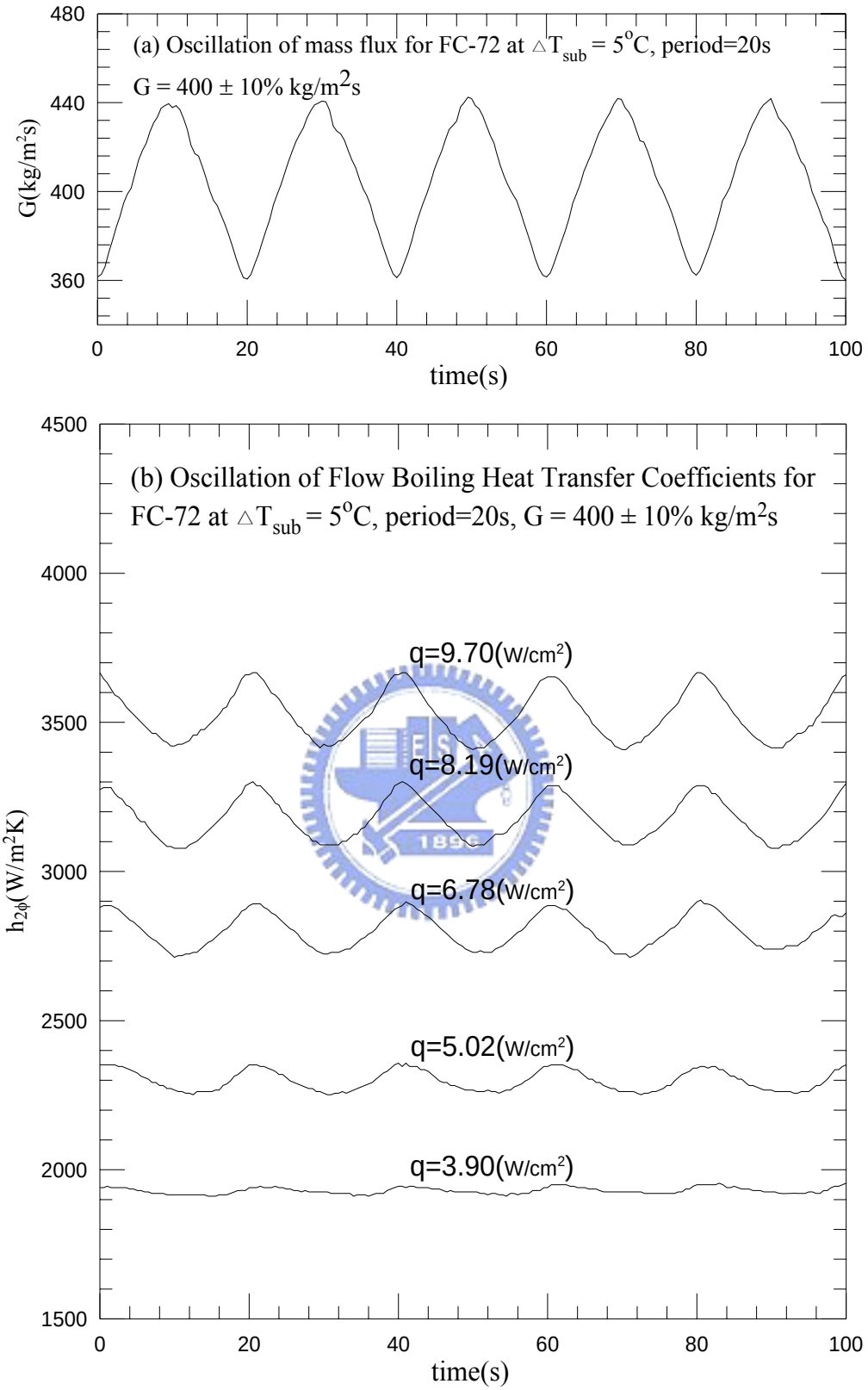

Fig. 5.58 Time variations of (a) imposed coolant mass flux and (b) flow boiling heat transfer coefficients in transient oscillatory subcooled flow boiling for various imposed heat fluxes for G=400±10% kg/m^{2}s with t_p=20 sec.

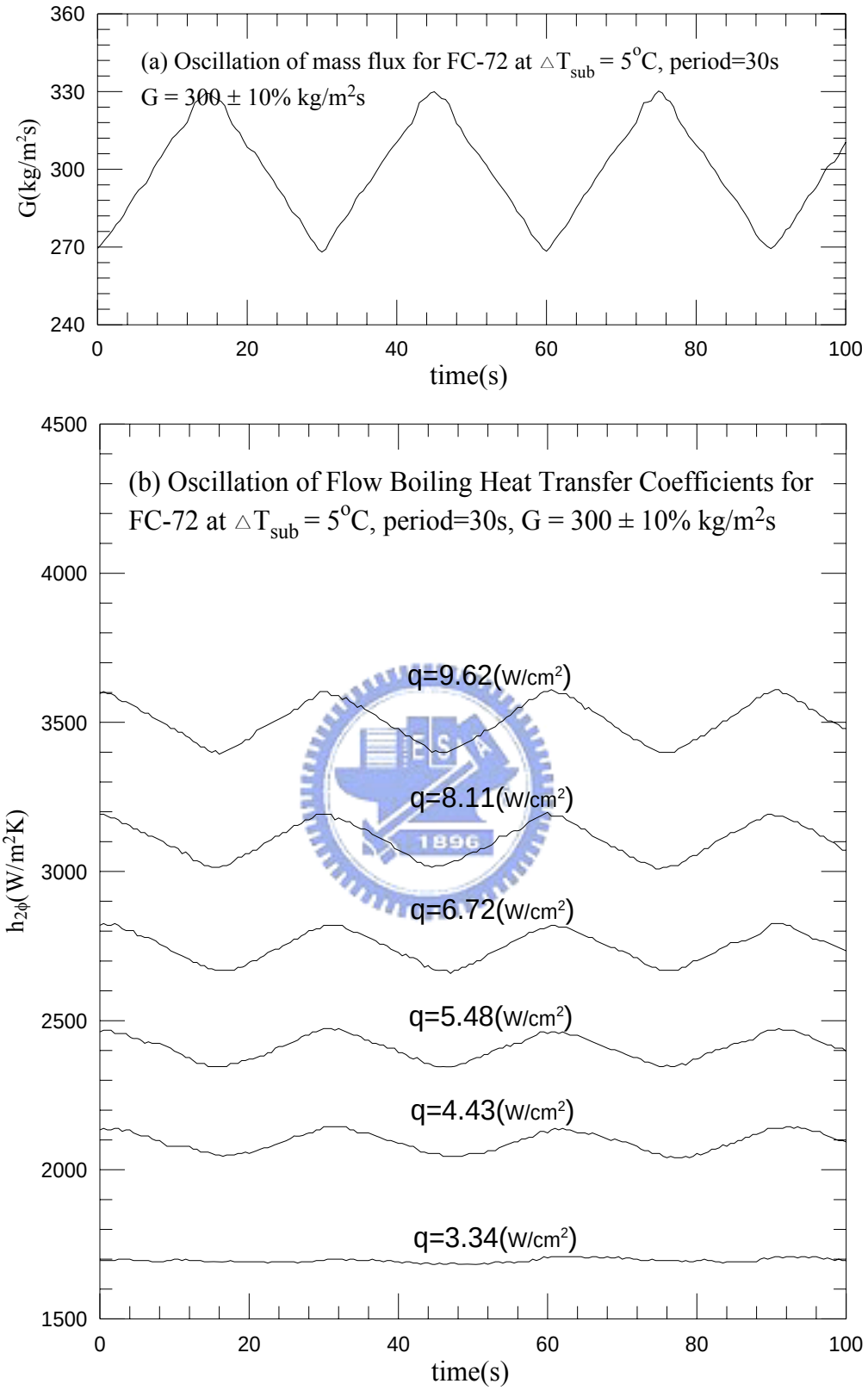

Fig. 5.59 Time variations of (a) imposed coolant mass flux and (b) flow boiling heat transfer coefficients in transient oscillatory subcooled flow boiling for various imposed heat fluxes for G=300±10% kg/m^{2}s with t_p=30 sec.

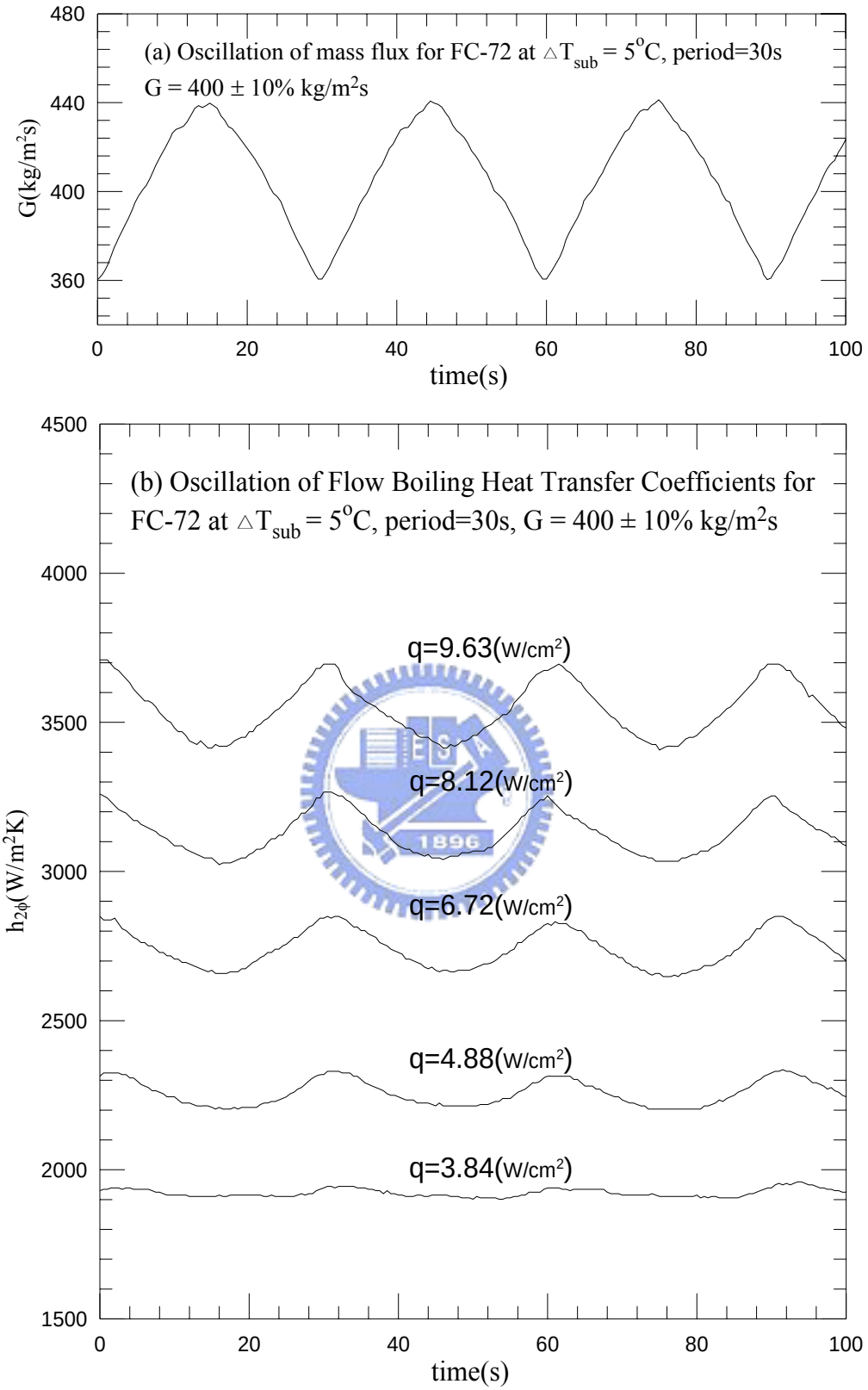

Fig. 5.60 Time variations of (a) imposed coolant mass flux and (b) flow boiling heat transfer coefficients in transient oscillatory subcooled flow boiling for various imposed heat fluxes for G=400±10% kg/m^{2}s with t_p=30 sec.

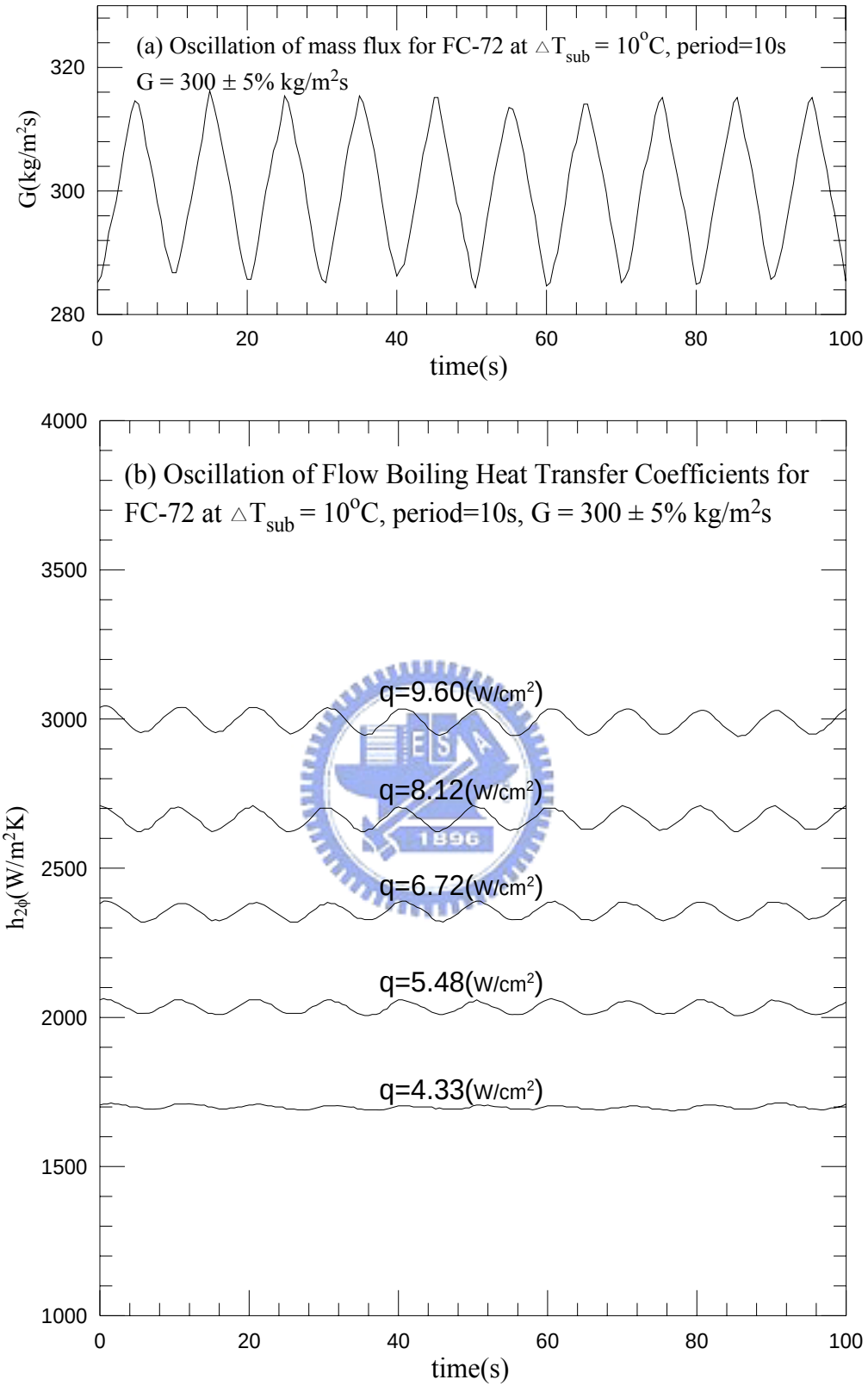

Fig. 5.61 Time variations of (a) imposed coolant mass flux and (b) flow boiling heat transfer coefficients in transient oscillatory subcooled flow boiling for various imposed heat fluxes for G=300±5% kg/m^{2}s with t_p=10 sec.

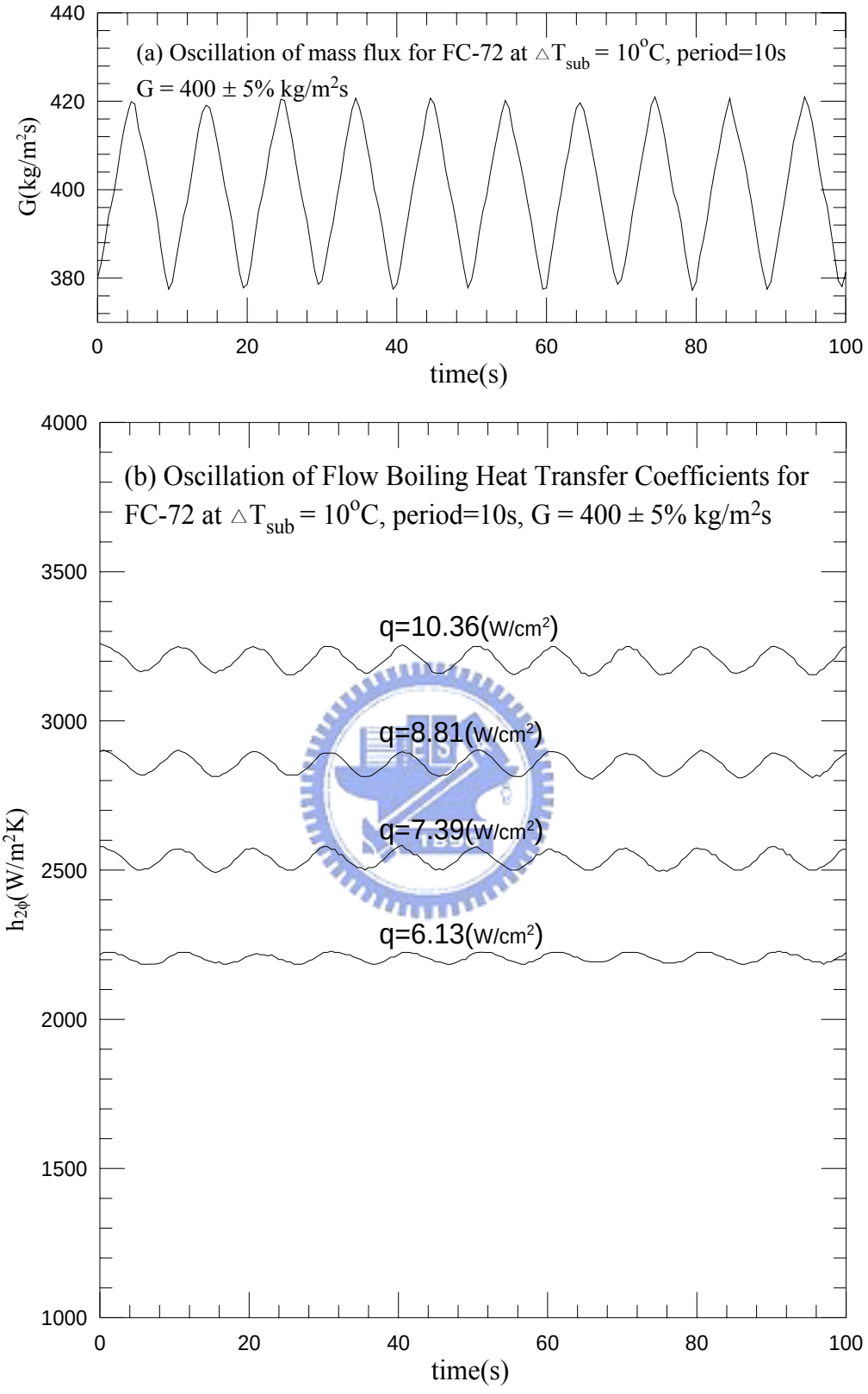

Fig. 5.62 Time variations of (a) imposed coolant mass flux and (b) flow boiling heat transfer coefficients in transient oscillatory subcooled flow boiling for various imposed heat fluxes for G=400±5% kg/m^{2}s with t_p=10 sec.

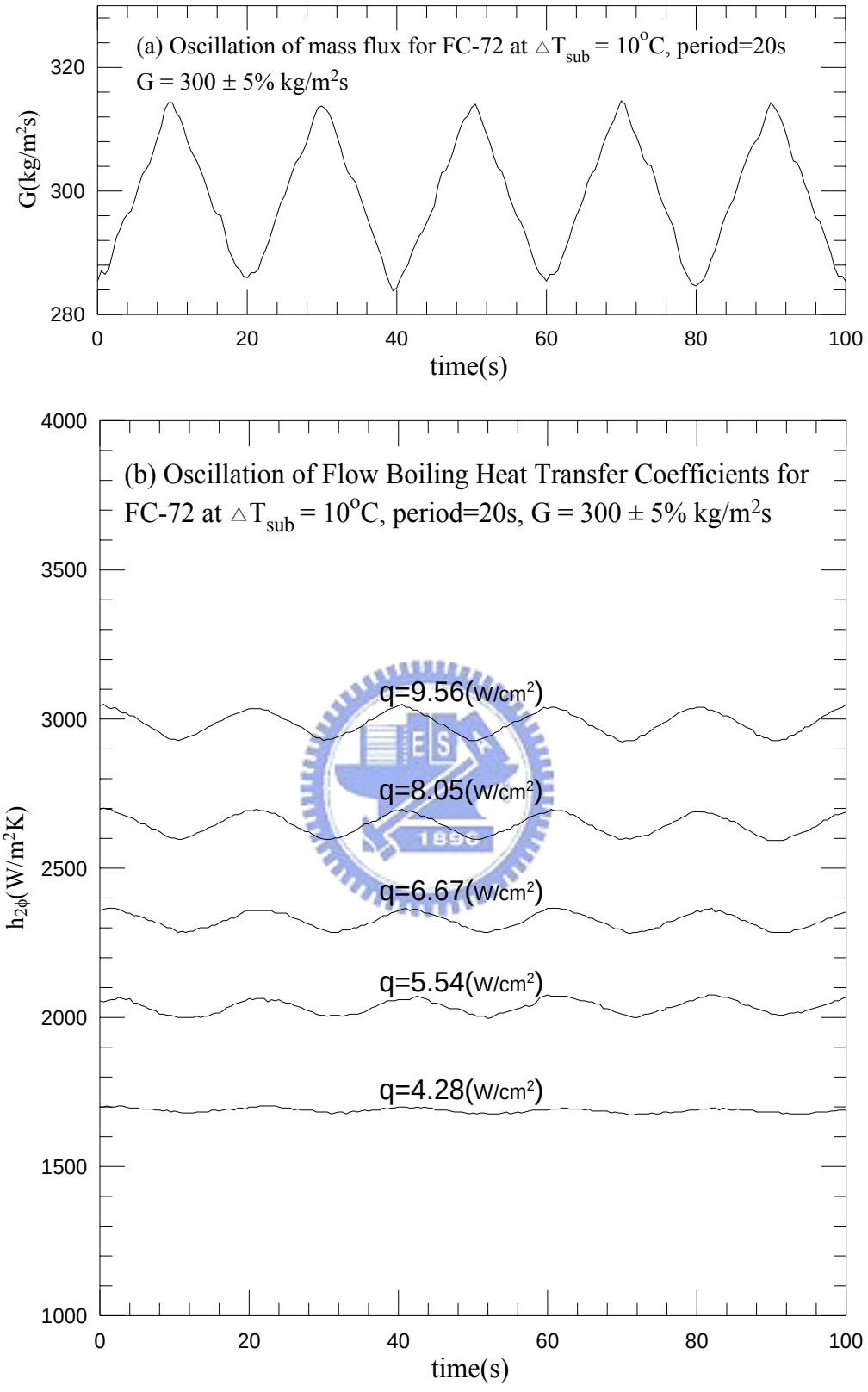

Fig. 5.63 Time variations of (a) imposed coolant mass flux and (b) flow boiling heat transfer coefficients in transient oscillatory subcooled flow boiling for various imposed heat fluxes for G=300±5% kg/m^{2}s with t_p=20 sec.

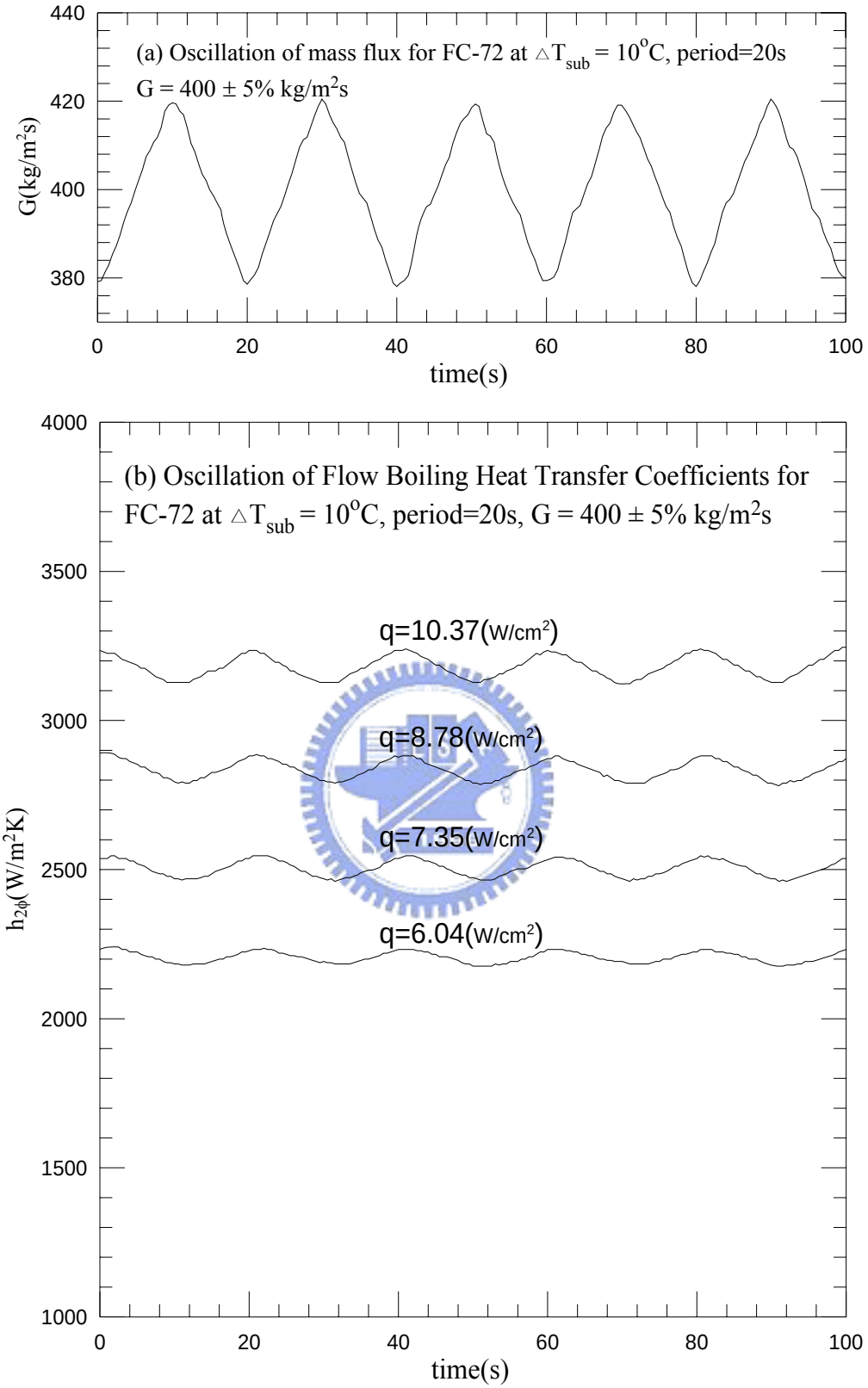

Fig. 5.64 Time variations of (a) imposed coolant mass flux and (b) flow boiling heat transfer coefficients in transient oscillatory subcooled flow boiling for various imposed heat fluxes for G=400±5% kg/m^{2}s with t_p=20 sec.

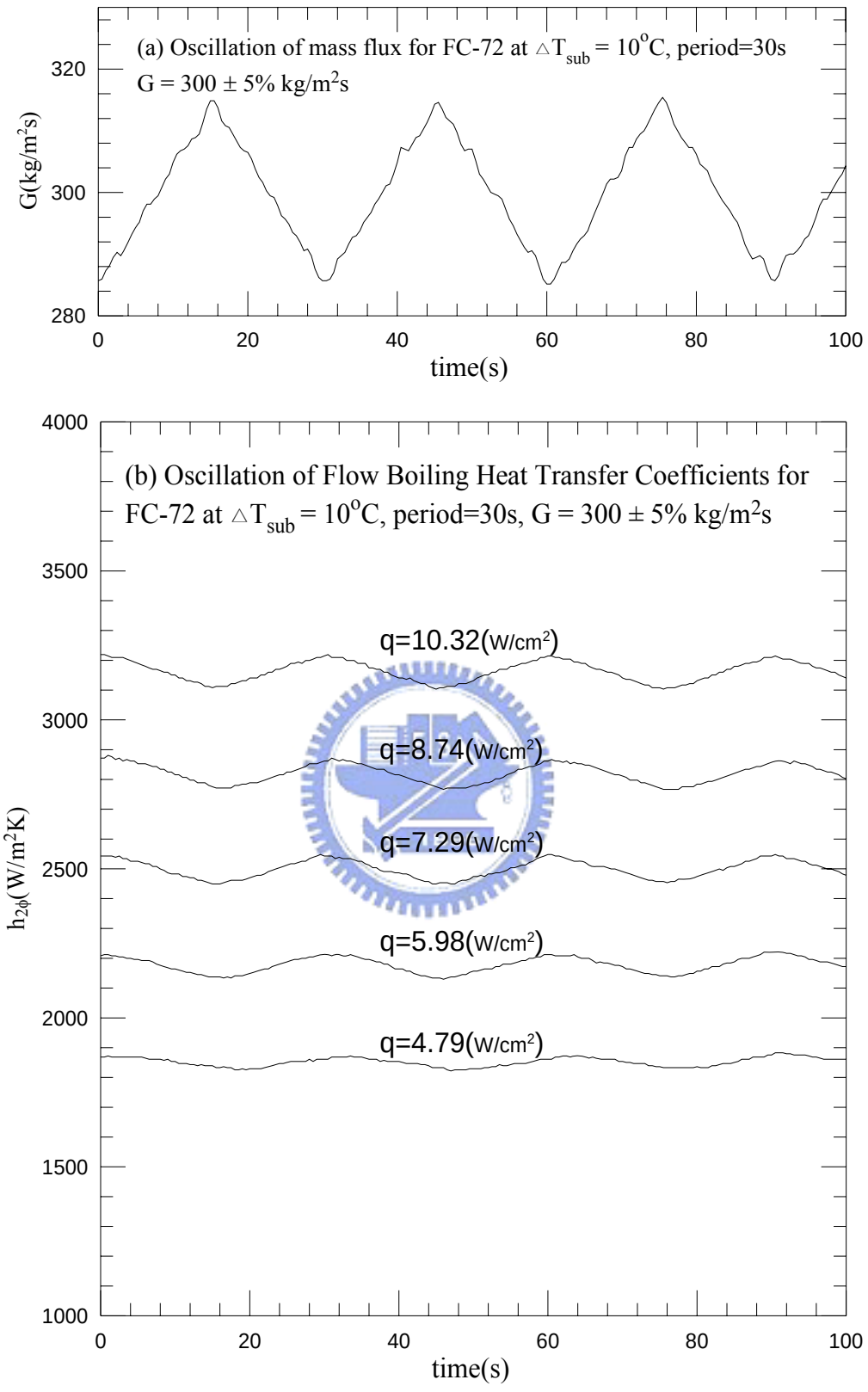

Fig. 5.65 Time variations of (a) imposed coolant mass flux and (b) flow boiling heat transfer coefficients in transient oscillatory subcooled flow boiling for various imposed heat fluxes for G=300±5% kg/m^{2}s with t_p=30 sec.

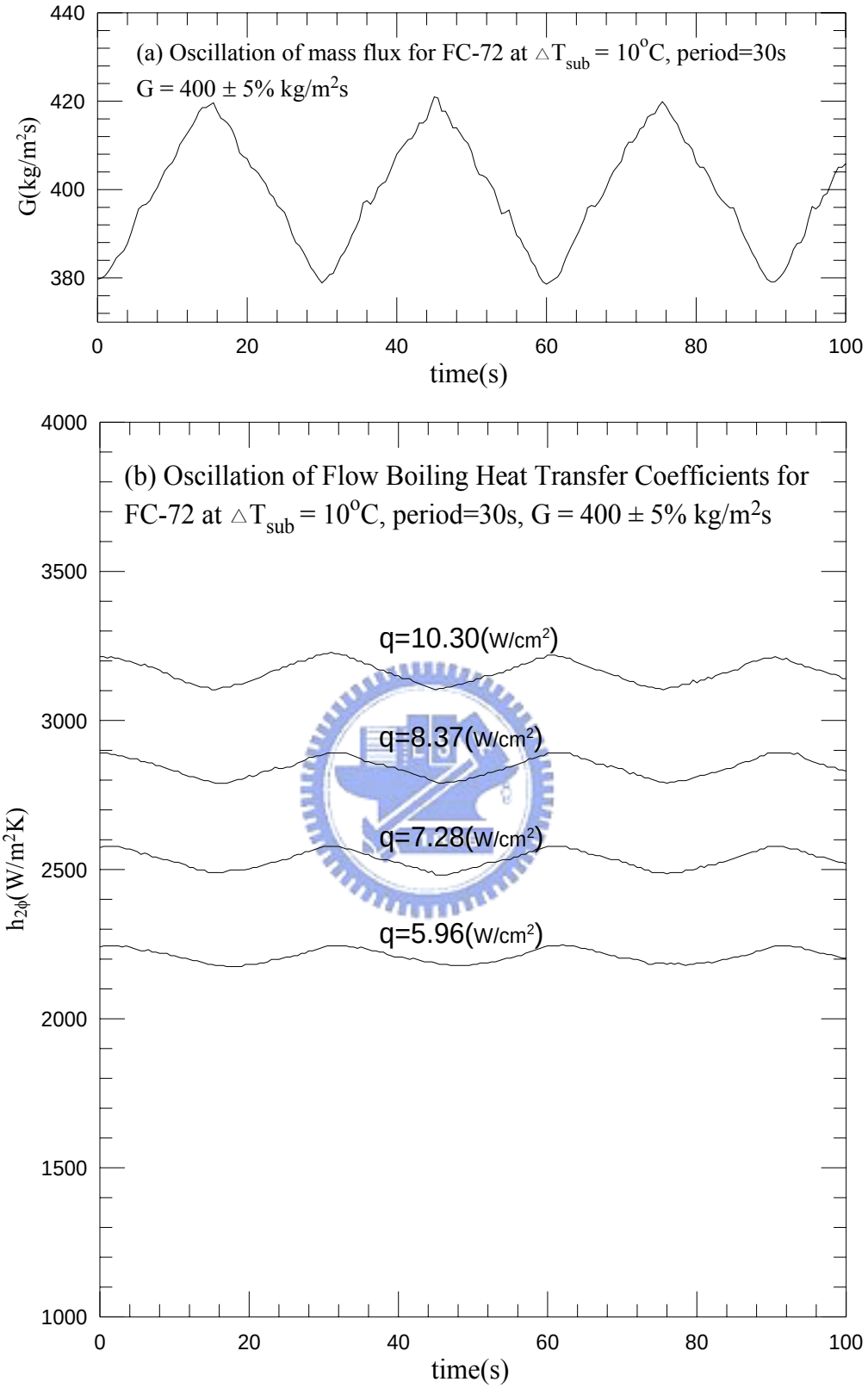

Fig. 5.66 Time variations of (a) imposed coolant mass flux and (b) flow boiling heat transfer coefficients in transient oscillatory subcooled flow boiling for various imposed heat fluxes for G=400±5% kg/m^{2}s with t_p=30 sec.

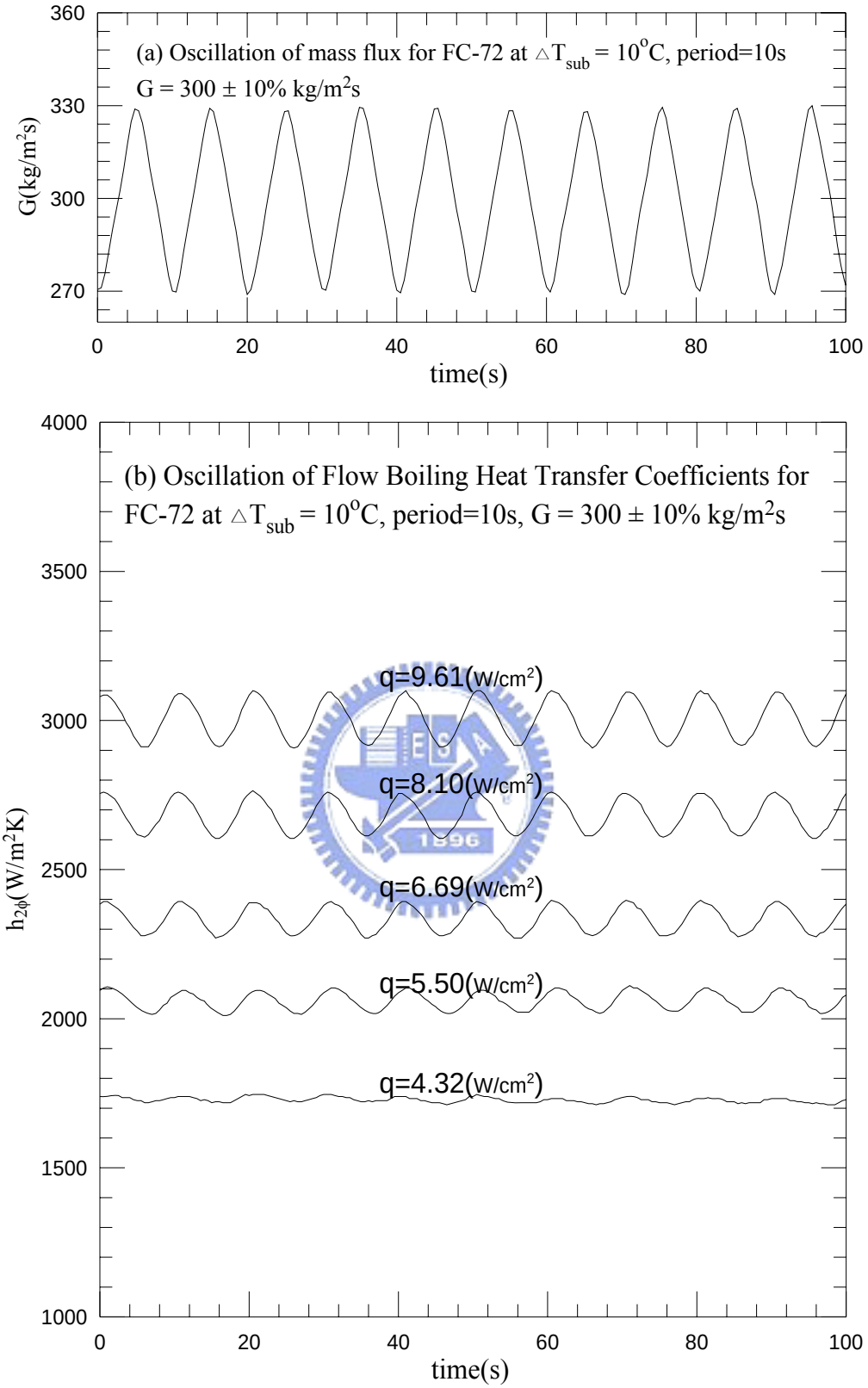

Fig. 5.67 Time variations of (a) imposed coolant mass flux and (b) flow boiling heat transfer coefficients in transient oscillatory subcooled flow boiling for various imposed heat fluxes for G=300±10% kg/m^{2}s with t_p=10 sec.

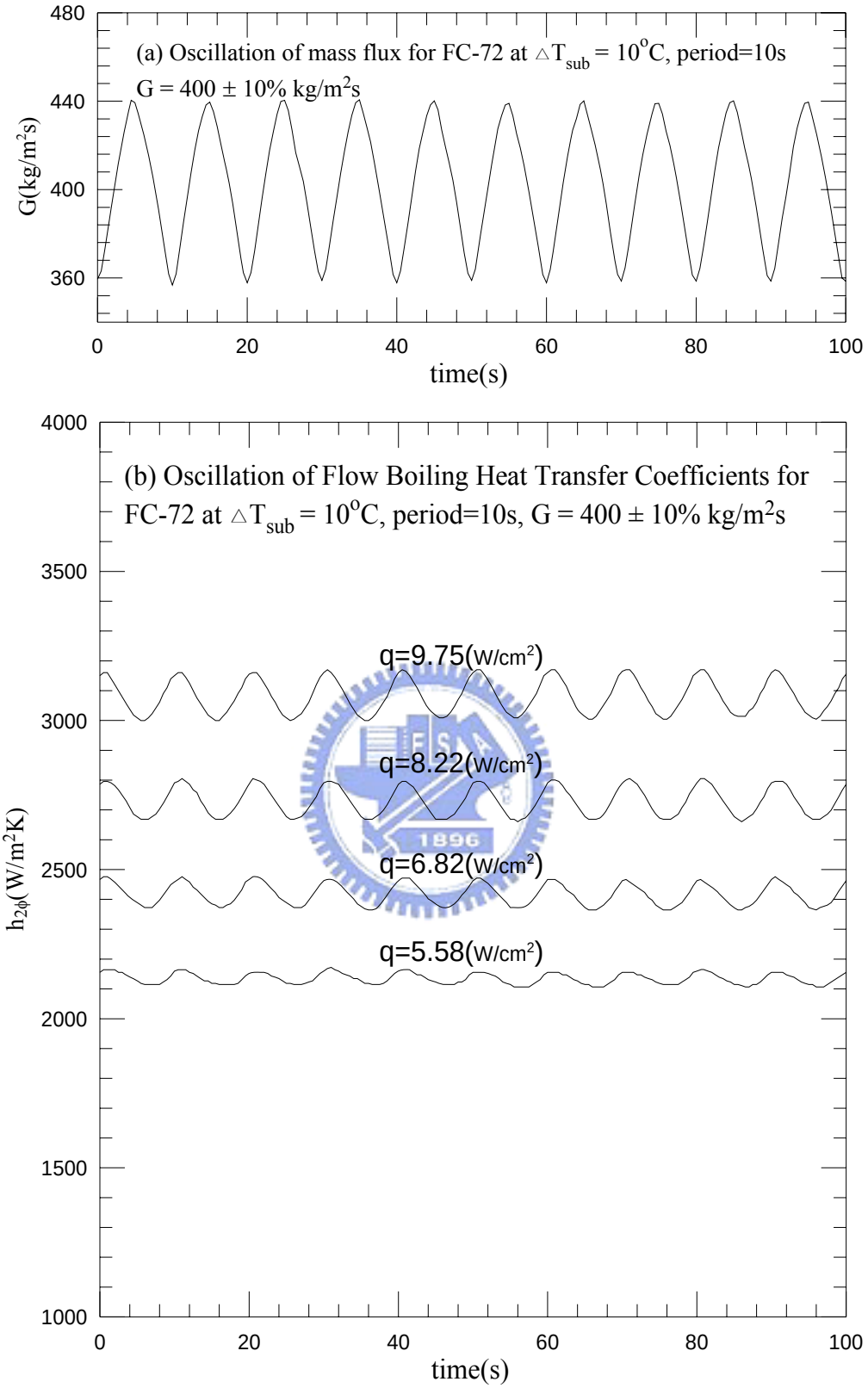

Fig. 5.68 Time variations of (a) imposed coolant mass flux and (b) flow boiling heat transfer coefficients in transient oscillatory subcooled flow boiling for various imposed heat fluxes for G=400±10% kg/m^{2}s with t_p=10 sec.

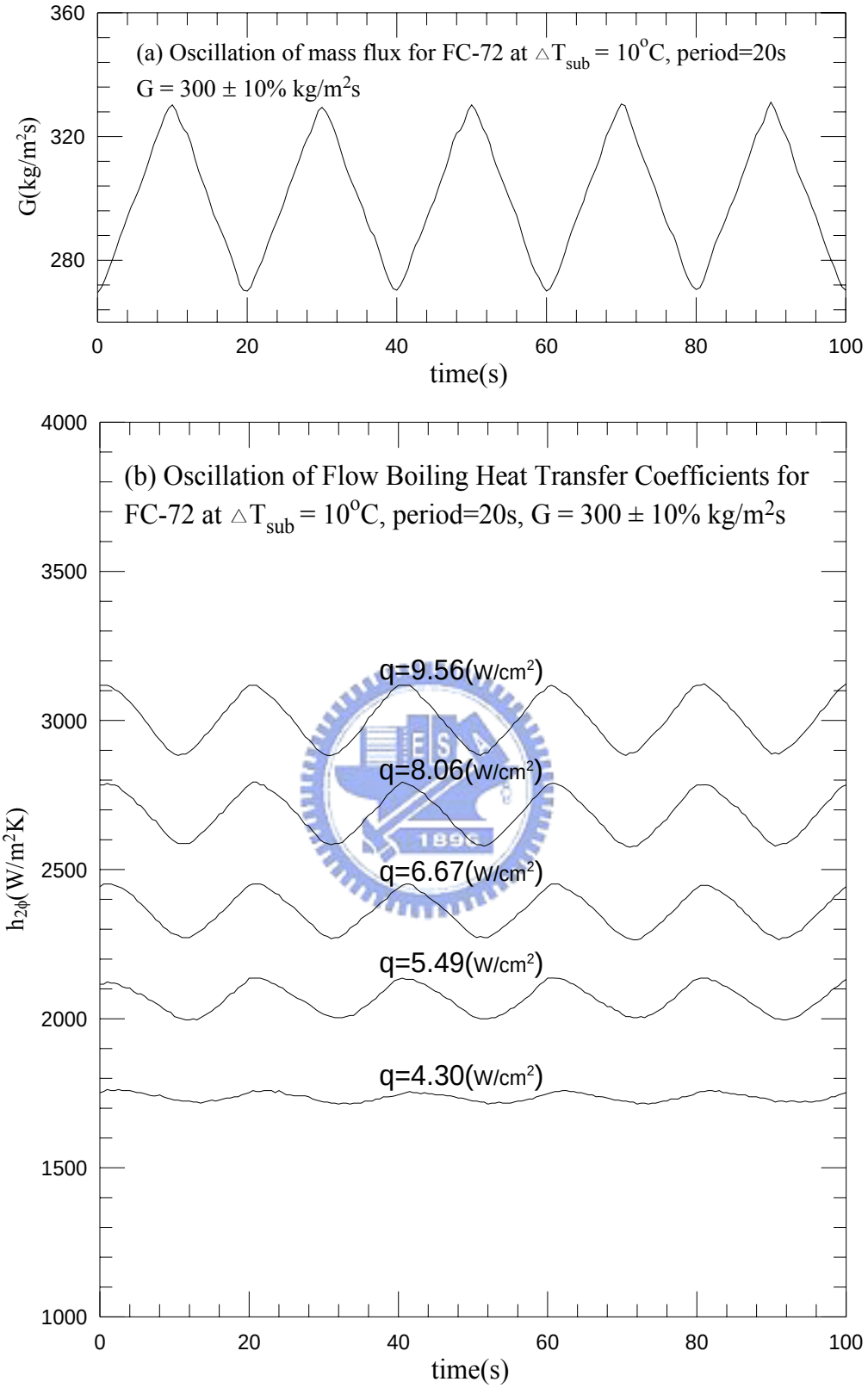

Fig. 5.69 Time variations of (a) imposed coolant mass flux and (b) flow boiling heat transfer coefficients in transient oscillatory subcooled flow boiling for various imposed heat fluxes for G=300±10% kg/m^{2}s with t_p=20 sec.

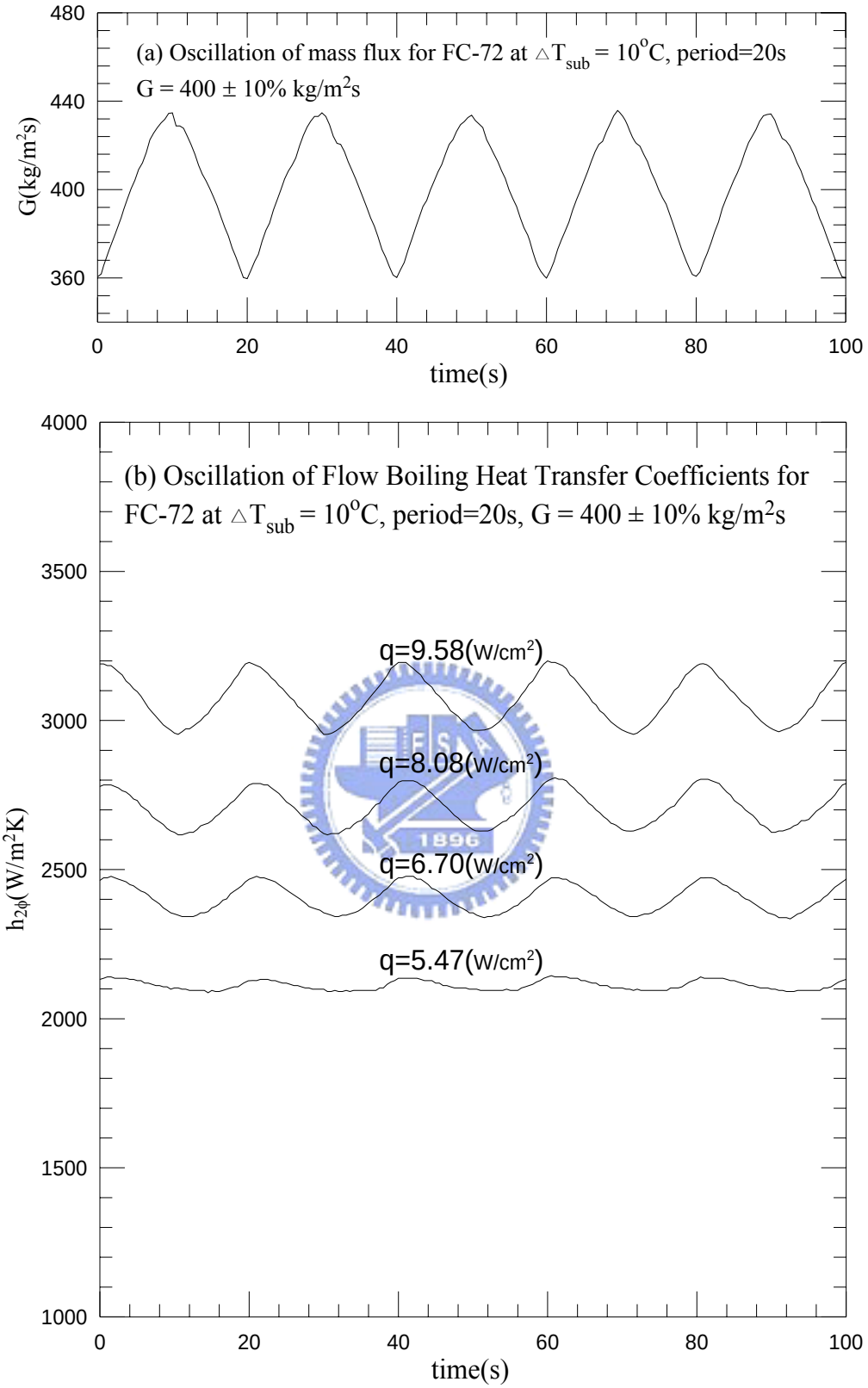

Fig. 5.70 Time variations of (a) imposed coolant mass flux and (b) flow boiling heat transfer coefficients in transient oscillatory subcooled flow boiling for various imposed heat fluxes for G=400±10% kg/m^{2}s with t_p=20 sec.

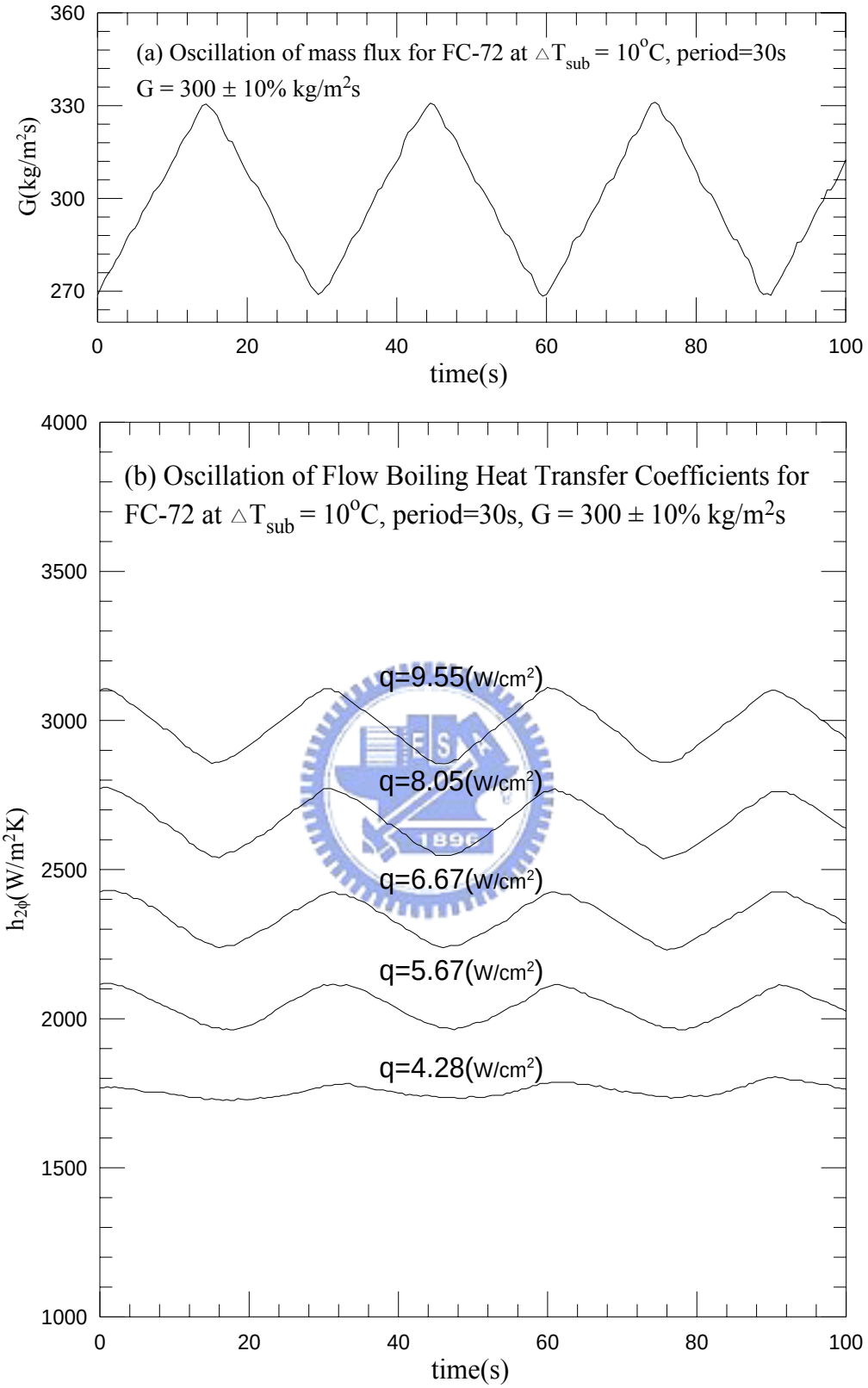

Fig. 5.71 Time variations of (a) imposed coolant mass flux and (b) flow boiling heat transfer coefficients in transient oscillatory subcooled flow boiling for various imposed heat fluxes for G=300±10% kg/m^{2}s with t_p=30 sec.

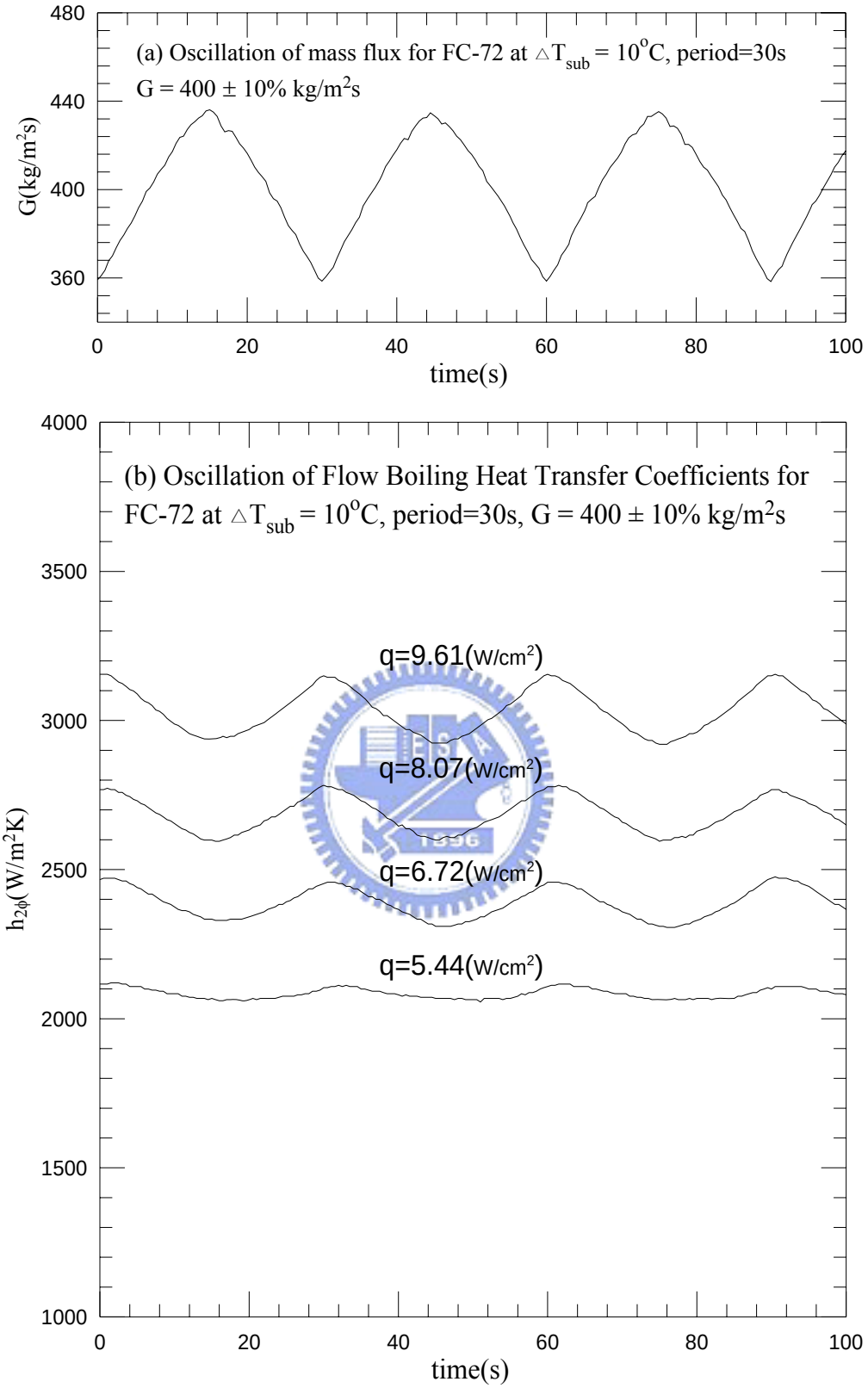

Fig. 5.72 Time variations of (a) imposed coolant mass flux and (b) flow boiling heat transfer coefficients in transient oscillatory subcooled flow boiling for various imposed heat fluxes for G=400±10% kg/m^{2}s with t_p=30 sec.

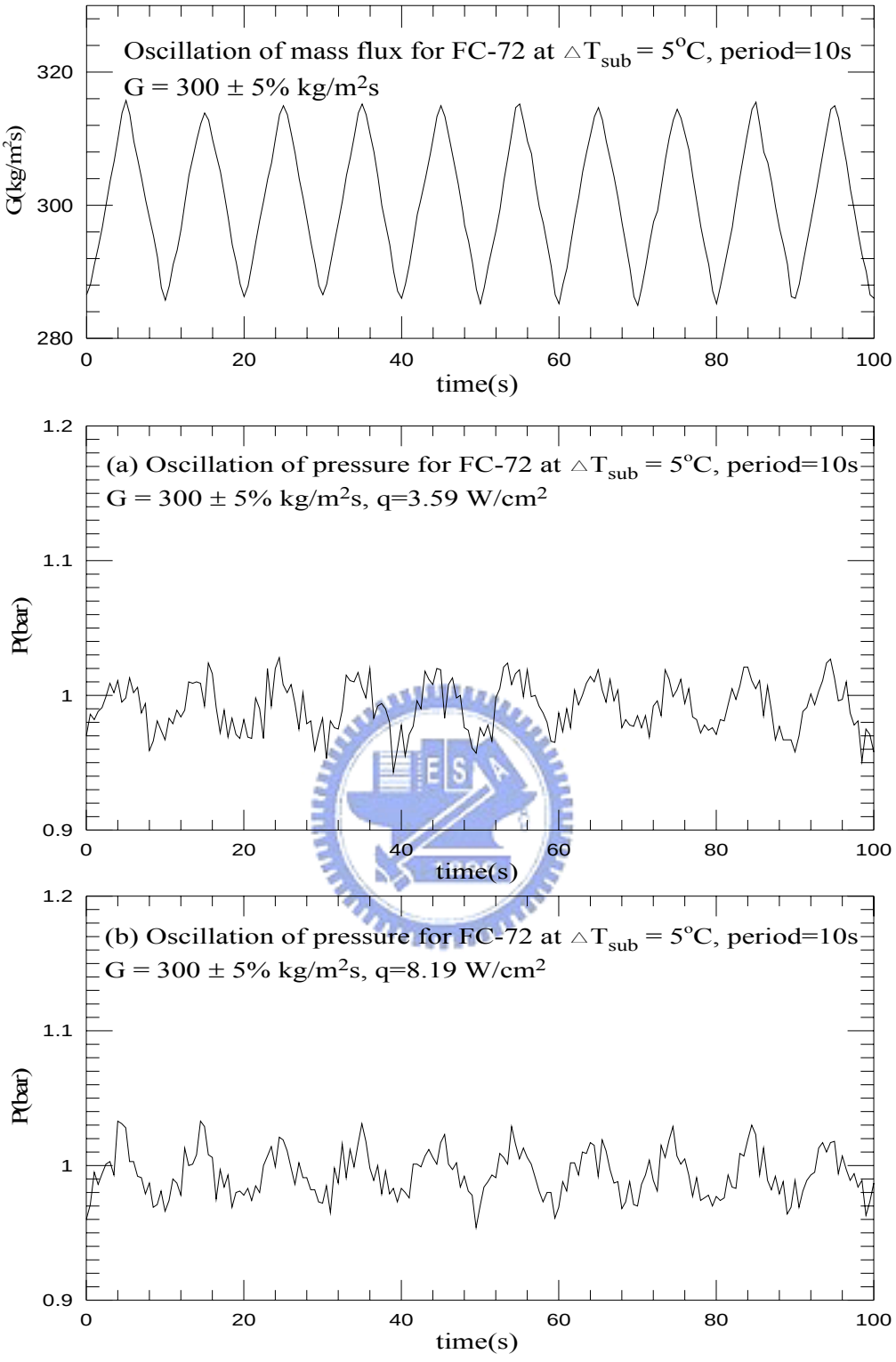

Fig.5.73 Time variations of coolant mass flux and inlet pressure in transient oscillatory subcooled flow boiling for various imposed heat fluxes at (a) q=3.59 W/cm^2 and (b) q=8.19 W/cm^2 for G=300±5% kg/m^{2}s with t_p=10 sec.

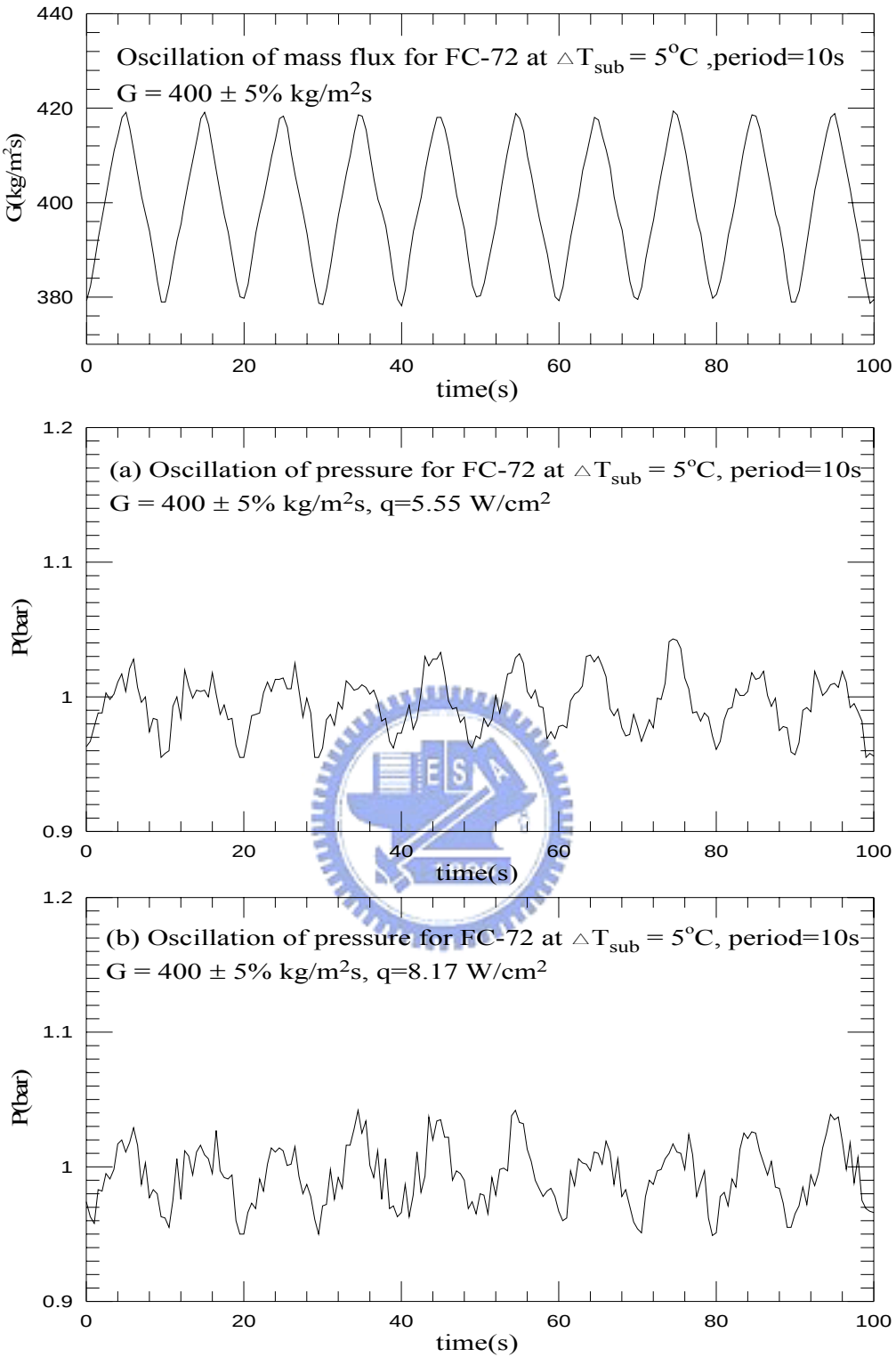

Fig.5.74 Time variations of coolant mass flux and inlet pressure in transient oscillatory subcooled flow boiling for various imposed heat fluxes at (a) q=5.55 W/cm^2 and (b) q=8.17 W/cm^2 for G=400±5% kg/m^{2}s with t_p=10 sec.

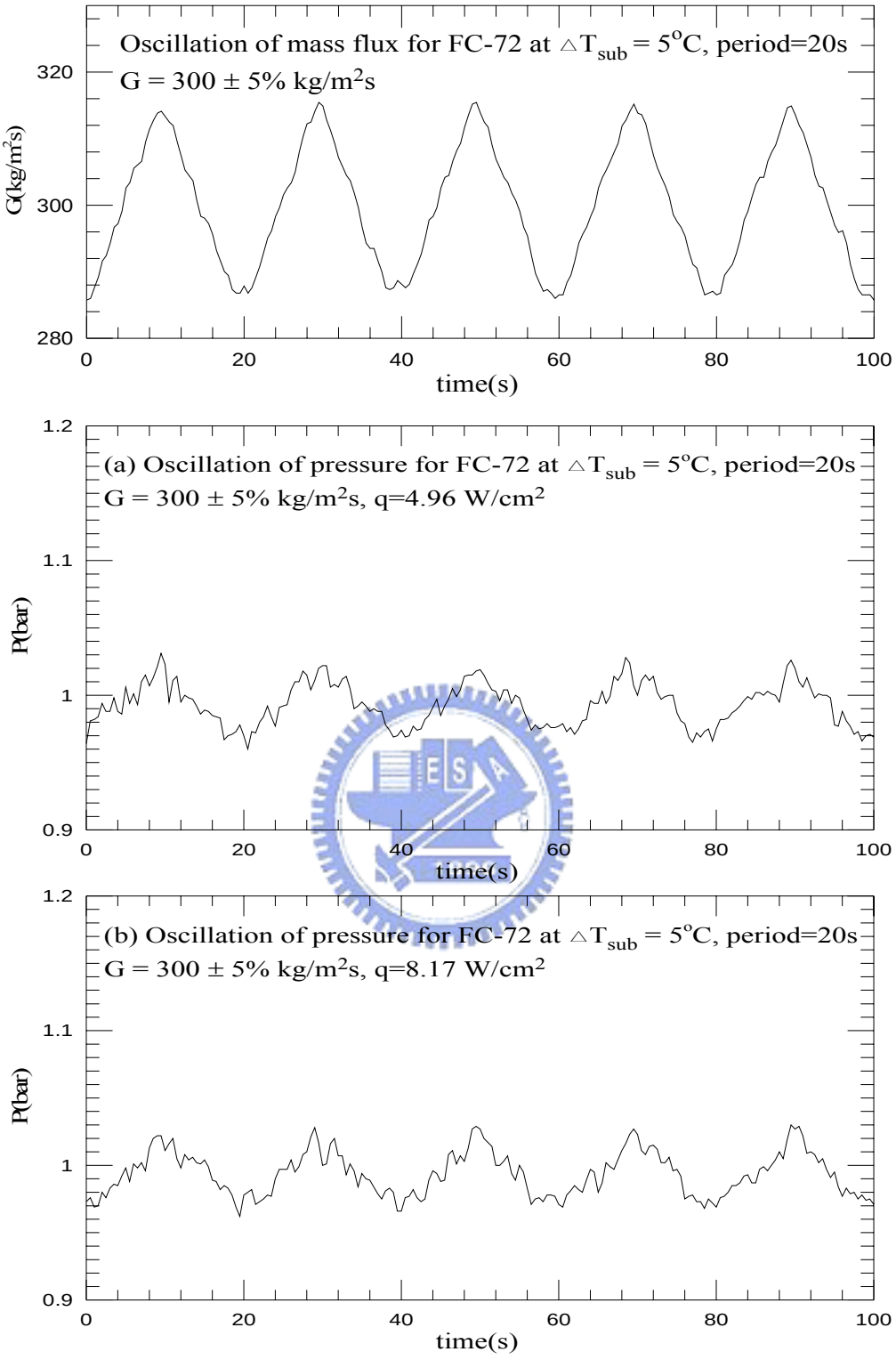

Fig.5.75 Time variations of coolant mass flux and inlet pressure in transient oscillatory subcooled flow boiling for various imposed heat fluxes at (a) q=4.96 W/cm^2 and (b) q=8.17 W/cm^2 for G=300±5% kg/m^{2}s with t_p=20 sec.

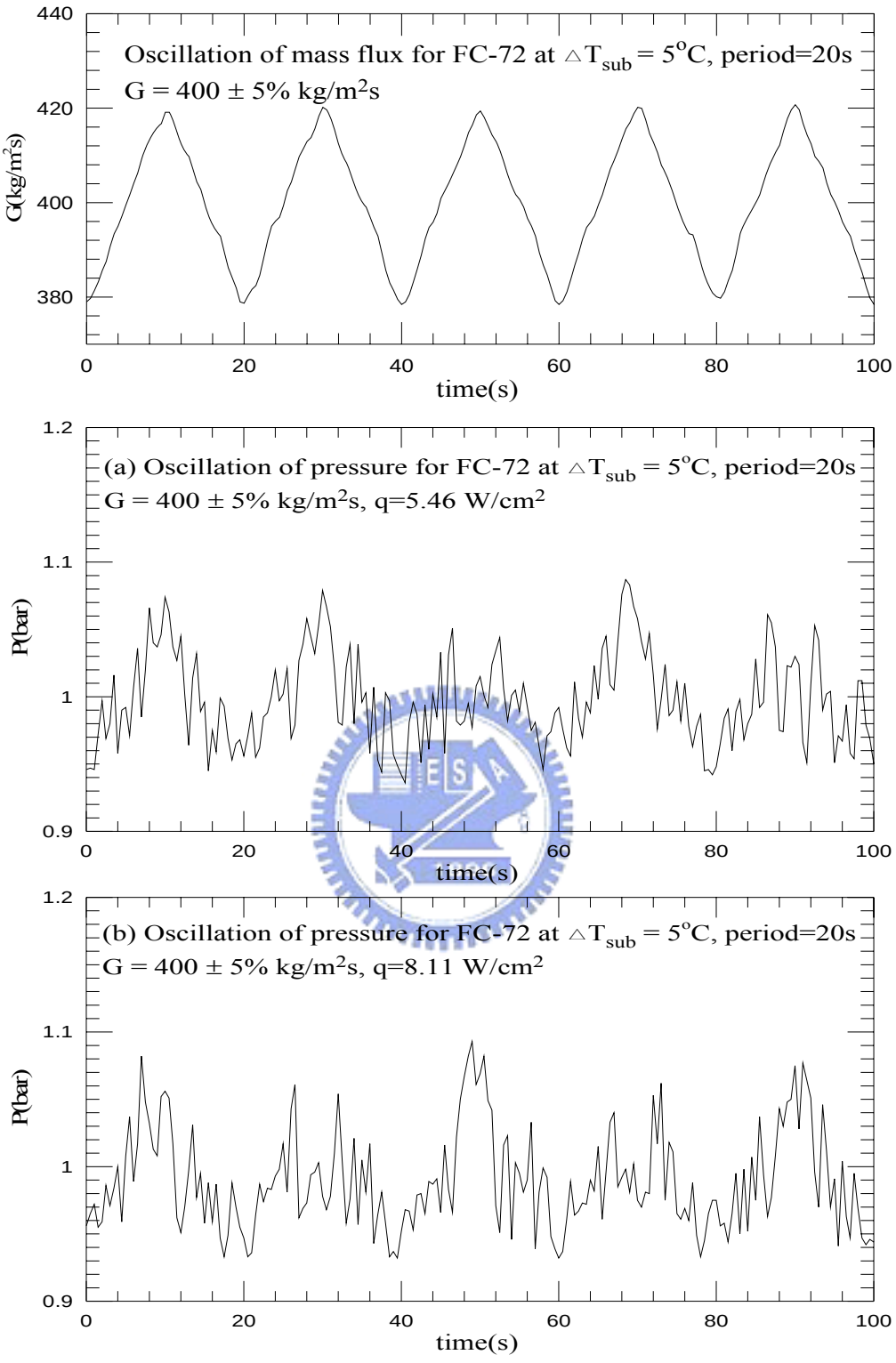

Fig.5.76 Time variations of coolant mass flux and inlet pressure in transient oscillatory subcooled flow boiling for various imposed heat fluxes at (a) q=5.46 W/cm^2 and (b) q=8.11 W/cm^2 for G=400±5% kg/m^{2}s with t_p=20 sec.

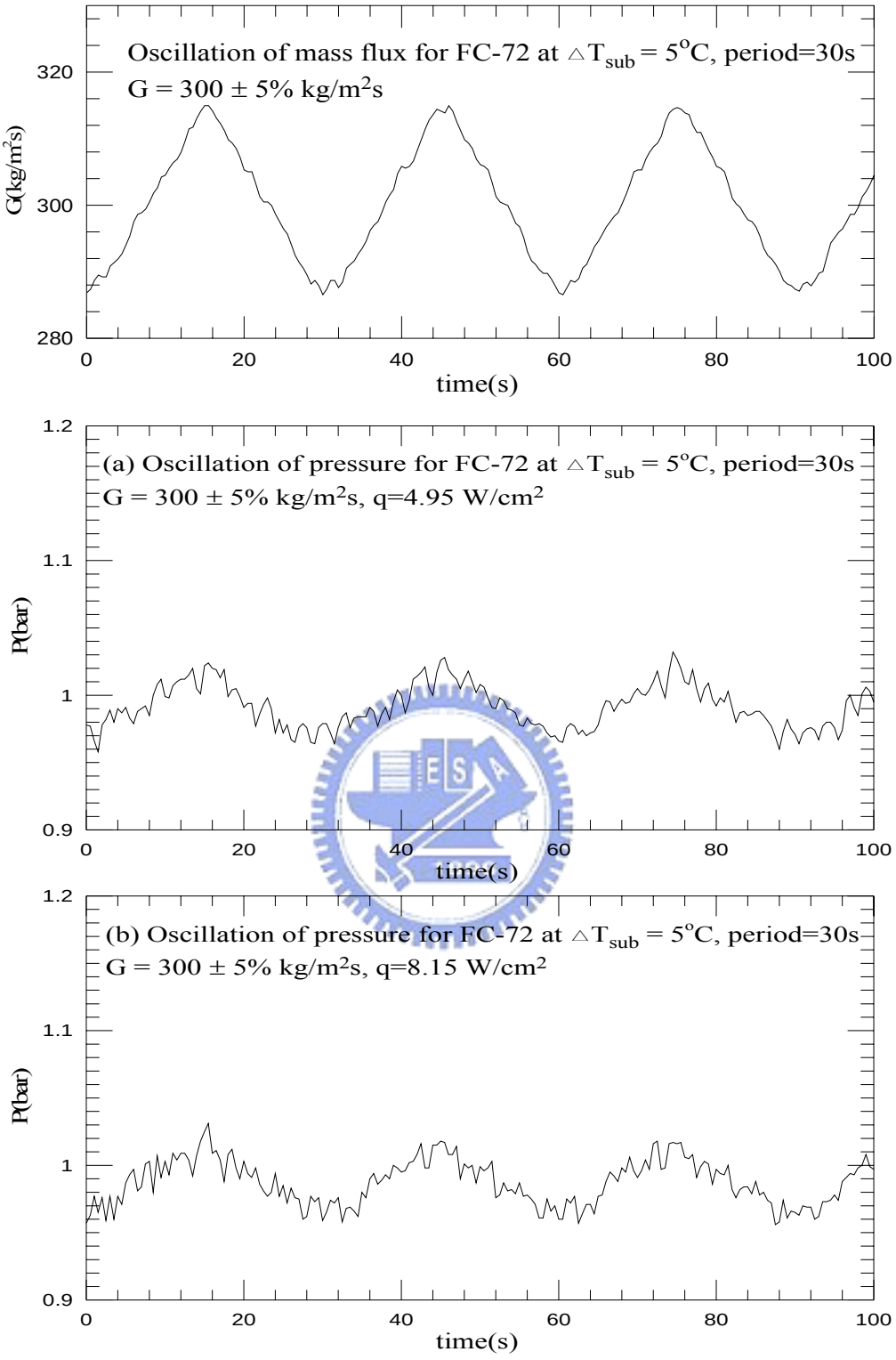

Fig.5.77 Time variations of coolant mass flux and inlet pressure in transient oscillatory subcooled flow boiling for various imposed heat fluxes at (a) q=4.95 W/cm^2 and (b) q=8.15 W/cm^2 for G=300±5% kg/m^{2}s with t_p=30 sec.

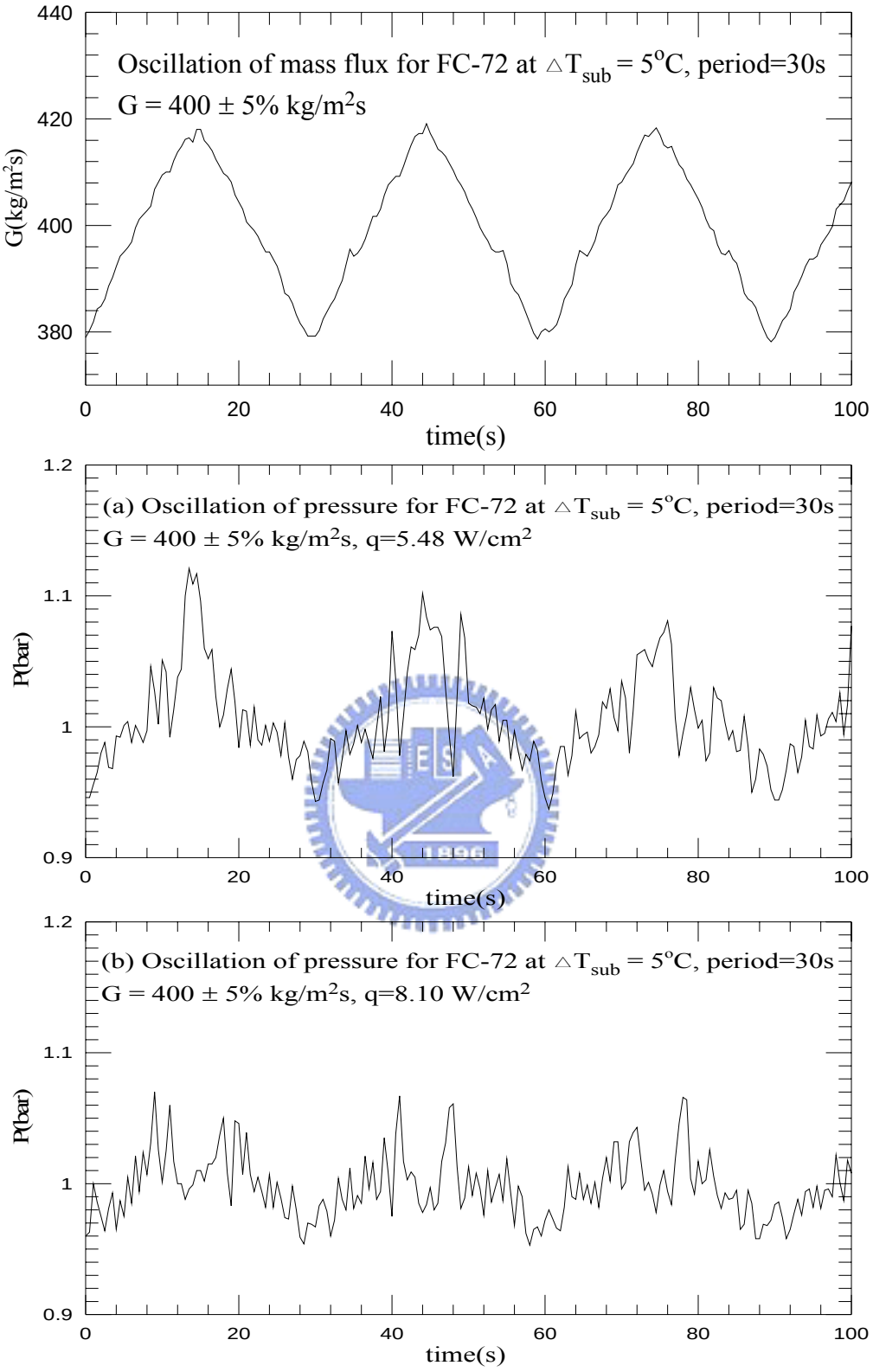

Fig.5.78 Time variations of coolant mass flux and inlet pressure in transient oscillatory subcooled flow boiling for various imposed heat fluxes at (a) q=5.48 W/cm^2 and (b) q=8.10 W/cm^2 for G=400±5% kg/m^{2}s with t_p=30 sec.

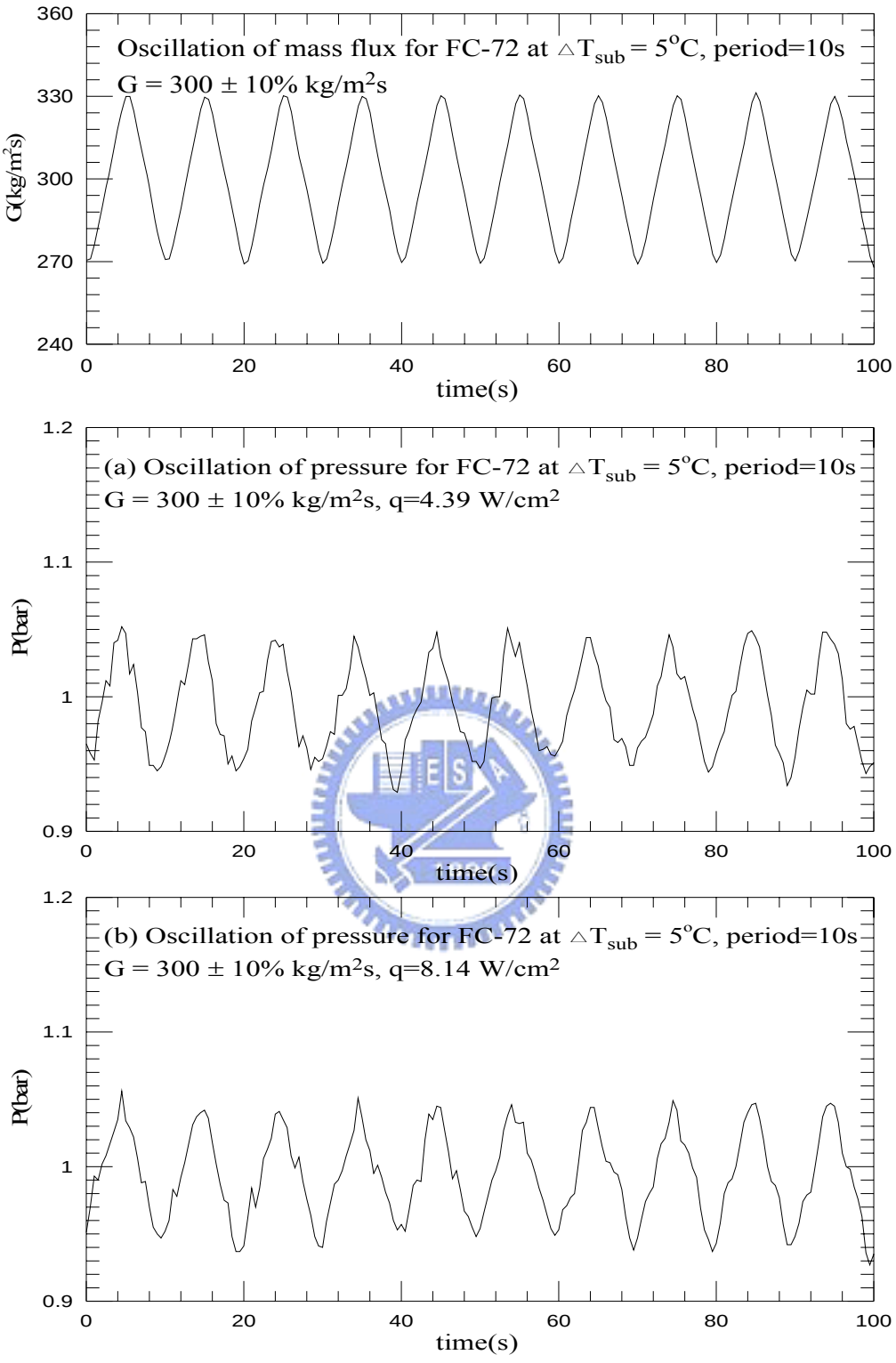

Fig.5.79 Time variations of coolant mass flux and inlet pressure in transient oscillatory subcooled flow boiling for various imposed heat fluxes at (a) q=4.39 W/cm^2 and (b) q=8.14 W/cm^2 for G=300±10% kg/m^{2}s with t_p=10 sec.

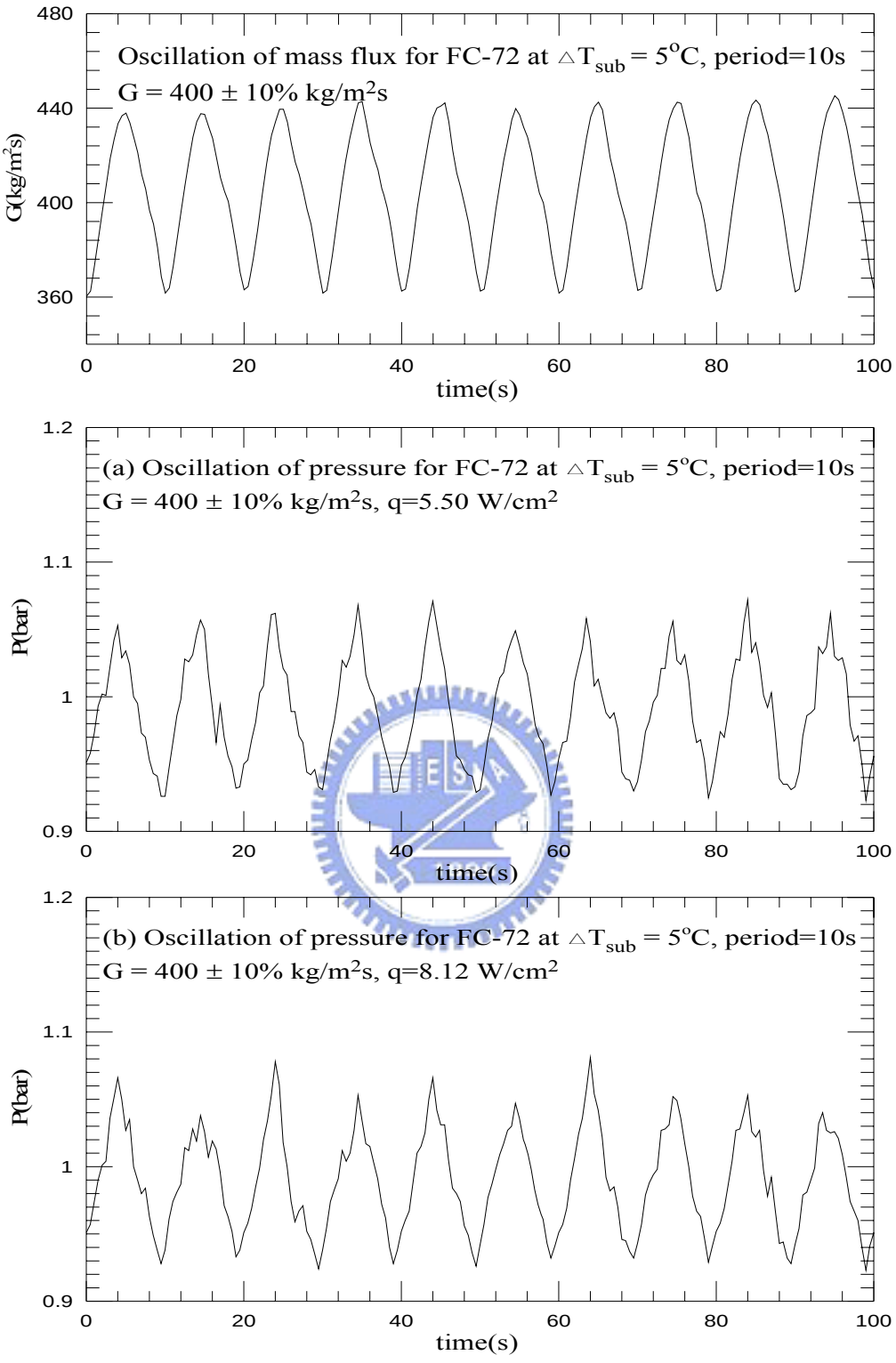

Fig.5.80 Time variations of coolant mass flux and inlet pressure in transient oscillatory subcooled flow boiling for various imposed heat fluxes at (a) q=5.50 W/cm^2 and (b) q=8.12 W/cm^2 for G=400±10% kg/m^{2}s with t_p=10 sec.

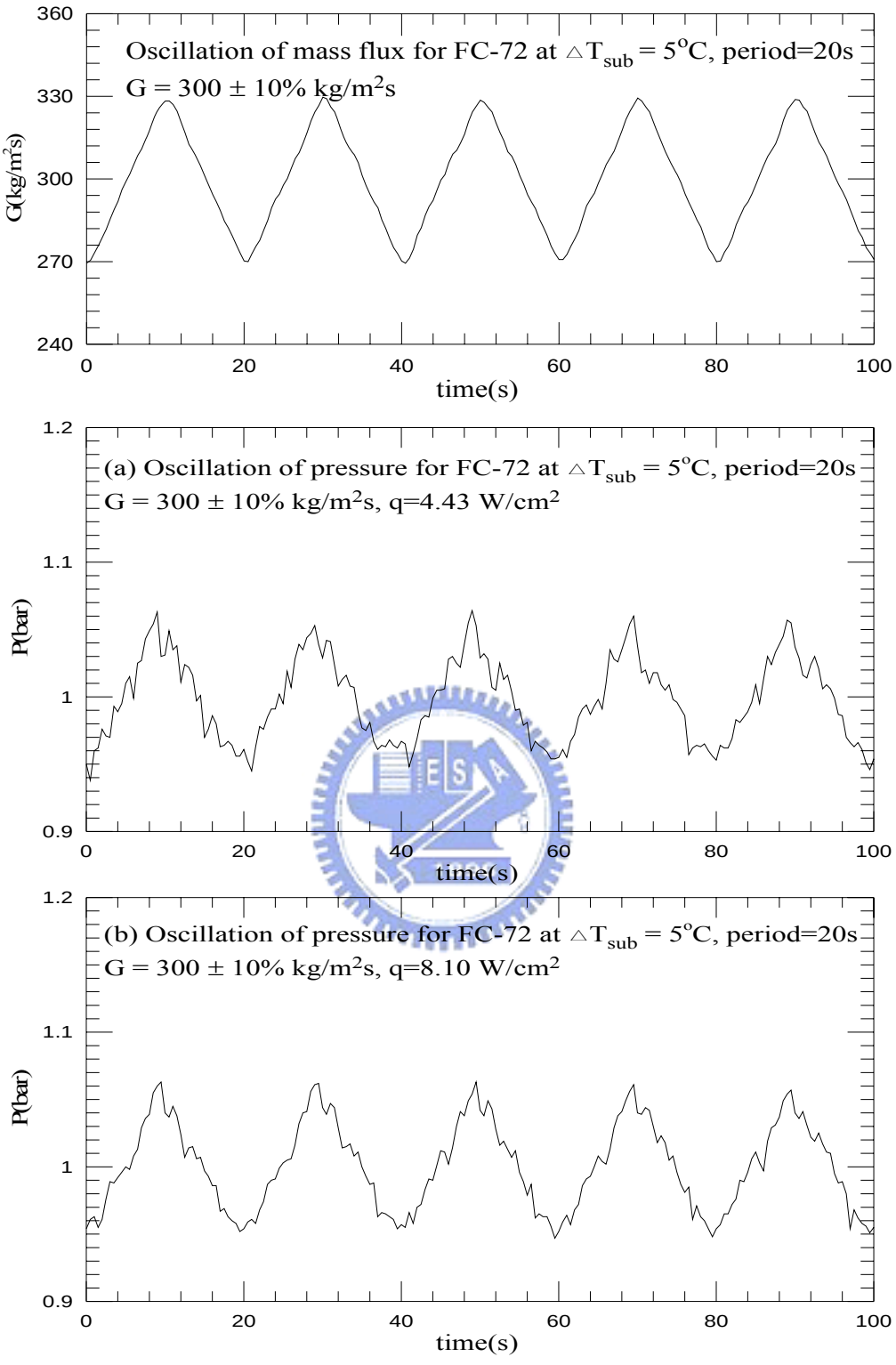

Fig.5.81 Time variations of coolant mass flux and inlet pressure in transient oscillatory subcooled flow boiling for various imposed heat fluxes at (a) q=4.43 W/cm^2 and (b) q=8.10 W/cm^2 for G=300±10% kg/m^{2}s with t_p=20 sec.

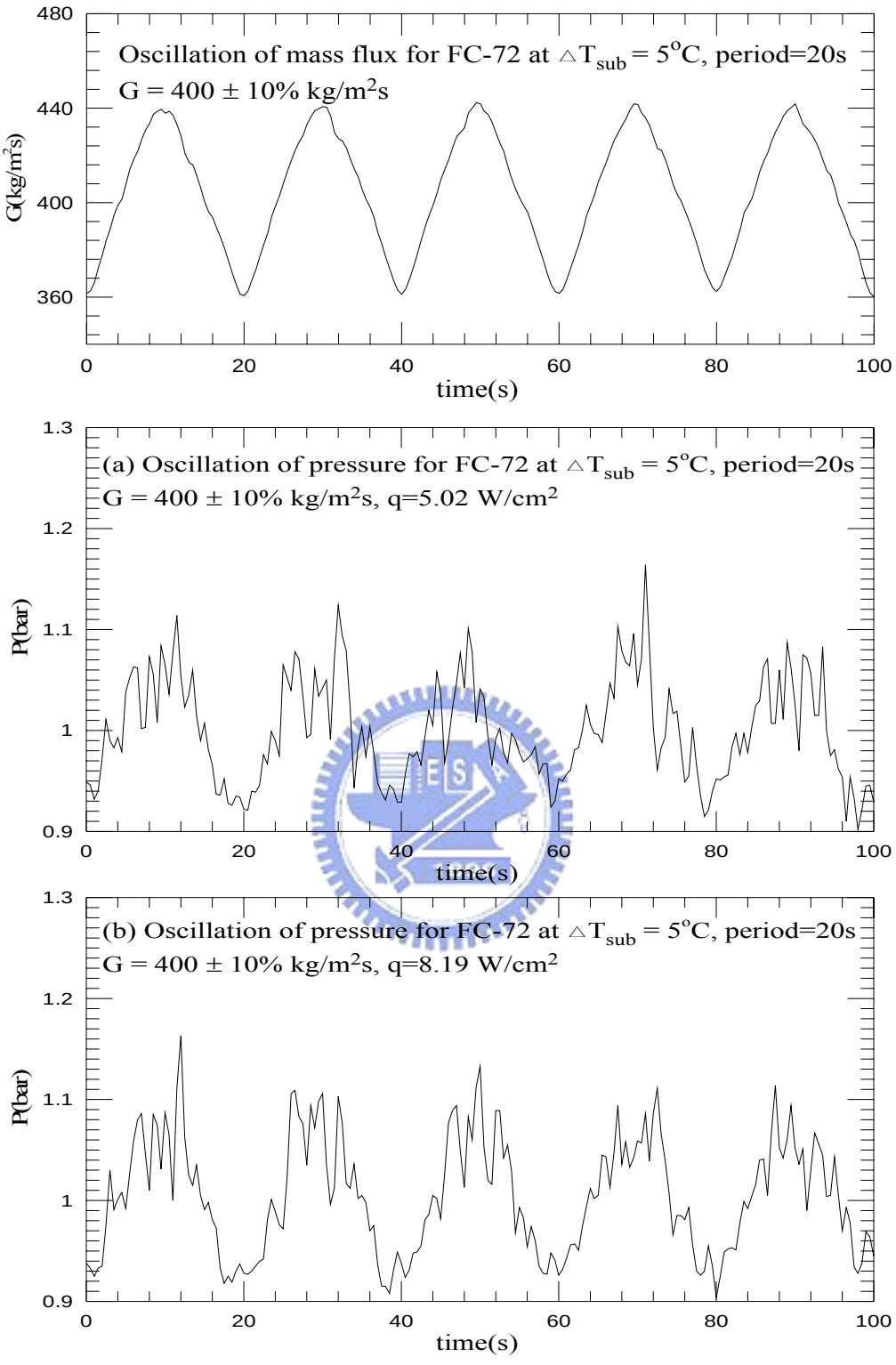

Fig.5.82 Time variations of coolant mass flux and inlet pressure in transient oscillatory subcooled flow boiling for various imposed heat fluxes at (a) q=5.02 W/cm^2 and (b) q=8.19 W/cm^2 for G=400±10% kg/m^{2}s with t_p=20 sec.

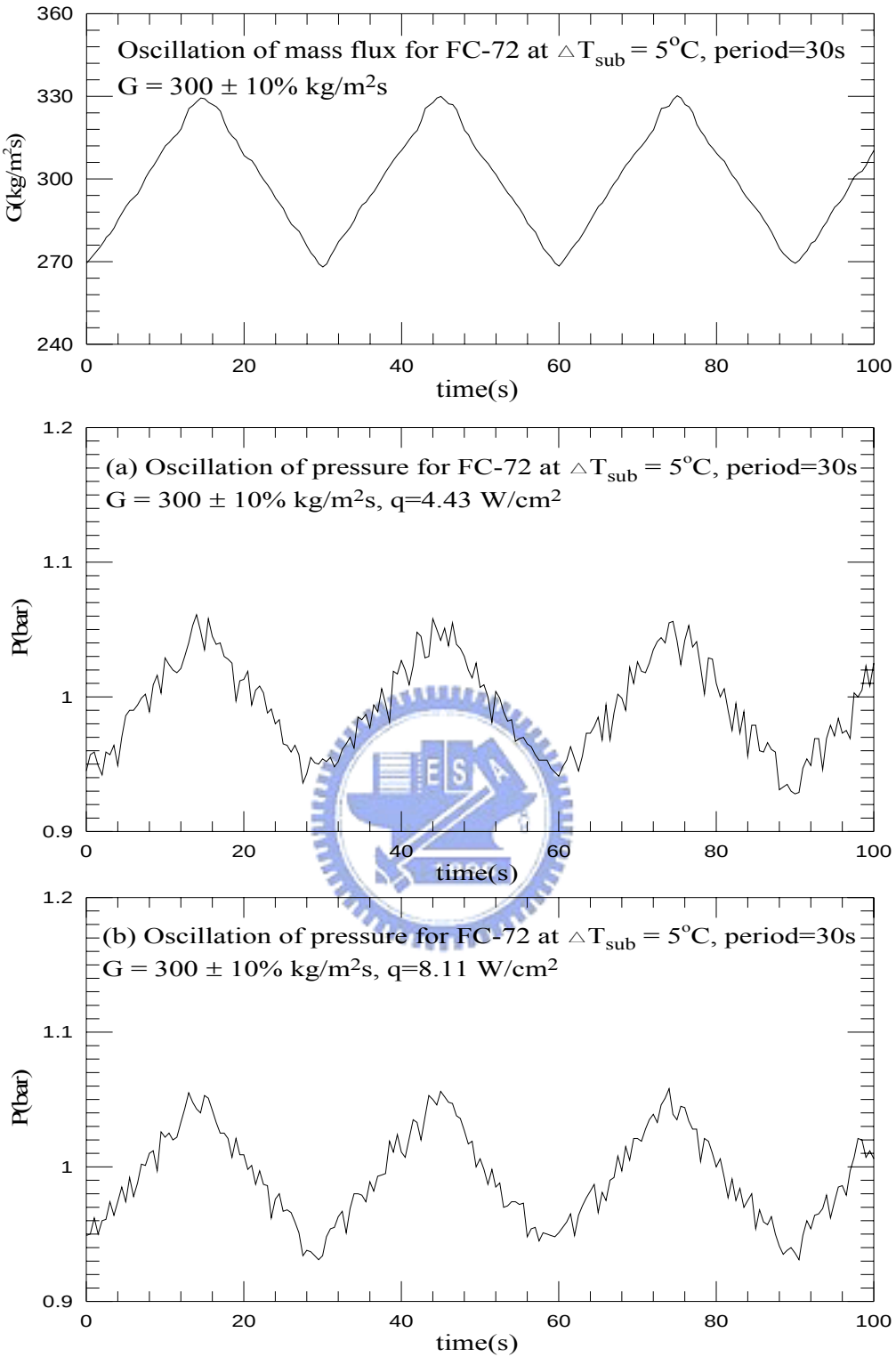

Fig.5.83 Time variations of coolant mass flux and inlet pressure in transient oscillatory subcooled flow boiling for various imposed heat fluxes at (a) q=4.43 W/cm^2 and (b) q=8.11 W/cm^2 for G=300±10% kg/m^{2}s with t_p=30 sec.

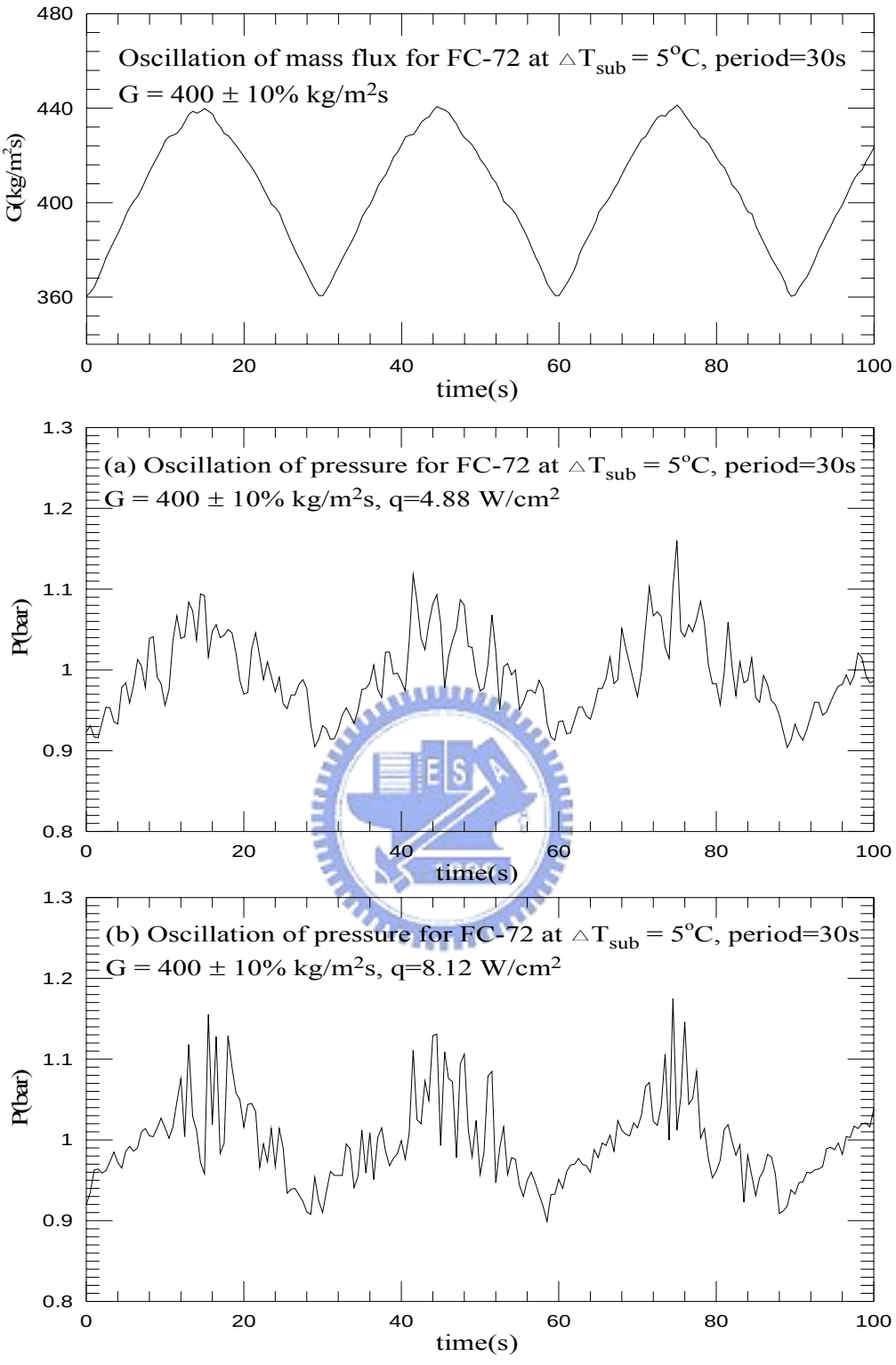

Fig.5.84 Time variations of coolant mass flux and inlet pressure in transient oscillatory subcooled flow boiling for various imposed heat fluxes at (a) q=4.88 W/cm^2 and (b) q=8.12 W/cm^2 for G=400±10% kg/m^{2}s with t_p=30 sec.

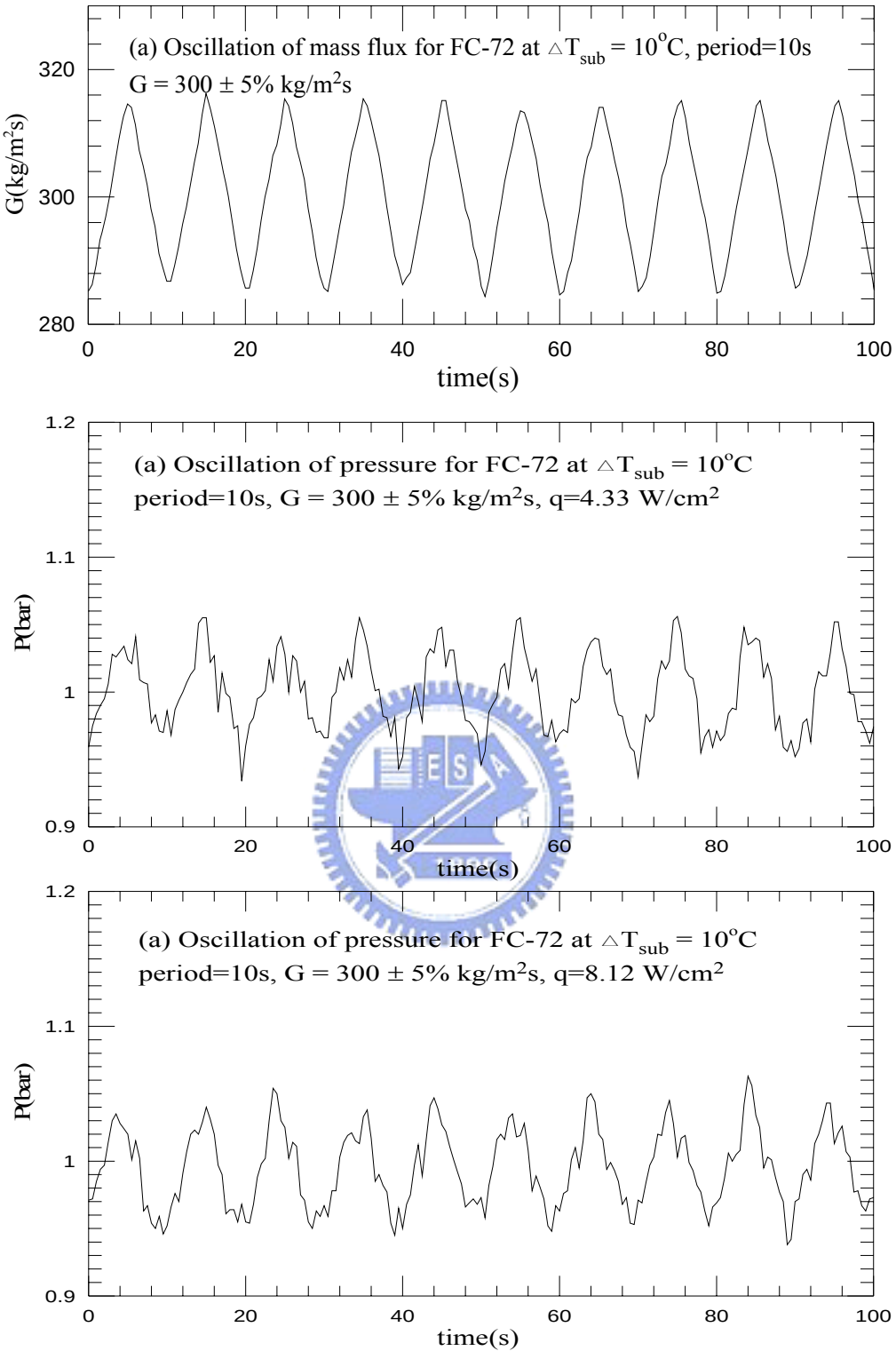

Fig.5.85 Time variations of coolant mass flux and inlet pressure in transient oscillatory subcooled flow boiling for various imposed heat fluxes at (a) q=4.33 W/cm^2 and (b) q=8.12 W/cm^2 for G=300±5% kg/m^{2}s with t_p=10 sec.

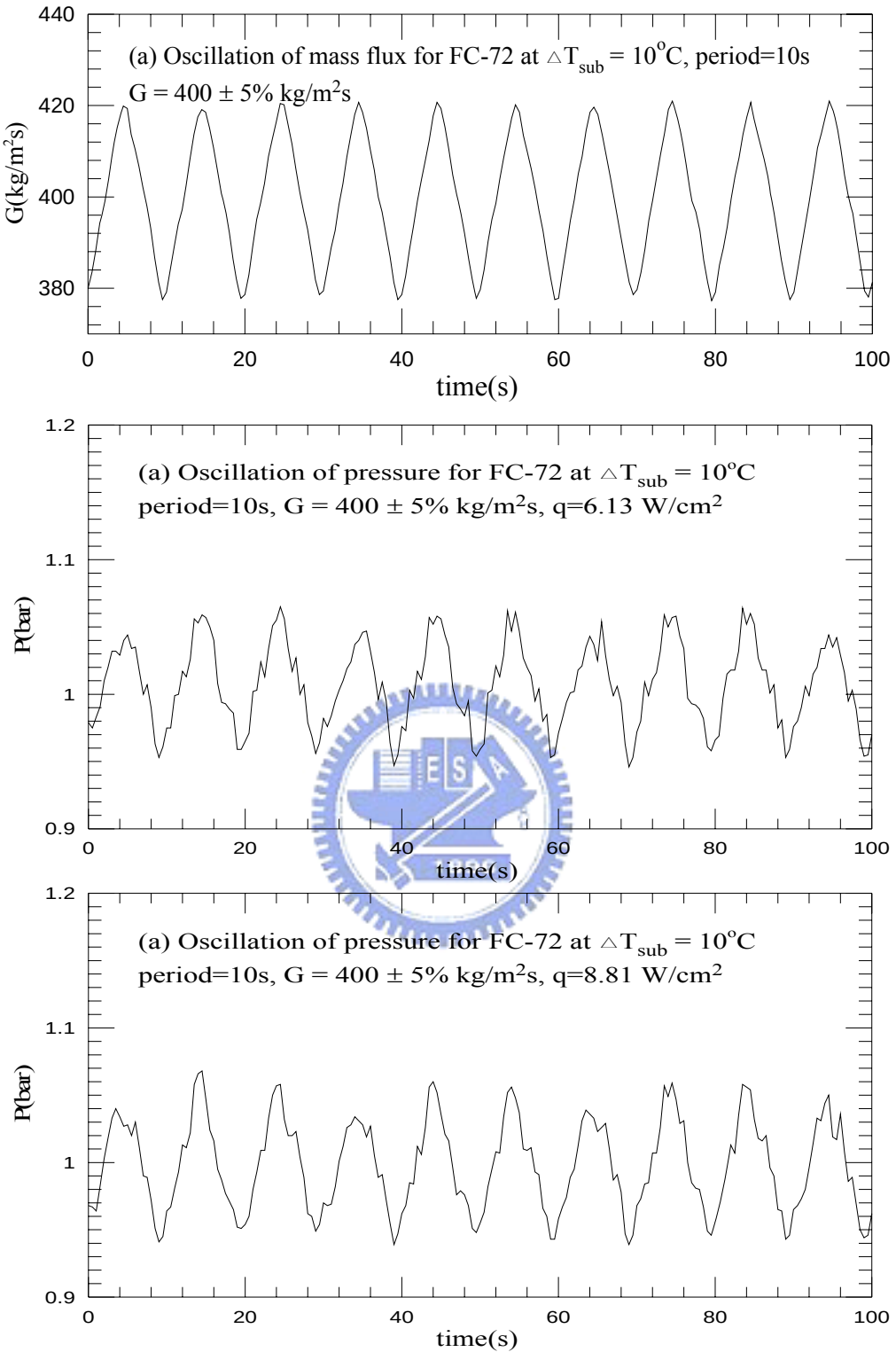

Fig.5.86 Time variations of coolant mass flux and inlet pressure in transient oscillatory subcooled flow boiling for various imposed heat fluxes at (a) q=6.13 W/cm^2 and (b) q=8.81 W/cm^2 for G=400±5% kg/m^{2}s with t_p=10 sec.

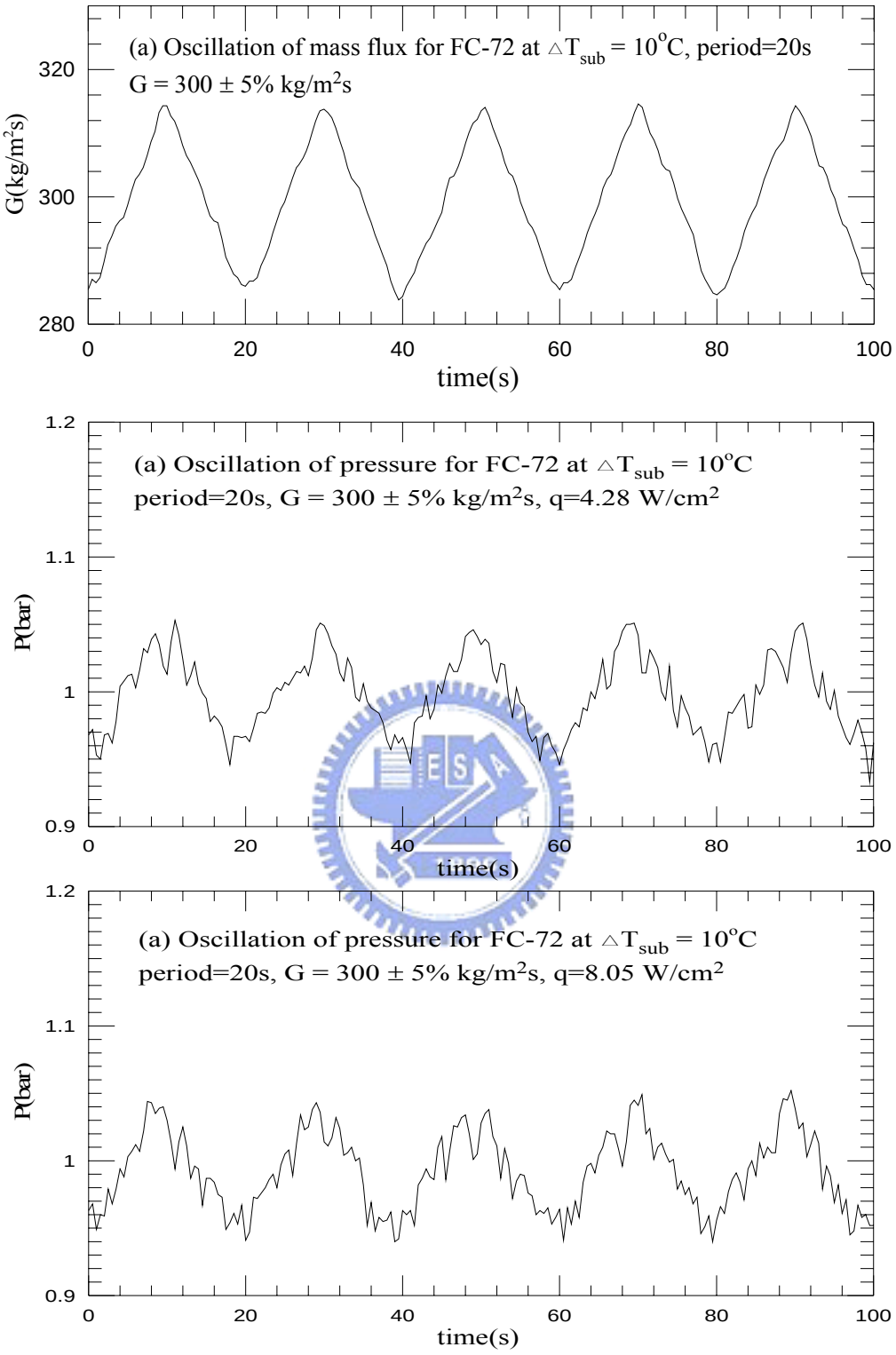

Fig.5.87 Time variations of coolant mass flux and inlet pressure in transient oscillatory subcooled flow boiling for various imposed heat fluxes at (a) q=4.28 W/cm^2 and (b) q=8.05 W/cm^2 for G=300±5% kg/m^{2}s with t_p=20 sec.

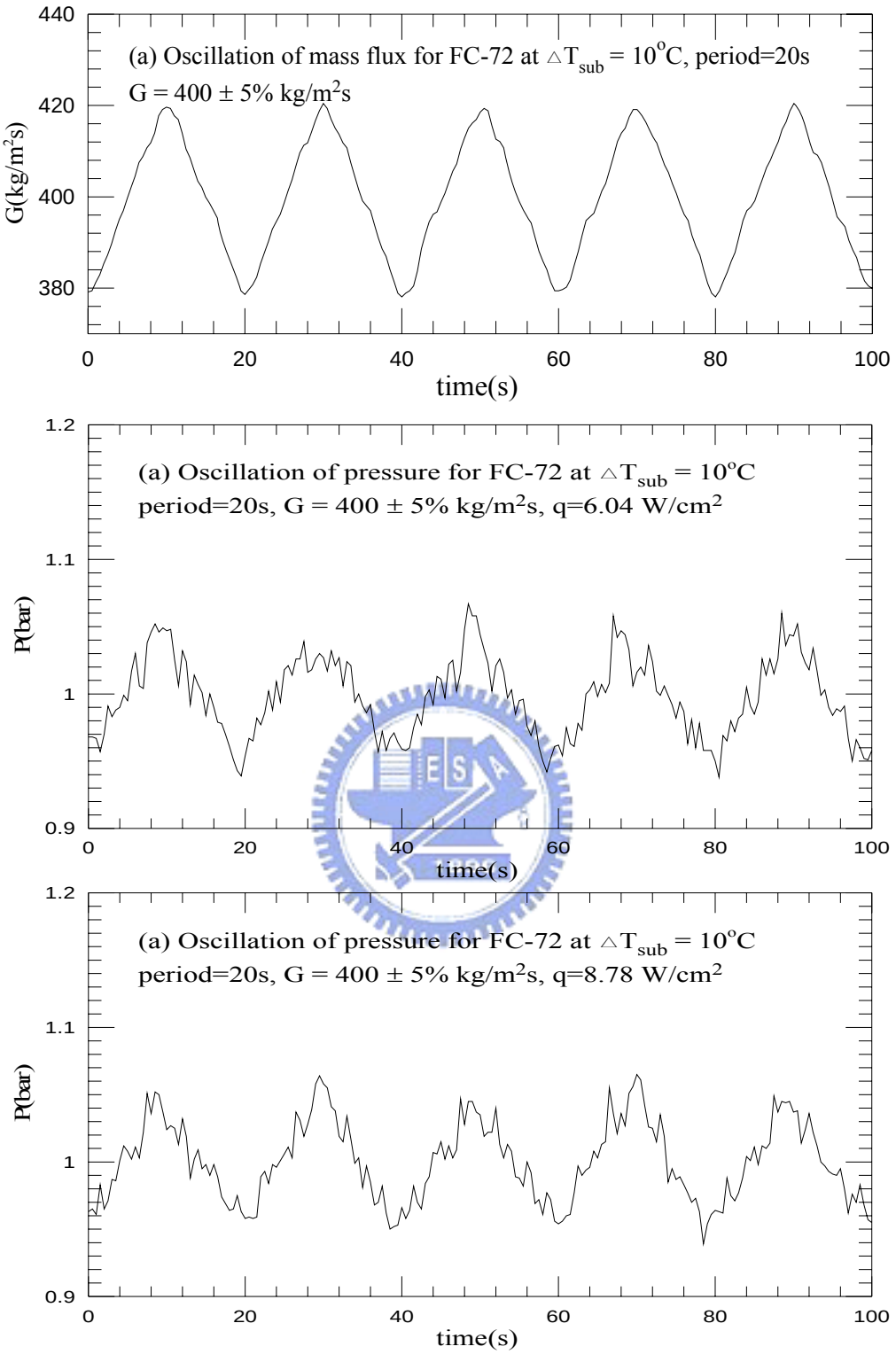

Fig.5.88 Time variations of coolant mass flux and inlet pressure in transient oscillatory subcooled flow boiling for various imposed heat fluxes at (a) q=6.04 W/cm^2 and (b) q=8.78 W/cm^2 for G=400±5% kg/m^{2}s with t_p=20 sec.

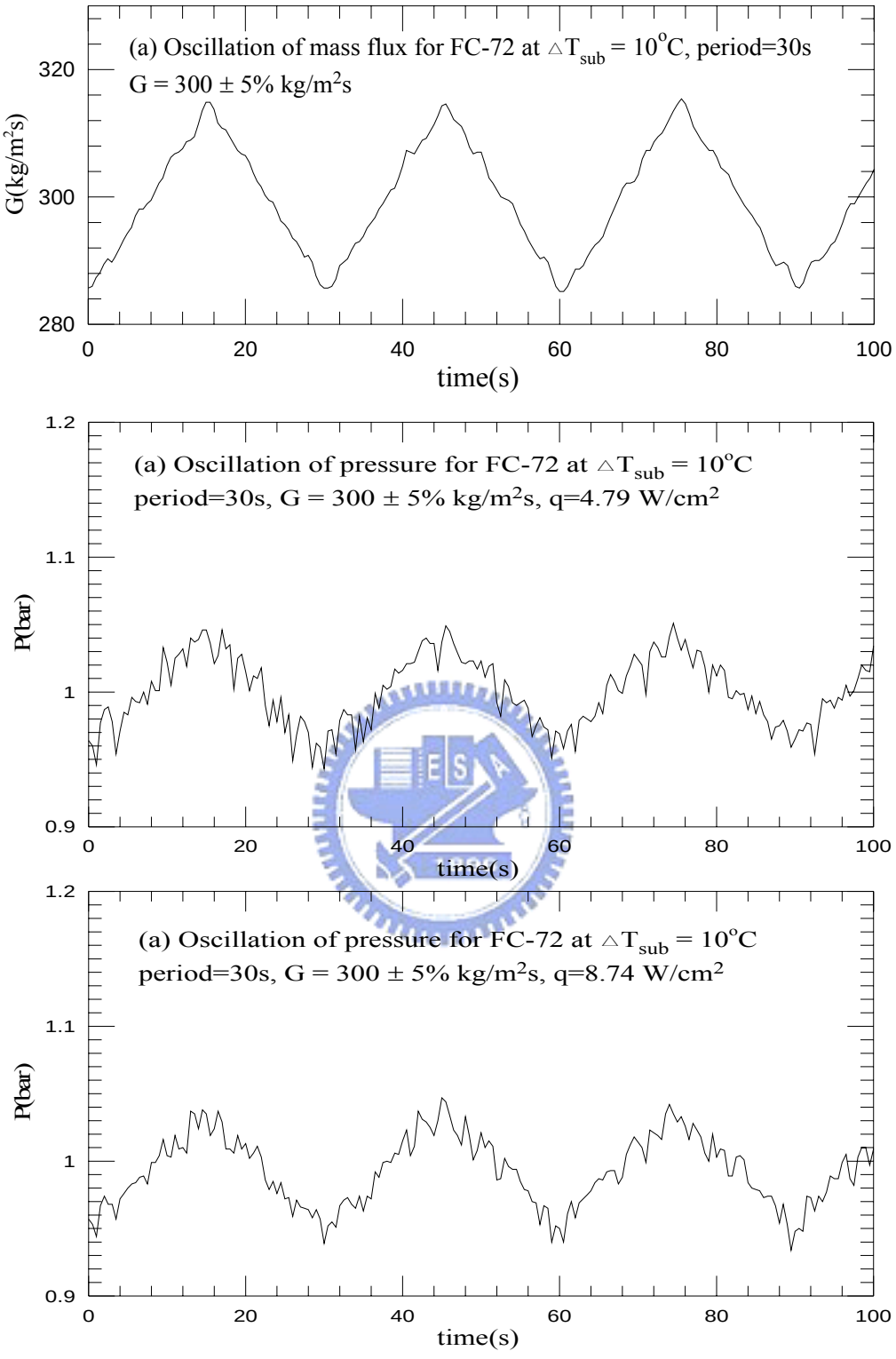

Fig.5.89 Time variations of coolant mass flux and inlet pressure in transient oscillatory subcooled flow boiling for various imposed heat fluxes at (a) q=4.79 W/cm^2 and (b) q=8.74 W/cm^2 for G=300±5% kg/m^{2}s with t_p=30 sec.

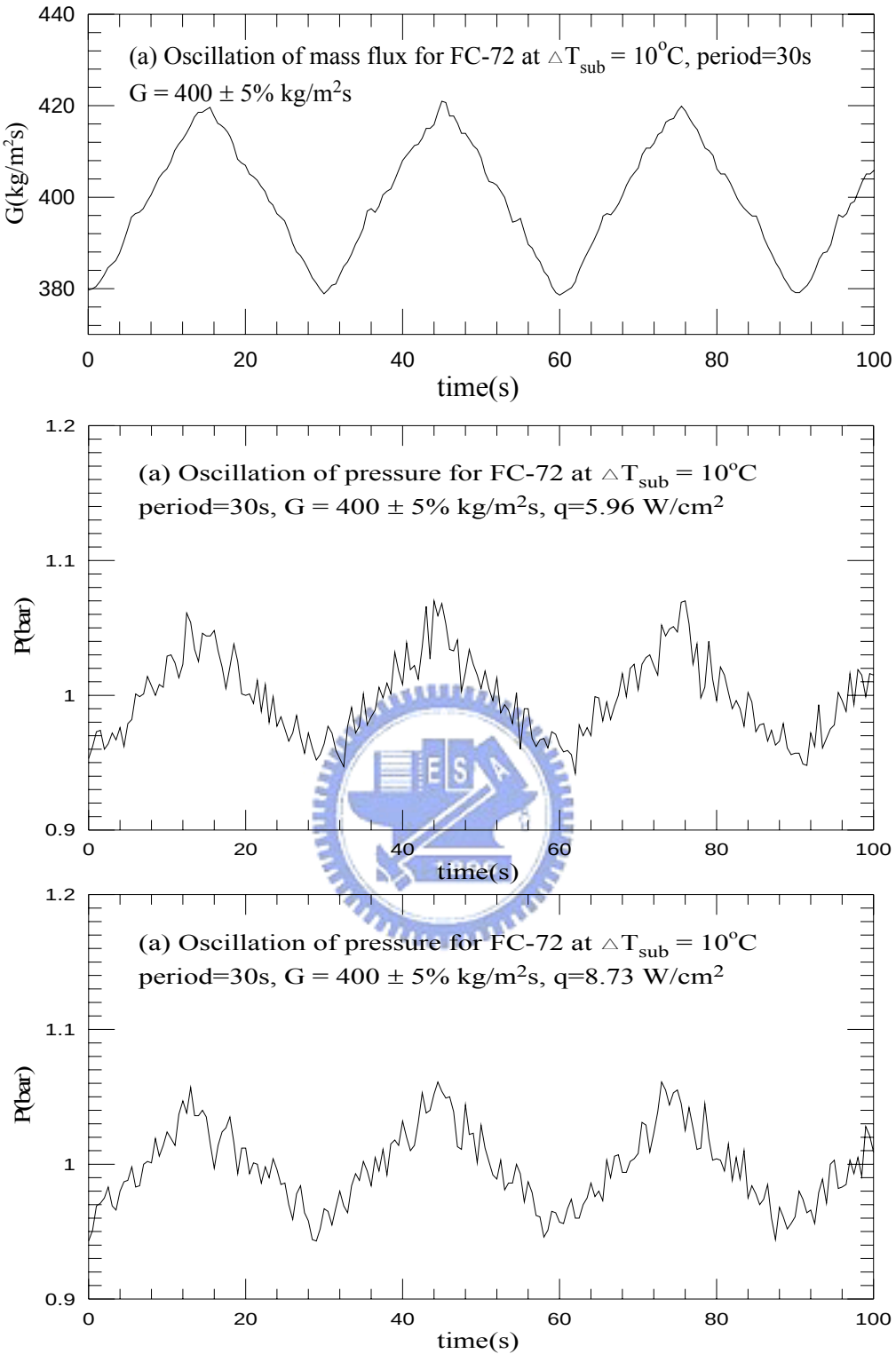

Fig.5.90 Time variations of coolant mass flux and inlet pressure in transient oscillatory subcooled flow boiling for various imposed heat fluxes at (a) q=5.96 W/cm^2 and (b) q=8.73 W/cm^2 for G=400±5% kg/m^{2}s with t_p=30 sec.

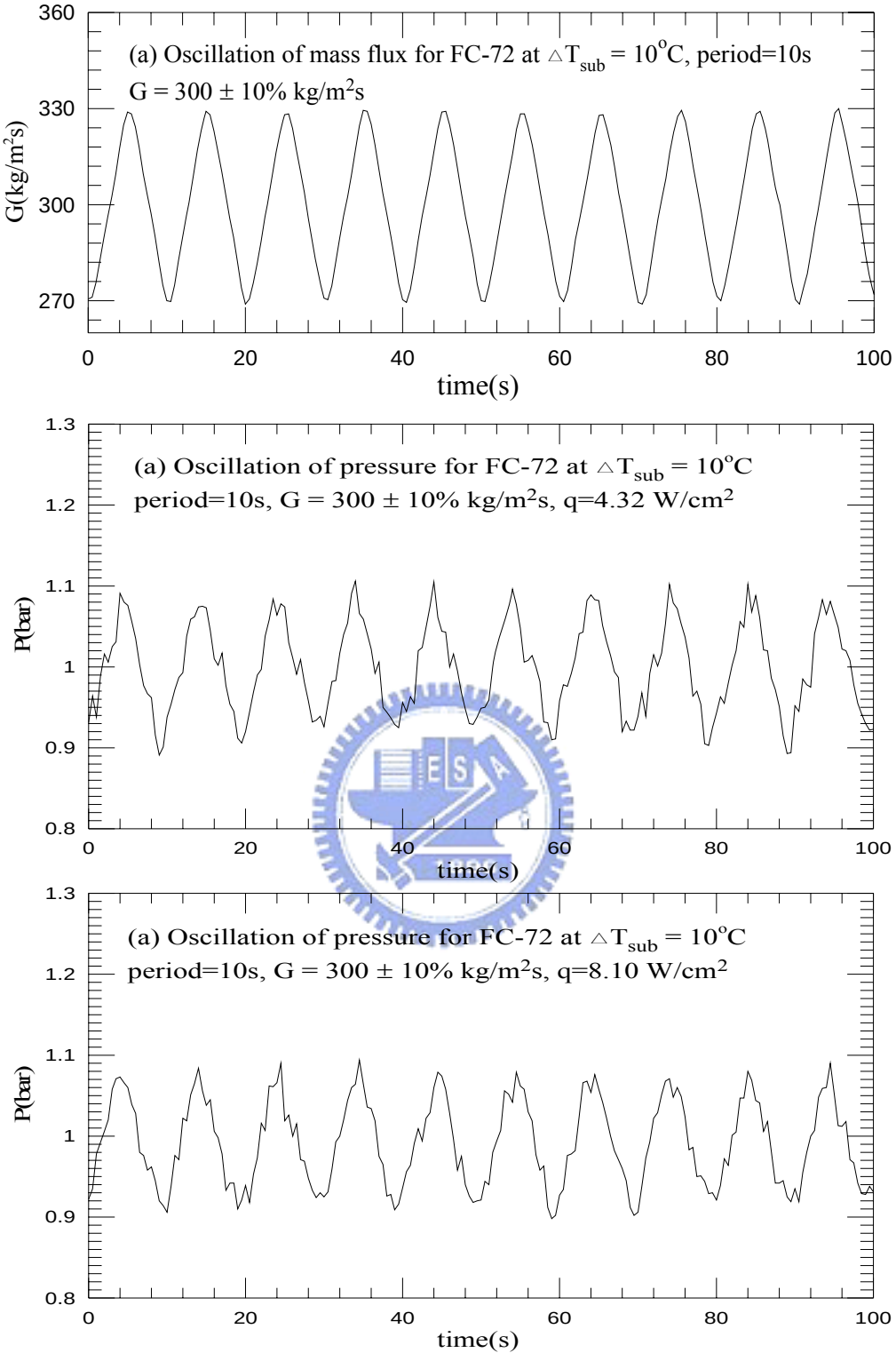

Fig.5.91 Time variations of coolant mass flux and inlet pressure in transient oscillatory subcooled flow boiling for various imposed heat fluxes at (a) q=4.32 W/cm^2 and (b) q=8.10 W/cm^2 for G=300±10% kg/m^{2}s with t_p=10 sec.

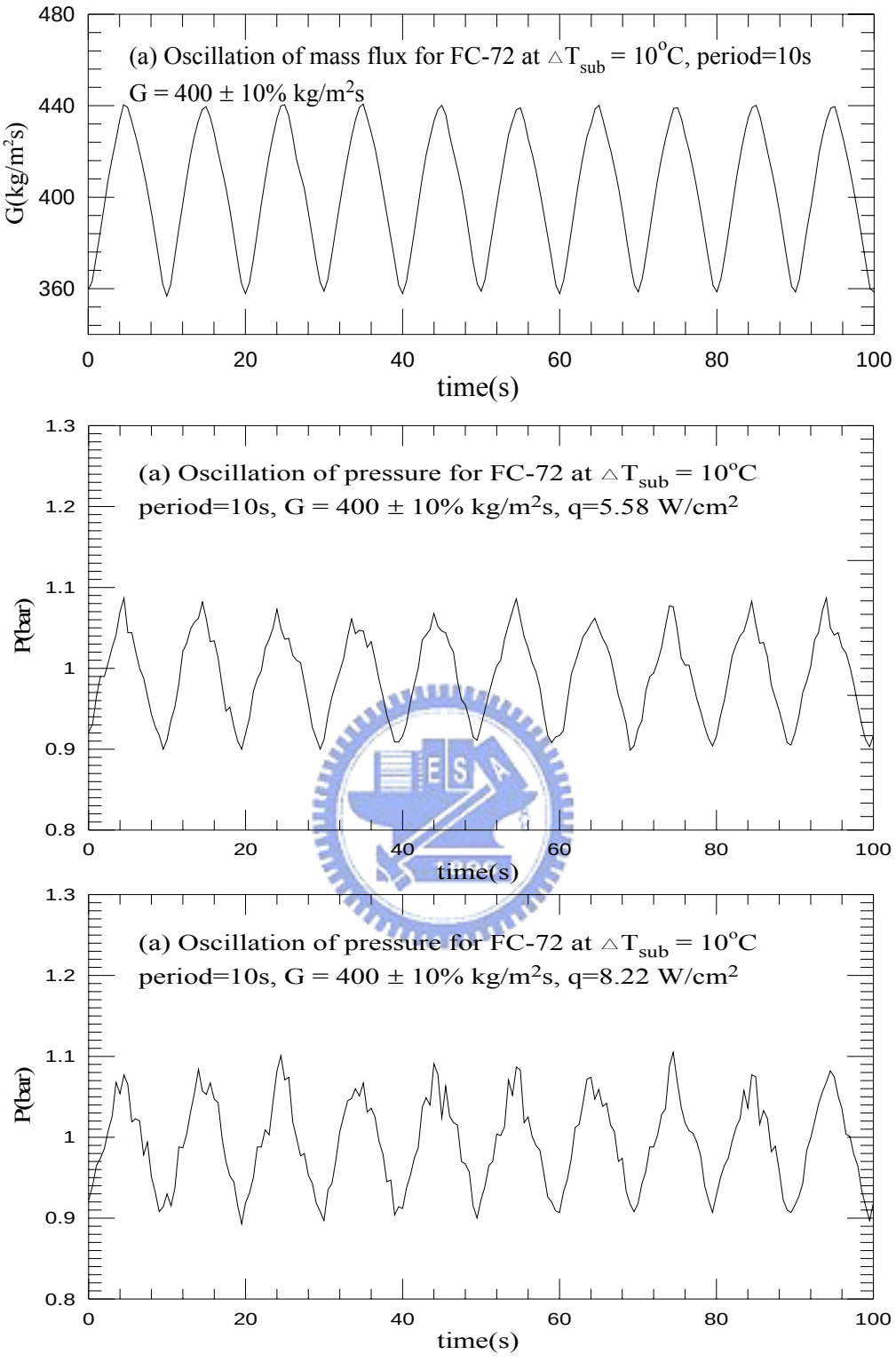

Fig.5.92 Time variations of coolant mass flux and inlet pressure in transient oscillatory subcooled flow boiling for various imposed heat fluxes at (a) q=5.58 W/cm^2 and (b) q=8.22 W/cm^2 for G=400±10% kg/m^{2}s with t_p=10 sec.

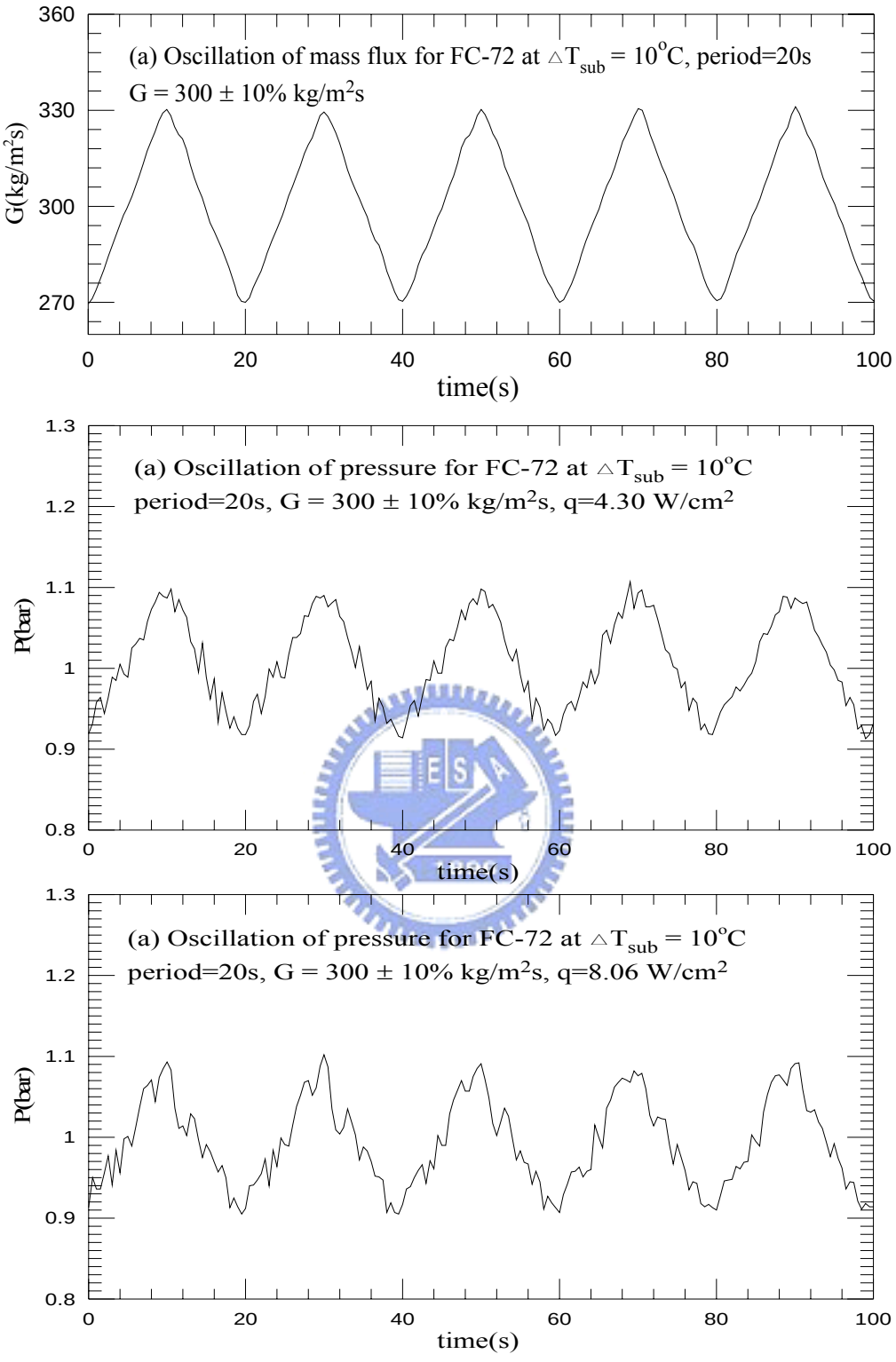

Fig.5.93 Time variations of coolant mass flux and inlet pressure in transient oscillatory subcooled flow boiling for various imposed heat fluxes at (a) q=4.30 W/cm^2 and (b) q=8.06 W/cm^2 for G=300±10% kg/m^{2}s with t_p=20 sec.

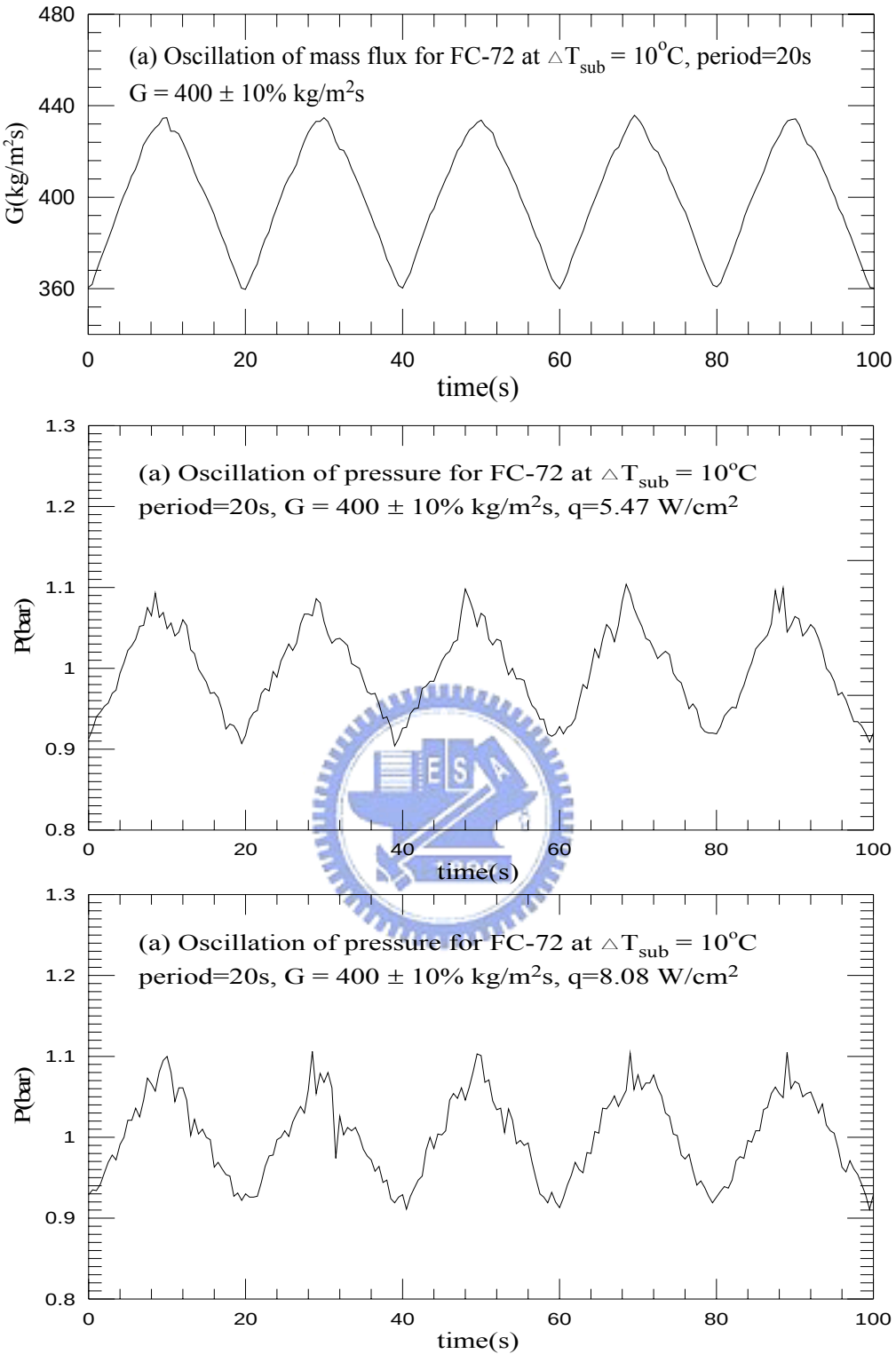

Fig.5.94 Time variations of coolant mass flux and inlet pressure in transient oscillatory subcooled flow boiling for various imposed heat fluxes at (a) q=5.47 W/cm^2 and (b) q=8.08 W/cm^2 for G=400±10% kg/m^{2}s with t_p=20 sec.

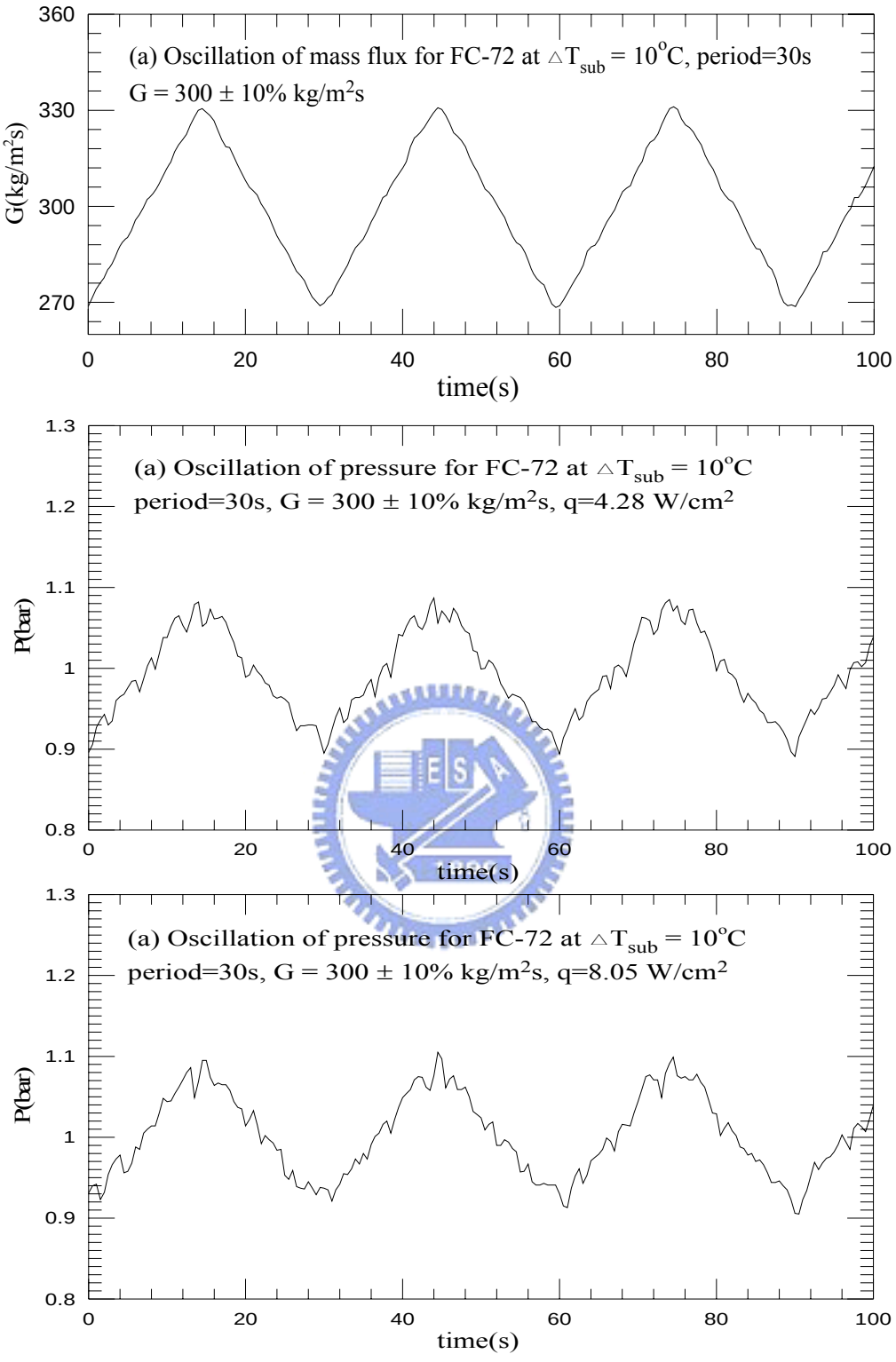

Fig.5.95 Time variations of coolant mass flux and inlet pressure in transient oscillatory subcooled flow boiling for various imposed heat fluxes at (a) q=4.28 W/cm^2 and (b) q=8.05 W/cm^2 for G=300±10% kg/m^{2}s with t_p=30 sec.

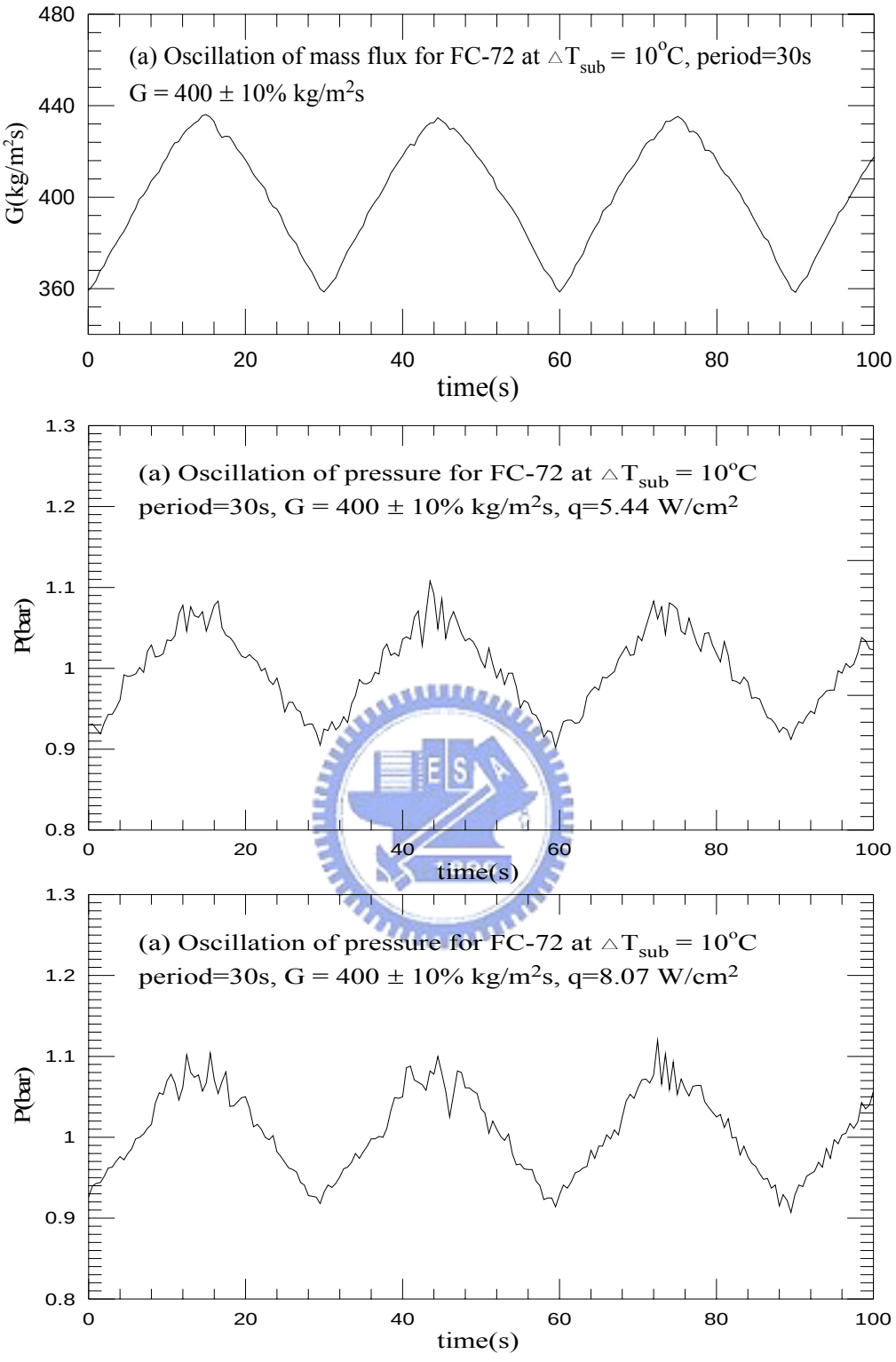

Fig.5.96 Time variations of coolant mass flux and inlet pressure in transient oscillatory subcooled flow boiling for various imposed heat fluxes at (a) q=5.44 W/cm^2 and (b) q=8.07 W/cm^2 for G=400±10% kg/m^{2}s with t_p=30 sec.